DISCOVERY OF CYTOSOLIC PHENYLALANINE BIOSYNTHETIC PATHWAY IN PLANTS

by

Yichun Qian

A Dissertation

Submitted to the Faculty of Purdue University

In Partial Fulfillment of the Requirements for the degree of

Doctor of Philosophy

Department of Horticulture

West Lafayette, Indiana

May 2019

THE PURDUE UNIVERSITY GRADUATE SCHOOL
STATEMENT OF COMMITTEE APPROVAL

Dr. Natalia Dudareva, Co-Chair
    Department of Biochemistry
    Department of Horticulture and Landscape Architecture
Dr. Joshua R. Widhalm, Co-Chair
    Department of Horticulture and Landscape Architecture
Dr. Avtar K. Handa
    Department of Horticulture and Landscape Architecture
Dr. Peter B. Goldsbrough
    Department of Botany and Plant Pathology

Approved by:
    Dr. Hazel Y. Wetzstein
        Head of the Graduate Program

To the beauty of life and everyone I love

ACKNOWLEDGMENTS

I would like to thank my advisor, Dr. Natalia Dudareva, for the opportunity to conduct my PhD research in her lab. Her mentorship will be a lifelong inspiration. I would also like to thank my previous and current advisory committee members, Dr. David Rhodes, Dr. Avtar Handa, Dr. Peter Goldsbrough and Dr. Joshua Widhalm, for their support and guidance along the progress of my research.

Thanks to my collaborators, Dr. John Morgan and Longyun Guo, for their generous contributions to this work. Thanks to my current and past lab mates, Joseph H Lynch, Joshua Widhalm, Heejin Yoo, Michael Gutensohn, Funmilayo Adebesin, Laura Henry, Rachel McCoy, Joëlle Mühlemann, Antje Klempien, and Anthony Qualley, for their valuable input to my research.

Last but not least, I would like to thank my family and friends for their sacrifice and support for the past years. I would not be able to achieve my goals without their unconditional love.

Chapter 2 contains both text and figures from a published manuscript entitled "An alternative pathway contributes to phenylalanine biosynthesis in plants via a cytosolic tyrosine: phenylpyruvate aminotransferase" (2013, *Nature communications, 4,* 2833. DOI: https://doi.org/10.1038/ncomms3833). This article is a product of joint efforts between myself, Heejin Yoo, Joshua Widhalm and principle investigator Dr. Natalia Dudareva. Additional assistance was provided by co-authors Hiroshi Maeda, Bruce R. Cooper, Amber S. Jannasch, Itay Gonda, Efraim Lewinsohn and David Rhodes.

My work involved biochemical characterization of PhPPY-AT (Tables 2.1, 2.2 and 2.3) and CmArAT1 (Tables 2.4 and 2.5) , PhPPY-AT subcellular localization (Figure 2.3), and analysis of the developmental, day/night rhythmic and tissue specific expression profiles of PhPPY-AT in petunia flowers (Figure 2.9). Heejin Yoo performed expression analysis (Figure 2.2) and metabolic profiling (Figure 2.7) of *PhADT1*x*PhPPA-AT* RNAi lines; PPY-AT activity assays from *E. coli* mutant expressing PhPPY-AT (Figure 2.8b); PDT activity assays from isolated plastids of petunia flowers (Figure 2.11); analysis of *PhPPY-AT* RNAi downregulation and overexpression (Figures 2.4 and 2.10); *AtTYDC* overexpression (Figure 2.5b) and ^{15}N-tyrosine labeling experiments (Figure 2.5a). Joshua Widhalm identified *PhPPY-AT* candidate and performed functional complementation experiment (Figure 2.8). Hiroshi Maeda generated the *PhADT1*x*PhPPA-AT* RNAi lines. Bruce R. Cooper and Amber S. Jannasch developed the phenylpyruvate detection method using triple quadrupole LC-MS. Dr. Efraim Lewinsohn and Itay Gonda provided us with the CmArAT1 protein expression construct.

Chapter 3 contains both text and figures from a published manuscript entitled "Identification of a plastidial phenylalanine exporter that influences flux distribution through the phenylalanine biosynthetic network" (2015, *Nature communications*, *6*, 8142. DOI: https://doi.org/10.1038/ncomms9142). The results in this chapter were generated by myself, Joshua Widhalm, Michael Gutensohn, Heejin Yoo, Funmilayo Adebesin, Longyun Guo, Joseph H. Lynch, and principle investigator Dr. Natalia Dudareva. Additional assistance was provided by co-authors Rohit Jaini, Rachel M. McCoy, Jacob T. Shreve, Jyothi Thimmapuram, David Rhodes and John A. Morgan.

My work involved generation of RNAi construct for *PhpCAT*; generation and metabolic profiling of *PhpCAT* RNAi and *PhpCAT* overexpression transgenic lines (Figures 3.5, 3.8 and 3.9). Joshua Widhalm identified *PhpCAT* candidate (Figure 3.1) and generated Figure 3.6a. Michael Gutensohn and Joshua Widhalm performed GFP subcellular localization (Figure 3.2a-f) and amino acid transport assays (Figure 3.4b) of PhpCAT together. Heejin Yoo performed metabolic profiling of *PhpCAT* RNAi and *PhpCAT* overexpression lines (Figure 3.5) and ^{15}N-tyrosine labeling experiments (Figure 3.10a). Funmilayo Adebesin performed the expression profiling of *PhpCAT* (Figure 3.3) and immunoblot experiments (Figures 3.2g, 3.4a and 3.7). Dr. John Morgan, Longyun guo and Rohit Jaini performed the metabolic flux modeling with ^{15}N-tyrosine labelling results (Table 3.1 and Figure 3.6b). Joseph H. Lynch performed the chorismate mutase assays from petunia plastids (Figure 3.11). Rachel M. McCoy generated the *PhpCAT* overexpression construct.

Chapter 4 contains both figures and text from a published manuscript entitles "Completion of the cytosolic post-chorismate phenylalanine biosynthetic pathway in plants (2019, *Nature communications, 10*(1), 15. DOI: https://doi.org/10.1038/s41467-018-07969-2). This article is a product of joint efforts between myself, Joseph H. Lynch, and principle investigator Dr. Natalia Dudareva. Additional assistance was provided by co-authors Longyun Guo, David Rhodes and John A. Morgan.

My work involved generation of *PhCM2* RNAi construct; generation and metabolic profiling of *PhCM2* RNAi transgenic lines (Figures 4.2, 4.10 and 4.11); expression profiling of *PhCM2* in petunia flowers (Figure 4.8); ^{15}N-tyrosine labeling experiments (Figure 4.12); shikimate feeding experiment (Figure 4.13); characterization of Arabidopsis *cm2* mutants (Figure 4.4); transient RNAi downregulation of *PhADT3* (Figure 4.6) and overexpression of *PhpCAT* (Figure 4.15); expression analysis of shikimate pathway genes (Figure 4.14a); preparation of plastidial and cytosolic fractions from petunia petals for the following CM (Figure 4.2b), PPA-AT and ADH (Figure 4.9), and ADT (Figure 4.14b) activity assays; identification of *PhADT3* alternative transcripts (Figure 4.5) and prediction of *AtADT6* alternative transcripts (Figure 4.22); expression profiles of *PhADT3* alternative transcripts (Figure 4.20); and immunoblots experiment of PhADT3 isoforms (Figure 4.5c and 4.19). Joseph H. Lynch performed biochemical characterization PhCM1, PhCM2 and PhADT3 isoforms (Tables 4.1 and 4.3, Figure 4.7); enzyme activity assays across the fractions obtained from non-aqueous fractionation of petunia petals (Figure 4.16); determination of relative enzyme activities distribution between plastids and cytosol (Figure 4.17); yeast mutant complementation assays (Figure 4.18); and subcellular localization of PhADT3S (Figure 4.21). Dr. John A. Morgan and Longyun Guo performed metabolic flux modeling with ^{15}N-tyrosine labelling results (Table 4.2 and Figure 4.3).

Chapter 5 contains both figures and text generated mostly by myself and principle investigator Dr. Natalia Dudareva. Additional assistance was provided by Joseph H. Lynch, Longyun Guo and John A. Morgan.

My work involved generation of *PhCM2* overexpression construct; transient overexpression of *PhCM2* (Figure 5.2a); generation and metabolic profiling of *PhCM2* overexpression transgenic lines (Figures 5.2b,c), as well as *AtVAS1xPhCM2* overexpression transgenic lines (Figures 5.3); ^{15}N-tyrosine labeling experiments (Figure 5.4); preparation of plastidial and cytosolic fractions from petunia petals for subsequent CM activity assays (Table 5.2, Figures 5.2b and 5.3b). Joseph H. Lynch generated the *AtVAS1* overexpression construct; prepared petunia petal tissues for transmission electron microscopy (Figure 5.5); and performed starch, IPA and IAA analysis from petunia petals (Figures 5.3c and 5.6). John A. Morgan and Longyun Guo performed metabolic flux modeling with ^{15}N-tyrosine labelling results (Table 5.1 and Figure 5.4).

TABLE OF CONTENTS

LIST OF TABLES 11

LIST OF FIGURES 12

ABSTRACT 15

CHAPTER 1. INTRODUCTION 17

- 1.1 Phenylalanine biosynthetic pathway in plants 17
- 1.2 Exploration of phenylalanine biosynthesis network in plants 18
- 1.3 Figure 21
- 1.4 References 22

CHAPTER 2. AN ALTERNATIVE PATHWAY CONTRIBUTES TO PHENYLALANINE BIOSYNTHESIS IN PLANTS VIA A CYTOSOLIC TYROSINE:PHENYLPYRUVATE AMINOTRANSFERASE[1] 27

- 2.1 Abstract 27
- 2.2 Introduction 28
- 2.3 Results 30
  - 2.3.1 *PhPPY-AT* suppression in PhADT1 RNAi lines rescues Phe levels 30
  - 2.3.2 PhPPY-AT prefers phenylpyruvate and Tyr as substrate 30
  - 2.3.3 PhPPY-AT is localized in the cytosol 32
  - 2.3.4 PhPPY-AT is involved in Phe biosynthesis *in vivo* 32
  - 2.3.5 Tyr catabolism and Phe biosynthesis are interconnected 33
- 2.4 Discussion 34
- 2.5 Materials and Methods 37
  - 2.5.1 Plant materials and metabolic analysis 37
  - 2.5.2 Gene expression analysis using qRT-PCR 37
  - 2.5.3 Expression and purification of recombinant proteins 38
  - 2.5.4 Functional complementation of the *E. coli* mutant DL39 39
  - 2.5.5 Enzyme assays 40
  - 2.5.6 Subcellular localization of PPY-AT 41
  - 2.5.7 *PhPPY-AT* downregulation and overexpression *in planta* 41

2.5.8 *AtTYDC* overexpression in petunia flowers 42
2.5.9 Labelling experiments 42
2.6 Tables and Figures 44
2.7 References 61
CHAPTER 3. IDENTIFICATION OF A PLASTIDIAL PHENYLALANINE EXPORTER THAT INFLUENCES FLUX DISTRIBUTION THROUGH THE PHENYLALANINE BIOSYNTHETIC NETWORK[2] 65
3.1 Abstract 65
3.2 Introduction 66
3.3 Results 68
3.3.1 *PhpCAT* is a homologue of *E. coli pheP* localized in plastids 68
3.3.2 *PhpCAT* is developmentally and rhythmically regulated 70
3.3.3 PhpCAT transports all three aromatic amino acids 70
3.3.4 PhpCAT links plastidial-cytosolic phenylalanine metabolism 71
3.3.5 PhpCAT controls phenylalanine biosynthetic flux 72
3.4 Discussion 73
3.5 Materials and Methods 76
3.5.1 Plant material, growth conditions and generation of *PhpCAT* RNAi and *PhpCAT* overexpression lines 76
3.5.2 qRT-PCR 76
3.5.3 Subcellular localization of PhpCAT 77
3.5.4 Heterologous expression of PhpCAT and transport assays 77
3.5.5 Metabolic flux analysis with ^{15}N-tyrosine labelling 78
3.5.6 Preparation of plastids 80
3.5.7 Immunoblots 80
3.5.8 Chorismate mutase assays 81
3.5.9 Targeted metabolite profiling 81
3.6 Table and Figures 82
3.7 References 96
CHAPTER 4. COMPLETION OF THE CYTOSOLIC POST-CHORISMATE PHENYLALANINE BIOSYNTHETIC PATHWAY IN PLANTS[3] 101

4.1 Abstract ... 101
4.2 Introduction ... 102
4.3 Results ... 104
  4.3.1 PhCM2 is required for cytosolic phenylalanine biosynthesis ... 104
  4.3.2 PhCM2 influences flux through both phenylalanine pathways ... 105
  4.3.3 CM2 contributes to phenylalanine biosynthesis in Arabidopsis ... 107
  4.3.4 Alternative transcription produces cytosolic PhADT3 isoform ... 108
4.4 Discussion ... 112
4.5 Materials and Methods ... 116
  4.5.1 Generation of *PhCM2*-RNAi transgenic plants ... 116
  4.5.2 Isolation of homozygous Arabidopsis *AtCM2* mutants ... 116
  4.5.3 qRT-PCR analysis and 5’-RLM-RACE ... 117
  4.5.4 Metabolic profiling ... 117
  4.5.5 Yeast complementation assays ... 119
  4.5.6 Enzyme assays ... 119
  4.5.7 Preparation of plastidial cytosolic fractions ... 122
  4.5.8 Non-aqueous fractionation and enzyme assays ... 123
  4.5.9 Shikimate feeding ... 124
  4.5.10 Metabolic flux analysis with ^{15}N-tyrosine labeling ... 124
  4.5.11 PhADT3 immunodetection and proteomic analyses ... 124
  4.5.12 Subcellular localization of PhADT3S ... 127
  4.5.13 *PhpCAT* overexpression and *PhADT3* downregulation in planta ... 127
4.6 Tables and Figures ... 129
4.7 References ... 156
CHAPTER 5. MODULATION OF AUXIN FORMATION BY THE CYTOSOLIC PHENYLALANINE BIOSYNTHETIC PATHWAY[4] ... 163
5.1 Abstract ... 163
5.2 Introduction ... 164
5.3 Results ... 165

5.3.1 Plastidial phenylalanine biosynthesis flux decreased in *PhCM2* overexpression lines. 165

5.3.2 Plastid development is impaired in *PhCM2* overexpression lines.......................... 166

5.3.3 Overexpressing *AtVAS1* in *PhCM2* overexpression line rescued phenylalanine levels 167

5.4 Discussion 167

5.5 Materials and Methods..................... 168

5.5.1 Generation of *PhCM2* overexpression and *AtVAS1xPhCM2* overexpression plants 168

5.5.2 RNA isolation and qRT-PCR analysis 169

5.5.3 Metabolic profiling 169

5.5.4 Enzyme assays 169

5.5.5 Preparation of plastidial and cytosolic fractions..................... 169

5.5.6 Metabolic flux analysis with ^{15}N-tyrosine labelling..................... 169

5.5.7 Starch extraction and analysis 170

5.5.8 IPA and IAA extraction and analysis 170

5.6 Tables and Figures 172

5.7 References..................... 184

CHAPTER 6. FUTURE DIRECTIONS 187

6.1 Introduction..................... 187

6.2 Objectives of future research 187

6.2.1 Understand regulation mechanism of plant DAHPS 187

6.2.2 Identify shikimate and chorismate transporters..................... 188

6.2.3 Characterize petunia TAA1 188

6.3 References..................... 189

PUBLICATIONS..................... 191

LIST OF TABLES

Table 2.1 Kinetic parameters of petunia PhPPY-AT 44

Table 2.2 Amino donor specificities of petunia PhPPY-AT for forward and reverse reactions. . 45

Table 2.3 Keto acid substrate specificities of petunia PhPPY-AT. 46

Table 2.4 Catalytic activity of CmArAT1 47

Table 2.5 Amino donor specificity of CmArAT1 with phenylpyruvate as the amino acceptor. .. 48

Table 2.6 Sequence information of primers used for qRT-PCR analysis 49

Table 3.1 Changes in flux in flowers from control and *PhpCAT*-RNAi petunia lines at t_{0h} and t_{6h} 82

Table 4.1 Kinetic parameters of recombinant petunia PhCM2 129

Table 4.2 Changes in flux in flowers from control and *PhCM2*-RNAi petunia lines at t_{0h} and t_{6h} 129

Table 4.3 Kinetic parameters of recombinant petunia PhADT3 isoforms with prephenate as substrate 129

Table 4.4 Primers used in this project 130

Table 5.1 Changes in flux in flowers from control and *PhCM2* overexpressing petunia lines at t_{0h} and t_{6h}. 172

Table 5.2 Protein yield from control and *PhCM2* overexpression petunia petals 172

Table 5.3 Primers used in this project 173

LIST OF FIGURES

Figure 1.1 Proposed phenylalanine biosynthetic network in plants 21

Figure 2.1 Proposed phenylalanine and tyrosine biosynthetic pathways in plants....................... 50

Figure 2.2 Effect of downregulating *PhPPA-AT* in the *PhADT1* RNAi line on phenylalanine levels in petunia flowers.. 51

Figure 2.3 Petunia PPY-AT is localized to the cytosol 52

Figure 2.4 Effect of *PhPPY-AT* downregulation and overexpression on phenylalanine and phenylalanine-derived volatile levels in wild-type and *PhADT1*x*PhPPA-AT* RNAi petunia flowers 53

Figure 2.5 *In planta* evidence for the interconnection between tyrosine catabolism and phenylalanine biosynthesis 54

Figure 2.6 Revised model for phenylalanine biosynthesis in plants.. 55

Figure 2.7 Effect of simultaneous *PhADT1* and *PhPPA-AT* downregulation on the levels of phenylalanine-derived volatiles, tyrosine, tryptophan, aromatic amino acid intermediates, and shikimate in petunia flowers. 56

Figure 2.8 Functional complementation of the phenylalanine auxotrophic *E. coli* mutant DL39 by *PhPPY-AT*.. 57

Figure 2.9 Expression profiles of *PhPPY-AT* in petunia flowers. 58

Figure 2.10 Effect of *PhPPY-AT* downregulation on phenylalanine and phenylalanine-derived volatile levels in petunia flowers of *PhADT1* and *PhPPA-AT* RNAi parental lines. 59

Figure 2.11 Effect of simultaneous *PhADT1* and *PhPPA-AT* downregulation on PDT activity, and expression levels of *PhADT2* and *PhADT3* in petunia flowers. 60

Figure 3.1 Identification of plastidial phenylalanine transporter candidates. 83

Figure 3.2 Ph21511 is localized to plastids 84

Figure 3.3 Expression profiles of *PhpCAT*... 85

Figure 3.4 PhpCAT aromatic amino acid transport activity 86

Figure 3.5 Metabolic profiling of petunia flowers from *PhpCAT*-RNAi and *PhpCAT*-overexpression lines.. 87

Figure 3.6 Metabolic modeling of the phenylalanine biosynthetic network in control and *PhpCAT*-RNAi lines 89

Figure 3.7 Immunoblot of PhpCAT in wild type and *PhpCAT*-RNAi transgenic line................. 91

Figure 3.8 Effect of *PhpCAT* RNAi downregulation on emission of individual phenylalanine-derived volatiles from petunia petals. 92

Figure 3.9 Effect of *PhpCAT* overexpression on emission of individual phenylalanine-derived volatiles from petunia petals 93

Figure 3.10 Effect of feeding ^{15}N-tyrosine on the labeling of phenylalanine and the levels of phenylalanine-derived volatiles 94

Figure 3.11 Phenylalanine inhibition of chorismate mutase activity in desalted petunia plastid extracts 95

Figure 4.1 Proposed plant phenylalanine biosynthetic pathways 132

Figure 4.2 Metabolic effects of *PhCM2* RNAi downregulation in petunia flowers 133

Figure 4.3 Metabolic modeling of phenylalanine biosynthetic pathways in control and *PhCM2* RNAi petunia flowers 135

Figure 4.4 Characterization of the Arabidopsis *cm2* mutants 136

Figure 4.5 Alternative *PhADT3* transcript yields a cytosolic isoform in petunia flowers 138

Figure 4.6 Effect of *PhADT3* RNAi down-regulation in wild type and *PhCM2* RNAi petunia flowers 139

Figure 4.7 Michaelis-Menten kinetics for PhCM1 (a), PhCM2 (b), PhADT3L (c) and PhADT3S (d). 140

Figure 4.8 Expression profiles of *PhCM2* in petunia flowers. 141

Figure 4.9 Activities of marker enzymes in WT and *PhCM2* RNAi petunia petals. 142

Figure 4.10 Levels of *PhCM2* transcripts (a), emitted phenylalanine-derived volatiles (b) and internal pools of aromatic amino acids (c) in petunia flowers of wild type (WT) and empty vector (EV) control lines. 143

Figure 4.11 Effect of *PhCM2* RNAi downregulation on emission of individual phenylalanine-derived volatiles from petunia flowers. 144

Figure 4.12 Isotopic labeling of phenylalanine from ^{15}N-tyrosine in petunia flowers. 145

Figure 4.13 Effects of feeding with exogenous shikimate on the levels of aromatic amino acids, arogenate, prephenate and phenylpyruvate in wild type and *PhCM2* RNAi petunia petals. 146

Figure 4.14 Effect of *PhCM2* downregulation on expression levels of shikimate pathway genes and ODO1 transcription factor, and plastidial ADT activity. 147

Figure 4.15 Effect of *PhpCAT* overexpression on levels of phenylalanine and phenylalanine-derived volatiles in wild-type and *PhCM2* RNAi petunia flowers. 148

Figure 4.16 Distribution of enzyme activities across the six fractions of decreasing density obtained by non-aqueous fractionation of petunia petals. 149

Figure 4.17 Relative distribution of enzyme activities between plastids and cytosol, as determined by non-aqueous fractionation. 150

Figure 4.18 Expression of *PhADTs* in a *pha2 S. cerevisiae* mutant. 151

Figure 4.19 Immunodetection of the cytosolic PhADT3 isoform. 152

Figure 4.20 Expression profiles of *PhADT3L* and *PhADT3S* transcripts in petunia flowers over a daily light/dark cycle.. 153

Figure 4.21 Subcellular localization of PhADT3S. 154

Figure 4.22 Potential alternative *AtADT6* transcripts. 155

Figure 5.1 Proposed plant phenylalanine biosynthetic pathways and feedback regulation by aromatic amino acids. 174

Figure 5.2 Metabolic effects of *PhCM2* overexpression in petunia flowers. 176

Figure 5.3 Metabolic effects of *AtVAS1* overexpression upon *PhCM2* overexpression petunia flowers.. 178

Figure 5.4 Metabolic modeling of phenylalanine biosynthetic pathways in control and *PhCM2* overexpression petunia flowers.. 180

Figure 5.5 Transmission electron microscopy of wild type and *PhCM2* overexpression petunia petal cells. 181

Figure 5.6 Effect of *PhCM2* overexpression on starch, IPA and IAA levels in petunia petals.. 182

Figure 5.7 Scheme of proposed metabolic crosstalk between phenylpyruvate pathway and tryptophan-dependent auxin biosynthesis... 183

ABSTRACT

Author: Qian, Yichun. PhD
Institution: Purdue University
Degree Received: May 2019
Title: Discovery of Cytosolic Phenylalanine Biosynthetic Pathway in Plants
Committee Chair: Natalia Dudareva

Phenylalanine (Phe) is a proteinogenic aromatic amino acid that also serves as a precursor for numerous primary and secondary metabolites in plants. Phe is synthesized from chorismate, the final product of the shikimate pathway. In plants, Phe is predominantly synthesized in the plastids via the arogenate pathway, while most Phe-derived compounds are produced in the cytoplasm, requiring exportation of Phe from plastids to the cytosol. Here, we provided genetic evidences that a *Petunia hybrida* plastidial cationic amino acid transporter (PhpCAT) participates in the exportation of Phe from plastids, as well as regulation of carbon flux through Phe biosynthesis.

By using reverse genetics, we demonstrated that a petunia phenylpyruvate aminotransferase (PhPPY-AT) is able to convert phenylpyruvate to Phe in the cytosol *in vivo*, and that a cytosolic chorismate mutase (CM2), which converts chorismate to prephenate, directs carbon flux from the plastidial Phe biosynthesis pathway towards the cytosolic pathway. Downregulation of *PhPPY-AT* and *PhCM2* resulted in significant decreases in Phe levels and emission of Phe-derived volatiles in petunia flowers, respectively. Metabolic flux analysis showed that the carbon flux through the cytosolic Phe biosynthesis pathway is significantly lower in *PhCM2* RNAi petunia flowers relative to wild type control. We also demonstrated that the conversion of prephenate to phenylpyruvate in the cytosol is catalyzed by a cytosolic prephenate dehydratase (PDT) produced from an alternative transcription start site of a known plastidial arogenate dehydratase (ADT). These results suggest that a microbial-like phenylpyruvate pathway for Phe biosynthesis operates in the cytosol of plant cells and the cytosolic pathway splits from the plastidial pathway at chorismate.

To evaluate the metabolic potential of the cytosolic phenylpyruvate pathway, *PhCM2* overexpressing transgenic petunia plants were generated. Unexpectedly, Phe levels and emission of Phe-derived volatiles were both reduced, even though the flux through the cytosolic pathway was increased relative to wild type control. Electron microscopy, metabolic profiling and

metabolic flux analysis revealed that the number of leucoplasts, starch levels and flux through the plastidial pathway were all reduced in *PhCM2* overexpression lines, while the concentrations of auxin and its biosynthetic intermediate, indole-3-pyruvic acid (IPA), were elevated. Overexpression of Arabidopsis aminotransferase VAS1, which converts IPA to Trp, in *PhCM2* overexpression petunia background recovered Phe levels and Phe-derived volatiles emission. These results indicate that there exists a metabolic crosstalk between cytosolic Phe production and Trp-dependent auxin biosynthesis .

Our research completed the post-chorismate cytosolic Phe biosynthesis pathway in plants and revealed possible metabolic crosstalk between cytosolic Phe production and auxin biosynthesis in plant cells, providing targets for future genetic modification of metabolites in plants.

CHAPTER 1. INTRODUCTION

1.1 Phenylalanine biosynthetic pathway in plants

The aromatic amino acids, phenylalanine (Phe), tyrosine (Tyr) and tryptophan (Trp), are not only constituents of proteins, but also precursors for numerous primary and secondary metabolites in all living organisms. In plants, up to ~30% of the carbon fixed from photosynthesis in plant cells goes into Phe and Phe-derived compounds[1], the highest among all aromatic amino acids. Phe is a precursor of > 8000 plant phenolic compounds involved in plant growth, development, reproduction, defense and architecture, such as the hormone salicylic acid[2], ubiquinone[3], phenylpropanoid/benzenoid volatiles[4,5], anthocyanins, (iso)flavonoids[6] and lignins[7]. Phe is also an essential nutrient in animal diets, because animals cannot synthesize Phe and must consume it from food. For humans, Phe is the precursor of neurotransmitters dopamine, norepinephrine and epinephrine, and can be used as supplement to treat mental disorders[8], as well as a broad range of human diseases[9]. The crucial roles of Phe in both plants and animals make it inevitable for us to investigate and understand Phe biosynthesis and metabolism.

Phe is synthesized from chorismate, the product of the shikimate pathway[10,11]. Chorismate is first converted to prephenate by chorismate mutase (CM). Prephenate is subsequently converted to Phe through two alternative pathways[12]. In the “phenylpyruvate pathway”, prephenate is first dehydrated/decarboxylated to phenylpyruvate by prephenate dehydratase (PDT) and then transaminated to Phe by phenylpyruvate aminotransferase (PPY-AT)[12]. In the “arogenate pathway”, prephenate is first transaminated to arogenate by prephenate aminotransferase (PPA-AT) and then dehydrated/decarboxylated to Phe by arogenate dehydratase (ADT)[12].

In most microorganisms, Phe is synthesized through the phenylpyruvate pathway[13-15]. The enzymatic reaction of PPY-AT in microorganisms is reported to be caused by broad substrate specificity of multiple aromatic amino acid aminotransferases[16-18], while PDT activity comes from either monofunctional PDT[13] or bifunctional CM/PDT[14,19].

Genetic evidences have demonstrated that, in plant cells, Phe is synthesized in the plastids via the arogenate pathway[20-24]. All enzymes involved in the arogenate pathway have been identified and characterized in plants (Figure 1.1). (1) A plastidial PhCM1 has been reported to be responsible for the production of Phe and Phe-derived volatiles in petunia flowers[25]. (2) PPA-AT activity has been described in many plants[26,27] and is shared in the tyrosine biosynthesis pathway[28]. The high catalytic efficiency of PPA-AT directs the carbon flux to predominantly go through the arogenate pathway in the plastids[21]. (3) Multiple genes encoding plastidial ADT have been identified in Plants (6 ADTs in Arabidopsis, 4 ADTs in rice and 3 ADTs in petunia)[20,22,23]. Their different expression profiles and enzymatic activities indicate that each ADT may be involved in different physiological functions[20,23]. It has been demonstrated in petunia that ADT1 is responsible for Phe biosynthesis through the arogenate pathway[20].

Plastidial Phe biosynthesis is subject to complex post-transcriptional feedback regulations, in which carbon flux is mainly controlled or redirected by 3-deoxy-D-arabino-heptulosonate 7-phosphate (DAHP) synthase (DAHPS), CM1 and ADT (Figure 1.1). DAPHS catalyzes the first step in shikimate pathway. *In vitro* assays have shown that the activities of plant DAHPS are inhibited by arogenate and prephenate[31,32], enhanced to Trp[33], but insensitive to Phe[34,35]. Overexpression of Phe-insensitive bacterial DAHPS (AroG) in Arabidopsis[36] and tomato[37] increased Phe levels up to 7- and 8-folds, respectively. The activity of plastidial CM1 has shown to be enhanced by Trp, but inhibited by its final product Phe and Tyr in *in vitro* assays[38-40]. Overexpressing a Phe-insensitive CM/PDT (PheA) in Arabidopsis increased Phe levels by up to 10 times[41]. ADT activity in plastids can be inhibited by its direct product Phe[22,42], due to the ACT regulatory domain on its C-terminal[20,43]. A rice mutant Mtr1, which contains a Phe-insensitive plastidial ADT with S298I mutation in the ACT domain, was shown to have Phe level 55 times higher than control Norin 8[22].

1.2 Exploration of phenylalanine biosynthesis network in plants

Other than the plastidial Phe biosynthetic pathway, recent discoveries also revealed the existence of an expanded Phe biosynthesis network in plants. The decrease of Phe levels in *PhPPA-AT* RNAi petunia flowers is not as significant as the decrease of Phe levels in *PhADT1* RNAi petunia flowers, raising the possibility that there is a redirection of carbon flux through an alternative Phe biosynthesis pathway in plants[21]. Furthermore, overexpression of the bi-functional CM/PDT (PheA) in Arabidopsis significantly increased Phe levels[41], suggesting that plants are able to use synthesize Phe from phenylpyruvate like microorganisms. Even though no dedicated PPY-AT candidates have been identified in plants yet, the PPY-AT activities in plant cells could either come from broad substrate specificity of other aminotransferases, or from the reverse reaction of aminotransferases that are involved in aromatic amino acid catabolism[49,50]. Biochemical characterization of such aminotransferases have been reported in Arabidopsis[49], opium poppy (*Papaver somniferum*)[50] and melon (*Cucumis melo* L., Cucurbitaceae)[44]. However, the *in vivo* functions of these aminotransferases have not been fully investigated yet as whether they are involved in Phe biosynthesis in planta.

If a microbial-like phenylpyruvate pathway does contribute to Phe biosynthesis in plants, PDT activity is required to convert prephenate to phenylpyruvate in plant cells. In plants, PDT activity has only been reported in etiolated Arabidopsis seedlings[29]. No dedicated PDT genes have been reported in plants but some ADTs are capable of using prephenate as substrates but with a much lower catalytic efficiency than arogenate[20,22,23,30]. A recent study revealed a PDT activity conferring (PAC) domain outside of ADT/PDT catalytic domain, in which a single residue Ala314 is responsible to trigger PDT activity[30]. However, PPA-AT converts prephenate to arogenate in the plastids with catalytic efficiency at least 900-fold higher than that of any ADT towards prephenate, making it very unlikely to produce phenylpyruvate in plastids[21]. Thus, in order to demonstrate a functional phenylpyruvate pathway in plant cells, further investigations will be conduct either to identify PDT candidates with higher catalytic efficiency towards prephenate to compete with PPA-AT, or to discover a Phe biosynthesis pathway that is physically separated from the plastidal pathway.

Over the past two decades, a cytosolic chorismate mutase (CM2) has been characterized in Arabidopsis[38,45], tobacco[46], petunia[25] and many other plant species[47]. Unlike CM1, the activity of CM2 is insensitive to the allosteric regulation by any of the three aromatic amino acids[38-40]. *In vitro* assays showed that Arabidopsis CM2 has higher affinity towards substrate chorismate than CM1 (K_m = 550 uM for AtCM1, K_m = 150 uM for AtCM2)[48]. However, the physiological functions of CM2 have remained unknown. The widespread existence of a cytosolic CM2 in plants provides a prospect for investigating the molecular structure and subcellular localization of alternative Phe biosynthetic pathways.

In plants, most Phe-derived compounds are produced in the cytoplasm[51], thus requiring exportation of enormous amount of plastidial Phe into cytosol. Since the lipid bilayer membrane is not permeable for Phe, simple diffusion would be too slow to meet the demand for the subsequent Phe-derived compound production and thus Phe transport requires facilitation of membrane proteins[52]. In plant cells, amino acid transporters have been shown to be localized on plasma membrane[54], vacuolar membrane[53,54] or endoplasmic reticulum[53], but no plastididal-localized amino acid transporters have been experimentally identified yet. Moreover, even though an Arabidopsis cationic amino acid transporter (AtCAT6)[55] and an aromatic and neutral transporter (AtANT1)[56] have been shown to uptake aromatic amino acids Phe, Tyr and Trp as substrates, no Phe-specific transporters have been reported in plants yet. On the other hand, Phe transport in microorganisms has been well understood. Phe uptake in *E.* coli occurs via two major systems: the Phe-specific permease (PheP) with substrate preference towards Phe (K_m = 2 μM for Phe)[57], and the general aromatic amino acid transporter (AroP) with high affinity towards Phe, Tyr and Trp (K_m = 0.47 μM, 0.57 μM and 0.4 μM, respectively)[58,60]. A branched-chain amino acid transporter (LIV-I/LS System) has also been shown to uptake Phe in *E.* coli with a relatively lower affinity (K_m = 19 μM for LIV-I system and K_m = 30 μM for LS system)[59]. Understanding the intracellular Phe transport system in plants will provide us with new insights into the regulation and interconnection within the Phe biosynthesis network.

Summary:

1) Phenylalanine biosynthesis in plants is a compartmentalized complex network with multiple molecular players involved.
2) The plastidial phenylalanine biosynthetic pathway is subject to stringent regulation at multiple steps throughout the pathway.
3) Metabolic engineering of the plastidial phenylalanine biosynthesis pathway, such as overexpressing feedback regulation insensitive enzymes, is able to increase phenylalanine production in plants.
4) Exploration of potential alternative Phe biosynthetic pathways will broaden our understanding of phenylalanine biosynthesis network in plants.

1.3 Figure

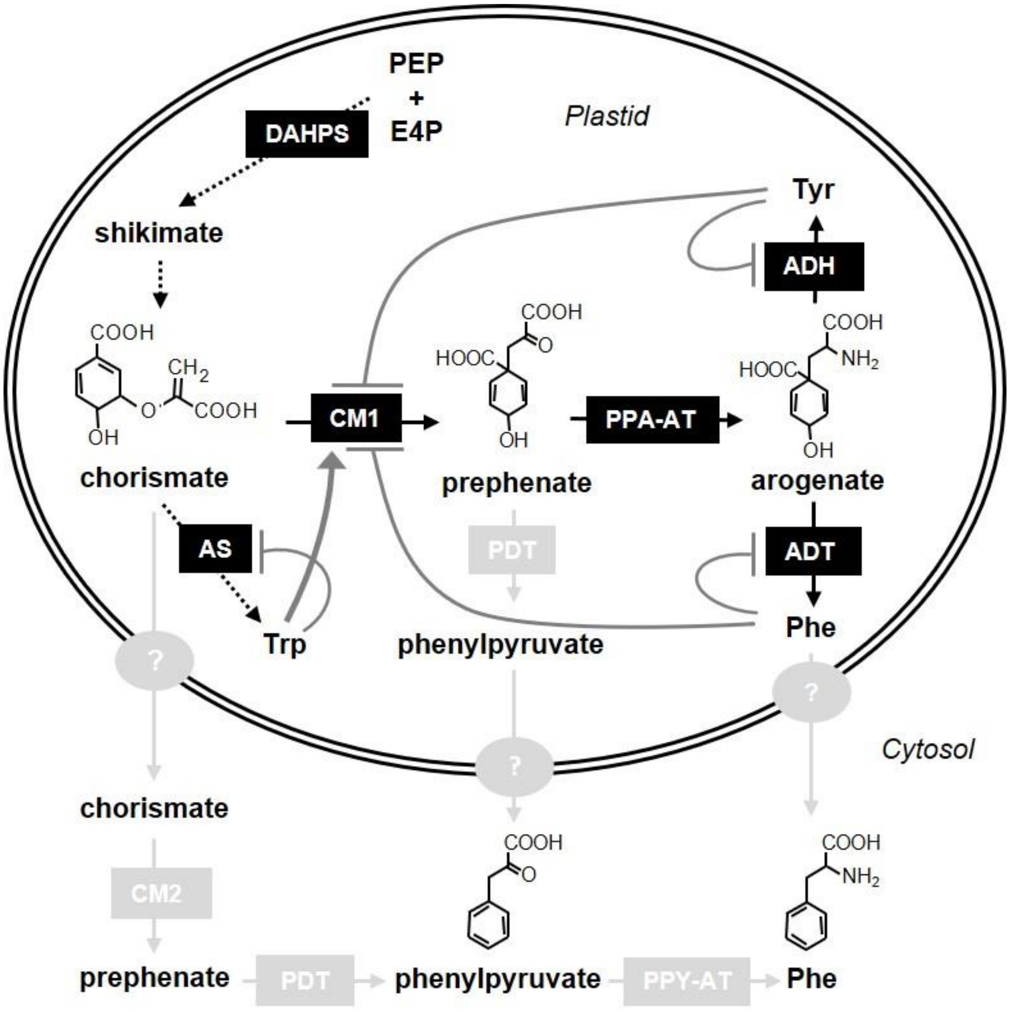
PEP
+
E4P
DAHPS
Plastid
shikimate
Tyr
ADH
COOH
CH2
O
COOH
OH
chorismate
CM1
HOOC
COOH
O
OH
prephenate
PPA-AT
HOOC
COOH
NH2
OH
arogenate
AS
PDT
ADT
Trp
phenylpyruvate
Phe
?
?
?
Cytosol
chorismate
COOH
O
COOH
NH2
CM2
prephenate
PDT
phenylpyruvate
PPY-AT
Phe

Figure 1.1 Proposed phenylalanine biosynthetic network in plants

Characterized enzymes and transporters are shown in black. Uncharacterized enzymatic and transport steps are shown in light grey. Dark grey lines depict activation and feedback inhibition of enzymes in the plastidial pathway. Abbreviations: ADH, arogenate dehydrogenase; ADT, arogenate dehydratase; AS, anthranilate synthase; CM, chorismate mutase; DAHPS, 3-deoxy-D-arabino-heptulosonate 7-phosphate synthase; E4P, erythrose 4-phosphate; PEP, phosphenolpyruvate; PDT, prephenate dehydratase; PPA-AT, prephenate aminotransferase; PPY-AT, phenylpyruvate aminotransferase.

1.4 References

1. Razal, R.A. *et al.* Nitrogen recycling in phenylpropanoid metabolism. *Phytochemistry* **41,** 31-35 (1996).
2. Vlot, A. C., Dempsey, D. A. & Klessig, D. F. Salicylic acid, a multifaceted hormone to combat disease. *Annu. Rev. Phytopathol.* **47,** 177–206 (2009).
3. Block, A. *et al.* The origin and biosynthesis of the benzenoid moiety of ubiquinone (Coenzyme Q) in Arabidopsis. *Plant Cell* **26,** 1938–1948 (2014).
4. Dudareva, N., Negre, F., Nagegowda, D. A. & Orlova, I. Plant volatiles: Recent advances and future perspectives. *Crit. Rev. Plant Sci.* **25,** 417–440 (2006).
5. Dudareva, N., Klempien, A., Muhlemann, J. K. & Kaplan, I. Biosynthesis, function and metabolic engineering of plant volatile organic compounds. *New Phytol.* **198,** 16-32 (2013).
6. Vogt, T. Phenylpropanoid biosynthesis. *Mol. Plant* **3,** 2–20 (2010).
7. Bonawitz, N. D. & Chapple, C. The genetics of lignin biosynthesis: Connecting genotype to phenotype. *Annu. Rev. Genet.* **44,** 337–363 (2010).
8. Fernstrom, J.D., and Fernstrom, M.H. Tyrosine, phenylalanine, and catecholamine synthesis and function in the brain. *The Journal of nutrition* **137,** 1539S-1547S (2007).
9. Huang, W. Y., Cai, Y. Z. & Zhang, Y. Natural phenolic compounds from medicinal herbs and dietary plants: Potential use for cancer prevention. *Nutr. Cancer* **62,** 1–20 (2010).
10. Herrmann, K. M., & Weaver, L. M. The shikimate pathway. *Annual review of plant biology* **50,** 473-503 (1999).
11. Maeda, H., & Dudareva, N. The shikimate pathway and aromatic amino acid biosynthesis in plants. *Annual review of plant biology* **63,** 73-105 (2012).
12. Siehl, D. L. The Biosynthesis of tryptophan, tyrosine. and phenylalanine from chorismate. *Plant Amino Acids* (CRC Press) pp. 185-218 (1998).
13. Prakash, P. et al. pheA (Rv3838c) of Mycobacterium tuberculosis encodes an allosterically regulated monofunctional prephenate dehydratase that requires both catalytic and regulatory domains for optimum activity. *J. of Biol. Chem.* **280,** 20666-20671 (2005).
14. Davidson, B. E. *et al.* Chorismate mutase-prephenate dehydratase from *Escherichia coli* K-12 I. Purification, molecular weight, and amino acid composition. *J. Biol. Chem.* **247,** 4441-4446 (1972).

15. Bentley, R., & Haslam, E. The shikimate pathway — a metabolic tree with many branche. *Critical reviews in biochemistry and molecular biology* **25,** 307-384 (1990).
16. Gelfand, D. H., & Steinberg, R. A. Escherichia coli mutants deficient in the aspartate and aromatic amino acid aminotransferases. *Journal of Bacteriology* **130,** 429-440 (1977).
17. Berry, A. *et al.* Enzymological features of aromatic amino acid biosynthesis reflect the phylogeny of mycoplasmas. *Microbiology* **133,** 2147-2154 (1987).
18. Fischer, R. S. *et al.* Clues from a halophilic methanogen about aromatic amino acid biosynthesis in archaebacteria. *Archives of microbiology*, **160,** 440-446 (1993).
19. Romero, R. M., Roberts, M. F., & Phillipson, J. D. Chorismate mutase in microorganisms and plants. *Phytochemistry* **40**, 1015–1025 (1995)
20. Maeda, H. *et al.* RNAi suppression of arogenate dehydratase1 reveals that phenylalanine is synthesized predominantly via the arogenate pathway in petunia petals. *Plant Cell* **22,** 832-849 (2010).
21. Maeda, H., Yoo, H. & Dudareva, N. Prephenate aminotransferase directs plant phenylalanine biosynthesis via arogenate. *Nature Chemical Biology* **7,** 19-21 (2011).
22. Yamada, T. *et al.* Mutation of a rice gene encoding a phenylalanine biosynthetic enzyme results in accumulation of phenylalanine and tryptophan. *Plant Cell* **20,** 1316-1329 (2008).
23. Cho, M. H. *et al.* Phenylalanine biosynthesis in Arabidopsis thaliana identification and characterization of Arogenate dehydratases. *J. Biol. Chem.* **282,** 30827-30835 (2007).
24. Rippert, P. *et al.* Tyrosine and phenylalanine are synthesized within the plastids in Arabidopsis. *Plant Physiology* **149,** 1251-1260 (2009).
25. Colquhoun, T.A. *et al.* A petunia chorismate mutase specialized for the production of floral volatiles. *Plant Journal* **61,** 145-155 (2010).
26. Bonner, C. A., & Jensen, R. A. Novel features of prephenate aminotransferase from cell cultures of Nicotiana silvestris. *Arch. Biochem. Biophys.* **238,** 237-246 (1985).
27. De-Eknamkul, W., & Ellis, B. E. Purification and characterization of prephenate aminotransferase from Anchusa officinalis cell cultures. *Archives of biochemistry and biophysics* **267,** 87-94 (1988).
28. Siehl, D. L., Connelly, J. A., & Conn, E. E. Tyrosine biosynthesis in Sorghum bicolor: characteristics of prephenate aminotransferase. *Zeitschrift für Naturforschung C*, **41,** 79-86 (1986).

29. Warpeha, K. M. *et al.* G-protein-coupled receptor 1, G-protein Gα-subunit 1, and prephenate dehydratase 1 are required for blue light-induced production of phenylalanine in etiolated Arabidopsis. *Plant physiology* **140,** 844-855 (2006).

30. El-Azaz, J. *et al.* Identification of a small protein domain present in all plant lineages that confers high prephenate dehydratase activity. *The Plant Journal* **87,** 215-229 (2016).

31. Rubin, J. L., & Jensen, R. A. Differentially regulated isozymes of 3-deoxy-D-arabino-heptulosonate-7-phosphate synthase from seedlings of Vigna radiata [L.] Wilczek. *Plant physiology* **79,** 711-718 (1985).

32. Doong, R. L., Ganson, R. J., & Jensen, R. A. Plastid-localized 3-deoxy-D-arabino-heptulosonate 7-phosphate synthase (DS-Mn): the early-pathway target of sequential feedback inhibition in higher plants. *Plant, Cell & Environment* **16,** 393-402 (1993).

33. Pinto, J. E., Suzich, J. A., & Herrmann, K. M. 3-Deoxy-D-arabino-heptulosonate 7-phosphate synthase from potato tuber (Solanum tuberosum L.). *Plant Physiol.* **82,** 1040-1044 (1986).

34. Huisman, O. C., & Kosuge, T. Regulation of aromatic amino acid biosynthesis in higher plants II. 3-Deoxy-arabino-heptulosonic acid 7-phosphate synthetase from cauliflower. *Journal of Biological Chemistry* **249,** 6842-6848 (1974).

35. Herrmann, K. M. The shikimate pathway: early steps in the biosynthesis of aromatic compounds. *Plant Cell* **7,** 907-919 (1995).

36. Tzin, V. *et al.* Expression of a bacterial feedback-insensitive 3-deoxy-d-arabino-heptulosonate 7-phosphate synthase of the shikimate pathway in Arabidopsis elucidates potential metabolic bottlenecks between primary and secondary metabolism. *New Phytologist* **194,** 430-439 (2012).

37. Tzin, V. *et al.* Tomato fruits expressing a bacterial feedback-insensitive 3-deoxy-D-arabino-heptulosonate 7-phosphate synthase of the shikimate pathway possess enhanced levels of multiple specialized metabolites and upgraded aroma. *J. Exp. Bot.* **64,** 4441-4452 (2013).

38. Eberhard, J. *et al.* Cytosolic and plastidic chorismate mutase isozymes from Arabidopsis thaliana: Molecular characterization and enzymatic properties. *Plant J.* **10,** 815-821 (1996).

39. Benesova, M., & Bode, R. Chorismate mutase isoforms from seeds and seedlings of Papaver somniferum. *Phytochemistry* **31,** 2983-2987 (1992).

40. Kuroki, G. W., & Conn, E. E. Differential activities of chorismate mutase isozymes in tubers and leaves of Solanum tuberosum L. *Plant Physiol.* **89,** 472-476 (1989).

41. Tzin, V. *et al.* Expression of a bacterial bi-functional chorismate mutase/prephenate dehydratase modulates primary and secondary metabolism associated with aromatic amino acids in Arabidopsis. *Plant J.* **60,** 156-167 (2009).

42. Siehl, D. L., & Conn, E. E. Kinetic and regulatory properties of arogenate dehydratase in seedlings of Sorghum bicolor (L.) Moench. *Arch. Biochem. Biophys.* **260,** 822-829 (1988).

43. Kleeb, A. C. *et al.* A monofunctional and thermostable prephenate dehydratase from the archaeon *Methanocaldococcus jannaschii*. *Biochemistry* **45,** 14101-14110 (2006).

44. Gonda, I. *et al.* Branched-chain and aromatic amino acid catabolism into aroma volatiles in *Cucumis melo* L. fruit. *J. Exp. Bot.* **61**, 1111–1123 (2010).

45. Mobley, E.M. *et al.* Identification, characterization and comparative analysis of a novel chorismate mutase gene in Arabidopsis thaliana. *Gene* **240,** 115-123 (1999).

46. Goers, S.K., and Jensen, R.A. Separation and characterization of 2 chorismate-mutase isoenzymes from Nicotiana-Silvestris. *Planta* **162,** 109-116 (1984).

47. Poulsen, C., and Verpoorte, R. Roles of chorismate mutase, isochorismate synthase and anthranilate synthase in plants. *Phytochemistry* **30,** 377-386 (1991).

48. Westfall, C. S. *et al.* Structural evolution of differential amino acid effector regulation in plant chorismate mutases. *Journal of Biological Chemistry* **289,** 28619-28628 (2014).

49. Prabhu, P.R. & Hudson, A.O. Identification and partial characterization of an L-Tyrosine aminotransferase (TAT) from *Arabidopsis thaliana*. *Biochem. Res. Int.* **2010**, 549572 (2010).

50. Lee, E.J. & Facchini, P.J. Tyrosine aminotransferase contributes to benzylisoquinoline alkaloid biosynthesis in *Opium Poppy*. *Plant Physiol.* **157**, 1067–1078 (2011).

51. Boatright, J. *et al.* Understanding in vivo benzenoid metabolism in petunia petal tissue. *Plant Physiol.* **135,** 1993-2011 (2004).

52. Chakrabarti, A. C. Permeability of membranes to amino acids and modified amino acids: Mechanisms involved in translocation. *Amino acids* **6,** 213-229 (1994).

53. Yang, H., Krebs, M., Stierhof, Y. & Ludewig, U. Characterization of the putative amino acid transporter genes AtCAT2, 3 & 4: The tonoplast localized AtCAT2 regulates soluble leaf amino acids. *J. Plant Physiol.* **171**, 594-601 (2014).

54. Su, Y., Frommer, W. B. & Ludewig, U. Molecular and functional characterization of a family of amino acid transporters from Arabidopsis. *Plant Physiol.* **136**, 3104-3113 (2004).
55. Hammes, U. Z., Nielsen, E., Honaas, L. A., Taylor, C. G. & Schachtman, D. P. AtCAT6, a sink-tissue-localized transporter for essential amino acids in Arabidopsis. *Plant J.* **48**, 414-426 (2006).
56. Chen, L., Ortiz-Lopez, A., Jung, A., & Bush, D. R. ANT1, an aromatic and neutral amino acid transporter in Arabidopsis. *Plant Physiol.* **125,** 1813-1820 (2001).
57. Pi, J., Wookey, P. J. & Pittard, A. J. Cloning and sequencing of the pheP gene, which encodes the phenylalanine-specific transport system of *Escherichia coli*. *J. Bacteriol.* **173**, 3622-3629 (1991).
58. Chye, M. L., Guest, J. R. & Pittard, J. Cloning of the aroP gene and identification of its product in *Escherichia coli* K-12. *J. Bacteriol*. **167**, 749-753 (1986).
59. Koyanagi, T., Katayama, T., Suzuki, H. & Kumagai, H. Identification of the LIV-I/LS system as the third phenylalanine transporter in *Escherichia coli* K-12. *J. Bacteriol*. **186**, 343-350 (2004).
60. Brown, K. D. Formation of aromatic amino acid pools in Escherichia coli K-12. *Journal of bacteriology* **104,** 177-188 (1970).

CHAPTER 2. AN ALTERNATIVE PATHWAY CONTRIBUTES TO PHENYLALANINE BIOSYNTHESIS IN PLANTS VIA A CYTOSOLIC TYROSINE:PHENYLPYRUVATE AMINOTRANSFERASE[1]

2.1 Abstract

Phenylalanine is a vital component of proteins in all living organisms, and in plants is a precursor for thousands of additional metabolites. Animals are incapable of synthesizing phenylalanine and must primarily obtain it directly or indirectly from plants. While plants can synthesize phenylalanine in plastids through arogenate, the contribution of an alternative pathway via phenylpyruvate, as it occurs in most microbes, has not been demonstrated. Here we establish that plants also utilize the microbial-like phenylpyruvate pathway to produce phenylalanine, and flux through this route is increased when the entry point to the arogenate pathway is limiting. Unexpectedly, we find the plant phenylpyruvate pathway utilizes a cytosolic aminotransferase that links the coordinated catabolism of tyrosine to serve as the amino donor, thus interconnecting the extra-plastidial metabolism of these amino acids. Our discovery unlocks another level of complexity in the plant aromatic amino acid regulatory network, unveiling new targets for metabolic engineering.

---

[1] This chapter has been published in Yoo *et al.* (2013) Nature Communications.

Yoo, H., Widhalm, J. R., Qian, Y., Maeda, H., Cooper, B. R., Jannasch, A. S., ... & Dudareva, N. (2013). An alternative pathway contributes to phenylalanine biosynthesis in plants via a cytosolic tyrosine: phenylpyruvate aminotransferase. *Nature communications, 4,* 2833. DOI: https://doi.org/10.1038/ncomms3833

2.2 Introduction

Aromatic amino acids are essential constituents of proteins in all living organisms, while in plants, phenylalanine and tyrosine also serve as precursors for thousands of vital and specialized compounds. Approximately 20-30% of photosynthetically fixed carbon is directed towards synthesis of phenylalanine, and in turn to lignin[1], the central structural component of plant cell walls and the major impediment to cellulosic biofuel production. In addition to structural roles, phenylalanine-derived compounds function in plant defense and UV protection (*e.g.* flavonoids and various phenolics)[2,3], signaling (*e.g.* isoflavonoids)[4], and reproduction (*e.g.* anthocyanins and phenylpropanoid/benzenoid volatiles)[3]. Moreover, tyrosine-derived metabolites, such as tocopherols (vitamin E)[5], plastoquinone[6], cyanogenic glycosides[7], and suberin[8] play crucial roles in plant fitness.

Phenylalanine and tyrosine are synthesized from chorismate, the final product of the shikimate pathway[9,10], which is converted by chorismate mutase to prephenate. Subsequent conversion of prephenate to phenylalanine and tyrosine occurs through alternative routes. In the first (the arogenate pathway), a shared transamination reaction catalyzed by prephenate aminotransferase (PPA-AT), produces L-arogenate, which can then either be dehydrated/decarboxylated to phenylalanine by arogenate dehydratase (ADT) or dehydrogenated/decarboxylated to tyrosine by arogenate dehydrogenase (ADH; Figure 2.1). In the other routes (the phenylpyruvate/4-hydroxyphenylpyruvate pathways), these reactions occur in reverse order: prephenate is first subjected to dehydration/decarboxylation or dehydrogenation/decarboxylation to form phenylpyruvate or 4-hydroxyphenylpyruvate, respectively. Then the corresponding products undergo transamination to phenylalanine and tyrosine (Figure 2.1). Most microorganisms appear to utilize only the phenylpyruvate/4-hydroxyphenylpyruvate pathways[11-13], with a few exceptions[14]. In contrast, phenylalanine and tyrosine biosynthesis in plants has only been described to occur via the arogenate pathway[15-18]. Nevertheless, overexpression of a bacterial bifunctional *chorismate mutase/prephenate dehydratase* (*PheA*) in Arabidopsis resulted in significantly increased phenylalanine production[19], implicating the presence of an aminotransferase capable of converting phenylpyruvate to phenylalanine in plants, as it occurs in the final step of the microbial phenylpyruvate pathway. Although several plant aminotransferases, mainly participating in aromatic amino acid catabolism, have recently been described[20-23], none of them have been demonstrated to function in phenylalanine biosynthesis.

Previously we demonstrated that *PhADT1* downregulation in *Petunia hybrida* flowers, which emit high levels of phenylalanine-derived volatiles[24,25], resulted in a greater decrease in phenylalanine levels compared to the effect of *PhPPA-AT* downregulation (up to 82% versus 20% reduction, respectively)[16,17]. Such a differential impact on phenylalanine levels from the downregulation of these individual genes was suggested to either be due to sufficient residual PPA-AT activity in the *PhPPA-AT* RNAi lines capable of sustaining the arogenate pathway, or the redirection of carbon flux from accumulated prephenate in the *PhPPA-AT* RNAi lines through the hitherto undetected alternative phenylpyruvate pathway[17]. Here, to test these hypotheses, we generated RNAi transgenic petunia plants in which both *PhADT1* and *PhPPA-AT* genes were simultaneously downregulated. If the phenylalanine and volatile phenotypes in *PhADT1* plants can be rescued by concurrent downregulation of *PhPPA-AT*, this would be consistent with redirection of flux from prephenate through an alternative pathway. Indeed, detailed metabolic profiling of *PhADT1xPhPPA-AT* RNAi lines provides evidence in agreement with the involvement of an alternative pathway. To provide further support, we identified a petunia phenylpyruvate aminotransferase gene (designated as PhPPY-AT, see below), downregulation of which leads to reduction of phenylalanine and phenylalanine-derived scent compounds. Extensive biochemical characterization of PhPPY-AT revealed that it preferentially converts phenylpyruvate to phenylalanine, and unexpectedly strongly favors tyrosine as the amino donor. Additionally, feeding experiments with petunia petals showed that the ^{15}N label from supplied ^{15}N-tyrosine is retrieved in phenylalanine, and higher phenylalanine labeling occurs in *PhADT1xPhPPA-AT* RNAi lines than wild-type, consistent with higher flux through the phenylpyruvate pathway when the flux into the arogenate pathway is limiting. Moreover, we have shown that PhPPY-AT is a cytosolic enzyme, and when the tyrosine pool is reduced via overexpression of a cytosolic tyrosine decarboxylase it leads to a decrease in phenylalanine levels. Taken together these results demonstrate for the first time that the microbial-like phenylpyruvate pathway operates in plants, phenylalanine biosynthesis is not limited to plastids, and that there is an interconnection between aromatic amino acid catabolism and biosynthesis *in planta*.

2.3 Results

2.3.1 *PhPPY-AT* suppression in PhADT1 RNAi lines rescues Phe levels

To examine the contribution of the undiscovered phenylpyruvate pathway towards phenylalanine biosynthesis in petunia flowers, *PhADT1* and *PhPPA-AT* RNAi lines were crossed to simultaneously downregulate both steps in the arogenate pathway. Five independent lines (A-E) were generated and found to display comparable degrees of *PhADT1* and *PhPPA-AT* mRNA suppression to those in the parental lines (Figure 2.2a,b). Phenylalanine levels in all five *PhADT1xPhPPA-AT* RNAi lines were rescued, not just to *PhPPA-AT* RNAi levele, but surprisingly to that of wild-type (Figure 2.2c), consistent with the hypothesized redirection of flux through an alternative pathway. One independent line (A) was selected for further biochemical analysis and metabolic profiling of emitted floral volatiles as well as internal pools of intermediates and end products. Similar to expression levels, ADT and PPA-AT activities in the flowers of the *PhADT1xPhPPA-AT* RNAi line (A) resembled the parents, while metabolic profiling revealed that similar to the *PhPPA-AT* RNAi line, prephenate and arogenate accumulated, while tyrosine, tryptophan, and shikimate levels matched the wild type (Figure 2.7). Moreover, like phenylalanine levels, phenylalanine-derived volatiles were rescued to those of wild type (Figures 2.2c and 2.7). Feeding petunia petals from *PhADT1xPhPPA-AT* RNAi flowers with 10 mM $^2H_5$-phenylpyruvate resulted in labelling of the phenylalanine pool by 24% (2.7-fold higher than wild type), further supporting the hypothesized increased flux through an alternative pathway when the arogenate route in limiting.

2.3.2 PhPPY-AT prefers phenylpyruvate and Tyr as substrate

Although most microorganisms utilize the phenylpyruvate route to synthesize phenylalanine[11-13], they rely on multiple functionally redundant aminotransferases with broad substrate specificity to convert phenylpyruvate to phenylalanine[26]. Since aminotransferase reactions are reversible in nature, we therefore used the *Cucumis melo* L., Cucurbitaceae enzyme CmArAT1 (ADC45389.1), which catalyzes the catabolism of phenylalanine to phenylpyruvate for production of melon fruit scent compounds[20], as query for a tBlastn search against our petunia RNA-seq database to identify a candidate phenylpyruvate aminotransferase (PPY-AT). The top hit in the tBLASTn search (E-value < e^{-170}) revealed a contig representing a full-length mRNA encoding a protein, later designated as the petunia phenylpyruvate aminotransferase (PhPPY-AT), of 447 amino acids sharing 66% identity/82% similarity to CmArAT1. To examine if PhPPY-AT is capable of converting phenylpyruvate to phenylalanine we initially assessed its ability to functionally complement the *Escherichia coli* (*E. coli*) phenylalanine auxotrophic mutant DL39[27]. This mutant lacks the three aminotransferases, AspC (aspartate aminotransferase), TyrB (L-Tyrosine aminotransferase), and IlvE (branched-chain aminotransferase), shown to participate in phenylalanine and tyrosine biosynthesis. The PhPPY-AT open reading frame, subcloned in the arabinose-inducible vector pBad33[28] and introduced into the DL39 mutant, restored the ability of the mutant to grow in the absence of exogenously supplied phenylalanine and tyrosine (Figure 2.8a). Moreover, *in vitro* enzyme assays using crude extracts from the DL39 mutant expressing PhPPY-AT in the presence of phenylpyruvate, glutamate as an amino donor and the pyridoxal phosphate cofactor, confirmed that PhPPY-AT transaminates phenylpyruvate to phenylalanine (Figure 2.8b).

For biochemical characterization of the isolated PhPPY-AT, its coding region was expressed in *E. coli* as an inducible fusion protein containing a hexahistidine tag, which was subsequently removed before analysis. Out of the 19 common L-amino acids (except phenylalanine, the product of the reaction) tested as amino donors, tyrosine by far most efficiently supplied the amino group for the conversion of phenylpyruvate to phenylalanine, while PPY-AT activities with glutamate, methionine, and leucine did not exceed 13% of the activity with tyrosine (Table 2.2). Of the five keto acids tested in the presence of tyrosine, only phenylpyruvate and α-ketoglutarate effectively served as substrates, and no activity was detected with prephenate (Table 2.3), the substrate of PhPPA-AT[17]. Similarly, with glutamate as the amino donor, phenylpyruvate was the best substrate and again no activity was detected with prephenate (Table 2.3), indicating that PhPPY-AT does not moonlight in the arogenate pathway. Apparent K_m values of PhPPY-AT for phenylpyruvate were 1.5 and 2.6 mM when tested with tyrosine and glutamate, respectively, as amino donors, while K_m values for tyrosine and glutamate in the presence of phenylpyruvate were 1.9 and 11.1 mM, respectively (Table 2.1). Catalytic efficiencies (k_{cat}/K_m) for phenylpyruvate and tyrosine were comparable (0.965 and 0.769 $\mathrm{mM}^{-1}\mathrm{s}^{-1}$) when used together. However, when tyrosine was substituted by glutamate the catalytic efficiency of PhPPY-AT for phenylpyruvate was reduced by half (0.461 $\mathrm{mM}^{-1}\mathrm{s}^{-1}$), and that for the amino donor (glutamate) was reduced 20-fold (0.039 $\mathrm{mM}^{-1}\mathrm{s}^{-1}$; Table 2.1).

PhPPY-AT also catalyzed the reverse reactions, conversion of phenylalanine to phenylpyruvate using 4-hydroxyphenylpyruvate or α-ketoglutarate as amino acceptors (Table 2.1). The forward and reverse reactions with glutamate and α-ketoglutarate, respectively, occurred with similar catalytic efficiencies (Table 2.1). However, catalytic efficiencies of the reverse reaction using 4-hydroxyphenylpyruvate and phenylalanine as substrates (0.089 and 0.039 $mM^{-1}s^{-1}$, respectively) were 11- and 20-fold lower than that in the forward reaction for phenylpyruvate (0.965 $mM^{-1}s^{-1}$) and tyrosine (0.769 $mM^{-1}s^{-1}$), respectively (Table 2.1). Since the reverse reaction with 4-hydroxyphenylpyruvate leads to tyrosine formation, we checked whether phenylalanine is the best amino donor. Indeed, phenylalanine showed the highest activity with 4-hydroxyphenylpyruvate as amino acceptor, although glutamate, methionine and leucine displayed comparable activities (Table 2.2).

2.3.3 PhPPY-AT is localized in the cytosol

In plants phenylalanine biosynthesis via the arogenate pathway takes place in plastids [10,16,18,29,30]. Surprisingly however, the protein targeting prediction programs (WolfPSort: http://wolfpsort.org/; Predotar: http://urgi.versailles.inra.fr/predotar/predotar.html; TargetP: http://www.cbs.dtu.dk/services/TargetP/) revealed the absence of an N-terminal transit peptide for plastidic localization in the PhPPY-AT protein. To experimentally determine PhPPY-AT subcellular localization, the complete coding region of the gene was fused to either the 5'- and 3'-ends of a green fluorescent protein (GFP) reporter gene. The resulting constructs were transferred to Arabidopsis protoplasts and the corresponding transient GFP expression was analyzed by confocal microscopy (Figure 2.3). Independent of PhPPY-AT position, GFP fluorescence was detected only in the cytosol (Figure 2.3a,b), similar to protoplasts expressing GFP alone (Figure 2.3c), and did not overlap with autofluorescence of chloroplasts or GFP fused to the transit peptide of ribulose-1,5-bis-phosphate carboxylase/oxygenase (Rubisco) small subunit (Figure 2.3d). These results indicate that PhPPY-AT is localized in the cytosol.

2.3.4 PhPPY-AT is involved in Phe biosynthesis *in vivo*

Genes involved in biosynthesis of phenylalanine and phenylalanine-derived volatile compounds in petunia flowers typically display a spatial, temporal, and rhythmic expression profile corresponding with floral volatile emission[16,17,25,31,32]. Thus, *PhPPY-AT* transcript levels were investigated by qRT-PCR with gene-specific primers. Although *PhPPY-AT* expression did not show a specific spatial profile or change over flower development, it did exhibit rhythmicity with maximum around 15:00 h, positively correlating with phenylalanine levels[16] and emission of phenylalanine-derived volatiles[24,25] over a daily light/dark cycle (Figure 2.9).

To further determine whether PhPPY-AT is involved in phenylalanine biosynthesis *in planta*, *PhPPY-AT* expression was transiently downregulated in flowers of wild-type petunia, the *PhADT1xPhPPA-AT* RNAi line, and the *PhADT1* and *PhPPA-AT* RNAi parental lines by infiltrating agrobacteria carrying the *PhPPY-AT* RNAi construct. Approximately 70-75% reduced expression levels of *PhPPY-AT* were achieved in all lines relative to their corresponding controls 2 d post infiltration (Figure 2.4a). Reduced *PhPPY-AT* expression led to a decrease in phenylalanine levels by 13% in wild-type flowers and by 28-33% in the *PhADT1xPhPPA-AT* RNAi (Figure 2.4a) and parental RNAi lines (Figure 2.10). Interestingly, downregulation of *PhPPY-AT* had a greater impact on phenylalanine-derived volatiles in the *PhADT1xPhPPA-AT* RNAi line compared to wild-type and the parental RNAi lines (64% versus 20-40%, respectively; Figures 2.4a and 2.10). Moreover, when *PhPPY-AT* was overexpressed in the wild-type and *PhADT1xPhPPA-AT* RNAi background, the levels of phenylalanine increased by 177% and 37%, respectively, and volatiles by 130% and 73%, respectively (Figure 2.4b). Taken together, these results provide *in vivo* evidence that cytosolic PhPPY-AT is involved in phenylalanine formation.

2.3.5 Tyr catabolism and Phe biosynthesis are interconnected

Previously it has been shown that the transamination of prephenate to arogenate by PhPPA-AT in petunia depends exclusively on aspartate and glutamate as amino donors[17]. In contrast, biochemical characterization of PhPPY-AT has revealed that tyrosine is by far the most efficient amino donor (Table 2.2). To verify if tyrosine participates in the transamination of phenylpyruvate *in vivo*, feeding experiments with ^{15}N-tyrosine were performed with 2-d old wild-type petunia flowers and the ^{15}N incorporation of the labeled amino group in phenylalanine was analyzed. After 6 h of continuous feeding with 10 mM ^{15}N-tyrosine, the tyrosine pool was labeled by more than 87% while the phenylalanine pool was labeled by 5% (Figure 2.5a). All other amino acids remained unlabeled, with the exception of glutamate and aspartate, which were both labeled by less than 1.3% after 6 h. No labeling was retrieved in phenylalanine when ring-labeled $^{2}H_4$-tyrosine was supplied instead, confirming that tyrosine is not converted to phenylalanine via dehydration.

When 10 mM ^{15}N-tyrosine was fed to flowers of the *PhADT1xPhPPA-AT* RNAi line, the phenylalanine pool was labeled approximately 52% higher than that detected in wild-type (Figure 2.5a). Labeling experiments with the *PhADT1 and PhPPA-AT* parental RNAi lines showed 25% lower and 31% higher incorporation of ^{15}N label into phenylalanine than wild-type, respectively (Figure 2.5a).

To investigate whether the cytosolic pool of tyrosine can influence phenylalanine levels *in vivo*, the level of tyrosine was depleted in petunia flowers of *PhADT1xPhPPA-AT* RNAi via transient overexpression of the cytosolic Arabidopsis *tyrosine decarboxylase* (AtTYDC), which exclusively catalyzes decarboxylation of L-tyrosine to tyramine[33,34]. *AtTYDC* overexpression resulted in 50% reduction of the tyrosine pool and a 9-fold increase in tyramine levels with a concomitant 50% decrease in phenylalanine levels (Figure 2.5b).

2.4 Discussion

Recent investigations into aromatic amino acid biosynthesis revealed that in contrast to most microbes, plants predominantly rely on the arogenate pathway to synthesize phenylalanine[15-18]. However, our results now demonstrate that downregulating *PhPPA-AT* in the *PhADT1* RNAi background rescues phenylalanine and phenylalanine-derived volatile levels (Figures 2.2c and 2.7), suggesting the redirection of carbon flux from prephenate via an alternative route and thus reopening *de facto* the search for plant genes participating in the microbial-like phenylpyruvate pathway (Figure 2.1). In this regard, we have identified a petunia aminotransferase, PhPPY-AT, which preferentially converts phenylpyruvate to phenylalanine and is unable to utilize prephenate as substrate (Table 2.3). Downregulation and overexpression of *PhPPY-AT* confirm participation of PhPPY-AT in phenylalanine biosynthesis *in vivo* (Figures 2.4 and 2.10), therefore establishing the existence of a functional alternative phenylpyruvate pathway in plants. Moreover, flux through the phenylpyruvate pathway is higher when the entry point into the arogenate pathway is blocked as it occurs in *PhPPA-AT* and *PhADT1xPhPPA-AT* RNAi lines (Figure 2.5a). It still remains enigmatic why phenylalanine and phenylalanine-derived volatile levels in the *PhADT1xPhPPA-AT* RNAi line were completely restored to those of wild-type and not just to those of the *PhPPA-AT* RNAi line (Figures 2.2c and 2.7), despite identical metabolic profiles (Figure 2.7) and comparable increases in flux through the phenylpyruvate pathway (Figure 2.5a). The decreased flux in the *PhADT1* RNAi line (Figure 2.5a) is likely due to the overall reduction in phenylalanine biosynthesis via the downregulation of the upstream shikimate pathway[16] (Figure 2.7).

To date it is believed that aromatic amino acids are exclusively synthesized in the plastid[10,16,18,29,30], and then transported into the cytosol to serve as building blocks for proteins and precursors of downstream metabolites. In light of the absence of an N-terminal targeting signal and the confirmed cytosolic localization of PhPPY-AT (Figure 2.3), the all-plastidial paradigm of phenylalanine biosynthesis should be shifted to now include a cytosolic component (Figure 2.6). This discovery may also alter the already complex post-transcriptional regulatory model of carbon flux through the shikimate pathway, which involves feedback mechanisms controlled by phenylalanine levels in plastids[10] (Figure 2.6). Furthermore, it can be envisioned that this will influence future metabolic engineering strategies for manipulating production of numerous important plant products.

The demonstration that phenylpyruvate serves as an intermediate in phenylalanine biosynthesis now implicates the existence of a functional PDT converting prephenate to phenylpyruvate in plants (Figure 2.1). To date, PDT activity and phenylpyruvate have rarely been reported in plant tissues[16,35]. However, using triple quadrupole LC-MS we were able to detect PDT activity in petunia plastids and found it to be increased by approximately two-fold in *PhADT1xPhPPA-AT* and parental RNAi lines (Figure 2.11a). Together with increased prephenate levels in the *PhADT1xPhPPA-AT* and *PhPPA-AT* RNAi lines (Figure 2.7), these results suggest that increased PDT activity efficiently redirects carbon flux through the alternative phenylpyruvate route, resulting in elevated phenylalanine levels compared to the *PhADT1 RNAi* line (Figure 2.2c). Although PDT activity also increased in the *PhADT1* RNAi line, it is likely that carbon flux was not redirected through the phenylpyruvate route because prephenate failed to accumulate and flux through the shikimate pathway was reduced[16] (Figure 2.7). It remains to be investigated if there is a dedicated PDT with strict specificity for prephenate catalyzing this reaction, or if plants rely on one or more of the known ADTs that can use prephenate as substrate at low catalytic efficiencies[15,16,36]. In petunia, PhADT2 and PhADT3, but not PhADT1, are capable of utilizing prephenate[16]. However, their expression levels did not correlate with increased PDT activity in the arogenate pathway knockdown lines (Figure 2.11b), indicating either the participation of an unknown enzyme(s) or post-transcriptional upregulation of the aforementioned ADTs. Projecting forward, it is additionally necessary to understand how phenylpyruvate is transported out of the plastid to serve as substrate for the cytosolic aminotransferase (Figure 2.6).

PhPPY-AT belongs to the class of tyrosine aminotransferases (EC 2.6.1.5) that are defined to catalyze the reversible conversion of tyrosine + 2-oxoglutarate to 4-hydroxyphenylpyruvate + glutamate. Although tyrosine is the preferred amino donor for PhPPY-AT (Table 2.2), the unique property of this plant enzyme is that instead of 2-oxoglutarate serving as the primary keto acid acceptor, it preferentially uses phenylpyruvate (Table 2.3), thus suggesting an interconnection of the catabolism of tyrosine with the production of phenylalanine in the cytosol (Figure 2.6). The greater catalytic efficiency of the forward reaction (tyrosine + phenylpyruvate → 4-hydroxyphenylpyruvate + phenylalanine) over the reverse (Table 2.1), as well as the impacts observed on the phenylalanine pool when PhPPY-AT expression is altered (Figure 2.4), further support such a relationship occurring *in planta*. The reduction in phenylalanine levels when the cytosolic tyrosine pool was depleted (Figure 2.5b), together with the labeling retrieved in the amino group of phenylalanine from ^{15}N-tyrosine (Figure 2.5a), provide direct *in vivo* evidence for the interconnection between these aromatic amino acids (Figure 2.6).

It is foreseeable that PPY-ATs directly interconnecting tyrosine and phenylalanine metabolism are not limited to petunia. Further examination of the melon aromatic amino acid aminotransferase, CmArAT1[20], revealed that similar to PhPPY-AT, it also converts phenylpyruvate to phenylalanine (Table 2.4) using tyrosine as the preferred amino donor (Table 2.5). In addition, similar to petunia flowers (Figure 2.5a), the phenylalanine pool in 5-week old Arabidopsis inflorescence shoots was labeled by 4.16 ± 0.23% after feeding 10 mM ^{15}N-tyrosine for 6 h. Moreover, a recent metabolic engineering study overexpressing *PheA*, a bacterial bifunctional *chorismate mutase/PDT,* in Arabidopsis plastids resulted in increased levels of phenylalanine and the tyrosine-derived metabolites homogentisate, tocopherols, and tocotrienols[19]. Interestingly, homogentisate serves as the aromatic head group of the tocopherols and tocotrienols, and is synthesized in the cytosol from 4-hydroxylphenylpyruvate via tyrosine[5] (Figure 2.6). Although at the time the basis for the enhanced pools of tyrosine-derived metabolites in transgenic *PheA* Arabidopsis plants was unexplained[19], in light of the current study, it is logical to suspect that increased flux from phenylpyruvate to phenylalanine drove that of tyrosine to 4-hydroxyphenylpyruvate via an aminotransferase orthologous to PhPPY-AT. Indeed, a Blastp search against Arabidopsis using PhPPY-AT as query retrieves as the best hit At5g53970, a recently characterized tyrosine aminotransferase demonstrated to be involved in tocopherol biosynthesis[23].

The discovery that the microbial-like phenylpyruvate pathway does in fact operate in plants raises many questions about the control of carbon flux towards phenylalanine and its downstream metabolites. One particularly crucial aspect that now must be taken into consideration is the role of compartmentalization and transport of intermediates in regulating flux through the phenylalanine biosynthetic pathways. It would also be interesting to explore the possibility of an analogous alternative pathway occurring for tyrosine biosynthesis from 4-hydroxyphenylpyruvate that *a priori* would be mediated by another aminotransferase (Figure 2.6) Finally, it should be emphasized that further studies are necessary to elucidate the functional relationship between the parallel pathways of phenylalanine biosynthesis, as well as that with tyrosine catabolism.

2.5 Materials and Methods

2.5.1 Plant materials and metabolic analysis

Petunia hybrida cv. Mitchell wild-type (Ball Seed Co., West Chicago, IL) and transgenic *PhADT1* RNAi, *PhPPA-AT* RNAi and crossed *PhADT1xPhPPA-AT* RNAi plants were grown under standard greenhouse conditions[37] with a light period from 6:00 h to 21:00 h. Crossed lines were screened for the presence of transgenes by PCR on genomic DNA using gene-specific primers: forward 5'-ATTTCGAACAAGCGTACACC-3' and reverse 5'-AATTGTGAGCGCCTTAGGTA-3' for *PhADT1*; forward 5'-GCTAAGCTGGAGTGCACATT-3' and reverse 5'-ACCTGGTATGACCTTCACGA-3' for *PhPPA-AT*. Scent collection and targeted metabolic profiling of petunia petals were performed as described previously[16], with exception of scent collection time, which was from 18:00 h to 22:00 h.

2.5.2 Gene expression analysis using qRT-PCR

For RNA isolation, petals from at least eight petunia flowers were harvested at 20:00 h, 2 days post-anthesis and immediately frozen in liquid nitrogen. Total RNA was isolated using a RNeasy plant mini kit (Qiagen, Valencia, CA, USA) and treated with DNase I to eliminate genomic DNA (Promega, Madison, WI, USA). One microgram of RNA was subsequently reverse transcribed to cDNA in a total volume of 100 μl using the High Capacity cDNA reverse transcription kit (Applied Biosystems, Foster City, CA, USA). qRT-PCR analysis relative to the reference gene *UBQ10* (ubiquitin 10) for *PhADT1*, *PhADT2*, *PhADT3*, *PhCM1* and *PhPPA-AT* were performed using gene-specific primer pairs (Table 2.6)[16,17]. Forward 5'-GCTTCTCACAAGTTCAATGGTTATGCT-3' and reverse 5'-CCAGAAAGGCAATTGCAGATTATTT-3' primers for *PhPPY-AT* were designed using PrimerExpress (Applied Biosystems, Foster City, CA, USA) and exhibited 93% efficiency at a final concentration of 500 nM. For absolute quantification of AtTYDC transcript levels, pCR4-TOPO vector carrying *AtTYDC* was digested with *BamHI* and *EcoRV*, and the resulting fragment was purified from agarose gel with a Qiaquick gel extraction kit (Qiagen, Valencia, CA, USA). Concentrations of purified DNA fragment was determined with the NanoDrop 100 spectrophotometer (Thermo Scientific, West Palm Beach, FL, USA). Several dilutions were prepared from 4 ng ml^{-1} to 6.4 pg ml^{-1} and used to obtain standard curves in qRT-PCR with gene-specific primers (Table 2.6). Individual qRT-PCR reactions contained 5 µl of the SYBR Green PCR master mix (Applied Biosystems, Foster City, CA, USA), 3 µl of 50-fold diluted cDNA, and 1 µl of 5 µM forward and reverse primers. Two-step qRT-PCR amplification (40 cycles of 95°C for 3 s followed by 60°C for 30 s) was performed using the StepOnePlus real-time PCR system (Applied Biosystems, Foster City, CA, USA). Each data point represents an average of three to five independent biological samples with three technical replicates for each sample.

2.5.3 Expression and purification of recombinant proteins

For functional expression, the coding region of *PhPPY-AT* was amplified with forward 5'-CGCGCGGCAGCCATATGATGGAGACGAATGTGGTGAAAGTGA-3' and reverse 5'-GTCATGCTAGCCATATGTCAACAGTGACCATTTTGTTGATATGAATG-3' primers designed using the In-Fusion® online tool (http://bioinfo.clontech.com/infusion). The amplified gene product was cloned into the *NdeI* site of pET28a containing an N-terminal (6xHis)-tag (Novagen, Madison, WI, USA) using In-Fusion® cloning (Clonetech, Mountain View, CA, USA). For functional expression of *CmArAT1*, its coding region was obtained by PCR using forward 5'-AACATATGCATCATCATCATCATCACGAGATTGGAGCTGTGAAC-3' and reverse 5'-GGATCCTTACAACATTAGTGTATGC-3' primers with the pBK-CMV-*CmArAT1*[20] as a template. The amplified gene product was cloned into a pET21a expression vector (Novagen, Madison, WI, USA) at the *NdeI* site with an N-terminal (6xHis)-tag. After sequence verification, recombinant PhPPY-AT and CmArAT1 were expressed in *E. coli* and purified on Ni-NTA resin

(Qiagen, Valencia, CA, USA). Expression in *E.coli* Rosetta^{TM} cells, induction, harvesting and crude extract preparation were performed as described previously[38] with the exception of lysis buffer, which contained 50 mM Tris-HCl (pH 7.5), 10 μM PLP, 5 mM β-mercaptoethanol, 300 mM NaCl, and 10% glycerol. Fractions with the highest PPY-AT activity were desalted on the Sephadex G-50 Fine column (GE Healthcare Bio-Sciences AB, Uppsala, Sweden) into the buffer containing 20 mM Tris-HCl, pH 8.0, 1 mM EDTA, and 10% glycerol and PLP was then added to 100μM. 6xHis tag from purified protein was removed by thrombin (Sigma-Aldrich, St. Louis, MO, USA) before biochemical and kinetic characterization of enzyme.

2.5.4 Functional complementation of the *E. coli* mutant DL39

For functional complementation, the coding region of *PhPPY-AT* was obtained by PCR using forward 5'-CCGGGGATCCTCTAGAATGGAGACGAATGTGGTGAAAGTGA-3' and reverse 5'-GCAGGTCGACTCTAGATCAACAGTGACCATTTTGTTGATATGAATG-3' primers designed with the In-Fusion online tool. The amplified *PhPPY-AT* coding sequence was cloned into *XbaI* site of pBad33[28] under control of an arabinose-inducible promoter using In-Fusion® cloning and introduced into the DL39 mutant (*LAM-, aspC13, fnr-25, rph-1, ilvE12, tyrB507*; Coli Genetic Stock Center, Yale University, New Haven, CT, USA)[27], which is auxotrophic for phenylalanine, tyrosine, aspartic acid, valine, leucine and isoleucine. Functional complementation was performed essentially as described[21]. Starter cultures of wild-type *E. coli* K-12 and DL39 cells harboring either empty pBad33 or the pBad33-*PhPPYAT* construct were grown in liquid M9 minimal medium containing 0.2% arabinose and 50 μg ml^{-1} phenylalanine, tyrosine, aspartic acid, valine, leucine and isoleucine. Chloramphenicol (25 μg mL^{-1}) was also added to DL39 cells for plasmid selection. After 36 h of growth at 37°C, cells were washed two times with M9 medium without antibiotics or amino acids, and resuspended to an OD_{600} of 0.1, which was further used to create cell dilutions with an OD_{600} of 1 x 10^{-2}, 10^{-3}, and 10^{-4}. Next, 5 μl of cells at each cell density were plated on M9 plates containing 0.2% arabinose and 50 μg ml^{-1} aspartic acid, valine, leucine and isoleucine, with and without 50 μg ml^{-1} phenylalanine and tyrosine. After 24 h at 37°C, a positive functional complementation was assessed by looking for the restored ability of the DL39 mutant to grow in the absence of phenylalanine and tyrosine.

2.5.5 Enzyme assays

Recombinant PhPPY-AT activity was analyzed in the reaction mixture (50 µL) containing 50 mM HEPES pH 10, 10 mM amino donor, 10 mM keto acid substrate and 200 µM PLP, which were preincubated at 30˚C for 5 min. The reaction was initiated by adding 5.6 µg of protein and incubated at 30˚C for 15 min. When Tyr was used as amino donor, 1.12 µg of protein was used and reactions were incubated for 3 min. For reverse reactions, 13.5 µg or 2.8 µg of enzymes were used for 4-hydroxyphenylpyruvate and α-ketoglutarate substrates, respectively. After termination of reaction with 50 µL of 1N HCl and centrifugation, 20 µL of the final reaction mixture was derivatized with o-phthalaldehyde and analyzed by HPLC (Agilent 1200 HPLC system, Palo Alto, CA, USA) as described[17].

Plastidic PDT activity was analyzed in the reaction mixtures (50 µL) containing 50 mM Na-phosphate (pH 8.0) and 3 mM prephenate, which were preincubated at 37˚C for 5 min. The reaction was initiated by adding 100 µg of plastidic protein and incubated at 37˚C for 60 min. The reaction was terminated by 50 µL of 100% MeOH. After protein precipitation, 10 µL of the final mixture was subjected to Triple Quadrupole LC/MS (Agilent 6460, Palo Alto, CA, USA). Chromatographic separation was performed using an Agilent 1200 LC system (Palo Alto, CA, USA) equipped with Atlantis dC18 column (3 µm, 150 x 2.1 mm; Waters, Milford, MA, USA) with a 20 min linear gradient of 0 to 95% acetonitrile in 1% formic acid. Phenylpyruvate was monitored in MRM (Multiple Reaction Monitoring) mode and quantified based on a standard calibration curve generated with an authentic phenylpyruvate standard. The d_0-phenylpyruvate data were acquired by monitoring the following transitions: 163.1→116.9 with a collision energy of 25 V, 163.1→100.9 with a collision energy of 25 V, and 163.1→91 with a collision energy of 5V. The d_1-prephenate data were acquired by monitoring the following transitions: 225→121 with a collision energy of 20 V, 225→109.1 with a collision energy of 10 V, and 225→91.1 with a collision energy of 5V. The dwell time for all data acquired was 50 ms and fragmentor voltage was 70V. The jet stream ESI interface had a gas temperature of 325°C, gas flow rate of 8 L/minute, nebulizer pressure of 35 psi, sheath gas temperature of 250°C, sheath gas flow rate of 7 L/minute, capillary voltage of 3000 V, and nozzle voltage of 500 V.

All enzyme assays were performed at an appropriate enzyme concentration so that reaction velocity was linear and proportional to enzyme concentration during the incubation time period.

Kinetic data were evaluated by hyperbolic regression analysis (HYPER.EXE, Version 1.00, 1992). At least triplicate assays were performed for all data points.

2.5.6 Subcellular localization of PPY-AT

Plasmid p326-sGFP containing the cauliflower mosaic virus 35S promoter was used for the generation of GFP fusion constructs. For the C-terminal GFP fusion (PhPPY-AT-GFP), the open reading frame of PhPPY-AT was amplified using forward primer 5’-GTCTAGAATGGAGACGAATGTGGTGAAAGTGA-3’, which introduced an *XbaI* site (underlined) upstream of ATG codon, and reverse primer 5’-CGGATCCACAGTGTGACCATTTTGTTGATATGAA-3’ containing a *BamHI* site (underlined). For the N-terminal GFP fusion (GFP-PhPPY-AT), the PhPPY-AT open reading frame was amplified by PCR using forward primer 5’-CTGTACAAGATGGAGACGAATGTGGTGAAAGTGA-3’, which introduced a *BsrGI* site (underlined) at the initiating ATG codon, in combination with reverse primer 5’-GGCGGCCGCTCAACAGTGACCATTTTGTTGATAT-3’, introducing a *NotI* site (underlined) after the stop codon. The PCR fragments were subcloned into the pGEM-T vector (Invitrogen, Carlsbad, CA, USA) and checked by sequencing for absence of errors during PCR amplifications. The *XbaI-BamH*I and *BsrGI-NotI* fragments were subcloned into the p326-sGFP vector in frame with GFP. Arabidopsis protoplasts were prepared and transformed as described previously[40]. The plasmids p326-sGFP and p326-RbTP-sGFP containing a plastidial Rubisco target peptide, were used as markers for cytosolic and plastidial localization, respectively. Transient expression of GFP fusion proteins was observed 16 to 20 hours after transformation, and images were acquired using Zeiss LSM710 laser spectral scanning confocal microscope with a C-Apochromat 40x/1.20 W objective (Zeiss, Thornwood, NY, USA). GFP was excited with an Argon laser at wavelength 488 nm and emissions were collected over a 493-598 nm bandpass. Chlorophyll fluorescence was excited by a HeNe laser at wavelength 633 nm and emissions were collected over a 647-721 nm bandpass.

2.5.7 *PhPPY-AT* downregulation and overexpression *in planta*

For the *PhPPY-AT* RNAi construct a synthetic DNA, containing two spliced *PhPPY-AT* cDNA fragments of the coding region corresponding to nucleotides 363 to 891 and 363 to 687, the latter in antisence orientation to form a hairpin structure, was synthesized (Genscript, Piscataway, NJ, USA). *EcoRI* and *BamHI* sites were introduced at the 5' and 3' ends during DNA synthesis and the resulting synthetic DNA fragment was subcloned into the *EcoRI*/*BamHI* site of pRNA69 vector containing *LIS* promoter[37]. Next, the part of constructed plasmid containing the *LIS* promoter and the two PPY-AT fragments in opposite orientation separated by the intron was cut out using *SacI*/*NotI* and subcloned into the pART27 simpler binary vector[41]. Transient *PhPPY-AT* downregulation was achieved using vacuum infiltration of 1-d old petunia flowers with *Agrobacterium tumefaciens* strain GV3101 containing pART27-LIS-PPY-AT RNAi and pART27-LIS vector (control) at OD_{600} of 0.4 as described previously. Forty eight hours after infiltration, scent was collected for 4 hours from 18:00 h to 22:00 h and analyzed by GC-MS[16]. For *PhPPY-AT* overexpression, the open reading frame of PhPPY-AT was amplified by PCR using forward 5'-CACCATGGAGACGAATGTGGTGAAAGTGA-3' and reverse 5'-TCAACAGTGACCATTTTGTTGATATGAATG-3' primers. The PCR fragment was subcloned into the pENTR/D-TOPO vector (Invitrogen, Carlsbad, CA, USA) and verified by sequencing for absence of errors during PCR amplifications. The Gataway cloning strategy was employed to subclone the *PhPPYAT* fragment into the destination vector pB2GW7 (Invitrogen, Carlsbad, CA, USA). Transient *PhPPY-AT* overexpression was performed as described previously[42].

2.5.8 *AtTYDC* overexpression in petunia flowers

The Arabidopsis *TYDC* coding region was PCR-amplified using forward primer 5'-CCATGGATGGAATTTGGTACCGGCAACG-3' and reverse primer 5'-TCCAAATTTACACGCAACGACCATTATTAACTGCAG-3' and subcloned into the pGEMT easy vector (Invitrogen, Carlsbad, CA, USA). After sequence verification, the fragment was subcloned into the *NcoI*/*PstI* site of the pEF1-LIS binary vector[43] and transient *AtTYDC* overexpression was performed as described above.

2.5.9 Labelling experiments

Feeding experiments were performed as described previously[25]. Corollas from 2 day old wild-type and transgenic petunia flowers were fed with 10 mM ^{15}N-Tyr or L-[ring-$^{2}H_{4}$]-Tyr (Cambridge Isotope Laboratories, Andover, MA, USA). Tissues were collected 2, 4 and 6 h after feeding starting at 18:00 h, followed by complete amino acid analysis as described previously[16]. The percentage of amino acid labeling was determined as the sum of the intensities of the shifted molecular ions divided by the sum of intensities for unshifted and shifted molecular ions, after correcting for natural isotope abundance.

2.6 Tables and Figures

Table 2.1 Kinetic parameters of petunia PhPPY-AT

Reactions : Phenylpyruvate + Tyrosine ↔ Phenylalanine + 4-hydroxyphenylpyruvate
Phenylpyruvate + Glutamate ↔ Phenylalanine + α-ketoglutarate

Substrate	**Co-substrate**	**K_m (mM)**	**V_{max} (nmol s^{-1} mg protein^{-1})**	**k_{cat} (s^{-1})**	**k_{cat}/K_m (mM^{-1}s^{-1})**
Forward					
phenylpyruvate	tyrosine[a]	1.5 ± 0.1	29.7 ± 0.5	1.46 ± 0.02	0.965 ± 0.014
phenylpyruvate	glutamate[b]	2.6 ± 0.6	24.2 ± 4.2	1.19 ± 0.19	0.461 ± 0.036
tyrosine	phenylpyruvate[a]	1.9 ± 0.1	30.2 ± 0.7	1.48 ± 0.04	0.769 ± 0.036
glutamate	phenylpyruvate[a]	11.1 ± 0.5	8.9 ± 0.3	0.44 ± 0.01	0.039 ± 0.003
Reverse					
4-hydroxy-phenylpyruvate	phenylalanine[c]	7.9 ± 0.5	14.2 ± 0.6	0.70 ± 0.03	0.089 ± 0.005
α-ketoglutarate	phenylalanine[d]	1.8 ± 0.7	18.8 ± 3.6	0.92 ± 0.17	0.508 ± 0.076
phenylalanine	4-hydroxy-phenylpyruvate[e]	4.3 ± 0.8	3.4 ± 0.3	0.17 ± 0.02	0.039 ± 0.005
phenylalanine	α-ketoglutarate[a]	13.8 ± 2.2	11.7 ± 0.8	0.57 ± 0.03	0.042 ± 0.007

[a] The concentration of co-substrates was 10 mM
[b] The concentration of co-substrate was 100 mM
[c] The concentration of co-substrate was 20 mM.
Kinetic parameters were estimated after truncation of data points where substrate inhibition was observed.
[d] The concentration of co-substrate was 60 mM
[e] The concentration of co-substrates was 4 mM which is highest co-substrate concentrations before inhibition was observed.
Data are means ± s.e.m. (*n* = 3 independent experiments).

Table 2.2 Amino donor specificities of petunia PhPPY-AT for forward and reverse reactions.

keto acid substrate	amino donor[c]	PhPPY-AT
Forward		
phenylpyruvate[a]	tyrosine	100[d]
	methionine	12.4 ± 0.45
	glutamate	12.3 ± 0.21
	leucine	10.6 ± 0.45
	tryptophan	6.6 ± 0.32
	histidine	3.0 ± 0.22
	glutamine	0.8 ± 0.04
	aspartate	0.2 ± 0.02
Reverse		
4-hydroxyphenylpyruvate[b]	phenylalanine	5.8 ± 0.19
	glutamate	5.2 ± 0.29
	methionine	5.0 ± 0.23
	leucine	4.6 ± 0.16
	tryptophan	2.7 ± 0.04
	histidine	1.4 ± 0.04
	glutamine	0.3 ± 0.05
	aspartate	0.1 ± 0.06

[a] Phenylpyruvate concentration was 10 mM.

[b] 4-hydroxyphenylpyruvate concentration was 4 mM since at higher concentrations inhibition was observed

[c] Amino donor substrate concentration was 10 mM.

[d] PhPPY-AT activity with phenylpyruvate and tyrosine as substrates was 23.6 nkat mg protein^{-1} and set as 100%.

Data are means ± s.e.m. (*n* = 3 independent experiments).

Table 2.3 Keto acid substrate specificities of petunia PhPPY-AT.

keto acid substrate[a]	**amino donor**[b]	**PhPPY-AT**
Phenylpyruvate	L-tyrosine	100[c]
α-ketoglutarate		44.0 ± 1.04
Oxaloacetate		2.1 ± 0.13
Prephenate		n.d.
Pyruvate		n.d.
Phenylpyruvate	L-glutamate	12.2 ± 0.96
Pyruvate		4.2 ± 0.23
Oxaloacetate		2.8 ± 0.40
4-hydroxyphenylpyruvate		2.5 ± 0.08
Prephenate		n.d.

[a] Keto acid and amino donor[b] substrate concentrations were 10 mM.
[c] PhPPY-AT activity with phenylpyruvate and tyrosine as substrates was 23.6 nkat mg protein^{-1} and set as 100%.
Data are means ± s.e.m. (*n* = 3 independent experiments).
n.d., not detectable

Table 2.4 Catalytic activity of CmArAT1

Reactions : Phenylpyruvate + Tyrosine ↔ Phenylalanine + 4-hydroxyphenylpyruvate

Phenylpyruvate + Glutamate ↔ Phenylalanine + α-ketoglutarate

keto acid substrate[a]	**amino donor**[b]	***Vmax*** **(nmol s^{-1} mg $protein^{-1}$)**
Forward		
Phenylpyruvate	tyrosine[a]	54.59 ± 1.94
Phenylpyruvate	glutamate[a]	1.47 ± 0.02
Reverse		
4-hydroxyphenylpyruvate	phenylalanine[b]	12.35 ± 0.39
a-ketoglutarate	phenylalanine[b]	8.19 ± 0.08

Enzymatic reactions were carried out at 30°C for 10 min in the presence of 5 µg of recombinant CmArAT1. When tyrosine was used as an amino donor, 0.3 µg of CmArAT1 was used and reactions were carried out at 30°C for 3 min.

[a]Keto acid and amino donor[b] substrate concentrations were 10 mM.

Data are means ± s.e.m. (*n* = 3 independent experiments).

Table 2.5 Amino donor specificity of CmArAT1 with phenylpyruvate as the amino acceptor.

keto acid substrate	**amino donor**[b]	**CmArAT1**
phenylpyruvate[a]	tyrosine	100.0[c]
	glutamate	2.7± 0.04
	methionine	2.6 ± 0.07
	leucine	3.8 ± 0.43
	tryptophan	3.5 ± 0.38
	histidine	0.96 ± 0.09
	glutamine	0.15 ± 0.008
	aspartate	n.d.

Enzymatic reactions were carried out at 30°C for 10 min in the presence of 5 µg of recombinant CmArAT1. When tyrosine was used as an amino donor, 0.3 µg of CmArAT1 was used and reactions were carried out at 30°C for 3 min.

[a] Phenylpyruvate and amino donor[b] substrate concentrations were 10 mM.

[c] CmArAT1 activity with phenylpyruvate and tyrosine as substrates was 54.6 nkat mg protein^{-1} and set as 100%.

Data are means ± s.e.m. (*n* = 3 independent experiments).

n.d., not detectable

Table 2.6 Sequence information of primers used for qRT-PCR analysis

Primers	**Sequence**
PhADT1 for[16]	5’-TAACTGCGAAGCCATTCCCTGC-3’
PhADT1 rev[16]	5’- CTCTACTGGTAGAACTGCGCG-3’
PhADT2 for[16]	5’-ACGAAGTTGGGTTTGGTCAG-3’
PhADT2 rev[16]	5’- TGCCCCTGCATCTTTTAGTT-3’
PhADT3 for[16]	5’-CAAAATGTGAAGCTATTCCTTGTG-3’
PhADT3 rev[16]	5’-TTCGATCGGTAAAACAGCACG-3’
PhCM1 for[16]	5’-CCTGCTGTTGAAGAGGCTATCA-3’
PhCM1 rev[16]	5’-CAGGGTCACCTCCATTTTCTG-3
PhPPA-AT for[17]	5'-GCAATGACTGGTTGGAGACTTG-3'
PhPPA-AT rev[17]	5'-TCACATCAGGTGCCAGTAGCA-3'
PhUBQ for[16]	5’-GTTAGATTGTCTGCTGTCGATGGT-3’
PhUBQ rev[16]	5’-AGGAGCCAATTAAAGCACTTATCAA-3’
AtTYDC for[34]	5’-GATCCAAGTTTTGAGGTTGTCACTA-3’
AtTYDC rev[34]	5’-ACGGTTACGTTCGTTACATTGG-3’

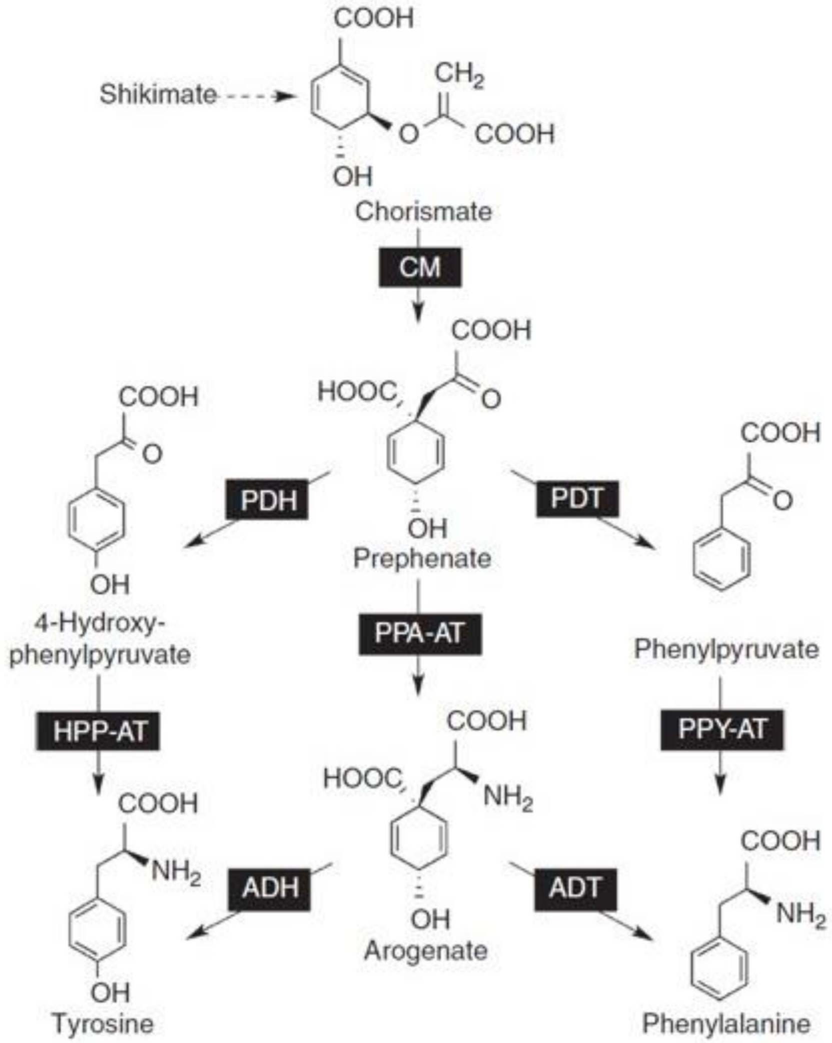
Shikimate
COOH
CH2
O
COOH
OH
Chorismate
CM
COOH
HOOC
O
OH
Prephenate
PDH
PDT
COOH
O
OH
4-Hydroxy-
phenylpyruvate
COOH
O
Phenylpyruvate
PPA-AT
HPP-AT
PPY-AT
COOH
HOOC
NH2
OH
Arogenate
COOH
NH2
OH
Tyrosine
ADH
ADT
COOH
NH2
Phenylalanine

Figure 2.1 Proposed phenylalanine and tyrosine biosynthetic pathways in plants

ADH, arogenate dehydrogenase; ADT, arogenate dehydratase; CM, chorismate mutase; HPP-AT, 4-hydroxyphenylpyruvate amino-transferase; PDH, prephenate dehydrogenase; PDT, prephenate dehydratase; PPA-AT, prephenate aminotransferase; PPY-AT, phenylpyruvate aminotransferase.

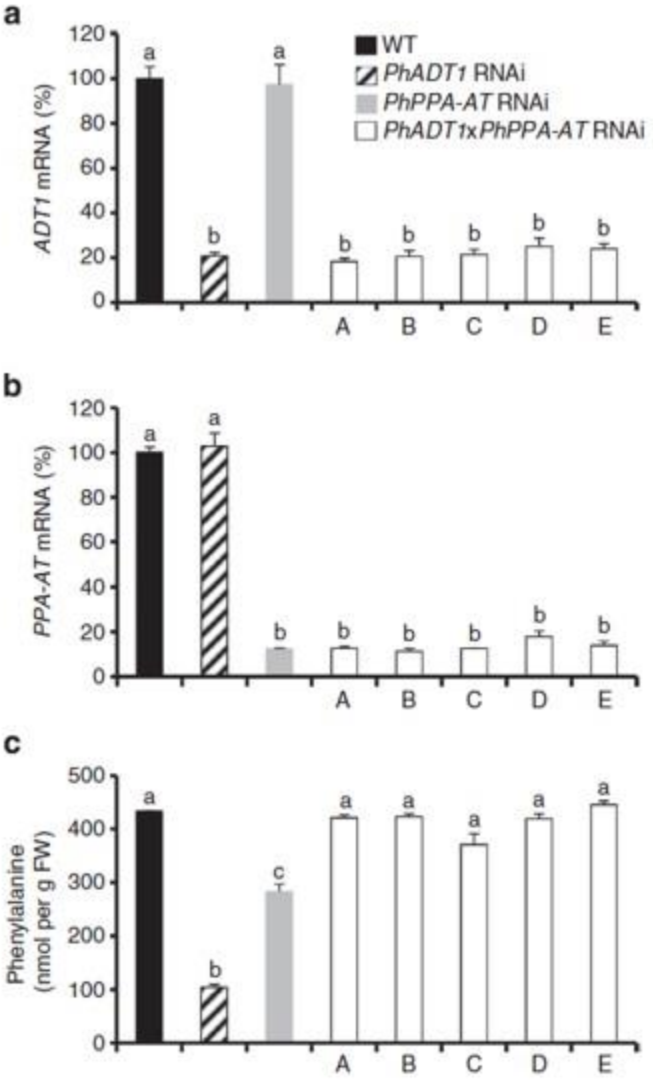

Figure 2.2 Effect of downregulating *PhPPA-AT* in the *PhADT1* RNAi line on phenylalanine levels in petunia flowers

The levels of *PhADT1* mRNA (a) and PhPPA-AT mRNA (b) were determined by qRT-PCR, and phenylalanine pools (c) were determined by LC-MS in petals of wild-type (WT; black), the *PhADT1* RNAi line (striped), the *PhPPA-AT* RNAi line (gray), and the *PhADT1*x*PhPPA-AT* RNAi line (white) petunia flowers harvested at 20:00 h, 2 days post-anthesis. Data are means ± s.e.m. (*n* = 5 biological replicates), Columns with the same letters above are not significantly different based on Tukey's test ($P < 0.05$; One-way ANOVA).

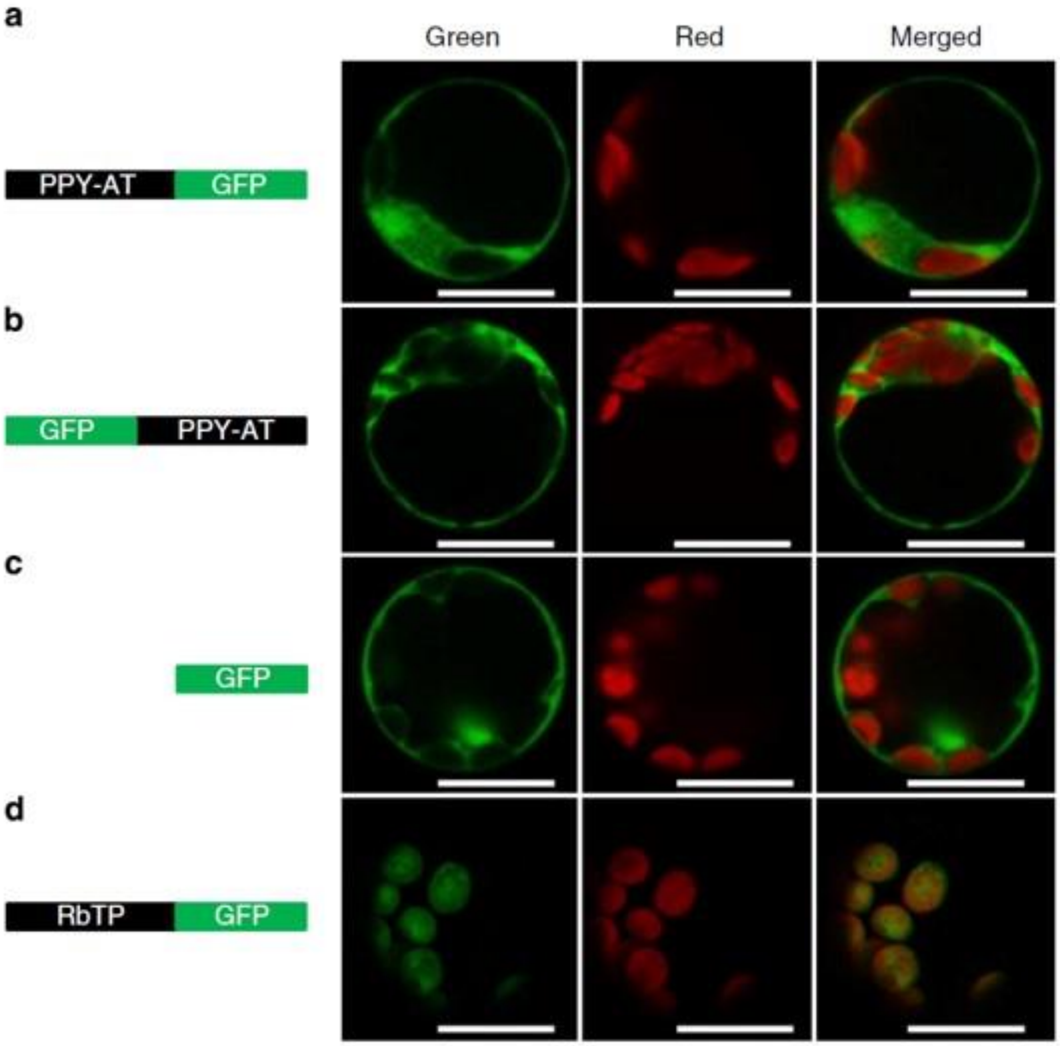

Figure 2.3 Petunia PPY-AT is localized to the cytosol

Schematic diagrams of GFP-fusion constructs are shown on the left with corresponding transient expression in Arabidopsis protoplasts on the right. GFP fluorescence and chloroplast autofluorescence are shown in the green and red panels, respectively. The merged panel shows the overlay of the green and red fluorescence images. GFP alone and RbTP (Rubisco transit peptide)-GFP were used as cytosolic and plastidic markers, respectively. Scale bars, 50µm.

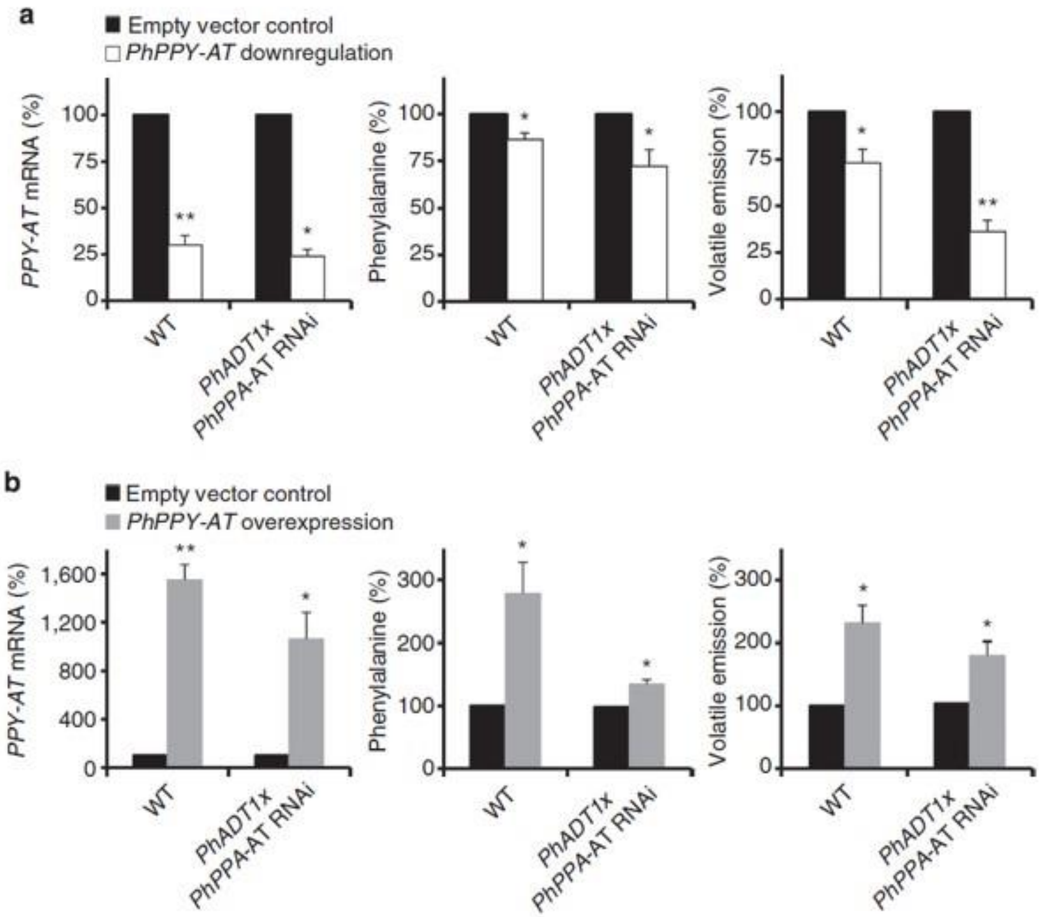

Figure 2.4 Effect of *PhPPY-AT* downregulation and overexpression on phenylalanine and phenylalanine-derived volatile levels in wild-type and *PhADT1*x*PhPPA-AT* RNAi petunia flowers

(**a**) Downregulation of *PhPPY-AT* in petunia flowers (left panel) significantly decreases the levels of phenylalanine (middle panel) and phenylalanine-derived volatiles (right panels). For each genetic background, black and white columns represent flowers infiltrated with the empty vector or the *PhPPY-AT* RNAi construct, respectively. (**b**) Overexpression of *PhPPY-AT* in petunia flowers (left panel) significantly increases the levels of phenylalanine (middle panel) and phenylalanine-derived volatiles (right panel). For each genetic background, black and gray columns represent flowers infiltrated with the empty vector or the *PhPPY-AT* overexpression construct, respectively. For **a** and **b**, data are presented as a percentage relative to the corresponding empty-vector reference. Data are means ± s.e.m. ($n \geq 3$ biological replicates). * $P < 0.05$ and ** $P < 0.01$ as determined by paired two-tailed Student's t-tests.

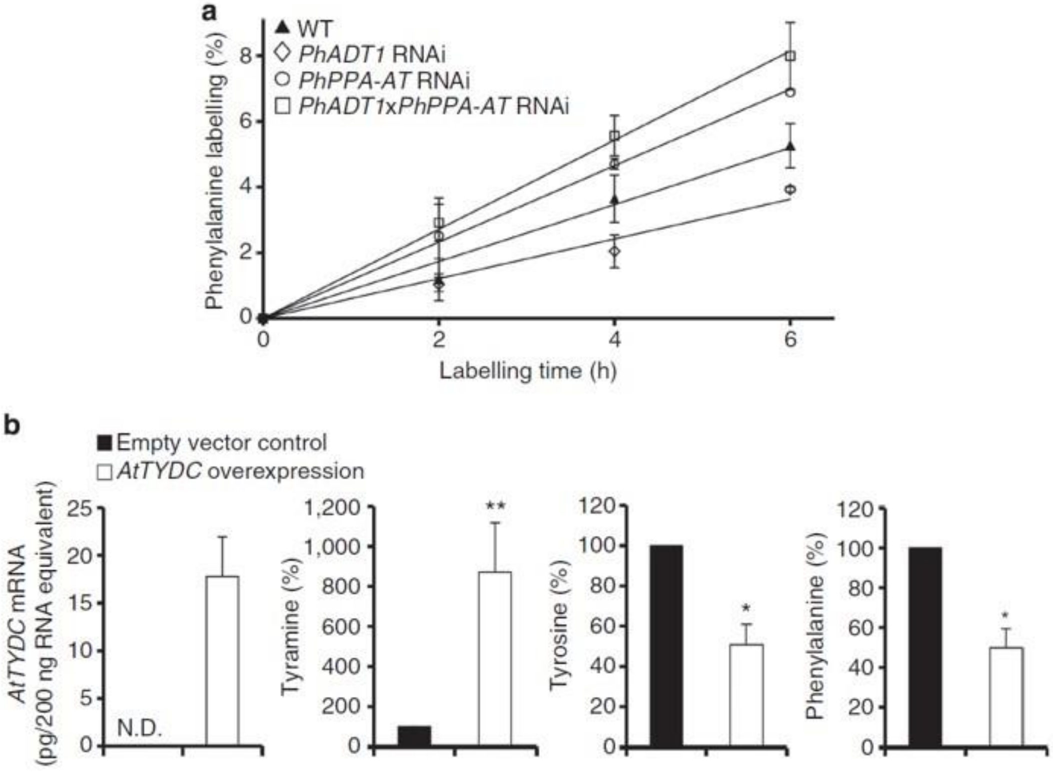

Figure 2.5 *In planta* evidence for the interconnection between tyrosine catabolism and phenylalanine biosynthesis

(a) ^{15}N-tyrosine labels phenylalanine in petunia flowers. 10 mM ^{15}N-tyrosine was fed to 2-d old petunia flowers of WT (solid triangle), and the *PhADT1* (open diamond), *PhPPA-AT* (open circle), and *PhADT1*x*PhPPA-AT* (open square) RNAi lines for 2, 4, and 6 h beginning at 6 PM. Labeling of phenylalanine pools were analyzed by LC-MS TOF. Data are means ± s.e.m. ($n \geq 3$ biological replicates except for the *PhPPA-AT* 6-h time point, $n = 1$). Incorporation of ^{15}N label in phenylalanine was linear over the 6-h time course ($R^2 = 0.9802$, 0.9693, 0.9982, and 0.9977 for WT and the *PhADT1*, *PhPPA-AT*, and *PhADT1*x*PhPPA-AT* RNAi lines, respectively). **(b)** Overexpression of Arabidopsis *Tyrosine decarboxylase (AtTYDC)* decreases phenylalanine levels in *PhADT1*x*PhPPA-AT* RNAi petunia flowers. Levels of *AtTYDC* mRNA, tyramine, tyrosine, and phenylalnine in petunia flowers of the *PhADT1*x*PhPPA-AT* RNAi line infiltrated with agrobacterium carrying the *AtTYDC* construct (white bars) relative to an empty-vector control (black bars). Absolute transcript levels of *AtTYDC* are shown as pg per 200 ng total RNA. Tyramine, tyrosine and phenylalanine levels are presented as a percentage relative to the corresponding empty-vector reference. Data are means ± s.e.m. ($n = 3$ biological replicates). * $P < 0.05$ and ** $P < 0.01$ as determined by paired two-tailed Student's t-tests. n.d., not detectable

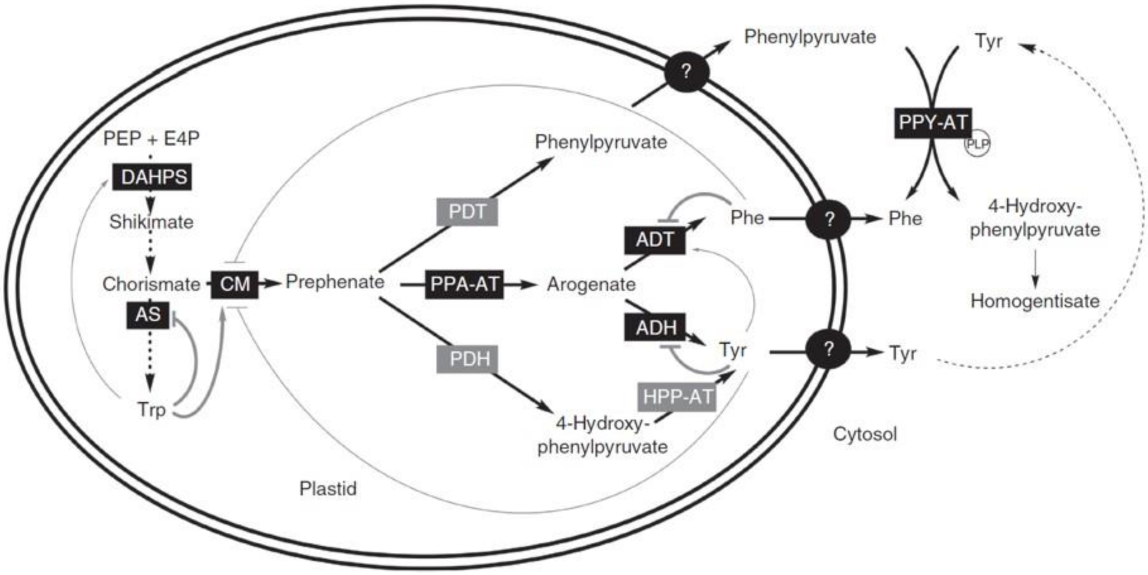
Phenylpyruvate
?
Tyr
PPY-AT
PLP
PEP + E4P
DAHPS
Shikimate
Chorismate
CM
Prephenate
AS
Trp
Phenylpyruvate
PDT
PPA-AT
Arogenate
PDH
ADT
Phe
?
Phe
4-Hydroxy-
phenylpyruvate
Homogentisate
ADH
Tyr
?
Tyr
HPP-AT
4-Hydroxy-
phenylpyruvate
Cytosol
Plastid

Figure 2.6 Revised model for phenylalanine biosynthesis in plants

The new model for phenylalanine biosynthesis in plants now includes a cytosolic step linked to the catabolism of tyrosine, which is mediated by PPY-AT. Circles with question marks correspond to undefined transport steps, while gray lines depict activation and feedback inhibition with thickness indicating the relative strength of allosteric regulation. Known enzymes are shown with a black background while those with a gray background are not yet characterized. ADH, arogenate dehydrogenase; ADT, arogenate dehydratase; AS, anthranilate synthase; CM, chorismate mutase; DAHPS, 3-deoxy-D-arabino-heptulosonate 7-phosphate synthase; E4P, D-erythrose 4-phosphate; HPP-AT, 4-hydroxyphenylpyruvate aminotransferase; PDH, prephenate dehydrogenase; PDT, prephenate dehydratase; PEP, phosphoenolpyruvate; PPA-AT, prephenate aminotransferase; PPY-AT, phenylpyruvate aminotransferase; Trp, tryptophan.

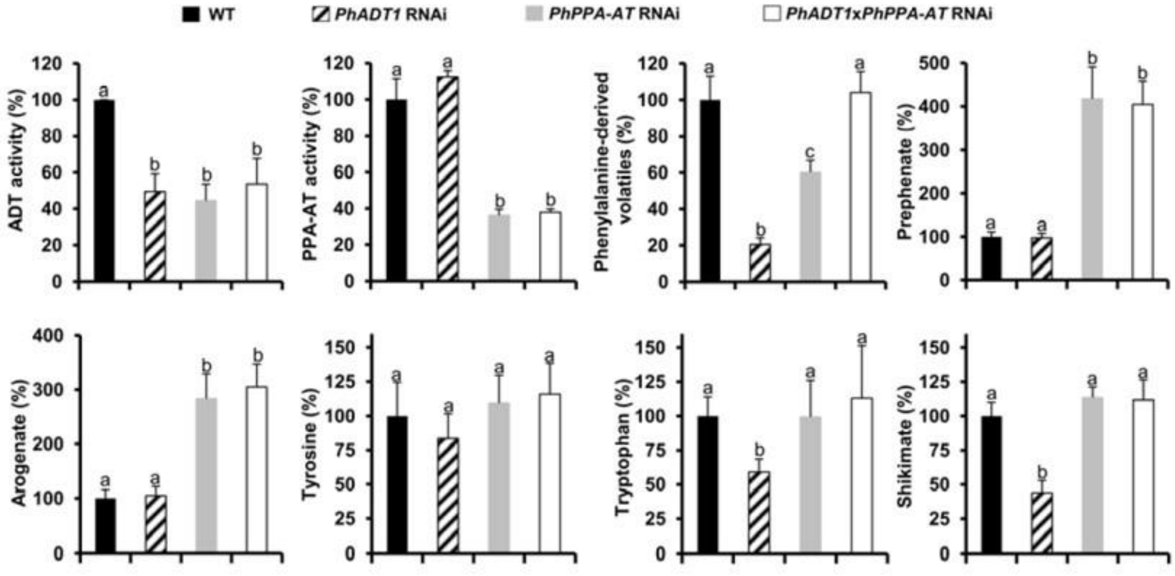

Figure 2.7 Effect of simultaneous *PhADT1* and *PhPPA-AT* downregulation on the levels of phenylalanine-derived volatiles, tyrosine, tryptophan, aromatic amino acid intermediates, and shikimate in petunia flowers.

The levels of plastidial ADT and PPA-AT activity (n = 5 biological replicates), phenylalanine-derived volatiles ($n \geq 5$), prephenate, arogenate, tyrosine, tryptophan and shikimate ($n \geq 6$) in petals of wild-type (WT; black) and the *PhADT1* (striped), *PhPPA-AT* (gray), and *PhADT1*x*PhPPA-AT* (white) RNAi lines harvested at 8 PM, 2 d postanthesis. Data are presented relative to corresponding WT controls set at 100% (687.5 nmol g FW^{-1} h^{-1} for phenylalanine-derived volatiles, 0.10 and 2.60 nkat mg $protein^{-1}$ for plastidial ADT1 and PPA-AT activities, respectively; 3.5, 21.4, 12.6, 16.0, 36.9 nmol g FW^{-1} for prephenate, arogenate, tyrosine, tryptophan, and shikimate, respectively). Columns with the same letters above are not significantly different based on Tukey's test ($P < 0.05$; One-way ANOVA).

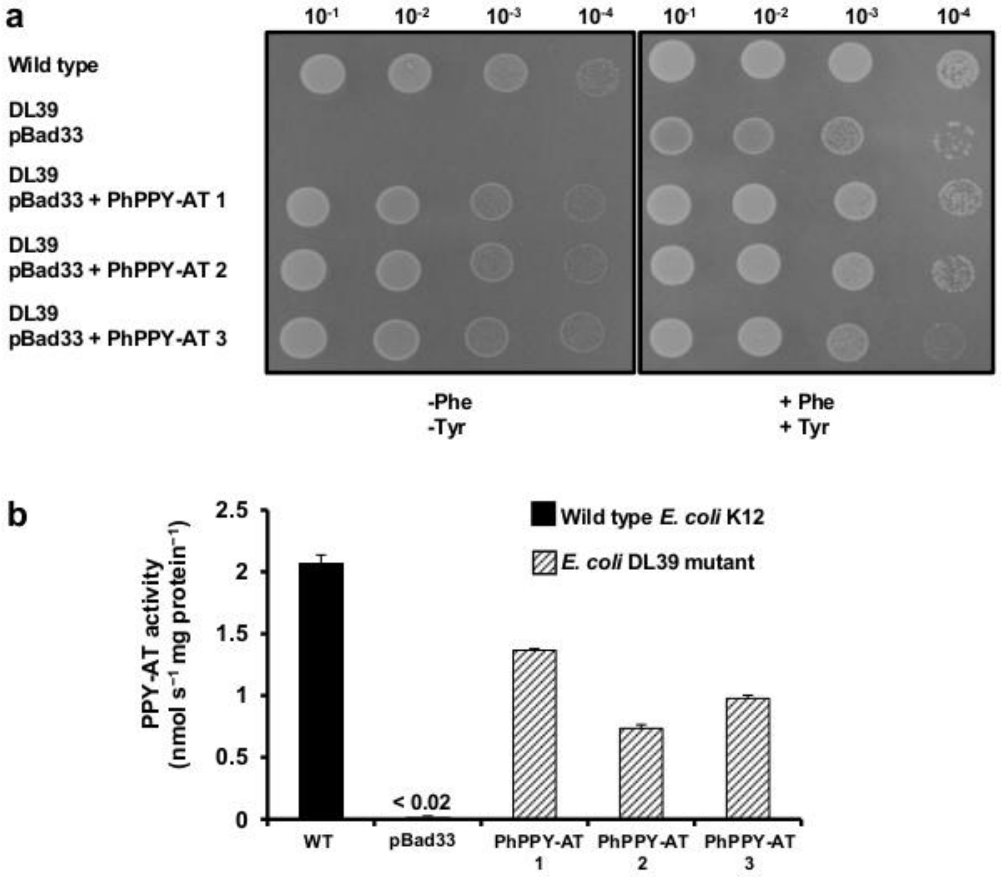

Figure 2.8 Functional complementation of the phenylalanine auxotrophic *E. coli* mutant DL39 by *PhPPY-AT*

(a) Wild-type *E. coli* (K12), the DL39 mutant transformed with pBad33 alone, and three independent clones of DL39 containing the pBad33-PhPPYAT construct were grown to an OD_{600} = 1 in M9 liquid media, washed, and serially diluted to $OD_{600} = 1 \times 10^{-1}$, 10^{-2}, 10^{-3} and 10^{-4}. Five µL of cells at each cell density were plated on M9 solid media containing 0.2% arabinose and 50 µg ml^{-1} aspartic acid, valine, leucine and isoleucine, with and without 50 µg ml^{-1} phenylalanine and tyrosine. **(b)** *In vitro* assays measuring PPY-AT activity with glutamate as an amino donor and phenylpyruvate as the keto acid acceptor were performed using crude extracts prepared from cells of wild-type (K12), the DL39 mutant transformed with empty pBad33, and the DL39 mutant harboring pBad33-PhPPYAT. Reactions were carried out at 30°C for 30 min with 74 µg of crude extract protein. Data are means ± s.e.m. (*n* = 3 independent experiments).

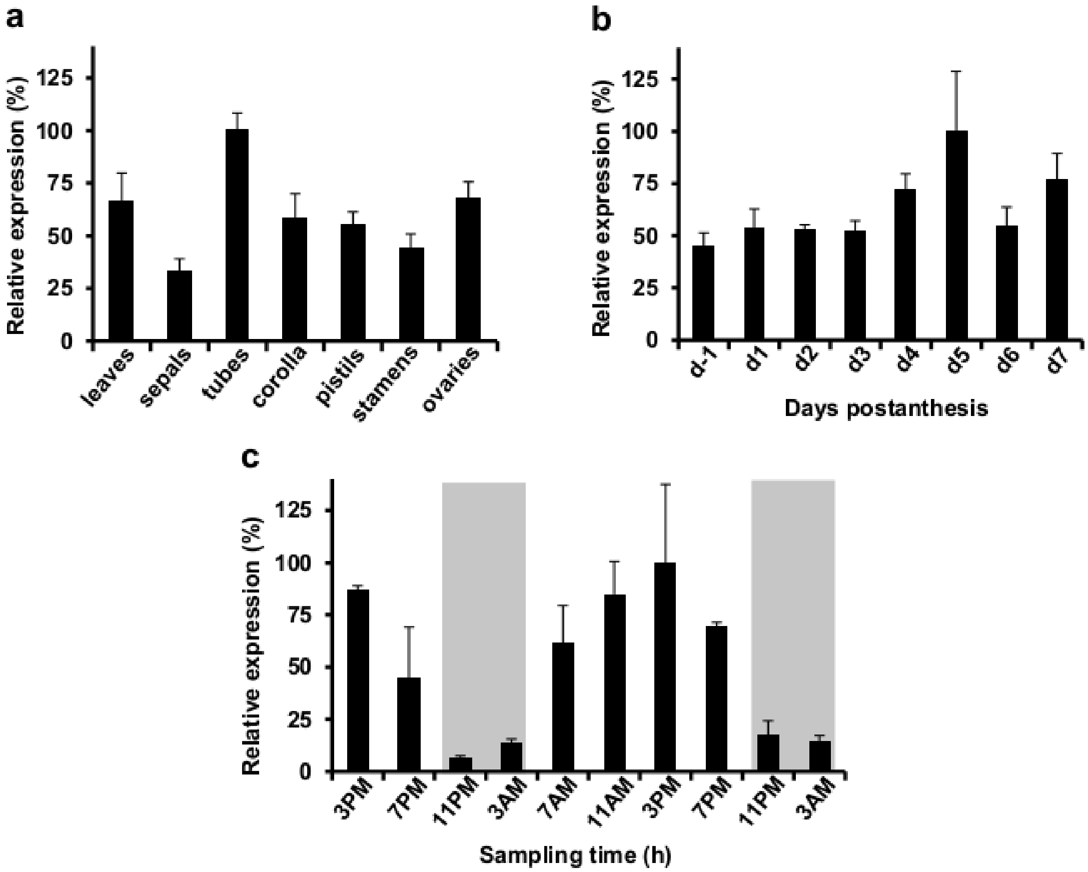

Figure 2.9 Expression profiles of *PhPPY-AT* in petunia flowers.

(a) Tissue specific expression of *PhPPY-AT* presented relative to levels in tubes set as 100%. **(b)** Developmental *PhPPY-AT* expression profile in corolla of petunia flowers from the mature bud stage (d -1) to 7 d postanthesis presented relative to level on d 5, set as 100%. **(c)** Diurnal expression profiles of *PhPPY-AT* in corolla of petunia flowers d 1 to d 3 postanthesis grown under a normal light/dark cycle presented relative to the level at 3 PM on d 2 postanthesis set as 100%. The dark cycles (9 PM to 6 AM) are shown with gray background. Data are means ± s.e.m. (*n* = 4 biological replicates)

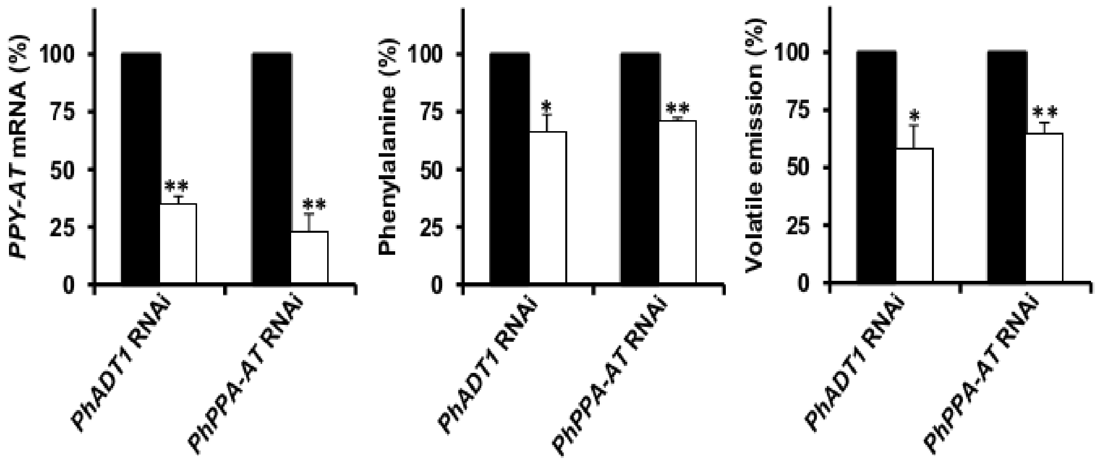

Figure 2.10 Effect of *PhPPY-AT* downregulation on phenylalanine and phenylalanine-derived volatile levels in petunia flowers of *PhADT1* and *PhPPA-AT* RNAi parental lines.

Downregulation of *PhPPY-AT* in petunia flowers (left panel) significantly decreases the levels of phenylalanine (middle panel) and phenylalanine-derived volatiles (right panels). For each genetic background, black and white columns represent flowers infiltrated with the empty vector or the *PhPPY-AT* RNAi construct, respectively. Data are presented as a percentage relative to the corresponding empty-vector reference. Data are means ± s.e.m. ($n \geq 3$ biological replicates). * $P < 0.05$ and ** $P < 0.01$ as determined by paired two-tailed Student's t-tests.

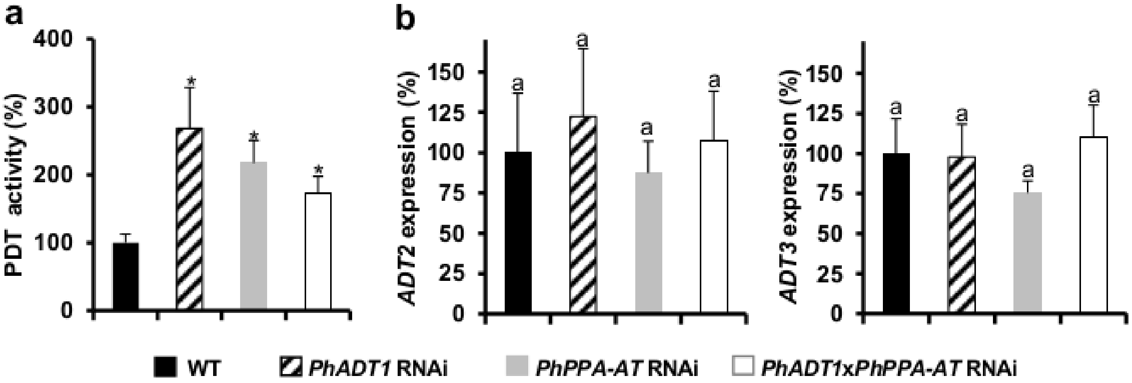

Figure 2.11 Effect of simultaneous *PhADT1* and *PhPPA-AT* downregulation on PDT activity, and expression levels of *PhADT2* and *PhADT3* in petunia flowers.

(a) PDT activities were determined using triple quadruple LC/MS in plastids isolated from d 1 to d 3 old petunia flowers of wild-type (WT; black) and the *PhADT1* (striped), *PhPPA-AT* (gray), and *PhADT1*x*PhPPA-AT* (white) RNAi lines harvested at 8 PM. Data are presented relative to the level in WT (0.468 pkat mg protein^{-1}) set as 100%. Data are means ± s.e.m. (*n* = 5 biological replicates). * $P < 0.05$ as determined by unpaired two-tailed Student's t-test between WT and each transgenic line. **(b)** *PhADT2* and *PhADT3* mRNA levels were determined by qRT-PCR with gene-specific primers in corollas of petunia flowers from WT (black) and the *PhADT1* (striped), *PhPPA-AT* (gray), and *PhADT1*x*PhPPA-AT* (white) RNAi lines harvested at 8 PM 2 d postanthesis. Data are presented relative to corresponding levels in WT set as 100%. Data are means ± s.e.m. (*n* = 3 biological replicates). Columns with the same letters above are not significantly different based on Tukey's test ($P < 0.05$; One-way ANOVA).

2.7 References

1. Bonawitz, N.D. & Chapple, C. The genetics of lignin biosynthesis: connecting genotype to phenotype. *Annu. Rev. Genet.* **44**, 337–363 (2010).
2. Winkel-Shirley, B. Flavonoid biosynthesis. A colorful model for genetics, biochemistry, cell biology, and biotechnology. *Plant Physiol.* **126**, 485–493 (2001).
3. Vogt, T. Phenylpropanoid biosynthesis. *Mol. Plant.* **3**, 2–20 (2010).
4. Dixon, R.A. Isoflavonoids: Biochemistry, molecular biology and biological functions. in *Comprehensive Natural Products Chemistry* (ed. Sankawa U), **1**, 773–823 (Elsevier, 1999).
5. DellaPenna D & Mène-Saffrané L. Vitamin E. in *Advances in Botanical Research* (eds. Rébeillé F & Douce R), **59**, 179–227 (Academic Press, 2011).
6. Nowicka, B. & Kruk, J. Occurrence, biosynthesis and function of isoprenoid quinones. *Biochim. Biophys. Acta.* **1797,** 1587–1605 (2010).
7. Mithöfer, A. & Boland, W. Plant defense against herbivores: chemical aspects. *Annu. Rev. Plant Biol.* **63**, 431–450 (2012).
8. Roppolo, D. & Geldner, N. Membrane and walls: who is master, who is servant? *Curr. Opin. Plant Biol.* **15**, 608–617 (2012).
9. Herrmann, K.M. & Weaver, L.M. The shikimate pathway. *Annu. Rev. Plant Physiol. Plant Mol. Biol.* **50**, 473–503 (1999).
10. Maeda, H. & Dudareva, N. The shikimate pathway and aromatic amino Acid biosynthesis in plants. *Annu. Rev. Plant Biol.* **63**, 73–105 (2012).
11. Berry, A., Ahmad, S., Liss, A. & Jensen, R.A. Enzymological features of aromatic amino acid biosynthesis reflect the phylogeny of mycoplasmas. *J. Gen. Microbiol.* **133**, 2147–2154 (1987).
12. Fischer, R.S., Bonner, C.A., Boone, D.R. & Jensen, R.A. Clues from a halophilic methanogen about aromatic amino acid biosynthesis in archaebacteria. *Arch. Microbiol.* **160**, 440–446 (1993).
13. Prakash, P., Pathak, N. & Hasnain, S.E. pheA (Rv3838c) of *Mycobacterium tuberculosis* encodes an allosterically regulated monofunctional prephenate dehydratase that requires catalytic and regulatory domains for optimum activity. *J. Biol. Chem.* **280**, 20666–20671 (2005).

14. Whitaker, R.J., Byng, G.S., Gherna, R.L. & Jensen, R.A. Diverse enzymological patterns of phenylalanine biosynthesis in pseudomonads are conserved in parallel with deoxyribonucleic acid homology groupings. *J. Bacteriol.* **147**, 526–534 (1981).
15. Cho, M.H. et al. Phenylalanine biosynthesis in *Arabidopsis thaliana*. Identification and characterization of arogenate dehydratases. *J. Biol. Chem.* **282**, 30827–30835 (2007).
16. Maeda, H. et al. RNAi suppression of Arogenate Dehydratase1 reveals that phenylalanine is synthesized predominantly via the arogenate pathway in petunia petals. *Plant Cell* **22**, 832–849 (2010).
17. Maeda, H. Yoo, H. & Dudareva, N. Prephenate aminotransferase directs plant phenylalanine biosynthesis via arogenate. *Nat. Chem. Biol.* **7**, 19–21 (2011).
18. Dal Cin, V. et al. Identification of Genes in the Phenylalanine Metabolic Pathway by Ectopic Expression of a MYB Transcription Factor in Tomato Fruit. *Plant Cell* **23**, 2738–2753 (2011).
19. Tzin, V., Malitsky, S., Aharoni, A. & Galili G. Expression of a bacterial bi-functional chorismate mutase/prephenate dehydratase modulates primary and secondary metabolism associated with aromatic amino acids in Arabidopsis. *Plant J.* **60**, 156–167 (2009).
20. Gonda, I. et al. Branched-chain and aromatic amino acid catabolism into aroma volatiles in *Cucumis melo* L. fruit. *J. Exp. Bot.* **61**, 1111–1123 (2010).
21. Prabhu, P.R. & Hudson, A.O. Identification and partial characterization of an L-Tyrosine aminotransferase (TAT) from *Arabidopsis thaliana*. *Biochem. Res. Int.* **2010**, 549572 (2010).
22. Lee, E.J. & Facchini, P.J. Tyrosine aminotransferase contributes to benzylisoquinoline alkaloid biosynthesis in *Opium Poppy*. *Plant Physiol.* **157**, 1067–1078 (2011).
23. Riewe, D. et al. A tyrosine aminotransferase involved in tocopherol synthesis in Arabidopsis. *Plant J.* **71**, 850–859 (2012).
24. Verdonk, J.C. et al. Regulation of floral scent production in petunia revealed by targeted metabolomics. *Phytochemistry* **62**, 997–1008 (2003).
25. Boatright, J. et al. Understanding *in vivo* benzenoid metabolism in petunia petal tissue. *Plant Physiol.* **135**, 1993–2011 (2004).
26. Gelfand, D.H. & Steinberg, R.A. Escherichia coli mutants deficient in the aspartate and aromatic amino acid aminotransferases. *J. Bacteriol.* **130**, 429–440 (1977).

27. LeMaster, D.M. & Richards, F.M. NMR sequential assignment of Escherichia coli thioredoxin utilizing random fractional deuteriation. *Biochemistry* **27**, 142–150 (1988).
28. Guzman, L.M., Belin, D., Carson, M.J. & Beckwith, J. Tight regulation, modulation, and high-level expression by vectors containing the arabinose PBAD promoter. *J. Bacteriol.* **177**, 4121–4130 (1995).
29. Rippert, P., Puyaubert, J., Grisollet, D., Derrier, L. & Matringe, M. Tyrosine and phenylalanine are synthesized within the plastids in Arabidopsis. *Plant Physiol.* **149**, 1251-1260 (2009).
30. Colquhoun, T.A. et al. A petunia chorismate mutase specialized for the production of floral volatiles. *Plant J*. **61**, 145–155 (2010).
31. Colquhoun, T.A. et al. Petunia floral volatile benzenoid/phenylpropanoid genes are regulated in a similar manner. *Phytochemistry* **71**, 158–167 (2010).
32. Klempien, A. et al. Contribution of CoA ligases to benzenoid biosynthesis in petunia Flowers, *Plant Cell* **24**, 2015–2030 (2012).
33. Lehmann, T. & Pollmann, S. Gene expression and characterization of a stress-induced tyrosine decarboxylase from *Arabidopsis thaliana*. *FEBS Lett.* **583**, 1895–1900 (2009).
34. Gutensohn, M. et al. Role of aromatic aldehyde synthase in wounding/herbivory response and flower scent production in different Arabidopsis ecotypes. *Plant J*. **66**, 591-602 (2011).
35. Warpeha, K.M. et al. G-protein-coupled receptor 1, G-protein G alpha-subunit 1, and prephenate dehydratase 1 are required for blue light-induced production of phenylalanine in etiolated Arabidopsis. *Plant Physiol*. **140**, 844-855 (2006).
36. Yamada, T. et al. Mutation of a rice gene encoding a phenylalanine biosynthetic enzyme results in accumulation of phenylalanine and tryptophan. *Plant Cell* **20**, 1316-1329 (2008).
37. Orlova, I. et al. Reduction of benzenoid synthesis in petunia flowers reveals multiple pathways to benzoic acid and enhancement in auxin transport. *Plant Cell* **18**, 3458-3475 (2006).
38. Kaminaga, Y. et al. Plant phenylacetaldehyde synthase is a bifunctional homotetrameric enzyme that catalyzes phenylalanine decarboxylation and oxidation. *J. Biol. Chem.* **281**, 23357–23366 (2006).
39. Kang, F. & Rawsthorne, S. Starch and fatty acid synthesis in plastids from developing embryos of oilseed rape. (*Brassica napus* L.) *Plant J*. **6**, 795–805 (1994).

40. Yoo, S.D., Cho, Y.H. & Sheen, J. Arabidopsis mesophyll protoplasts: a versatile cell system for transient gene expression analysis. *Nat Protoc.* **2**, 1565-1572 (2007).
41. Gleave, A.P. A versatile binary vector system with a T-DNA organisational structure conducive to efficient integration of cloned DNA into the plant genome. *Plant Mol. Biol.* **20**, 1203–1207 (1992).
42. Long, M.C. et al. Involvement of snapdragon benzaldehyde dehydrogenase in benzoic acid biosynthesis. *Plant J.* **59**, 256–265 (2009).
43. Orlova, I. et al. The small subunit of snapdragon geranyl diphosphate synthase modifies the chain length specificity of tobacco geranylgeranyl diphosphate synthase in planta. *Plant Cell* **21**, 4002–4017 (2009).

CHAPTER 3. IDENTIFICATION OF A PLASTIDIAL PHENYLALANINE EXPORTER THAT INFLUENCES FLUX DISTRIBUTION THROUGH THE PHENYLALANINE BIOSYNTHETIC NETWORK[2]

3.1 Abstract

L-phenylalanine is a versatile precursor for thousands of plant metabolites. Production of phenylalanine-derived compounds is a complex multi-compartmental process using phenylalanine synthesized predominantly in plastids as precursor. However, the transporter(s) exporting phenylalanine from plastids still remains unknown. Here, a gene encoding a *Petunia hybrida* plastidial cationic amino acid transporter (PhpCAT) functioning in plastidial phenylalanine export was identified based on homology to an *E. coli* phenylalanine transporter and co-expression with phenylalanine metabolic genes. *PhpCAT* downregulation and overexpression resulted in decreased and increased levels, respectively, of phenylalanine-derived volatiles, as well as phenylalanine, tyrosine, and their biosynthetic intermediates. Metabolic flux analysis revealed that flux through the plastidial phenylalanine biosynthetic pathway is reduced in *PhpCAT* RNAi lines, suggesting that the rate of phenylalanine export from plastids contributes to regulating flux through the aromatic amino acid network.

[2] This chapter has been published in Widhalm *et al.* (2015) Nature Communications.

Widhalm, J. R., Gutensohn, M., Yoo, H., Adebesin, F., Qian, Y., Guo, L., ... & Dudareva, N. (2015). Identification of a plastidial phenylalanine exporter that influences flux distribution through the phenylalanine biosynthetic network. *Nature communications*, *6*, 8142. DOI: https://doi.org/10.1038/ncomms9142

3.2 Introduction

The aromatic amino acid L-phenylalanine is a vital constituent of proteins in all living organisms and serves as a precursor for thousands of indispensable metabolites[1]. In humans, phenylalanine is an essential amino acid obtained through the diet primarily from plant-based sources, either directly or indirectly. Humans can convert phenylalanine to L-tyrosine for incorporation into proteins, as well as to synthesize thyroid hormones[2] and brain chemicals such as L-dopamine, epinephrine, and norepinephrine[3]. In plants, phenylalanine metabolism is even more prevalent and diverse. In fact, plants direct 20-30% of photosynthetically fixed carbon to the production of phenylalanine[4] and phenylalanine-derived compounds, which constitute approximately 30-45% of plant organic matter[5] and have profound impacts on growth and development (*e.g.* lignin[6]), reproduction (*e.g.* phenylpropanoids and benzenoids[7]) and defense (*e.g.* salicylic acid[8], tannins and flavonoids[9]).

Production of phenylalanine-derived compounds in plants is a complex multi-compartmental process relying on phenylalanine mainly synthesized in plastid stroma[10-12] to first be exported to the cytosol across both the inner and outer plastid envelope membranes. Due to its low permeability coefficient (2.5×10^{-10} cm s^{-1} for phenylalanine vs. 2×10^{-4} cm s^{-1} for water in egg phosphatidylcholine)[13, 14], simple diffusion of phenylalanine through membranes cannot meet the cytosolic demand, and therefore its passage is predicted to be protein mediated. In general, the plastid outer envelope is believed to contain pores and channels that confer partial discriminatory transport of metabolites, while the inner membrane, in conjunction with over 100 different transporters, serves as a selective permeability barrier[15]. Within the outer plastid envelope, an outer envelope protein, OEP16[16], a member of the plant preprotein and amino acid transporter superfamily[17], forms cation-selective high conductance channels with remarkable permeability for amines and amino acids, including phenylalanine[18]. However, there are still no reports on the characterization of an inner envelope amino acid transporters[19], despite the presence of several amino acid biosynthetic pathways in plastids[20]. Phenylalanine is utilized throughout the cell in plant primary and specialized metabolism, thus its transport across membranes is not limited to plastids. While intercellular amino acid transporters have been uncovered through recent studies on long-distance nitrogen transport in plants, to date very little is known about intracellular transport of amino acids[21-24].

Phenylalanine transport (uptake) has been well studied in microbes. In yeast (*Saccharomyces cerevisiae*) phenylalanine uptake occurs via the broad substrate transporters AGP1 and GAP1, the high-affinity tryptophan permease TAT2, and the branched-chain amino acid permeases BAP2 and BAP3[25]. In *Escherichia coli*, phenylalanine uptake proceeds via four distinct systems: (i) PheP (T.C. 2.A.3.1.1), a specific transport system that prefers phenylalanine over tyrosine and does not accept L-tryptophan[26]; (ii) AroP, a general aromatic amino acid transport system actively transporting phenylalanine, tyrosine, and tryptophan with high affinity[27]; (iii) TyrP, a tyrosine-specific system transporting phenylalanine at mM, but not μM, concentrations[28]; and (iv) LIV-I/LS, a branched-chain amino acid transporter system with broad substrate specificity capable of transporting phenylalanine only at very high concentrations[29].

The flowers of *Petunia hybrida* cv Mitchell have emerged as an ideal model system for studying plant phenylalanine metabolism. The primary fate of phenylalanine in mature petunia flowers is towards production of cytosolically synthesized volatiles[30,31]. However, it has been shown that phenylalanine is predominantly synthesized in plastids[10-12], implicating the involvement of an unknown transporter to move phenylalanine to the cytosol. Based on homology with *E. coli* PheP and coexpression with phenylalanine metabolic genes, we have identified a gene encoding a *P. hybrida* plastidial cationic amino acid transporter (PhpCAT) that participates in plastidial phenylalanine transport. Green fluorescent protein (GFP) fusion experiments and subcellular fractionation combined with immunoblotting confirmed that PhpCAT is localized to plastids. Expression of *PhpCAT* was found to be spatially, developmentally, and temporally consistent with genes involved in biosynthesis of phenylalanine and phenylalanine-derived volatiles. Radiolabel uptake assays performed using *E. coli* overexpressing PhpCAT suggest that this transporter is capable of transporting all three aromatic amino acids. RNAi downregulation of *PhpCAT* resulted in reduced emission of phenylalanine-derived volatiles and lowered levels of phenylalanine and tyrosine, and to a lesser extent tryptophan. In contrast, *PhpCAT* overexpression led to increased flux to phenylalanine-derived volatiles and elevated aromatic amino acid pools. Metabolic flux analysis further showed that when *PhpCAT* is downregulated flux is increased through the alternative phenylpyruvate route, which synthesizes phenylalanine in the cytosol. Based on these data we conclude that PhpCAT is involved in export of phenylalanine from plastids and contributes to controlling carbon flux through the phenylalanine biosynthetic network.

3.3 Results

3.3.1 *PhpCAT* is a homologue of *E. coli pheP* localized in plastids

With recent advances in gene expression technology, coexpression analysis is becoming an effective tool for discovery of missing genes, including those encoding for plastidial transporters[46,47]. Therefore, we took advantage of petunia flowers since they synthesize high levels of phenylalanine and phenylalanine-derived volatiles, production of which is coordinately regulated over development and a daily light/dark cycle[10,11,32,33,48,49]. We generated an RNA-Seq dataset based on RNA isolated from corolla tissue harvested at 8 PM at two developmental stages, day -1 (bud) and day 2 postanthesis (the tissues containing the lowest and highest levels of phenylalanine, respectively[10]) to accurately detect and quantify low abundance transcripts not represented in our petunia petal-specific EST database[30] as well as the Sol genomics network (http://solgenomics.net). To identify candidate phenylalanine transporters a tblastn search (cutoff e^{-08}) of the petunia RNA-Seq *de novo* assembly transcriptome was performed for genes encoding proteins homologous to *E. coli* PheP[26]. Based on the cutoff, three distinct genes, corresponding to contigs *Ph21511*, *Ph18042*, and *Ph19221*, were retrieved and appeared to represent full-length mRNAs encoding proteins comprised of at least 467 amino acids and that share 24%/41%, 22%/43%, and 22%/41% identity/similarity to *E. coli* PheP, respectively. The cognate proteins of contigs *Ph21511* and *Ph18042* were found to contain 14 and 13 transmembrane helices, respectively, and were annotated by BLAST2GO in the RNA-Seq datasets as putative cationic amino acid transporters (CATs; T.C. 2.A.3.3.4), which are proton-energized members[34] of the Amino acid-polyamine-organocation (APC) family[15]. Contig *Ph19221* was predicted to encode for a putative amino acid transporter with nine transmembrane domains.

In petunia, it has been shown that expression of phenylalanine metabolic genes increases concomitantly with increased phenylalanine levels[10,11] and emitted volatiles[32,33] as the flower opens. We hypothesized that a phenylalanine transporter(s) may also be transcriptionally upregulated at this time. Since RNA-Seq is a quantitative approach, gene expression on day 2 after flower opening relative to buds was investigated based on the number of counts corresponding to each contig in the generated datasets. The counts are based on the number of reads that map to a given contig, correcting for the total number of reads and length of the contig. First, higher expression of genes encoding plastidial phenylalanine biosynthetic enzymes (chorismate mutase 1, CM1; prephenate aminotransferase, PPA-AT; arogenate dehydratase 1, ADT1) and cytosolic phenylalanine-utilizing enzymes involved in scent formation (phenylalanine ammonia-lyase 1,PAL1; phenylacetaldehyde synthase, PAAS) on day 2 relative to buds (Figure 3.1) was confirmed to validate the RNA-Seq datasets. Next, expression of the three petunia *pheP* homologs was examined. This analysis revealed that contig *Ph19221* showed an average 1.8-fold decrease in counts on day 2 relative to buds, while contigs *Ph21511* and *Ph18042* both showed a 2-fold average increase (Figure 3.1). Therefore, only *Ph21511* and *Ph18042* were further examined as plastidial phenylalanine transporter candidate genes.

Recent analysis of the 5800 transmembrane proteins in *Arabidopsis thaliana* revealed that 660 contained putative N-terminal plastid transit peptides[15]. Therefore, it was hypothesized that if contigs *Ph21511* and *Ph18042* encode plastidial transporters their cognate proteins should bear detectable N-terminal transit peptides. Analysis of the encoded *Ph18042* protein by multiple subcellular prediction programs (WoLF PSORT: http://www.genscript.com/psort/wolf_psort.html; Predotar: https://urgi.versailles.inra.fr/predotar/predotar.html; TargetP: http://www.cbs.dtu.dk/services/TargetP/) revealed that it does not contain a transit peptide. In contrast, the first 43 amino acids of the encoded *Ph21511* protein were predicted with a score of 0.837 by TargetP to serve as a plastid-targeting signal. To experimentally test for plastidial localization, the first 52 amino acids of Ph21511, which includes all the residues prior to the first predicted transmembrane domain, were fused to the N-terminus of the GFP reporter protein and transiently expressed in tobacco leaves (Figure 3.2a-f). Whereas the GFP control displayed fluorescence confined to the cytosol (Figure 3.2a-c), the green fluorescence of the Ph21511$_{1-52}$-GFP construct resulted in co-localization with the red autofluorescence of chlorophyll in plastids (Figure 3.2d-f). To independently verify the confocal microscopy result, total crude extracts and isolated plastids were prepared from 2 day old petunia flowers and examined by immunoblotting using purified anti-Ph21511 antibodies. The apparent molecular mass of the detected protein, which migrated above the 50 kDa marker, from both crude extract and the plastid fraction was consistent with the calculated size (57.9 kDa) for mature (*i.e.* without transit peptide) Ph21511 (Figure 3.2g). Moreover, the detected signal from equal amounts (60 μg) of loaded protein was drastically enriched in the plastid fraction compared to crude extract (Figure 3.2g), thus confirming that Ph21511 is targeted to plastids. Based on the experimentally determined localization and the work presented below, the protein encoded by *Ph21511* was designated as PhpCAT for *Petunia hybrida* plastidial cationic amino acid transporter.

3.3.2 *PhpCAT* is developmentally and rhythmically regulated

Petunia flowers predominantly emit high levels of phenylalanine-derived volatiles at night[30,50]. To accomplish this, petunia flowers have evolved synchronized developmental and temporal expression patterns for genes involved in synthesis of phenylalanine[10,11,33] and phenylalanine-derived volatiles[32,48,49]. Investigation of *PhpCAT* transcript levels by qRT-PCR with gene-specific primers revealed that it is expressed in all flower organs, as well as in leaves (Figure 3.3a). Moreover, *PhpCAT* expression was lowest at the bud stage (day -1) and increased upon flower opening (Figure 3.3b), displaying a typical pattern for petunia flower genes involved in biosynthesis of phenylalanine[10,11,33] and phenylalanine-derived scent compounds[32,48,49] (Figure 3.1). Remarkably, *PhpCAT* was also found to exhibit rhythmic expression over a daily light cycle, with the highest transcript abundance occurring at night on day 2 postanthesis (Figure 3.3c), which corresponds to the time of highest emission of phenylalanine-derived volatiles[30,50]. Thus, the developmental and temporal expression of *PhpCAT* is consistent with that of a transporter *a priori* needed to export phenylalanine out of plastids for production of floral volatiles.

3.3.3 PhpCAT transports all three aromatic amino acids

The use of whole cell uptake assays in a heterologous *E. coli* expression system has been an informative approach for elucidating the biochemical function of plastid transporters[51-56]. To determine if PhpCAT is capable of transporting phenylalanine and/or the other aromatic amino acids, uptake assays with ^{14}C-phenylalanine, ^{14}C-tyrosine, and ^{14}C-tryptophan were performed with intact *E. coli* cells expressing recombinant PhpCAT$_{53\text{-}583}$ (N-terminal 6XHis-tagged PhpCAT without its predicted transit peptide) or carrying an empty vector as a control. An immunoblot using purified anti-PhpCAT (anti-Ph21511) antibodies against *E. coli* crude extracts verified that recombinant PhpCAT$_{53\text{-}583}$ was expressed in IPTG-induced cells carrying the pET28a:*PhpCAT*$_{157\text{-}1749}$ construct, but not empty pET28a vector (Figure 3.4a). As a negative control, ^{14}C-glucose was used to test if overexpression of PhpCAT affected endogenous *E. coli* uptake activities. First, glucose was selected because it was not expected to be a substrate of PhpCAT. In addition, one of the native glucose transport systems is proton driven similar to the *E. coli* AroP uptake system, which is responsible for 80-90% of aromatic amino acid transport. Since no difference in ^{14}C-glucose uptake was detected between *E. coli* harboring the empty vector and cells expressing PhpCAT$_{53\text{-}583}$ this indicates that the endogenous aromatic amino acid uptake system was not perturbed (Figure 3.4b). On the other hand, *E. coli* cells expressing $\mathrm{PhpCAT}_{53\text{-}583}$ accumulated significantly lower levels of ^{14}C-phenylalanine (Figure 3.4c), ^{14}C-tyrosine (Figure 3.4d), and to a lesser extent, ^{14}C-tryptophan (Figure 3.4e), compared to the empty-vector control. The detected levels of radiolabeled amino acids results from the net difference between uptake into and efflux out of the cell. Since no decrease in uptake via the endogenous aromatic amino acid *E. coli* transport systems is presumably occurring, the reduced accumulation of aromatic amino acids in cells expressing $\mathrm{PhpCAT}_{53\text{-}583}$ is due to efflux via PhpCAT. These results demonstrate that all three aromatic amino acids are substrates of PhpCAT.

3.3.4 PhpCAT links plastidial-cytosolic phenylalanine metabolism

To examine if PhpCAT functions *in vivo* as an exporter of phenylalanine from plastids, *PhpCAT* expression was downregulated using an RNAi strategy under control of a petal-specific promoter[35]. Three independent lines with 75-80% downregulated *PhpCAT* transcript levels (Figure 3.5a) were selected for subsequent detailed metabolic profiling. Moreover, an immunoblot using purified anti-PhpCAT (anti-Ph21511) antibodies against crude extracts and purified plastid fractions from RNAi line 17 verified PhpCAT was downregulated at the protein level (Figure 3.7). Consistent with an *in planta* role in plastidial phenylalanine export, downregulation of *PhpCAT* led to 20-42% reduction in total emission of phenylalanine-derived volatiles relative to control (Figure 3.5a), but the extent of decrease varied for each compound (Figure 3.8). Phenylalanine and tyrosine levels were also decreased in *PhpCAT*-RNAi lines by up to 42% compared to control (Figure 3.5a), which was likely due to reduced amounts of their biosynthetic intermediates prephenate (25-52% decreased in *PhpCAT*-RNAi lines versus control) and arogenate (54-61% decreased in *PhpCAT*-RNAi lines versus control) (Figure 3.5a). At the same time, only minimal decreases were observed in the pool sizes of tryptophan (5-18% reduced) and shikimate (up to 9% reduced) in *PhpCAT*-RNAi lines compared to control (Figure 3.5a).

To further investigate the role of PhpCAT *in vivo*, *PhpCAT* was overexpressed under control of a petal-specific promoter[35]. Three different lines showing 4.5 to 100-fold increase in *PhpCAT* transcript levels (Figure 3.5b) were chosen for further metabolite analysis. Total emission of phenylalanine-derived volatiles in detached flowers increased by up to 18% in *PhpCAT* overexpressors compared to control (Figure 3.5b), although the degree of increase differed for individual compounds (Figure 3.9). In addition, the levels of phenylalanine and tyrosine increased from 23-53% in *PhpCAT* overexpressors compared to control (Figure 3.5b), likely as a result of elevated pools of phenylalanine biosynthetic intermediates prephenate and arogenate (11-16% and 22-48% increase in *PhpCAT* overexpressors versus control, respectively) (Figure 3.5b). Moreover, the tryptophan pool displayed an increasing trend and no changes were detected in shikimate levels in *PhpCAT* overexpressors compared to control (Figure 3.5b). Taken together these data indicate that PhpCAT is involved in plastidial phenylalanine export *in planta*. Moreover, profiling of plastidial phenylalanine biosynthetic intermediates suggest that PhpCAT is involved in regulating flux through the aromatic amino acid biosynthetic network.

3.3.5 PhpCAT controls phenylalanine biosynthetic flux

Since downregulation of *PhpCAT* led to a decrease in the levels of phenylalanine, tyrosine, and their shared precursors prephenate and arogenate (Figure 3.5a), we hypothesized that phenylalanine and tyrosine accumulate inside plastids of *PhpCAT*-RNAi lines and feedback inhibit the arogenate pathway (Figure 3.6a). Recently we showed that plants also contain an alternative pathway that proceeds via phenylpyruvate to produce phenylalanine in the cytosol, flux through which increases when the plastidial biosynthetic pathway (via arogenate) is impaired[12]. In the alternative pathway, a cytosolic phenylpyruvate aminotransferase (PPY-AT) preferentially converts phenylpyruvate to phenylalanine using tyrosine as an amino donor[12] (Figure 3.6a). Interestingly, tyrosine cannot serve as an amino donor for PPA-AT in the plastidal arogenate pathway[11]. Taking advantage of this characteristic to distinguish between the two pathways, we employed metabolic flux analysis with stable isotopic labeling using ^{15}N-tyrosine to determine the effect of reduced plastidial phenylalanine export on carbon flux through the parallel phenylalanine biosynthetic pathways.

Excised 2 day-old petunia flowers from control and *PhpCAT*-RNAi lines 9 and 17 were fed with 10 mM ^{15}N-tyrosine starting at 18:00 h, harvested after 2, 4, and 6 h, and analyzed by liquid chromatography-mass spectrometry (LC-MS) to determine phenylalanine and tyrosine pool sizes and isotope abundances. Similar to what was observed previously[12], the labeling percentage of phenylalanine increased linearly over 6 h, as did the level of emitted volatiles (Figure 3.10). To assess the control PhpCAT exerts on metabolic fluxes through the phenylalanine biosynthetic network, a metabolic flux model was developed. The simulation revealed that v_1, the rate of synthesis through the plastidial arogenate pathway, was 32% and 44% lower ($p < 0.05$) at t_0 and

t_6, respectively, in *PhpCAT*-RNAi lines compared to control (Figure 3.6b and Table 3.1). This finding is consistent with our hypothesis that reduced export of phenylalanine and tyrosine from plastids in *PhpCAT*-RNAi lines leads to feedback inhibition of the arogenate pathway. At the same time, the flux analysis showed that in both control and the *PhpCAT*-RNAi lines v_2, the flux through the cytosolic phenylpyruvate pathway, was minor at t_0, but significantly increased over the 6-h period (Figure 3.6b and Table 3.1). In addition, increase in the rate of v_2 in *PhpCAT* knockdowns was more rapid than in control (Figure 3.6b and Table 3.1), suggesting that more carbon flux is directed through the cytosolic pathway. Taking this into account with the decrease in flux through the arogenate pathway, the relative contribution of cytosolic phenylalanine production is considerably higher in *PhpCAT*-RNAi lines compared to control (a v_2/v_1 flux ratio of 0.44 versus 0.18, respectively, at t_6) (Figure 3.6b and Table 3.1).

3.4 Discussion

Eukaryotic metabolic networks are often spread throughout multiple subcellular compartments separated by organelle membrane barriers, through which precursors, intermediates, and end-products must pass. While some metabolites may passively diffuse across membranes, others require protein-mediated transport, as is the case for phenylalanine synthesized in plastids. The current study took advantage of the distinctive transcriptional developmental regulation of phenylalanine metabolism in petunia flowers to identify a plastidial amino acid transporter, PhpCAT, which is capable of transporting all three aromatic amino acids (Figure 3.4). Respective increases and decreases in the levels of phenylalanine-derived volatiles, as well as in phenylalanine, tyrosine, and their biosynthetic intermediates prephenate and arogenate in *PhpCAT* overexpression and RNAi lines (Figure 3.5) support an *in vivo* role for PhpCAT as a plastidial phenylalanine and tyrosine exporter. Moreover, flux through the phenylpyruvate pathway, which produces phenylalanine in the cytosol, was increased when *PhpCAT* was downregulated (Figure 3.6b).

It is likely that while the total cellular pools of phenylalanine and tyrosine decrease in *PhpCAT*-RNAi lines compared to control (Figure 3.5a), these amino acids accumulate inside the plastid and feedback inhibit the shikimate and/or aromatic amino acid biosynthetic pathways. Disproportional effects on the concentrations of phenylalanine, tyrosine, and their precursors prephenate and arogenate compared to shikimate and tryptophan (Figure 3.5a) may point to feedback inhibition of CM1 (Figure 3.6a) in *PhpCAT*-RNAi lines. Previously it was shown that petunia CM1 activity is not inhibited at the same concentration (50 μM) of phenylalanine and tyrosine[33] known to regulate Arabidopsis CM1[36]. However, in light of the high demand for phenylalanine in petunia flowers, and the fact that inhibition constants (K_i) of other plant CMs are in the range of 0.3-1.1 mM[1], it is possible that petunia CM1 is inhibited at higher concentrations of phenylalanine. To test this, we assayed preparations of petunia plastids for CM activity in the presence of a range of phenylalanine concentrations. Indeed, petunia plastidial CM activity was found to be inhibited by phenylalanine with an IC_{50} of 748 μM (Figure 3.11). Thus, the metabolic phenotype on the arogenate pathway observed in *PhpCAT*-RNAi lines (Figure 3.5a) could be attributed to feedback inhibition of petunia CM1. Conversely, in *PhpCAT* overexpression lines, levels of phenylalanine, tyrosine, prephenate, and arogenate were increased compared to control (Figure 3.5b), which may indicate reduced levels of phenylalanine and tyrosine in plastids leading to the relaxation of naturally-occurring feedback regulation of their biosynthetic enzymes, including CM1. The fact that tryptophan also trended to increase in *PhpCAT* overexpression lines compared to control (Figure 3.5b) might further imply reduced feedback restrictions on tryptophan biosynthesis and/or the shikimate pathway.

Downregulation of *PhpCAT* expression in petunia flowers by 75-80% led to 20-42% reduction in the emission of phenylalanine-derived volatiles (Figure 3.5a). The smaller reduction in volatiles relative to *PhpCAT* expression is likely the result of one or a combination of several factors. (i) It is possible that the remaining amount of PhpCAT transporter activity was sufficient to sustain the observed volatile emission rate. (ii) In addition or alternatively, there could be other specific and/or non-specific amino acid transporters, which are not homologous to *E. coli* PheP, involved in exporting phenylalanine from plastids. (iii) Another possibility is the contribution of a phenylalanine storage pool in the vacuole to the production of phenylalanine-derived products. Vacuoles, which are separated from cytosol by a single, semi-permeable membrane called the tonoplast, are involved in temporary and long-term storage of numerous metabolites[37], including free phenylalanine[38]. In recent years, tonoplast-localized transporters have been discovered in plants and shown to be an integral part of a complex cellular network controlling plant metabolism[48]. Two Arabidopsis amino acid transporters, AtCAT2 and AtCAT4, have been shown to localize to the vacuolar membrane[22,23]. Though the physiological function of AtCAT4 is still unknown, AtCAT2 has been shown to regulate free amino acid levels in Arabidopsis leaves[22]. Interestingly, AtCAT2 is the most similar Arabidopsis CAT homolog to Ph18042, the other *E. coli*

PheP homolog with increased gene expression in petunia flowers on day 2 postanthesis. Similar to AtCAT2, Ph18042 is also predicted to localize to the vacuole and it seems conceivable that it may contribute to modulating cytosolic phenylalanine levels in petunia flowers. (iv) Finally, in *PhpCAT*-RNAi lines the phenylpyruvate pathway could partially compensate for the shortage of phenylalanine being exported from the plastid. Recently it was shown that flux through the cytosolic phenylpyruvate pathway (Figure 3.6a) increases when entry into the arogenate pathway is genetically blocked[12]. Similarly, the present study shows that the phenylpyruvate pathway has higher relative contribution when plastidial phenylalanine export is impeded in *PhpCAT*-RNAi lines (Figure 3.6b). It still remains an open question at which upstream step flux is redirected towards the phenylpyruvate pathway. If CM1 is indeed feedback inhibited *PhpCAT*-RNAi lines, then one possibility is at the level of chorismate (Figure 3.6a). Plants contain a cytosolic isoform of CM, CM2, with higher affinity for chorismate than their plastidial CM1 counterparts[1], which may produce prephenate in the cytosol for the alternative phenylalanine biosynthetic pathway (Figure 3.6a). This scenario implicates the involvement of a plastidial chorismate transporter and cytosolic prephenate dehydratase (PDT), neither of which has been discovered. Alternatively, phenylpyruvate may be generated in the plastid via dehydration/decarboxylation of prephenate by moonlighting ADT (or an unidentified PDT) and then exported through an unknown transporter to the cytosol (Figure 3.6a). However, *PhpCAT*-RNAi lines have reduced prephenate levels and the catalytic efficiency of PPA-AT[11] is much higher than those of the known ADTs with moonlighting PDT activity[10]. Thus, together these factors likely preclude formation of a sufficient quantity of phenylpyruvate in plastids to sustain the cytosolic pathway.

The occurrence of a plastidial CAT transporter does not appear to be unique to petunia. Phylogenetic reconstruction with the Arabidopsis CAT family reveals that the closest homologs of PhpCAT are CAT7 (73% identity/85% similarity) and AtCAT6 (73% identity/84% similarity). While Arabidopsis CAT7 has unknown function, it possesses a putative transit peptide predicted to serve as a plastid targeting signal[23]. On the other hand, AtCAT6 has previously been shown to function in sink tissues as a transporter of amino acids, including phenylalanine[34]. Fusion of GFP to the N-terminus of AtCAT6 revealed that it is localized to the plasma membrane[34]. However, it should be further investigated if AtCAT6 is dual localized, because similar to Arabidopsis CAT7 and PhpCAT, it contains a predicted transit peptide[23] (with a TargetP score of 0.949).

At the cellular level, transporters are integral parts of metabolic networks as they mediate interactions between multiple pathways across different subcellular compartments. Metabolic flux analysis performed in the current study strongly supports the idea that transporters, such as PhpCAT, further exert control over fluxes through metabolic networks by influencing organellar metabolite concentrations, which in turn biochemically regulate enzymes. Thus, development of organellar metabolite profiling techniques[39,40], coupled with stable isotope labeling will be needed to further dissect the role PhpCAT plays in feedback control of the aromatic amino acid network.

3.5 Materials and Methods

3.5.1 Plant material, growth conditions and generation of *PhpCAT* RNAi and *PhpCAT* overexpression lines

Wild type and transgenic *Petunia hybrida* cv. Mitchell plants were grown under standard greenhouse conditions[35] with a light period from 6:00 h to 21:00 h. For the *PhpCAT*-RNAi construct, DNA containing two spliced *PhpCAT* cDNA fragments of the coding region corresponding to nucleotides 30-577 and 30-368, the latter in antisense orientation to create a hairpin structure, was synthesized (Genscript, Piscataway, NJ). 5'-*EcoRI* and 3'-*BamHI* sites were added for directional subcloning into pRNA69 containing the *Clarkia breweri linalool synthase (LIS)* petal-specific promoter[35]. The resulting plasmid containing the *LIS* promoter and the synthetic *PhpCAT* hairpin fragment was cut out using *SacI/NotI* and subcloned into the pART27 simpler binary vector[41]. For the *PhpCAT* overexpression construct, *PhpCAT* was amplified using the forward primer 5'-GAATTCATGGAGACCCATAGCTCCTCTTTCTCTAACATAAA-3' and reverse primer 5'-GGATCCTTACACTTTGAGAGTATGGTCCTGGTTTTCAATAG-3' and directionally subcloned into the *EcoRI* and *BamHI* sites (underlined in the respective primers) of pRNA69 in frame with the *LIS* promoter. The resulting cassette was cut out with *SacI/NotI* and subcloned into the pART27 binary vector. The final *PhpCAT*-RNAi and *PhpCAT* overexpression constructs were used for *Agrobacterium tumefaciens* (GV3101)-mediated transformation of *Petunia hybrida* cv. Mitchell diploid using the standard leaf disk transformation method[42].

3.5.2 qRT-PCR

Sample collection, RNA isolation and qRT-PCR were performed as previously described[32]. RNA was isolated from petals of at least eight wild type or transgenic petunia flowers (per biological replicate) at 23:00 h on day 2 post-anthesis using an RNeasy plant mini kit (Qiagen, Valencia, CA).

RNA was treated with DNase I (Promega, Madison, WI, USA) to eliminate genomic DNA and was reverse transcribed to cDNA using the High Capacity cDNA Reverse Transcription Kit (Applied Biosystems). *PhpCAT* expression was analyzed relative to the reference gene *elongation factor 1-α (EF1-α). PhpCAT*-specific primers 5*'*-AGCACTTTCCGATACCCCAA-3*'* and 5*'*-GAACTCGGCTTGTTTCTTCGA-3*'*, and *EF1-α*-specific primers 5*'*-CCTGGTCAAATTGGAAACGG-3*'* and 5*'*-CAGATCGCCTGTCAATCTTGG-3*'* were used respectively.

3.5.3 Subcellular localization of PhpCAT

The first 156 nucleotides encoding the 52 amino acids preceding the first predicted transmembrane domain of *PhpCAT* (*Ph21511*) were amplified using the forward primer 5*'*-CACCATGGAGACCCATAGCTCCTCTTTCTCTAACATAAA-3*'* and reverse primer 5*'*-CCGTTTCATATCACCACCAGACCG-3*'*. The resulting fragment was subcloned into pENTR^{TM}/D-TOPO (Invitrogen^{TM}, Carlsbad, CA), sequenced verified, and transferred into pK7FWG2[45] via Gateway^{TM} technology, resulting in an in-frame fusion with the N-terminal end of GFP. The Ph21511$_{1-52}$-GFP construct and an empty GFP vector were transformed into *Agrobacterium tumefaciens* strain GV3101, infiltrated into *Nicotiana benthamiana* leaves, and imaged 48 h later Images were acquired using a Zeiss LSM710 laser spectral scanning confocal microscope with a C-Apochromat 40 X /1.20 W objective (Zeiss, Thornwood, NY). GFP was excited with an argon laser at wavelength 488 nm and emission were collected over a 493-598 nm bandpass. Chlorophyll fluorescence was excited by a HeNe laser at wavelength 633 nm and emission were collected over a 647-721 nm bandpass.

3.5.4 Heterologous expression of PhpCAT and transport assays

The coding sequence of *PhpCAT* was synthesized (Genscript, Piscataway, NJ) with codon optimization for expression in *E. coli* using GenScript's OptimumGene™ Gene Design system. A truncated version (minus the predicted transit peptide) of codon-optimized *PhpCAT* was amplified with the forward primer 5*'*-CATATGAGTCTGCGTTGGTACGACCTGGTT-3*'* and reverse primer 5*'*-CTCGAGTTAGACTTTCAGGGTATGGTCTTGGTTTTCA-3*'*, which introduced NdeI and XhoI sites (underlined), respectively, for directional cloning into pET28a (Novagen) in frame with an N-terminal 6XHis-tag. The resulting codon optimized pET28a:*PhpCAT*$_{157-1749}$

construct was sequenced verified and transformed into Lemo21(DE3) *E. coli* (New England Biosciences, Ipswich, MA). Starter cultures containing kanamycin and chloramphenicol were used to inoculate 25 ml of Luria-Bertani (LB) at an A_{600} of 0.05. When A_{600} reached approximately 0.4, isopropyl-1-thio-β-D-galacatopyranoside (IPTG) was added to a final concentration of 0.5 mM and incubation was continued for 2 h at 18°C. Cells were harvested by centrifugation, and nickel-affinity purification of PhpCAT$_{53\text{-}583}$ under denaturing conditions was performed according to *The QIAexpressionist^{TM}* (5th Ed., 2003) protocols 10 and 17.

For the radiolabel uptake assays IPTG induction and preparation of cells carrying empty pET28a or codon optimized pET28a:*PhpCAT$_{157\text{-}1749}$* was performed as described above except that cells were washed and resuspended to an A_{600} of 4.0 in M9 minimal media. To initiate the assays, 100 μl of prepared cells were added to 100 μl of M9 incubation media containing ^{14}C-labeled glucose (0.25 μCi), phenylalanine (0.35 μCi), tyrosine (0.35 μCi), or tryptophan (0.2 μCi). Concentrations of substrates were pre-adjusted in the M9 incubation media to 200 μM with cold substrate. Uptake assays were carried out at 30°C in 1.5 ml Eppendorf microfuge tubes and terminated after the indicated time periods by rapid filtration of the reaction through a 0.45 μm Whatman filter (GE Healthcare Life Sciences, Pittsburgh, PA) under vacuum. Filters were washed two times with 1 ml M9 media and then transferred into a 20 ml scintillation vial containing 10 ml of EcoLite(+) scintillation cocktail (MP Biochemicals, Santa Ana, CA). Radioactivity in the samples was quantified by scintillation counting.

3.5.5 Metabolic flux analysis with ^{15}N-tyrosine labelling

We generated a metabolic flux model that utilizes experimentally determined pool sizes and isotopic enrichment of phenylalanine from exogenously fed ^{15}N-tyrosine. Feeding of 10 mM ^{15}N-tyrosine (Cambridge Isotope Laboratories, Andover, MA) to 2-day-old corollas of control and *PhpCAT*-RNAi lines was performed as previously described[12]. Similar to our previous labeling study[12], the labeling percentage of tyrosine quickly reached >80% and pseudo-steady state within 2 hours upon feeding, and stayed constant for the rest of the experimental period. The model was based on the dynamic mass balance around phenylalanine as defined as:

$$\frac{dC_{Phe}}{dt} = v_1 + v_2 - v_c \qquad (1)$$

where C_{Phe} is the phenylalanine pool size, v_1 is the flux through the plastidial arogenate pathway, v_2 is the flux through the cytosolic phenylpyruvate pathway, v_c is the consumption rate of phenylalanine. To determine v_2, it was also required to know the mass balance of isotopic enrichment for phenylalanine as defined as:

$$\frac{df_{Phe}C_{Phe}}{dt} = f_{Tyr} * v_2 - f_{Phe} * v_c \qquad (2)$$

where f_{Phe} and f_{Tyr} represent isotopic abundance of phenylalanine and tyrosine, respectively, in the total pools. With (1) and (2), v_1 and v_2 can be derived as follows:

$$v_1 = \frac{(f_{Tyr}-f_{Phe})\frac{dC_{Phe}}{dt}-C_{Phe}\frac{df_{Phe}}{dt}}{f_{Tyr}} + \frac{f_{Tyr}-f_{Phe}}{f_{Tyr}}v_c \qquad (3)$$

$$v_2 = \frac{f_{Phe}\frac{dC_{Phe}}{dt}+C_{Phe}\frac{df_{Phe}}{dt}}{f_{Tyr}} + \frac{f_{Phe}}{f_{Tyr}}v_c \qquad (4)$$

Since the labeling percentage and concentration of phenylalanine increased linearly over 6 h, $\frac{dC_{Phe}}{dt}$ and $\frac{df_{Phe}}{dt}$ were computed from the slopes of the time-series data. Then every 6 min estimates of C_{Phe} and f_{Phe} were derived based on $\frac{dC_{Phe}}{dt}$ and $\frac{df_{Phe}}{dt}$. f_{Tyr} was the average labeling percentage of tyrosine along the experiment. To determine the control v_c, emitted volatiles from day 2 control flowers fed with 10 mM tyrosine were collected for 2, 4, and 6 h starting at 18:00 h. No statistical differences were found in the scent profiles of flowers fed with 10 mM tyrosine compared to control. Since the volatile amount was found to increase linearly, v_c was assumed to be constant during the experimental period, and was derived from the slope of the time-series data. The v_c for *PhpCAT* RNAi lines was subsequently determined by multiplying the control v_c by the average fractional decrease of total emission observed in lines 9 and 17 (Figure 3.5a). With these obtained values, v_1 and v_2 were calculated along the experimental period every 6 min by (3) and (4). The whole simulation was performed in Matlab R2013a environment (The MathWorks, Inc., Natick, MA). Variances in the estimated slopes were derived with a standard linear regression procedure as described[43], while setting the intercepts as constants was based on experimental measurements. Since flux values are the function of the estimated trend slopes and other experimental measurements, flux variances can then be derived by considering the propagation of errors based on:

$$\sigma_y^2 = \sum_{i=1}^{n} \sigma_{x_i}^2 \left(\frac{\partial y}{\partial x_i}\right)^2$$

$$\text{where } y = f(x_1, \dots x_n)$$

3.5.6 Preparation of plastids

Plastids were isolated from approximately 25 g of 1-3 day-old petals of control, *PhpCAT*-RNAi line 9, and *PhpCAT* overexpression line 3 petunia plants. Flowers were kept in the dark for 2 h prior to plastid preparations to deplete starch. Petals were placed in a chilled blender containing 200 ml ice-cold medium A (0.5 M sorbitol, 10 mM MES/NaOH pH 6.3, 4 mM Na-ascorbate, 4 mM cysteine, 2 mM $MgCl_2$, 1.5 mM KH_2PO_4, 1 mM $MnCl_2$, 1 mM EDTA-Na_2) and homogenized with three 2 s pulses. The resulting homogenate was filtered through two layers of Miracloth (Calbiochem, La Jolla, CA). An aliquot of filtrate (crude extract) was taken from each preparation and set aside, and the remainder was centrifuged at 6,000 *g*, 4°C for 5 min. The pellet was washed twice in medium B (0.33 M sorbitol, 10 mM MES/NaOH pH 7.6), resuspended in 2 ml of medium B, and layered over a discontinuous Percoll^{TM} gradient consisting of 80% (2 ml) and 25% (6 ml) Percoll^{TM} prepared in medium B. After centrifugation (9,200 *g*, 4°C for 20 min in a swinging bucket rotor with no brake applied), the intact plastid fractions (approximately 1.5 ml) were collected from the interface of the Percoll^{TM} layers, washed two times in medium B, and finally resuspended in 50 mM NaH_2PO_4 (pH 8.0) with 5% (v/v) glycerol, flash frozen, and stored at -80°C.

3.5.7 Immunoblots

Immunoblot analysis was performed essentially as described previously[44] using petunia crude extracts and plastids, *E. coli* crude extracts, and the purified PhpCAT$_{53\text{-}583}$. Protein sample concentration was determined by the Bio-Rad Bradford protein assay. To solubilize membrane proteins, protein loading dye containing 10% SDS was added to protein samples, which were then incubated at room temperature for three hours, and centrifuged at 5,000 *g* for 5 min to pellet debris. Immunodetection was performed on 2.5 μg protein using purified rabbit anti-PhpCAT polyclonal antibodies (1:3,000) generated against a synthetic peptide CMIDPDAPFSGAFMG (Genscript, Piscataway, NJ). A goat anti-rabbit IgG horseradish peroxidase conjugate (1:30,000) was used as secondary antibody (Bio-Rad, Hercules, CA). Antigen bands were visualized using an enhanced chemiluminescence reagent (PerkinElmer, Waltham, MA) according to the manufacturer's protocol, and exposing the gels on Eastman Kodak X-OMART AR film.

3.5.8 Chorismate mutase assays

CM assays were performed as described previously[10], except that they were adapted to HPLC detection as follows. Following reaction incubation and subsequent conversion of prephenate to phenylpyruvate by acid hydrolysis, reactions were neutralized by addition of 50 µl of 1 M NaOH, and 10 µl of the reaction mixture was analyzed by HPLC using the Waters Atlantis dC18 column (3µm, 2.1 x 150 mm) held at 35°C, with an 8-min linear gradient of 5-70% acetonitrile in 1% formic acid at a flow rate of 0.4 ml min^{-1}. Phenylpyruvate and chorismate were detected by absorbance at 288 nm and quantified by comparison to authentic standards.

3.5.9 Targeted metabolite profiling

Petunia volatiles were collected from detached 2-day-old flowers of wild type, *PhpCAT*-RNAi, and *PhpCAT* overexpression lines (three flowers per biological replicate) from 18:00 to 22:00 h using a closed-loop stripping method and analyzed by GC-MS as previously described[35]. Internal pools of the aromatic amino acids and organic acids (shikimate, prephenate, and arogenate) from control and transgenic tissues collected (minimum of eight flowers per biological replicate) were extracted at 20:00 h on day 2 post-anthesis were analyzed by LC-MS as previously described[10].

3.6 Table and Figures

Table 3.1 Changes in flux in flowers from control and *PhpCAT*-RNAi petunia lines at t_{0h} and t_{6h}

	Plastidial synthesis rate v_1 (μmol gFW^{-1} h^{-1})			**Cytosolic synthesis rate v_2 (μnmol gFW^{-1} h^{-1})**		
	t_{0h}	t_{6h}	Relative change at t_{6h}	t_{0h}	t_{6h}	Relative change at t_{6h}
Control	1.051±0.227	0.896±0.191	-14.7%	0.0067±0.0017	0.161±0.048	+2303%
PhpCAT RNAi	0.711±0.089	0.500±0.065	-29.7%	0.0068±0.0010	0.218±0.041	+3106%
Relative change in *PhpCAT* RNAi	-32.4%	-44.2%		+1.5%	+35.4%	

v_1 – absolute flux through the plastidial arogenate pathway;
v_2 – absolute flux through the cytosolic phenylpyruvate pathway;
(-) - indicates a decrease in flux at t_{6h} versus t_{0h} or in *PhpCAT* RNAi versus control
(+) - indicates an increase in flux at t_{6h} versus t_{0h}

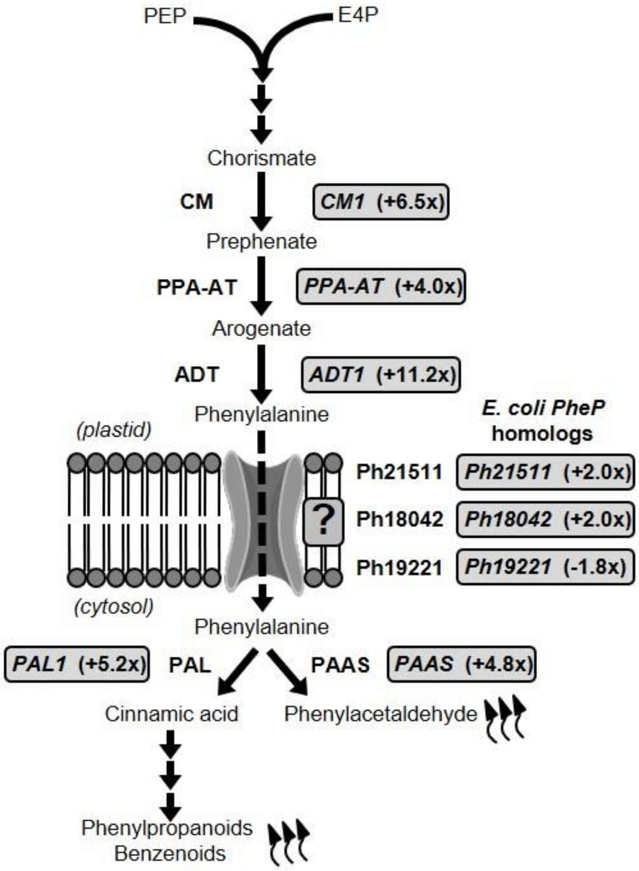
PEP
E4P
Chorismate
CM
CM1 (+6.5x)
Prephenate
PPA-AT
PPA-AT (+4.0x)
Arogenate
ADT
ADT1 (+11.2x)
Phenylalanine
(plastid)
E. coli PheP homologs
Ph21511
Ph21511 (+2.0x)
?
Ph18042
Ph18042 (+2.0x)
Ph19221
Ph19221 (-1.8x)
(cytosol)
Phenylalanine
PAL1 (+5.2x)
PAL
PAAS
PAAS (+4.8x)
Cinnamic acid
Phenylacetaldehyde
Phenylpropanoids
Benzenoids

Figure 3.1 Identification of plastidial phenylalanine transporter candidates.

Gray boxes depict average fold-change in gene expression in petunia flowers on day 2 postanthesis relative to the bud stage. Changes in expression are shown for petunia homologs of *E. coli pheP*, genes encoding plastidial phenylalanine biosynthetic enzymes chorismate mutase 1 (CM1), prephenate aminotransferase (PPA-AT), and arogenate dehydratase 1 (ADT1), as well as genes for the cytosolic phenylalanine-utilizing enzymes phenylalanine ammonia lyase 1 (PAL1) and phenylacetaldehyde synthase (PAAS). Measurement of gene expression is based on the average number of sequenced fragments ± s.e.m. (*n* = 3 biological replicates) found for a given contig (gene) per kilobase of sequence per million reads (FPKM) from RNA-Seq analysis of petunia flowers collected at 8 PM at the bud stage (day -1) and on day 2 postanthesis.

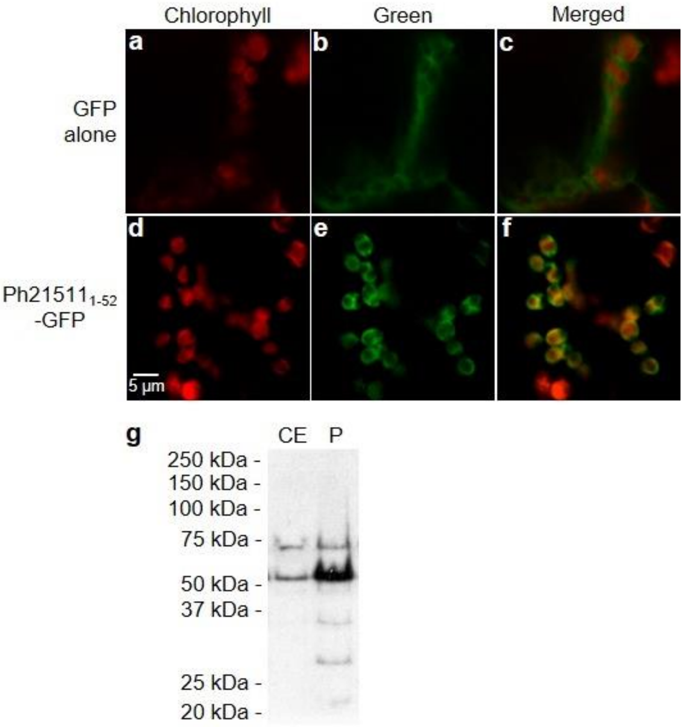
Chlorophyll
Green
Merged
a
b
c
GFP alone
d
e
f
Ph21511$_{1-52}$ -GFP
5 µm
g
CE
P
250 kDa -
150 kDa -
100 kDa -
75 kDa -
50 kDa -
37 kDa -
25 kDa -
20 kDa -

Figure 3.2 Ph21511 is localized to plastids

(a-c) Transient expression of GFP alone in leaves of *Nicotiana benthamiana*. **(d-f)** Transient expression of the first 52 amino acids of Ph21511 fused to the N-terminal end of GFP in leaves of *Nicotiana benthamiana*. Red pseudocolor of chlorophyll autofluorescence is shown in panels **a** and **d**. Green pseudocolor of GFP fluorescence is shown in panels **b** and **e**. Merged images of red and green pseudocolor from **a** and **b** and from **d** and **e** are shown in **c** and **f**, respectively. **(g)** Immunoblot using anti-Ph21511 antibodies against 60 µg protein from total crude extract and plastids prepared from day 2 petunia flowers

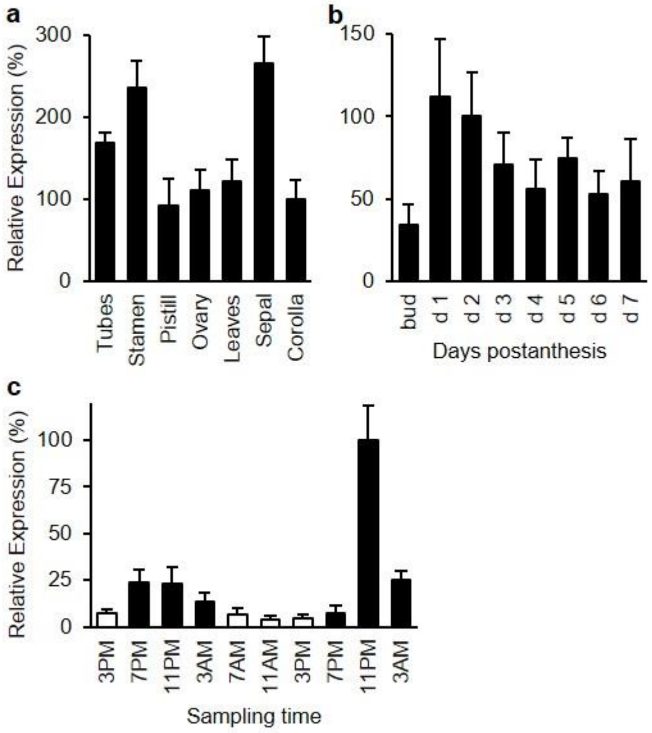

Figure 3.3 Expression profiles of *PhpCAT*

(a) Tissue-specific expression of *PhpCAT* in leaves and floral organs at 3 PM on day 2 postanthesis relative to corolla set at 100%. **(b)** Developmental *PhpCAT* expression profile at 3 PM in petunia flowers starting from the bud stage and on days 1 through 7 postanthesis relative to expression on day 2 set at 100%. **(c)** Rhythmic changes in *PhpCAT* expression in corollas of petunia flowers from day 1 to day 3 postanthesis during a normal light/dark cycle shown relative to expression at 11 PM on day 2 set at 100%. All transcript levels were determined by qRT-PCR and obtained relative to the reference gene (*elongation factor 1-α*). Data are means ± s.e.m. ($n = 3$ biological replicates).

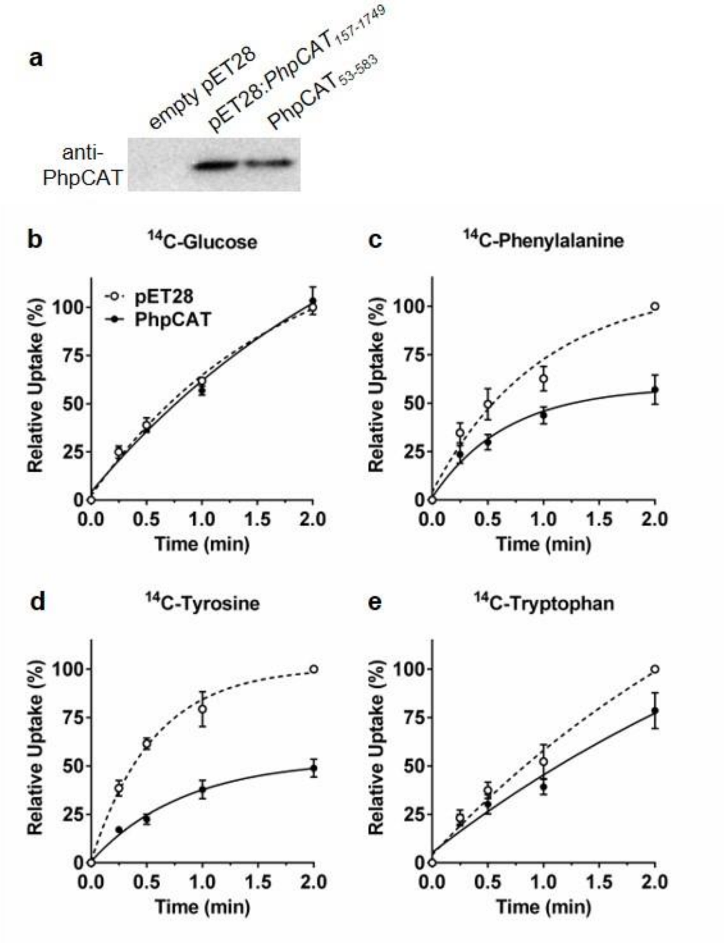

Figure 3.4 PhpCAT aromatic amino acid transport activity

(a) Immunoblots on 2.5 µg of whole cell crude extracts prepared from *E. coli* carrying an empty pET28a vector or codon optimized pET28a:*PhpCAT*$_{157\text{-}1749}$, and 2.5 µg of purified PhpCAT$_{53\text{-}583}$. **(b-e)** Transport assays on whole *E. coli* cells carrying empty pET28a (white circles) or pET28a:*PhpCAT*$_{157\text{-}1749}$ (black circles). An equal number of cells were incubated with 100 µM ^{14}C-glucose as a negative control (**b**), ^{14}C- phenylalanine (**c**), ^{14}C- tyrosine (**d**), or ^{14}C- tryptophan (**e**) for the indicated time periods until termination of the assays by rapid filtration. Data are presented as a percentage relative to the corresponding empty-vector control two minute time point set at 100%. Data are means ± s.e.m. (*n* ≥ 3 biological replicates). Two-tailed Student's *t-tests* revealed that relative accumulation of radiolabeled aromatic amino acids was statistically different in *E. coli*-expressing *PhpCAT* versus empty vector control ($p<0.01$).

Figure 3.5 Metabolic profiling of petunia flowers from *PhpCAT*-RNAi and *PhpCAT*-overexpression lines

(a) Effects of *PhpCAT* RNAi downregulation. **(b)** Effects of *PhpCAT* overexpression. *PhpCAT* mRNA levels (n = 3 biological replicates), internal pools of shikimate, prephenate, arogenate, phenylalanine, tyrosine, and tryptophan (n = 4), and total emission of phenylalalnine-derived volatiles ($n \geq 3$) were measured in three independent *PhpCAT*-RNAi downregulated and *PhpCAT* overexpression lines (white bars) and compared to wild type control (black bars), which were set at 100%. Data are means ± s.e.m. * = $p < 0.05$, ** = $p < 0.01$ by paired two-tailed Student's t-tests. Dotted lines indicate trafficking steps. White boxes with question marks indicate unknown transporters/transport steps. In (**a**) the "x" over PhpCAT depicts downregulation. In (**b**) the arrow with "OX" depicts overexpression. ADH, arogenate dehydrogenase; ADT, arogenate dehydratase; CHA, chorismate; CM, chorismate mutase; E4P, erythrose 4-phosphate; PPA-AT, prephenate aminotransferase; PDT, prephenate dehydratase; PEP, phosph*enol*pyruvate; PPY-AT, phenylpyruvate aminotransferase.

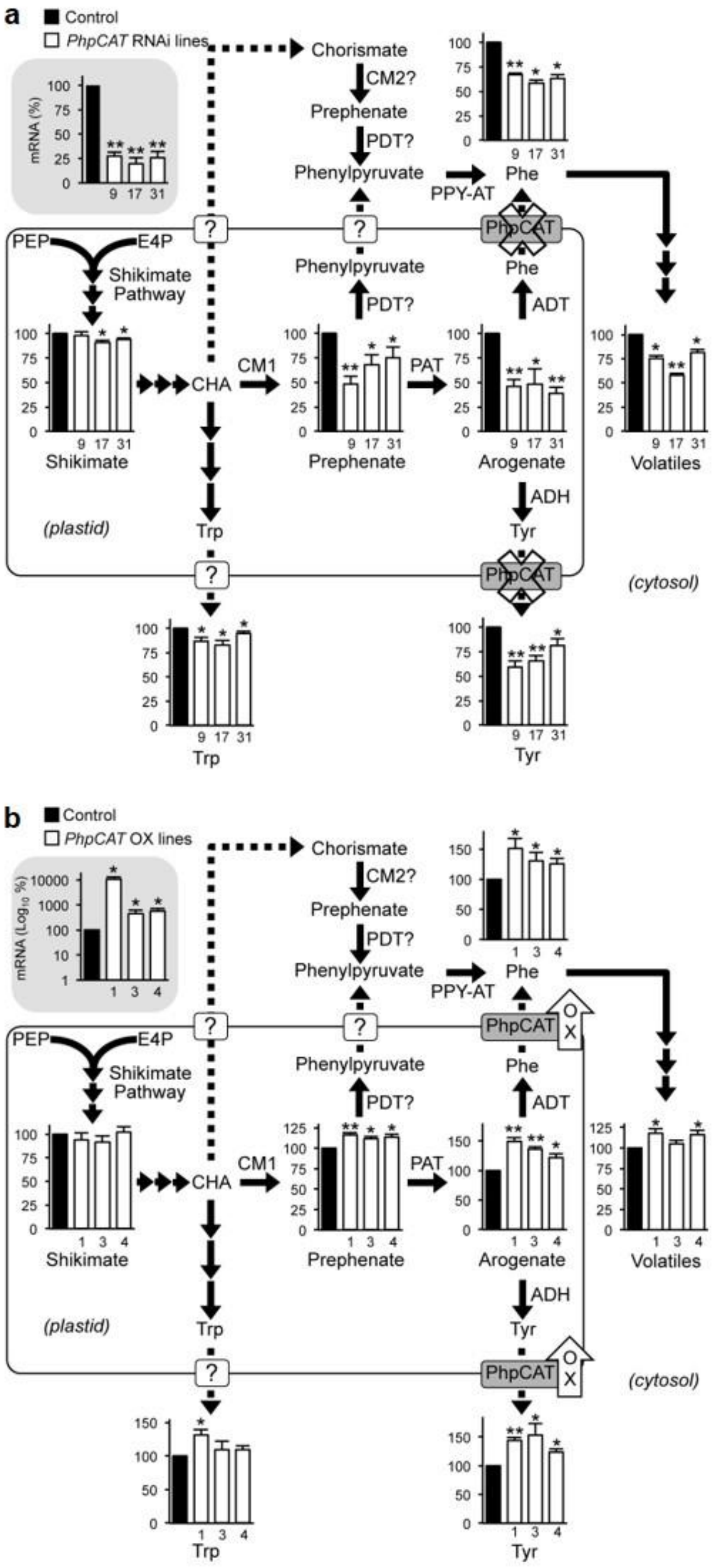
a
Control
PhpCAT RNAi lines
mRNA (%)
9 17 31
Chorismate
CM2?
Prephenate
PDT?
Phenylpyruvate
PPY-AT
Phe
?
PhpCAT
PEP
E4P
Shikimate Pathway
Phenylpyruvate
PDT?
Phe
ADT
CHA
CM1
PAT
Shikimate
Prephenate
Arogenate
Volatiles
ADH
(plastid)
Trp
Tyr
(cytosol)
Trp
Tyr
b
Control
PhpCAT OX lines
mRNA (Log10 %)
1 3 4
Chorismate
CM2?
Prephenate
PDT?
Phenylpyruvate
PPY-AT
Phe
PhpCAT
OX
PEP
E4P
Shikimate Pathway
Phenylpyruvate
PDT?
Phe
ADT
CHA
CM1
PAT
Shikimate
Prephenate
Arogenate
Volatiles
ADH
(plastid)
Trp
Tyr
(cytosol)
Trp
Tyr

Figure 3.6 Metabolic modeling of the phenylalanine biosynthetic network in control and *PhpCAT*-RNAi lines

(**a**)Scheme depicting cytosolic formation of phenylalanine and potential feedback inhibition mechanisms involved in plastidial phenylalanine biosynthesis[1]. In *PhpCAT*-RNAi lines, phenylalanine and tyrosine may accumulate in plastids and feedback inhibit arogenate dehydratase (ADT) and arogenate dehydrogenase (ADH), respectively, as well as chorismate mutase 1 (CM1). If plastidial ADTs also function as prephenate dehydratases (PDTs), then the enzymatic conversion of prephenate to phenylpyruvate may also be subject to feedback inhibition by phenylalanine. It is unclear if phenylpyruvate utilized in the alternative phenylalanine biosynthetic pathway originates from the plastid, or from cytosolic conversion of chorismate exported from the plastid. White boxes with question marks indicate unknown transporters/transport steps. AS, anthranilate synthase. For remaining abbreviations, see Figure 3.1. **(b)** Flux models representing the phenylalanine biosynthetic network in 2-day old petunia flowers from control and *PhpCAT*-RNAi lines. Computer-assisted metabolic modeling was performed using pool sizes and isotopic abundances of phenylalanine and tyrosine, and measurements of phenylalanine-derived volatile emission from petunia petal tissue supplied with 10 mM ^{15}N-tyrosine for up to 6 h. The rate of plastidial flux (v_1) in *PhpCAT*-RNAi lines was found to be significantly lower than control based on comparisons of absolute fluxes and two-tailed Student's *t-tests* corrected by Bonferroni method ($p < 0.05$). The rate of change in cytosolic flux (v_2) in *PhpCAT*-RNAi lines was found to be significantly higher than control ($p < 0.01$) based on paired sample two-tailed Student's *t-tests* of slopes. $n = 3$ for control and $n = 6$ for *PhpCAT*-RNAi lines.

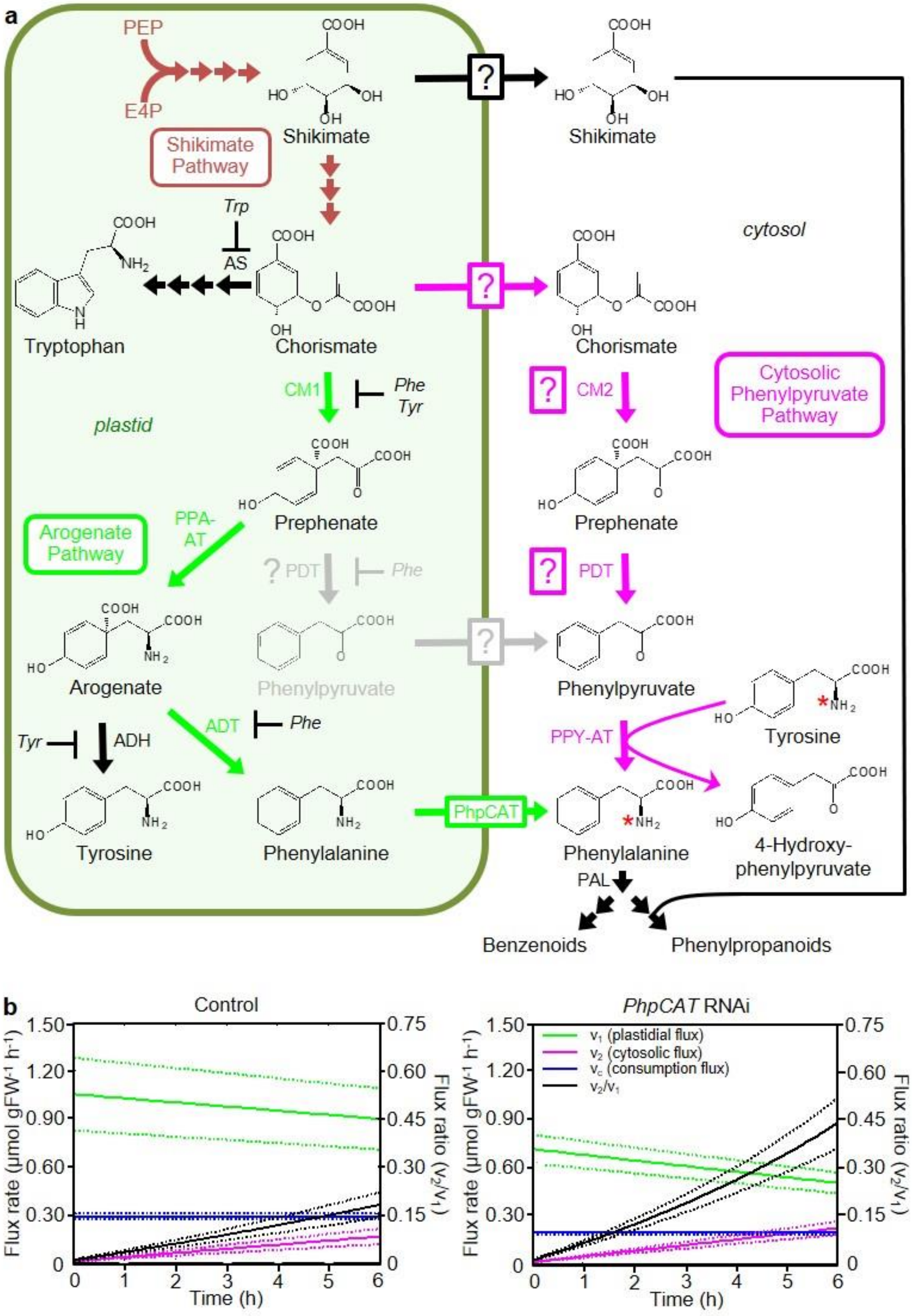
a
PEP
E4P
Shikimate Pathway
Shikimate
Trp
AS
Tryptophan
Chorismate
CM1
Phe
Tyr
plastid
Prephenate
Arogenate Pathway
PPA-AT
? PDT
Phe
Arogenate
Phenylpyruvate
ADT
Phe
Tyr
ADH
Tyrosine
Phenylalanine
PhpCAT
?
Shikimate
cytosol
?
Chorismate
? CM2
Cytosolic Phenylpyruvate Pathway
Prephenate
? PDT
?
Phenylpyruvate
Tyrosine
PPY-AT
Phenylalanine
4-Hydroxy-phenylpyruvate
PAL
Benzenoids
Phenylpropanoids
COOH
HO
OH
NH2
b
Control
PhpCAT RNAi
Flux rate (μmol gFW⁻¹ h⁻¹)
Flux ratio (v2/v1)
Time (h)
0
0.30
0.60
0.90
1.20
1.50
0.15
0.30
0.45
0.60
0.75
0 1 2 3 4 5 6
v1 (plastidial flux)
v2 (cytosolic flux)
vc (consumption flux)
v2/v1

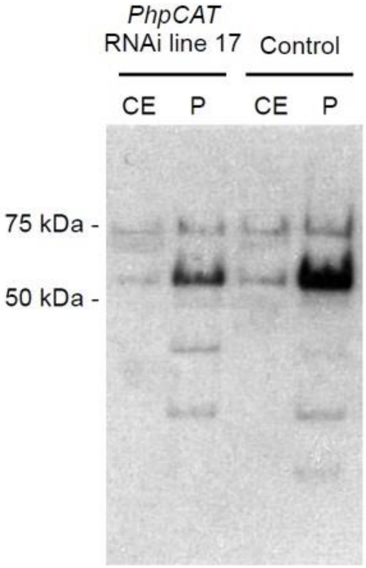
PhpCAT
RNAi line 17
Control
CE
P
CE
P
75 kDa -
50 kDa -

Figure 3.7 Immunoblot of PhpCAT in wild type and *PhpCAT*-RNAi transgenic line

Anti-PhpCAT (anti-Ph21511) antibodies were used against 60 ug protein isolated from crude extract (CE) and plastids (P) of day 2 petunia flowers from wild type control and *PhpCAT*-RNAi line 17. Mature PhpCAT is predicted to be 57.9kDa

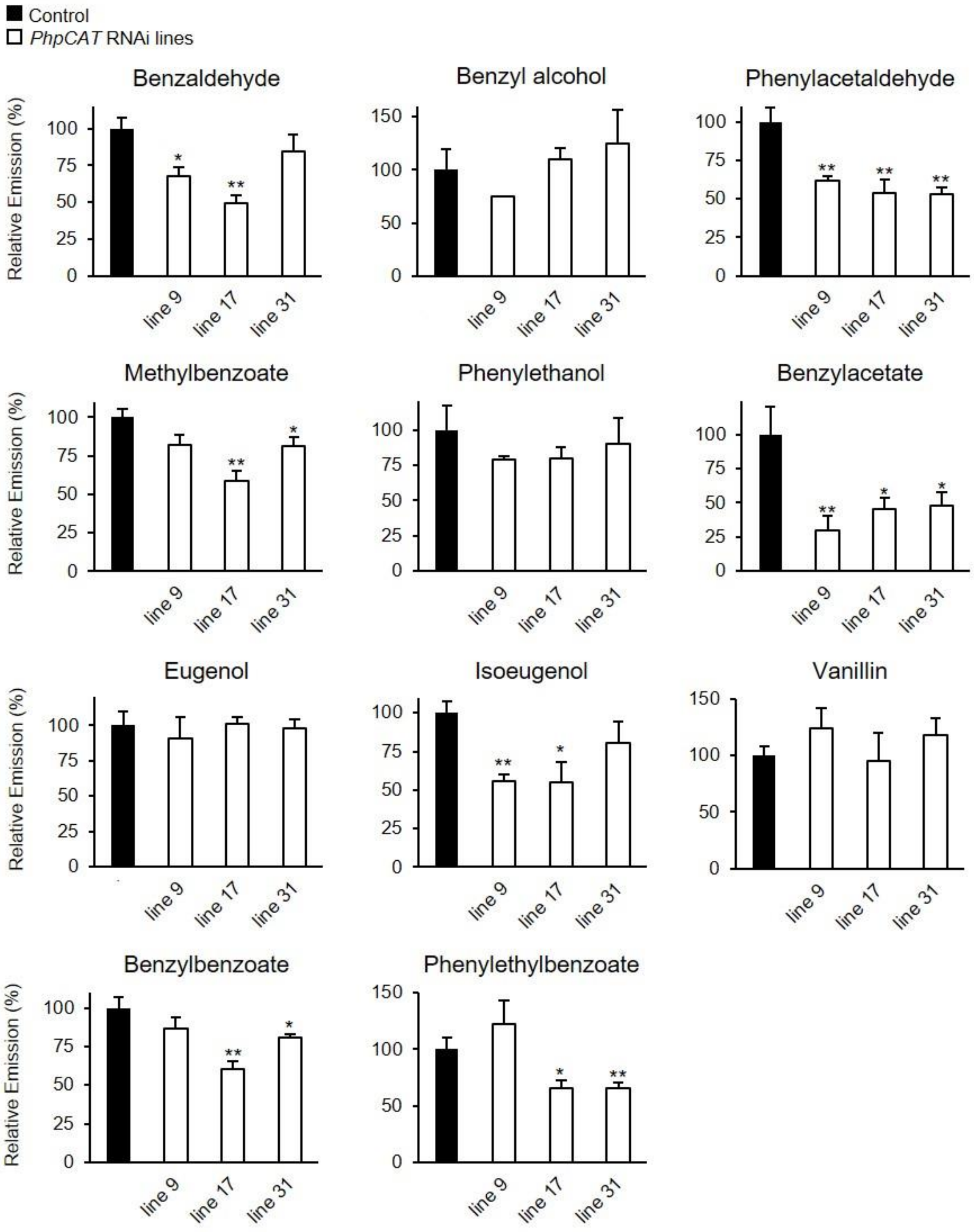

Figure 3.8 Effect of *PhpCAT* RNAi downregulation on emission of individual phenylalanine-derived volatiles from petunia petals.

Volatiles were collected from 6:00-10:00 PM on day 2 postanthesis and are presented as percentages of levels in wild-type set at 100%. Data are means ± s.e.m. ($n \geq 3$ biological replicates). * = $p < 0.05$, ** = $p < 0.01$ by paired two-tailed Student's t-tests.

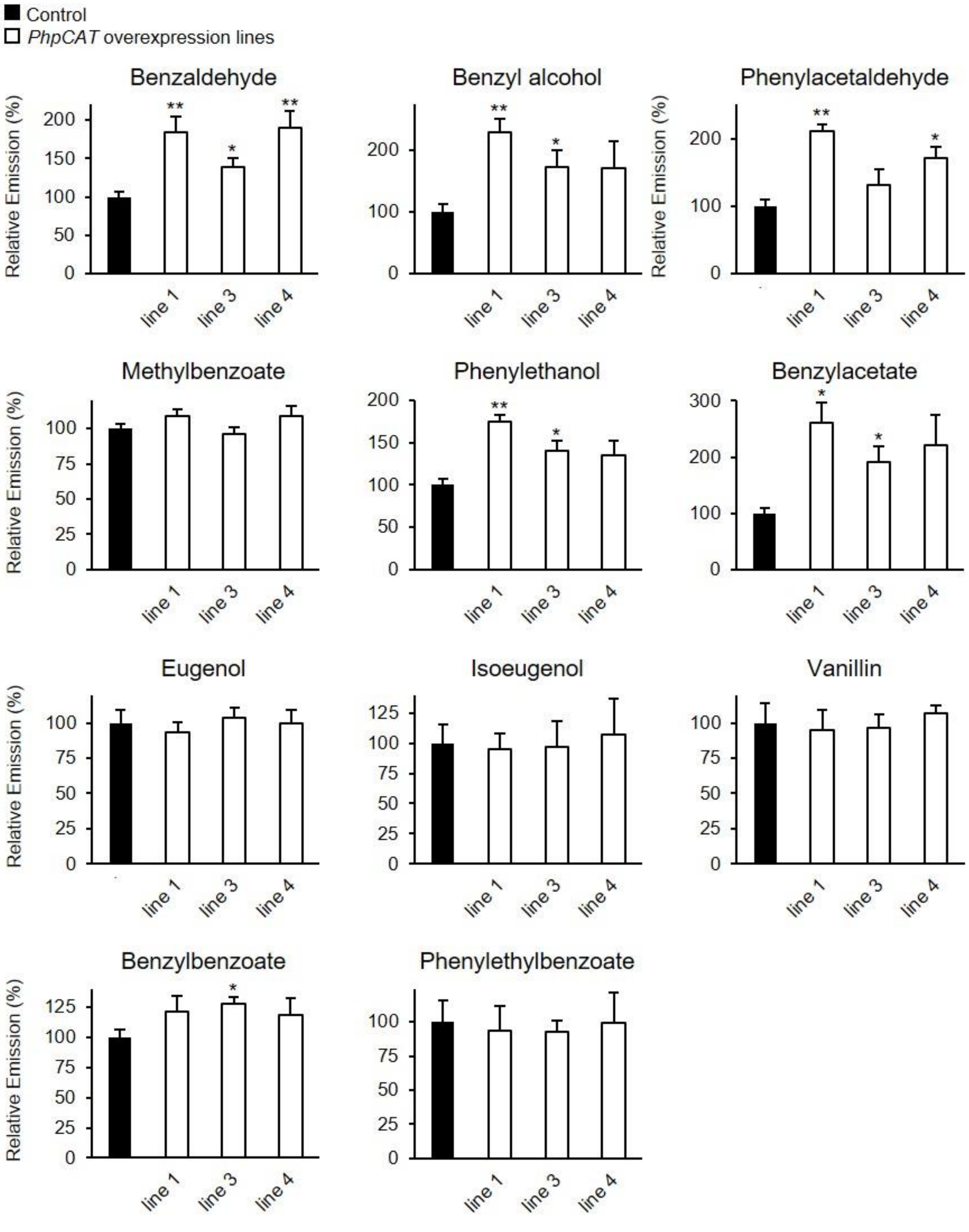

Figure 3.9 Effect of *PhpCAT* overexpression on emission of individual phenylalanine-derived volatiles from petunia petals

Volatiles were collected from 6:00-10:00 PM on day 2 postanthesis and are presented as percentages of levels in wild-type set at 100%. Data are means ± s.e.m. ($n \geq 3$ biological replicates). * = $p < 0.05$, ** = $p < 0.01$ by paired two-tailed Student's t-tests.

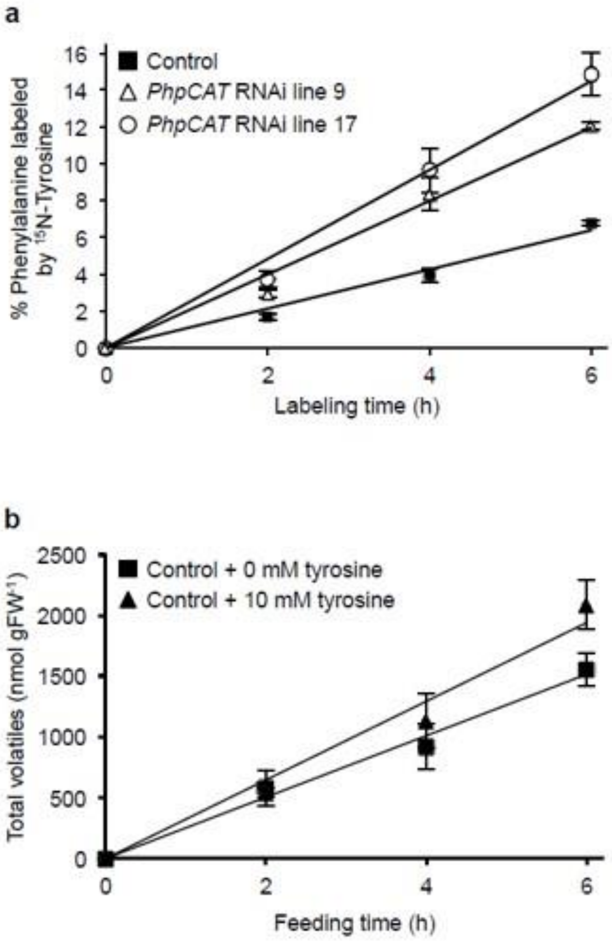

Figure 3.10 Effect of feeding ^{15}N-tyrosine on the labeling of phenylalanine and the levels of phenylalanine-derived volatiles

(a)Phenylalanine is more highly labeled by ^{15}N-tyrosine in *PhpCAT*-RNAi lines than control. 10 mM ^{15}N-tyrosine was fed to 2-day-old petunia flowers from control (solid square) and *PhpCAT*-RNAi lines 9 (open triangle) and 17 (open circle) for 2, 4, and 6 h beginning at 18:00 h. Labeling of phenylalanine pools were analyzed by TOF LC-MS. Data are means ± s.e.m. (n = 3 biological replicates, except for control 6-h time point, n = 2). Incorporation of ^{15}N-label into phenylalanine was linear over the 6-h time course (R^2 = 0.9834, 0.9858, and 0.9895 for control and *PhpCAT*-RNAi lines 9 and 17, respectively). (**b**) Feeding with tyrosine does not affect the emission rate of phenylalanine-derived volatiles. Two-day-old wild-type petunia flowers were fed with 0 (black squares) or 10 mM tyrosine (black triangles) for 2, 4, and 6 h beginning at 18:00 h. The total amount of phenylalanine-derived volatiles emitted was analyzed by GC-MS. Data are means ± s.e.m. (n = 3 biological replicates). The total amount of volatiles released remained constant over the 6-h time course (R^2 = 0.9878 and 0.9746 for control and 10 mM tyrosine-fed flowers, respectively), with no significant differences in slopes.

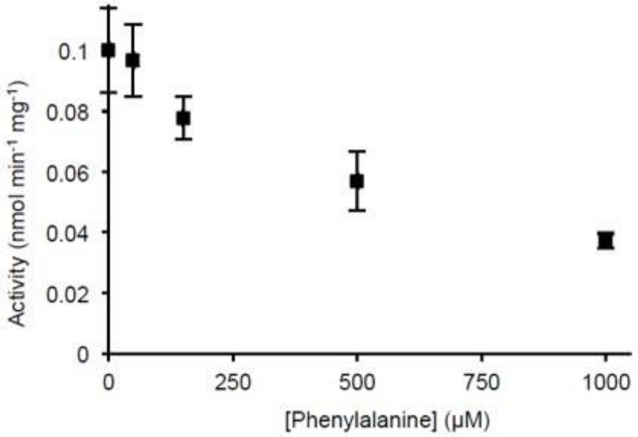

Figure 3.11 Phenylalanine inhibition of chorismate mutase activity in desalted petunia plastid extracts

Chorismate mutase activity was measured in desalted plastid extracts with the presence of various phenylalanine concentrations. Activity was measured by acidifying the reaction after incubation to convert enzymatically-formed prephenate to phenylpyruvate, which was quantified by HPLC. Plastids were isolated from day 2 petunia flowers at 21:00 h. Data are means ± s.e.m. (*n* = 3 biological replicates).

3.7 References

1. Maeda, H. & Dudareva, N. The shikimate pathway and aromatic amino acid biosynthesis in plants. *Annu. Rev. Plant Biol.* **63**, 73-105 (2012).
2. Ekholm, R. Biosynthesis of thyroid hormones. *Int. Rev. Cytol.* **120**, 243-288 (1990).
3. Fernstrom, J. D. & Fernstrom, M. H. Tyrosine, phenylalanine, and catecholamine synthesis and function in the brain. *J. Nutr.* **137**, 1539S-1547S (2007).
4. Haslam, E. In *Shikimic acid: metabolism and metabolites* (Wiley, 1993).
5. Razal, R. A., Ellis, S., Singh, S., Lewis, N. G. & Towers, G. H. N. Nitrogen recycling in phenylpropanoid metabolism. *Phytochemistry* **41**, 31-35 (1996).
6. Bonawitz, N. D. & Chapple, C. The genetics of lignin biosynthesis: connecting genotype to phenotype. *Annu. Rev. Genet.* **44**, 337-363 (2010).
7. Dudareva, N., Klempien, A., Muhlemann, J. K. & Kaplan, I. Biosynthesis, function and metabolic engineering of plant volatile organic compounds. *New Phytol.* **198**, 16-32 (2013).
8. Vlot, A. C., Dempsey, D. & Klessig, D. F. Salicylic acid, a multifaceted hormone to combat disease. *Annu. Rev. Phytopathol.* **47**, 177-206 (2009).
9. Vogt, T. Phenylpropanoid biosynthesis: invited review. *Mol. Plant* **3**, 2-20 (2009).
10. Maeda, H. *et al*. RNAi suppression of arogenate dehydratase1 reveals that phenylalanine is synthesized predominantly via the arogenate pathway in petunia petals. *Plant Cell* **22**, 832-849 (2010).
11. Maeda, H., Yoo, H. & Dudareva, N. Prephenate aminotransferase directs plant phenylalanine biosynthesis via arogenate. *Nat. Chem. Biol.* **7**, 19-21 (2011).
12. Yoo, H. *et al*. An alternative pathway contributes to phenylalanine biosynthesis in plants via a cytosolic tyrosine:phenylpyruvate aminotransferase. *Nat. Commun.* **4**: 2833 (2013).
13. Carruthers, A. & Melchior, D. L. Study of the relationship between bilayer water permeability and bilayer physical state. *Biochemistry* **22**, 5797-5807 (1983).
14. Chakrabarti, A. C. & Deamer, D. W. Permeability of lipid bilayers to amino acids and phosphate. *Biochimica et Biophysica Acta (BBA) - Biomembranes* **1111**, 171-177 (1992).
15. Weber, A. P. M., Schwacke, R. & Flügge, U. Solute transporters of the plastid envelope membrane. *Annu. Rev. Plant Biol.* **56**, 133-164 (2005).

16. Pohlmeyer, K., Soll, J., Steinkamp, T., Hinnah, S. & Wagner, R. Isolation and characterization of an amino acid-selective channel protein present in the chloroplastic outer envelope membrane. *Proc. Natl. Acad. Sci. USA* **94**, 9504-9509 (1997).
17. Pudelski, B., Kraus, S., Soll, J. & Philippar, K. The plant PRAT proteins - preprotein and amino acid transport in mitochondria and chloroplasts. *Plant Biol.* **12**, 42-55 (2010).
18. Pudelski, B. *et al*. The plastid outer envelope protein OEP16 affects metabolic fluxes during ABA-controlled seed development and germination. *J. Exp. Bot.* **63**,1919-1936 (2012).
19. Weber, A. P. M. & Linka, N. Connecting the plastid: transporters of the plastid envelope and their role in linking plastidial with cytosolic metabolism. *Annu. Rev. Plant Biol.* **62**, 53-77 (2011).
20. Reyes-Prieto, A. & Moustafa, A. Plastid-localized amino acid biosynthetic pathways of Plantae are predominantly composed of non-cyanobacterial enzymes. *Sci. Rep.* **2**: 955 (2012).
21. Yang, H., Bogner, M., Stierhof, Y. & Ludewig, U. H^+-independent glutamine transport in plant root tips. *PLoS ONE* **5**, e8917 (2010).
22. Yang, H., Krebs, M., Stierhof, Y. & Ludewig, U. Characterization of the putative amino acid transporter genes AtCAT2, 3 & 4: The tonoplast localized AtCAT2 regulates soluble leaf amino acids. *J. Plant Physiol.* **171**, 594-601 (2014).
23. Su, Y., Frommer, W. B. & Ludewig, U. Molecular and functional characterization of a family of amino acid transporters from Arabidopsis. *Plant Physiol.* **136**, 3104-3113 (2004).
24. Tegeder, M. & Rentsch, D. Uptake and partitioning of amino acids and peptides. *Mol. Plant* **3**, 997-1011 (2010).
25. Ljungdahl, P. O. & Daignan-Fornier, B. Regulation of amino acid, nucleotide, and phosphate metabolism in *Saccharomyces cerevisiae*. *Genetics* **190**, 885-929 (2012).
26. Pi, J., Wookey, P. J. & Pittard, A. J. Cloning and sequencing of the pheP gene, which encodes the phenylalanine-specific transport system of *Escherichia coli*. *J. Bacteriol.* **173**, 3622-3629 (1991).
27. Chye, M. L., Guest, J. R. & Pittard, J. Cloning of the aroP gene and identification of its product in *Escherichia coli* K-12. *J. Bacteriol.* **167**, 749-753 (1986).
28. Brown, K. D. Formation of aromatic amino acid pools in *Escherichia coli* K-12. *J. Bacteriol.* **104**, 177-188 (1970).

29. Koyanagi, T., Katayama, T., Suzuki, H. & Kumagai, H. Identification of the LIV-I/LS system as the third phenylalanine transporter in *Escherichia coli* K-12. *J. Bacteriol*. **186**, 343-350 (2004).
30. Boatright, J. *et al*. Understanding in vivo benzenoid metabolism in petunia petal tissue. *Plant Physiol.* **135**, 1993-2011 (2004).
31. Verdonk, J. C. *et al.* Regulation of floral scent production in petunia revealed by targeted metabolomics. *Phytochemistry* **62**, 997-1008 (2003).
32. Klempien, A. *et al*. Contribution of CoA ligases to benzenoid biosynthesis in petunia flowers. *Plant Cell* **24**, 2015-2030 (2012).
33. Colquhoun, T. A. *et al*. A petunia chorismate mutase specialized for the production of floral volatiles. *Plant J.* **61**, 145-155 (2010).
34. Hammes, U. Z., Nielsen, E., Honaas, L. A., Taylor, C. G. & Schachtman, D. P. AtCAT6, a sink-tissue-localized transporter for essential amino acids in Arabidopsis. *Plant J.* **48**, 414-426 (2006).
35. Orlova, I. *et al*. Reduction of benzenoid synthesis in petunia flowers reveals multiple pathways to benzoic acid and enhancement in auxin transport. *Plant Cell* **18**, 3458-3475 (2006).
36. Eberhard, J. *et al*. Cytosolic and plastidic chorismate mutase isozymes from *Arabidopsis thaliana*: molecular characterization and enzymatic properties. *Plant J.* **10**, 815-821 (1996).
37. Martinoia, E., Meyer, S., De Angeli, A. & Nagy, R. Vacuolar transporters in their physiological context. *Annu. Rev. Plant Biol.* **63**, 183-213 (2012).
38. Tohge, T. *et al*. Toward the storage metabolome: profiling the barley vacuole. *Plant Physiol.* **157**, 1469-1482 (2011).
39. Benkeblia, N., Shinano, T. & Osaki, M. Metabolite profiling and assessment of metabolome compartmentation of soybean leaves using non-aqueous fractionation and GC-MS analysis. *Metabolomics* **3**, 297-305 (2007).
40. Heinig, U., Gutensohn, M., Dudareva, N. & Aharoni, A. The challenges of cellular compartmentalization in plant metabolic engineering. *Curr. Opin. Biotechnol.* **24**, 239-246 (2013).

41. Gleave, A. A versatile binary vector system with a T-DNA organisational structure conducive to efficient integration of cloned DNA into the plant genome. *Plant Mol. Biol.* **20**, 1203-1207 (1992).

42. Horsch, R. B. *et al*. A simple and general method for transferring genes into plants. *Science* **227**, 1229-1231 (1985).

43. Press, W.H. In *Numberical recipes 3rd edition: The art of scientific computing* (Cambridge University Press, 2007).

44. Dudareva, N. *et al.* Developmental Regulation of Methyl Benzoate Biosynthesis and Emission in Snapdragon Flowers. *Plant Cell.* **12**, 949-961 (2000).

45. Karimi, M., Inze, D. & Depicker, A. GATEWAY vectors for Agrobacterium-mediated plant transformation. *Trends Plant Sci.* **7**, 193-195 (2002).

46. Bordych, C., Eisenhut, M., Pick, T. R., Kuelahoglu, C. & Weber, A. P. M. Co-expression analysis as tool for the discovery of transport proteins in photorespiration. *Plant Biol.* **15**, 686-693 (2013).

47. Pick, T. R. *et al*. PLGG1, a plastidic glycolate glycerate transporter, is required for photorespiration and defines a unique class of metabolite transporters. *Proc. Natl. Acad. Sci. USA* **110**, 3185-3190 (2013).

48. Qualley, A. V., Widhalm, J. R., Adebesin, F., Kish, C. M. & Dudareva, N. Completion of the core β-oxidative pathway of benzoic acid biosynthesis in plants. *Proc. Natl. Acad. Sci. USA* **109**, 16383-16388 (2012).

49. Van Moerkercke, A., Schauvinhold, I., Pichersky, E., Haring, M. A. & Schuurink, R. C. A plant thiolase involved in benzoic acid biosynthesis and volatile benzenoid production. *Plant J.* **60**, 292-302 (2009).

50. Kolosova, N., Gorenstein, N., Kish, C. M. & Dudareva, N. Regulation of circadian methyl benzoate emission in diurnally and nocturnally emitting plants. *Plant Cell* **13**, 2333-2347 (2001).

51. Tjaden, J., Schwöppe, C., Möhlmann, T., Quick, P. W. & Neuhaus, H. E. Expression of a plastidic ATP/ADP transporter gene in *Escherichia coli* leads to a functional adenine nucleotide transport system in the bacterial cytoplasmic membrane. *J. Biol. Chem.* **273**, 9630-9636 (1998).

52. Klaus, S. M. J. *et al*. Higher plant plastids and cyanobacteria have folate carriers related to those of trypanosomatids. *J. Biol. Chem.* **280**, 38457-38463 (2005).
53. Bedhomme, M. *et al*. Folate metabolism in plants: an Arabidopsis homolog of the mammalian mitochondrial folate transporter mediates folate import into chloroplasts. *J. Biol. Chem.* **280**, 34823-34831 (2005).
54. Pavón, L. R. *et al*. Arabidopsis ANTR1 is a thylakoid Na+-dependent phosphate transporter: functional characterization in *Escherichia coli*. *J. Biol. Chem.* **283**, 13520-13527 (2008).
55. Eudes, A. *et al*. Identification of transport-critical residues in a folate transporter from the folate-biopterin transporter (FBT) Family. *J. Biol. Chem.* **285**, 2867-2875 (2010).
56. Furumoto, T. *et al*. A plastidial sodium-dependent pyruvate transporter. *Nature* **476**, 472-475 (2011).

CHAPTER 4. COMPLETION OF THE CYTOSOLIC POST-CHORISMATE PHENYLALANINE BIOSYNTHETIC PATHWAY IN PLANTS[3]

4.1 Abstract

In addition to being a vital component of proteins, phenylalanine is also a precursor of numerous aromatic primary and secondary metabolites with broad physiological functions. In plants phenylalanine is synthesized predominantly via the arogenate pathway in plastids. Here, we describe the structure, molecular players and subcellular localization of a microbial-like phenylpyruvate pathway for phenylalanine biosynthesis in plants. Using a reverse genetic approach and metabolic flux analysis, we provide evidence that the cytosolic chorismate mutase is responsible for directing carbon flux towards cytosolic phenylalanine production via the phenylpyruvate pathway. We also show that an alternative transcription start site of a known plastidial enzyme produces a functional cytosolic prephenate dehydratase that catalyzes the conversion of prephenate to phenylpyruvate, the intermediate step between chorismate mutase and phenylpyruvate aminotransferase. Thus, our results complete elucidation of phenylalanine biosynthesis via phenylpyruvate in plants, showing that this pathway splits from the known plastidial arogenate pathway at chorismate, instead of prephenate as previously thought, and the complete pathway is localized in the cytosol.

---

[3] This chapter has been published in Qian *et al.* (2019) Nature Communications.

Qian, Y., Lynch, J. H., Guo, L., Rhodes, D., Morgan, J. A., & Dudareva, N. (2019). Completion of the cytosolic post-chorismate phenylalanine biosynthetic pathway in plants. *Nature communications, 10*(1), 15. DOI: https://doi.org/10.1038/s41467-018-07969-2

4.2 Introduction

Plants have a high demand for the aromatic amino acids L-phenylalanine, L-tyrosine, and L-tryptophan, as they serve as precursors for the formation of proteins and numerous aromatic primary and secondary metabolites[1]. Phenylalanine, for example, is a precursor of > 8000 plant phenolic compounds, including the hormone salicylic acid[2], quinones (ubiquinone)[3], pigments (anthocyanins), aromatic volatiles[4,5], phytoalexins, feeding deterrents (tannins), UV protectants (flavonoids), signal molecules (isoflavonoids)[6], and structural components (lignin, suberin, and cell wall-associated phenolics)[6,7]. Broad physiological functions of these compounds and their importance for plant growth, development, reproduction, defense, and environmental responses explain the high carbon flux through the phenylalanine metabolic network[1]. In contrast to plants, animals lack the ability to synthesize phenylalanine and rely on a dietary supply. Moreover, phenylalanine-derived plant natural products possess biological activities and provide protection against a broad range of human diseases[8]. They are also used by humans as flavors, fragrances, biofuels and insecticides[9].

In plants, biosynthesis of phenylalanine occurs via two alternative pathways, both requiring conversion of chorismate, the final product of the shikimate pathway, to prephenate by chorismate mutase. Genetic studies showed that out of the two pathways the major carbon flux is directed through the arogenate pathway[10–12], which is initiated by transamination of prephenate to arogenate, followed by its decarboxylation/dehydration to phenylalanine (Figure 4.1). In the alternative phenylpyruvate pathway, the order of reactions is reversed, and prephenate is first decarboxylated/dehydrated to phenylpyruvate, which is then transaminated to phenylalanine. Most microorganisms use the phenylpyruvate pathway to synthesize phenylalanine, but knowledge about this route in plants is still very fragmented[1,13]. The contribution of phenylpyruvate to phenylalanine biosynthesis has been demonstrated in Arabidopsis and petunia expressing a bacterial bifunctional CM/PDT in plastids[14,15]. However, to date no genes involved in this route have been identified in plants, except for a phenylpyruvate aminotransferase (PPY-AT) preferentially converting phenylpyruvate to phenylalanine[16]. While the enzymes involved in the arogenate pathway are localized in plastids, PPY-AT is instead localized in the cytosol[16]. This discovery raised the question of the origin of the phenylpyruvate used by the cytosolic PPY-AT in the microbial-like phenylpuryvate pathway in plants, and by extension, the subcellular localization of the entire pathway and its branching point from the known plastidial arogenate pathway.

It is possible that phenylpyruvate originates from the action of plastidial arogenate dehydratases (ADTs) with moonlighting prephenate dehydratase (PDT) activity[10,17–19] (Figure 4.1). To date, six, nine, four and three ADT genes have been identified in Arabidopsis, pine, rice and petunia, respectively[10,17–19], encoding enzymes that are all localized in plastids[10,19,20]. Although some of these ADTs can use prephenate as substrate, the presence of prephenate aminotransferase (PPA-AT) converting prephenate to arogenate in the same subcellular compartment with catalytic efficiency that is at least 50- (Arabidopsis) to 900-fold (petunia) higher than that of respective ADTs with prephenate likely prevents formation of phenylpyruvate to support cytosolic phenylalanine biosynthesis (Figure 4.1)[21]. Alternatively, formation of phenylpyruvate could take place in the cytosol, requiring a cytosolic pool of prephenate (Figure 4.1).

Previously it has been shown that a plastidial chorismate mutase (CM1) is predominantly responsible for phenylalanine production in petunia[22]. Nevertheless, for many years it has been known that plants also contain cytosolic chorismate mutase (CM2)[23–27], but its physiological function remains unknown. The wide acceptance of plastids being the exclusive site of aromatic amino acid biosynthesis, *a priori* excluded the consideration of CM2 involvement in phenylalanine biosynthesis but instead led to multiple proposals of alternative functions[22,23,28]. However, recent discovery of cytosolic PPY-AT[16] and the widespread occurrence of cytosolic CM2s in plant species urge reconsideration of CM2 function and raise the prospect that plants contain a complete phenylpyruvate pathway for phenylalanine biosynthesis in the cytosol.

Here we used flowers of *Petunia hybrida* cv Mitchell, which have high carbon flux through the phenylalanine biosynthetic network and emit high levels of exclusively phenylalanine-derived volatiles[29,30] to identify architecture and subcellular localization of the phenylpyruvate pathway for phenylalanine biosynthesis. By combining reverse genetic and metabolic flux analyses, we demonstrated that the cytosolic CM2 catalyzes the first step in the cytosolic phenylpyruvate pathway. We also show that the intermediate step between chorismate mutase and phenylpyruvate aminotransferase is catalyzed by prephenate dehydratase, the cytosolic localization of which is the result of transcription from an alternative transcription start site of a known gene encoding a plastidial enzyme. Together these data complete elucidation of the microbial-like phenylpyruvate pathway in petunia and show that the whole pathway is localized in the cytosol.

4.3 Results

4.3.1 PhCM2 is required for cytosolic phenylalanine biosynthesis

Like all flowering plants[28], *Petunia hybrida* contains both a plastidial CM (PhCM1) and a cytosolic CM (PhCM2)[22]. Biochemical characterization of both recombinant petunia enzymes revealed that, as it has been reported in Arabidopsis (K_m for chorismate 550 μM and 150 μM for AtCM1 and AtCM2, respectively;[28]), PhCM2 has higher affinity towards chorismate (K_m for chorismate 174 μM and 8.6 μM for PhCM1 and PhCM2, respectively) (Table 4.1 and Figure 4.7a and b). Moreover, both petunia enzymes are catalytically more efficient (k_{cat}/K_m) and differences between their catalytic efficiencies are more pronounced than those for Arabidopsis enzymes likely reflecting the need to sustain the high flux towards phenylalanine and subsequently phenylalanine-derived volatiles in the floral tissue. Indeed, apparent catalytic efficiency of PhCM2 is 49.7-fold higher than that of PhCM1 (Table 4.1), while in Arabidopsis this difference is only 8.8-fold[28].

Previous report of *PhCM1* RNAi downregulation supports its *in planta* role in phenylalanine biosynthesis in plastids[22], however, an *in vivo* function of PhCM2, or CM2 from any plant species, has not been established. To determine if *PhCM2* expression correlates with known phenylalanine biosynthetic genes, either the arogenate or phenylpyruvate pathways, *PhCM2* transcript levels were analyzed in petunia flowers by quantitative RT-PCR (qRT-PCR) with gene-specific primers. Like *PhPPY-AT*, *PhCM2* transcripts were found in all floral tissues and leaves (Figure 4.8a) demonstrating that *PhCM2* expression does not exhibit spatial profile typical for genes involved in the arogenate pathway, *PhADT1* and *PhPPA-AT*,[10,16,21]. However, similar to *PhADT1* and *PhPPA-AT*, *PhCM2* mRNA levels in corolla increased after flower opening although to a lesser extent (Figure 4.8b). In addition, *PhCM2* transcripts exhibited rhythmicity with the highest levels at 19:00 and 23:00 h (Figure 4.8c), which corresponds to the peak of phenylalanine content[10] and emission of phenylalanine-derived volatiles[29,30] over a daily light/dark cycle.

To examine the *in vivo* function of PhCM2, its expression was down-regulated in petunia flowers using RNAi approach under the control of a petal-specific promoter[31]. Thirty independent transgenic lines were generated and three lines with the greatest decrease in *PhCM2* transcript levels (~90%) were selected for further analysis and metabolic profiling (Figure 4.2a). RNAi suppression of *PhCM2* expression resulted in 66% - 81% reduction in CM activity detected in cytosolic fraction relative to wild type (Figure 4.2b). It should be noted that the reduction in the cytosolic CM activity in transgenic lines is underestimated since cytosolic fraction contained some plastidial proteins, including PhCM1, based on PPA-AT activity used as plastidial marker (Figure 4.9a). In plastids, which were free from cytosolic contamination based on alcohol dehydrogenase activity assays (Figure 4.9b), CM activity remained unchanged and showed similar enrichment relative to crude extract (2.5-fold on average across *PhCM2*-RNAi lines) (Figure 4.2b) as PPA-AT activity (2.4-fold on average across *PhCM2*-RNAi lines and wild type (Figure 4.9a). Reduced *PhCM2* expression led to a decrease in endogenous phenylalanine levels in the petals by 33% to 64% compared to wild type (Figure 4.2c), which was metabolically indistinguishable from empty vector control (Figure 4.10). Transgenic flowers also emitted 30% to 37% less phenylalanine-derived volatiles relative to wild type (Figure 4.2c), but the extent of decrease varied among the individual compounds (Figure 4.11). In addition, tyrosine levels in the petals of *PhCM2* RNAi lines were increased by 31% to 41% at least in two transgenic lines relative to controls (Figure 4.2c). Tyrosine is a known amino donor for PhPPY-AT[16], an enzyme which is downstream of CM2 in the phenylpyruvate pathway (Figure 4.1), thus its accumulation is consistent with reduced flux towards cytosolic phenylalanine biosynthesis. In contrast to tyrosine, tryptophan levels were decreased by 52% to 65% in transgenics (Figure 4.2c). At the same time, analysis of internal pools of shikimate and phenylalanine biosynthetic intermediates revealed that prephenate was reduced by 25% to 33% (Figure 4.2c) and arogenate by 19% to 53% relative to controls, while shikimate remained unchanged except for transgenic line 15, which exhibited 15% reduction (Figure 4.2c). The levels of phenylpyruvate remained below detection limit, while we were unable to detect chorismate in plant tissue.

4.3.2 PhCM2 influences flux through both phenylalanine pathways

We previously developed a strategy to determine the relative flux through the phenylpyruvate pathway based on the unique property of cytosolic PhPPY-AT to use tyrosine as its amino donor[16,32]. Since the plastidial PPA-AT is unable to use tyrosine[21], the incorporation of ^{15}N label into the amino group of phenylalanine from ^{15}N-tyrosine allows assessment of flux through the phenylpyruvate pathway[16]. To determine the effect of *PhCM2*-RNAi downregulation on the carbon flux through the phenylalanine biosynthetic pathways, 2-day-old control and *PhCM2* RNAi line 17 flowers were fed with 10mM ^{15}N-tyrosine starting at 18:00 h. After 2, 4 and 6 h of feeding, phenylalanine and tyrosine pool sizes and their isotopic abundances were analyzed by liquid chromatography-mass spectrometry (LC-MS) and used in our recently developed metabolic flux model of the phenylalanine biosynthetic network[32]. As previously reported[16,32], the labeling percentage of phenylalanine increased linearly over a 6 h period (Figure 4.12). The model revealed that v_2, the flux through the cytosolic phenylpyruvate pathway, was 76% and 85% lower ($p < 0.0005$, two tailed Student's *t*-test, n=3, Bonferroni corrected) at t_0 and t_6, respectively, in *PhCM2* RNAi plants relative to control (Figure 4.3 and Table 4.2), further supporting that PhCM2 contributes to phenylalanine biosynthesis via the cytosolic phenylpyruvate pathway. At the same time, the flux analysis showed that in *PhCM2*-RNAi line, v_1, the flux through the plastidial arogenate pathway, was also decreased by 39% and 37% ($p < 0.005$, two tailed Student's *t*-test, n=3, Bonferroni corrected) at t_0, and t_6, respectively, relative to control (Figure 4.3 and Table 4.2). The decrease in plastidial aromatic amino acid biosynthesis is consistent with observed decrease in internal pools of arogenate and tryptophan (Figure 4.2c).

The decreased flux through the arogenate pathway in *PhCM2* transgenics could be the result of a decreased consumption of cytosolic chorismate, accumulation of which could reduce export of chorismate from plastids, and redirecting it to the formation of aromatic amino acids in this organelle. If the resulting increase in plastidial phenylalanine and tyrosine pools then exceeds transport capability of PhpCAT, a plastidial aromatic amino acid transporter[32], it would lead to their buildup, and inhibit upstream enzymes within the network. To test if such feedback regulation occurs and can be overcome by feeding of shikimate pathway intermediate, 2-day-old *PhCM2*-RNAi and control petunia petals were fed with 100 mM shikimate for 7 h starting at 15:00 h and pool sizes of arogenate, prephenate and phenylpyruvate as well as aromatic amino acids were analyzed. Feeding of shikimate increased internal pools of phenylalanine biosynthetic intermediates, arogenate, prephenate and phenylpyruvate, as well as tyrosine, in both genetic backgrounds such that there were no statistical differences between control and transgenics for any of those compounds after feeding except for arogenate, which still remained 30% lower in transgenics (Figure 4.13). In contrast, phenylalanine and tryptophan were increased only in the *PhCM2* RNAi background, with phenylalanine, but not tryptophan, still remaining below wild type levels. These results indicate that increased availability of shikimate recovers the plastidial aromatic amino acid flux in the *PhCM2* RNAi line to wild type levels, while cytosolic flux remains depressed. A decrease in the cytosolic flux persists despite a dramatic accumulation in phenylpyruvate. This may indicate that phenylpyruvate is being formed within the plastid by PDT activity of ADTs and is inaccessible to the cytosolic PhPPY-AT due to limited transport out of plastids.

To determine whether a reduced flux through the arogenate pathways is the result of transcriptional regulation of: (*i*) 3-deoxy-D-*arabino*-heptulosonate 7-phosphate synthase (DAHPS), which catalyzes the first committed step in the shikimate pathway[33,34]; (*ii*) other genes encoding key enzymes of the shikimate pathway (e.g. 5-enolpyruvylshikimate 3-phosphate synthase, EPSPS, and CM1), or (*iii*) petunia shikimate pathway transcriptional regulator ODORANT1 (ODO1)[35], their transcript levels were analyzed in petals of transgenic and control plants using qRT-PCR. This analysis revealed that expression of these genes remained unchanged in *PhCM2*-RNAi plants relative to control (Figure 4.14a). Likewise, activities of PPA-AT and ADT in plastids were unaffected by *PhCM2* down-regulation (Figures 4.9a and 4.14b).

To assess whether feedback regulation within the plastidial aromatic amino acid network can be overcome by an increased capacity of a plastidial Phe transporter, *PhpCAT* was transiently overexpressed in *PhCM2*-RNAi flowers and compared to that in wild type control. *PhpCAT* overexpression led to a significant increase in phenylalanine levels and emission of phenylalanine-derived volatiles in both backgrounds (Figure 4.15), demonstrating that the increased consumption flux of phenylalanine corresponds to an increase in its plastidial biosynthesis, supporting the feedback regulation hypothesis.

4.3.3 CM2 contributes to phenylalanine biosynthesis in Arabidopsis

To determine whether CM2 is involved in phenylalanine biosynthesis via the phenylpyruvate pathway in other plant species, we searched TAIR database for Arabidopsis *AtCM2* T-DNA insertion mutants. Two T-DNA insertion lines were identified: a N414383 (*cm2-1*) line, carrying a T-DNA insertion within the 3rd exon of the *AtCM2* gene (At5g10870), and a CS849985 (*cm2-2*) line with a T-DNA insertion in the 3rd intron (Figure 4.4a). The genotypes of obtained homozygous *cm2* plants were confirmed by genomic PCR analysis with gene-specific primers flanking the insertion sites, which failed to amplify the respective gene regions (Figure 4.4b). No *AtCM2* transcripts were detected in *cm2* mutants by RT-PCR (Figure 4.4c). Analysis of aromatic amino acid internal pools in leaves revealed no differences between *cm2* mutants and wild type plants (Figure 4.4d). We have previously shown that mechanical wounding of Arabidopsis leaves increases emission of phenylacetaldehyde, which is formed directly from phenylalanine by aromatic aldehyde synthase (AtAAS), a bifunctional enzyme that catalyzes phenylalanine decarboxylation/deamination[36]. While mechanical wounding increased phenylacetaldehyde emission in wild type leaves, there were no changes in phenylacetaldehyde emission in wounded leaves of either *cm2-1* or *cm2-2* mutants, levels of which were similar to that in unwounded wild type leaves (Figure 4.4e). Analysis of *AtAAS* expression by qRT-PCR revealed that its transcript levels were increased to the same degree in *cm2* mutant as in wild type leaves upon wounding (Figure 4.4f). Furthermore, wounding of wild type leaves increased expression of *AtCM2* by 2-fold (Figure 4.4g). Taken together, these results indicate that AtCM2 contributes to phenylalanine biosynthesis and subsequently to phenylpropanoid metabolism in Arabidopsis, especially when demand for phenylpropanoids is increased as a part of plant defense.

4.3.4 Alternative transcription produces cytosolic PhADT3 isoform

In the cytosol, PhCM2 produces prephenate and PhPPY-AT converts phenylpyruvate to phenylalanine, thus we hypothesized that the conversion of prephenate to phenylpyruvate by PDT takes place in the same subcellular compartment (Figure 4.1). To date, PDT activity has been detected only in etiolated Arabidopsis seedlings[37]. Since PDT activity was below detection limit when analyzed in cytosolic fraction obtained from petal tissue, petunia petals were subjected to non-aqueous fractionation and PDT activity as well as activities of compartment-specific marker enzymes (phospho*enol*pyruvate carboxylase, PEPC, and NADPH-dependent glyceraldehyde-3-phosphate dehydrogenase, GAPDH, for cytosol and plastid, respectively) were analyzed within the gradient fractions to assess subcellular enrichment (Figure 4.16), which was determined using best fit algorithm[38]. In parallel, activities of several enzymes with established subcellular localizations were used to validate this approach. Indeed, phenylalanine ammonia lyase, PAL[39], PPA-AT[12] and PPY-AT[16] were correctly found to be localized in the cytosol, plastids, and cytosol, respectively (Figures 4.16 and 4.17). Moreover, CM activity in the presence of 20 µM and 500 µM chorismate was predominantly distributed in the cytosol and plastids, respectively, consistent with high and lower affinity of petunia cytosolic and plastidial CM isoforms for this substrate (Table 4.1). Plastidial, but not cytosolic, CMs have previously been shown to be activated by tryptophan[28]. Assays performed in the presence of 1 mM tryptophan resulted in almost exclusive plastidial localization of CM activity (Figures 4.16 and 4.17). Analysis of PDT activity revealed a split at nearly a 1:1 ratio between cytosol and plastids (Figures 4.16 and 4.17), the latter is likely due to PDT activities of plastidial PhADT2 and PhADT3[10].

To date, no dedicated PDTs have been identified in plants, although certain ADTs from Arabidopsis, rice, pine, and petunia (PhADT2 and PhADT3) have been shown to utilize prephenate as substrate[10,17–19]. Recent studies in pine identified, outside of ADT/PDT catalytic domain, a 22-amino acid PDT-activity conferring (PAC) domain in which a single residue Ala314 is thought to trigger PDT activity based on yeast complementation assays[19]. Out of two petunia ADTs displaying PDT activities *in vitro*[10], only PhADT2 retained this residue. Therefore, to test for bona fide PDT activities of petunia ADTs, complementation of the *Saccharomyces cerevisiae pha2* mutant, which lacks PDT activity and is unable to grow without phenylalanine supplementation, was performed. Both PhADT2 and PhADT3 were able to restore growth of *pha2* mutant, which reached stationary phase after 2 and 4 days, respectively (Figure 4.18), while yeast strain expressing PhADT1 displayed significant delay in growth. Consistent with our previously reported catalytic efficiencies of recombinant petunia ADTs[10] these results confirm that PhADT2 and PhADT3 possess PDT activity *in vivo*, and additional factors beyond Ala314 are involved in determining substrate specificity.

All characterized ADTs, however, contain N-terminal transit peptides targeting the proteins to plastids[10,19,20]. Even so, dual subcellular localization of proteins often could be achieved by using two alternative in-frame translation initiation codons, where the isoform produced from the first methionine possesses a plastid-targeting peptide while a truncated isoform generated from the second methionine could be targeted to the cytosol[40–43]. Examination of protein sequences revealed that PhADT2 and PhADT3 each contain a second in-frame ATG codon located 99 and 133 amino acids downstream from their respective first translation initiation codon (Figure 4.5a).

Previously, assemblies of overlapping EST sequences with homology to Arabidopsis ADTs resulted in identification of *PhADT2* and *PhADT3* transcripts, which contain full-length open reading frames and respective 5′-UTRs of 176 and 121 bp in size[10]. To test for a second transcription start site (TSS) for these transcripts, the 5′-RNA ligase-mediated rapid amplification of the cDNA ends (5′-RLM-RACE) was performed using RNA extracted from 2-day-old petals at 20:00 h and gene-specific primers. The use of the GeneRacer^{TM} Kit (Invitrogen) enables the amplification of only full-length transcripts while eliminating truncated (5′ degraded) messages from the amplification process. 5′-RLM-RACE with *PhADT2* specific primer designed downstream of the second in-frame ATG codon produced a PCR product of ~ 0.9 kb in size, sequence of which corresponded to 5′-UTR already recovered from EST sequences. There were no PCR products between 450 and 747 bp in length corresponding to the putative TSS located between first and second ATG codons (Figure 4.5a). In contrast, *PhADT3* specific primer designed downstream of the second in-frame ATG codon produced a PCR fragment of about 1 kb in size. Sequencing of this fragment revealed the existence of a second TSS (TSS2) located 133 bp upstream of the second ATG codon (Figure 4.5a). A potential TATA box was identified using Plant-CARE program[44] 29 bp upstream from this TSS2. The shorter *PhADT3* transcript, designated as *PhADT3S*, encodes PhADT3S isoform containing intact ADT/PDT catalytic and ACT regulatory domains, but lacking a plastid targeting peptide (Figure 4.19a).

To independently test for the presence of shorter *PhADT3* transcripts, qRT-PCR was performed with two pairs of gene-specific primers targeted to different regions of the cDNA generated from RNA extracted from petals at 20:00 h on day 2 post-anthesis, the time with the highest expression of *PhADTs*[10]. One set of gene-specific primers was designed upstream of the TSS2 (set 5) to detect only the long transcripts, designated *PhADT3L*, encoding long PhADT3 isoform (PhADT3L), and the other (set 6) was situated downstream of the second ATG codon to detect the entire *PhADT3* transcript population (*PhADT3L* plus *PhADT3S*) (Figure 4.5b). Both pairs of primers were found to have similar efficiencies (>99%) based on amplification from a dilution series of purified full-length *PhADT3* template. The absolute amount of *PhADT3* transcripts obtained with set 6 primers (1.14 pg/200 ng RNA equivalent) was almost 2-fold higher than that with set 5 primers (0.62 pg/200 ng RNA equivalent) (Figure 4.5b), suggesting that both types of transcripts, *PhADT3L* and *PhADT3S*, are produced in the cell at nearly similar levels. In contrast, similar experiment targeting *PhADT2* with sets 3 and 4 of *PhADT2*-specific primers revealed no differences (Figure 4.5b), consistent with 5′-RLM-RACE data showing the absence of alternative TSS. In line with these experiments, *PhADT1* was included despite not possessing PDT activity. Similar to *PhADT2*, one type of transcript was detected for *PhADT1* (Figure 4.5b). Previously it has been shown that *PhADT3* is expressed in petunia flowers and exhibits rhythmic expression corresponding to production of phenylalanine and emission of phenylalanine-derived volatiles[10]. Interestingly, both *PhADT3L* and *PhADT3S* display similar rhythmicity in their expression patterns over a day/night cycle (Figure 4.20).

To experimentally determine whether the *PhADT3S* transcript encodes a cytosolically localized protein, its coding region was fused to either N- or C- terminus of the green fluorescent protein (GFP) reporter coding sequence. The resulting constructs were transiently expressed in *Nicotiana benthamiana* leaves along with GFP as a positive cytosolic control[45]. When samples were analyzed by confocal laser scanning microscopy, GFP fluorescence for all fusion proteins was found in the cytosol (Figure 4.21), thus confirming the predicted cytosolic localization of PhADT3S.

To verify if the cytosolic PhADT3S isoform is catalytically active, the recombinant protein starting from a second ATG codon as well as PhADT3L (Figure 4.19a) were produced in *E. coli*, purified and found to retain dehydratase activities with both prephenate and arogenate substrates. Further analysis of PDT activity revealed that both isoforms have similar affinity for prephenate (K_m for prephenate 358 ± 32 μM and 433 ± 73 μM for PhADT3L and PhADT3S, respectively), while the apparent catalytic efficiency of PhADT3S is slightly (1.6-fold) lower than that of PhADT3L (Table 4.3 and Figure 4.7c and d).

In silico sequence analysis predicted that the sizes of mature PhADT3L protein (*i.e.* without transit peptide that is cleaved *in vivo*) and PhADT3S are 42 kD, and 33 kD, respectively (Figure 4.19a). To experimentally determine if *in planta* alternative TSSs in *PhADT3* produce PhADT3 isoforms with different sizes and subsequently different subcellular localization, we performed immunoprecipitation of PhADT3 proteins followed by immunoblot analysis with anti-PhADT3 antibodies. Antibodies generated against synthetic PhADT3 peptide, localized after the second methionine, recognized both recombinant long mature and short PhADT3 proteins and did not cross hybridize with the PhADT1 (Figure 4.19b), the ADT protein with the highest expression and homology to PhADT3 (84% amino acid identity) in petunia petals[10]. Western blot analysis of the PhADT3 proteins immunoprecipitated from crude protein extracts prepared from 2-day old petunia flowers revealed two bands of ~42kD and ~33kD in size (Figure 4.5c), which were nearly equally abundant, consistent with their transcript levels (Figure 4.5b) and subcellular distribution of detected PDT activity (Figure 4.17). Proteomic analysis revealed the presence of PhADT3-specific peptides in both bands, indicating the existence of two PhADT3 isoforms in petunia flowers.

To further determine whether PhADT3 is involved in cytosolic phenylalanine biosynthesis *in planta*, its expression was transiently down-regulated in flowers of wild type and *PhCM2* RNAi line 15. Reduction by 41% - 57% in *PhADT3* expression without an effect on *PhADT1* mRNA levels led to a decrease in phenylalanine levels and phenylalanine-derived volatiles by 19% and 35%, respectively, in wild type flowers but did not impact their levels in *PhCM2* RNAi background (Figure 4.6). Taken together, these results suggest that PhADT3 does indeed act in series with PhCM2 within the same phenylalanine biosynthetic pathway.

4.4 Discussion

In plants, up to 30% of photosynthetically fixed carbon is directed to phenylalanine biosynthesis[46], which can occur via two alternative routes (Figure 4.1). Genetic evidence suggests that the majority of this carbon flux proceeds via the plastidial arogenate pathway[10–12], discovery of which was only recently completed[21,47]. However, until recently it remained unknown whether the alternative microbial-like phenylpyruvate route also contributes to phenylalanine biosynthesis. Evidence for the presence of a functional alternative route to phenylalanine production in plants first came from experiments in petunia flowers[16]. While downregulation of either of two consecutive steps in the arogenate pathway, catalyzed by PhADT1 and PhPPA-AT, resulted in reduced phenylalanine chemotype, their simultaneous downregulation restored phenylalanine to wild type levels[16]. The subsequent isolation of a gene encoding a cytosolic PhPPY-AT, which transaminates phenylpyruvate to phenylalanine[16], further supported the existence of alternative route, although it still remained unclear where the substrate for PhPPY-AT is synthesized.

Most microorganisms utilize only the phenylpyruvate pathway[48–50] with a few exceptions[51] and contain a bifunctional CM-PDT, which produces phenylpyruvate. In contrast, flowering plants contain multiple monofunctional CMs, with at least one isoform always being localized in the cytosol in species in which CMs have been analyzed[1,52]. The first gene encoding a cytosolic CM isoform in Arabidopsis (*AtCM2)* was isolated nearly two decades ago[23], but the physiological role of the corresponding enzyme still remained unknown. The results presented here show that downregulation of *PhCM2* expression in petunia flowers leads to reduction of flux via the phenylpyruvate pathway (Figure 4.3 and Table 4.2) with a concomitant decrease in the levels of phenylalanine and phenylalanine-derived volatile compounds (Figure 4.2c), providing direct *in vivo* evidence for the involvement of PhCM2 in phenylalanine biosynthesis via the microbial-like phenylpyruvate route.

The contribution of a cytosolic CM to phenylalanine biosynthesis is not unique to petunia flowers. Under normal growth conditions, in leaves of wild type and *cm2* Arabidopsis mutants there are no differences in phenylalanine internal pools (Figure 4.4d) or in emission of phenylacetadehyde (Figure 4.4e). However, in response to mechanical wounding, only in leaves of wild type, but not *cm2*-mutant, emission of phenylacetadehyde is increased by 2.3-fold relative to unwounded controls (Figure 4.4e). As phenylacetadehyde is derived directly from phenylalanine by AtAAS and *AtAAS* expression is similar in wild type and *cm2*-mutant wounded leaves (Figure 4.4f), these results suggest that *cm2* mutants are unable to produce substrate for AtAAS and that the excess of phenylalanine required for the phenylacetadehyde production upon wounding is produced by the phenylpyruvate route.

The cytosolic production of prephenate by PhCM2 and conversion of phenylpyruvate to phenylalanine by PhPPY-AT in the same subcellular compartment implies the existence of a functional cytosolic PDT converting prephenate to phenylpyruvate (Figure 4.1). Alternatively, phenylpyruvate could be synthesized in plastids and transported to the cytosol. In general, phenylpyruvate is undetectable in most plant tissues[10,37], but its level drastically increases upon shikimate feeding in petunia petals (Figure 4.13 and [10]). Despite the fact that cytosolic phenylpyruvate production is blocked at CM2, feeding of *PhCM2*-RNAi flowers with exogenous shikimate increased the phenylpyruvate pool to the same level as in wild type flowers, yet it did not lead to recovery of phenylalanine levels (Figure 4.13). The reason for Its inability to be converted to phenylalanine is currently unknown but could be due to a plastidial localization of this phenylpyruvate pool, where it is inaccessible to the cytosolic PhPPY-AT. We do not exclude that under shikimate feeding, as well as under overexpression of a bacterial CM/PDT in Arabidopsis and petunia plastids[14,15], phenylpyruvate could be converted to phenylalanine in plastids by unknown aminotransferase(s) with low affinity towards phenylpyruvate or by moonlight activities of some aminotransferase(s). Nevertheless, this activity was unable to bypass the blockage in the cytosolic pathway in *PhCM2*-RNAi flowers and recover phenylalanine levels (Figure 4.13).

To date, PDT activity has rarely been reported in plant tissues[37]. While monofunctional PDTs exist in yeast, fungi and bacteria[53,54], no such dedicated enzymes have been identified in plants. Moreover, only some of characterized plant ADTs utilize prephenate as substrate in addition to arogenate[10,17,19,53]. All characterized and putative plant ADTs/PDTs contain an N-terminal transit peptide targeting the proteins to plastids[10,17,19,20]. However, using non-aqueous fractionation, we show that PDT activity exists in the cytosol (Figure 4.17). One of the mechanisms to direct the same protein to two different subcellular locations is the use of multiple TSSs to produce two in-frame proteins differing only in their N-termini[40–42]. Recent large-scale full-length cDNA and genome sequence analyses in yeast[55], humans[56] and plants[57,58] predicted that significant fraction of genes likely contains alternative TSS(s). 5′-RLM-RACE, qRT-PCR with two sets of primers upstream and downstream of the alternative TSS (Figure 4.5a and b) and proteomics analysis of immunoprecipitated PhADT3 separated on and extracted from the SDS-PAGE (Figure 4.5c) revealed that PhADT3 contains an alternative TSS located 134 bp upstream of its second ATG codon (Figure 4.5a), which encodes a functional PhADT3S isoform with PDT activity (Table 4.3) lacking the N-terminal transit peptide and thus localized in the cytosol (Figure 4.21). Moreover, RNAi down-regulation of *PhADT3* had no effect on levels of phenylalanine and phenylalanine-derived volatiles in *PhCM2* RNAi petunia flowers while reducing their levels in wild type (Figure 4.6), further supporting the participation of PhADT3 in the cytosolic phenylpyruvate pathway.

Arabidopsis encodes six ADTs, with AtADT1, AtADT2 and AtADT6 being capable of utilizing prephenate as substrate *in vitro*[17] and AtADT1 and AtADT2 furthermore being able to complement the *Saccharomyces cerevisiae* PDT-deficient *pha2* knockout mutant[53]. Similar to PhADT3, these three Arabidopsis proteins have in-frame ATG start codon located 86, 68 and 76 amino acids downstream from the first translation initiation codon in AtADT1, AtADT2 and AtADT6, respectively, but upstream of PDT/ADT catalytic domain. *In silico* analysis of corresponding genes using the Plant Promoter Databases[59]; www.softberry.com) predicted that *AtADT6*, but not *AtADT1* or *AtADT2*, contains two alternative TSS(s), suggesting that, similar to petunia, Arabidopsis can contain a cytosolic enzyme with PDT activity. Indeed, qRT-PCR with two pairs of *AtADT6* gene-specific primers revealed that region of cDNA downstream of predicted alternative TSS is 6.6-fold more abundant than upstream region, further suggesting that two types of *AtADT6* transcripts exist in Arabidopsis (Figure 4.22a and b). Moreover, similar to *AtCM2*, expression of both *AtADT6* transcripts was upregulated by wounding, with a more profound effect on *AtADT6S* (Figure 4.22c and d). Recently the existence of different subcellular localizations, cytosolic and plastidial, was shown for AtADT3 depending on developmental stage and light conditions[60]. However, neither the mechanism of such dual localization nor the precise biochemical function in the cytosol of AtADT3, which does not possess PDT activity, were established. Interestingly, *in silico* analysis of all nine ADT genes previously identified in gymnosperm *Pinus pinaster*, four of which encode proteins with PDT activity *in vitro*[19], using the

Plant Promoter Databases, revealed that none of them contain alternative TSS capable of producing a cytosolically localized protein. A search of the SustainPine database[61] using Arabidopsis CMs as queries identified two CMs (unigenes 37772 and 37813), both of which contain N-terminal plastid transit peptides based on TargetP. The absence of both cytosolically localized CM and ADT transcripts is consistent with a lack of the cytosolic phenylpyruvate pathway in gymnosperms, which requires further experimental validation. Likewise, the apparent lack of cytosolic CM isoforms in mosses and ferns[28], suggests non-seed plants also lack the cytosolic phenylpyruvate pathway, consistent with a gain of the pathway in the angiosperm lineage, rather than the loss of an ancestral pathway in gymnosperms.

The discovery of CM2 function and a cytosolically localized enzyme with PDT activity in petunia completes the elucidation of the microbial-like phenylpyruvate route for phenylalanine biosynthesis. It also shows that the phenylpyruvate pathway branches from the known plastidial arogenate pathway at chorismate, and not at prephenate as previously thought, and that the entire pathway is localized in the cytosol. This discovery reinforces the long-standing suggestion that some plant species may possess a cytosolic pre-chorismate shikimate pathway, as extra-plastidic DAHPS and EPSPS isoforms as well as a gene encoding cytosolically localized 3-dehydroquinate dehydratase/shikimate dehydrogenase (DHD-SDH) have been reported (reviewed in [52]).

Given that the major carbon flux to phenylalanine is flowing via the arogenate pathway, an open question is why plants contain a functional phenylpyruvate route. The plastidial arogenate pathway in plants is subjected to complex feedback regulation at the entry and branch points catalyzed by CM1 and ADT, respectively[1,13,62]. In contrast, the phenylpyruvate route is subject to less stringent feedback regulation, because CM2, catalyzing the entry step in the phenylpyruvate pathway, is insensitive to allosteric regulation by aromatic amino acids[28].

One remaining question about the cytosolic pathway is how significant it is *in planta*. Data available in petunia flowers show that the phenylpyruvate pathway can compensate for the phenylalanine production when the major route is impaired[16] and for the shortage of phenylalanine when phenylalanine export out of plastids is impeded[32]. The blockage of the cytosolic phenylpyruvate pathway at CM2 causes a reduction in flux through the plastidial arogenate route (Figure 4.3 and Table 4.2) via yet unknown mechanism. This effect points to a role of a cytosolic pathway in maintaining overall phenylalanine homeostasis in the cell, despite its relatively low direct contribution to phenylalanine biosynthesis. In addition, our results demonstrate that the phenylpyruvate route contributes to phenylacetaldehyde emission upon mechanical wounding in Arabidopsis (Figure 4.4e). The experimental evidence that the use of multiple TSS is tissue-specific and stress-responsive[41,63] and that cytosolic localization of PDT isoform is the result of transcription from an alternative TSS of a gene encoding a plastidial enzyme, suggests that the phenylpyruvate pathway likely contributes to phenylalanine biosynthesis when demand for phenylpropanoids is increased as a part of plant biotic and abiotic stress responses. Similarly, tyrosine biosynthesis via a cytosolic prephenate dehydrogenase in legumes has been attributed to demand of specialized lineage-specific metabolites[64].

4.5 Materials and Methods

4.5.1 Generation of *PhCM2*-RNAi transgenic plants

Petunia hybrida cv Mitchell plants were grown under standard greenhouse conditions with a light period from 6:00 h to 21:00 h. For the *PhCM2*-RNAi construct, a fragment of *PhCM2* coding region (334 bp in size, corresponding to nucleotides 100 to 434) was amplified by PCR using forward 5'-CTCGAGTCTAGAATCAAATTCCCAATAAATTCCACC-3' and reverse 5'-GAATTCGGATCCTGAATATCACAGGCAGCAGT-3' primers. The PCR fragment was subcloned into the polylinker site (*Xho*I/*Eco*RI) upstream of the intron of a modified pRNA69 vector, containing the *Clarkia breweri linalool synthase* (*LIS*) petal specific promoter[31], and in the inverted orientation into the polylinker site (*BamH*I/*Xba*I) downstream of the intron. The entire cassette containing the *LIS* promoter and the *PhCM2* hairpin structure was released by *Sac*I/*Not*I digestion and ligated into the corresponding sites of the pART27 binary vector[65]. The final *PhCM2* RNAi construct in the binary vector was used for *Agrobacterium tumefaciens* (GV3101) mediated transformation of *Petunia hybrida* cv. Mitchell using the standard leaf disk transformation method.

4.5.2 Isolation of homozygous Arabidopsis *AtCM2* mutants

Arabidopsis thaliana AtCM2 T-DNA insertion lines N414383/*cm2-1* (Nottingham Arabidopsis Stock Centre, UK) and CS849985/*cm2-2* (Arabidopsis Biological Research Center, Ohio State University, USA) were grown under standard greenhouse conditions with a light period from 6:00 h to 22:00 h. Homozygous *cm2* mutant plants were identified by PCR analysis on isolated genomic DNA using gene-specific primers flanking the T-DNA insertions (CM2-L/CM2-R) as well as T-DNA border-specific primers (o8409 and p745 for *cm2-1* and *cm2-2*, respectively) (Table 4.4).

Rosette leaves of 4-week-old wild-type and *cm2* mutant plants were wounded using an array of 50 household needles, and volatiles were collected for 24 h[36].

4.5.3 qRT-PCR analysis and 5'-RLM-RACE

Sample collection, RNA isolation and qRT-PCR were performed using established protocols[66]. Unless otherwise specified, tissues were harvested at 20:00 h. Briefly, total RNA was isolated using a Spectrum™ Plant Total RNA Kit (Sigma, St. Louis, MO, USA) and treated with DNase I (Promega, Madison, WI, USA) to eliminate genomic DNA. One microgram of total RNA was reverse transcribed to cDNA using a 5X All-In-One RT MasterMix (Applied Biological Materials, Richmond, BC, Canada). Relative quantification of *AtAAS*, *AtCM2, AtADT6, PhCM1*, *PhCM2*, *PhADT1*, *PhADT2*, *PhADT3*, *DAHPS*, *EPSPS* and *ODO1* transcript levels were performed by qRT-PCR analysis with gene specific primers (Table 4.4) relative to the reference genes *UBQ10* for petunia and *Ubc* for Arabidopsis[10,16,36]. Changes in *PhADT3S, PhADT3L* and *PhCM2* transcript levels during a normal light/day cycle were analyzed by qRT-PCR using elongation factor 1-α (*EF1-α*) as a reference gene[67]. Each data point represents an average of three independent biological replicates, unless indicated. *AtCM2* transcript levels in wild type, *cm2-1* and *cm2-2* were analyzed by RT-PCR[36].

The 5′-RNA ligase-mediated rapid amplification of the cDNA ends (5′-RLM-RACE) was performed using the GeneRacer™ Kit (Invitrogen) according to manufacturer's instructions. Obtained PCR fragments were subcloned into pCR-TOPO vector (Invitrogen) and sequenced.

4.5.4 Metabolic profiling

Volatiles were collected from detached 2-day-old flowers of control and transgenic lines from 18:00 to 22:00 h using the closed-loop stripping method[31]. Trapped volatiles were eluted from Porapak Q traps (80/100 mesh size; Waters, Milford, MA) with 300 µl dichloromethane containing naphthalene (200 µg/ml) as an internal standard. Samples were analyzed by gas chromatography-MS using 5975 inert XL EI/CI mass spectrometer detector combined with 6890N GC (Agilent Technologies, Santa Clara, CA) with an Agilent 19091S-433 HP-5MS capillary column (30 m × 0.25 mm; film thickness 0.25 µm)[10]. Two µl of sample were injected in pulsed splitless mode with an injector temperature of 250°C. Column temperature was held at 40°C for 3 min and then heated to 220°C at 8°C min^{-1}. Electron ionization energy was set at 70 eV. Mass spectra were obtained in scan mode scanning across 50 to 550 amu. All volatile compounds were identified by comparing their retention times and mass spectra with those of corresponding authentic compounds. Quantification was performed using calibration curves generated from individual authentic standards.

Internal pools of aromatic amino acids and organic acids (shikimate, prephenate, arogenate and phenylpyruvate) from control and transgenic petals (minimum of six flowers per biological replicate) were extracted at 20:00 h on day 2 post-anthesis and analyzed by LC-MS[10]. Each data point represents an average of six to nine independent biological replicates. For analysis of aromatic amino acids and arogenate, 0.2 g tissue was ground in liquid N_2 and homogenized in 0.8 ml of 75% ethanol containing 0.5% 2-amino-2-methyl-1-propanol HCl (pH 10) with 30 nmol of α-aminoadipic acid as an internal standard. After centrifugation, 500 µl of the supernatant was filtered through an Amicon Ultra filter (Ultracel-10K, MilleporeSigma, Darmstadt, Germany), vacuum dried and dissolved in 50 µl water. 10 µl of sample was derivatized with *o*-phthaldialdehyde and injected into LC-MS. Chromatographic separations were performed using an Agilent 1100 HPLC system and a Luna C18 (2) column (3 µm, 100Å, 250 x 4.6 mm; Phenomenex) with a 25 min linear gradient of 25 - 90% methanol in 0.1% ammonium acetate (v/v) at a 0.3 ml/min flow rate. The column effluent was then introduced by negative electrospray ionization (ESI) into an Agilent 6210 MSD time-of-flight mass spectrometer[10]. Compounds were quantified based on a calibration curves generated by authentic standards.

For analysis of shikimate, 0.5 g of tissue was ground in liquid N_2 and homogenized in 1 ml of 0.25N HCl. After 20-min centrifugation, the supernatant was filtered through a 0.45 µm SFCA Nalgene syringe filter (Thermo Scientific) and analyzed by LC-MS as above using an Agilent ZORBAX SB-C18 column (4.6 x 150 mm x 3.5 µm) with an isocratic elution of 0.1% formic acid (v/v) in ddH_2O at a 0.5 ml/min flow rate. Shikimic acid was quantified based on a calibration curve generated with authentic standard.

For prephenate and phenylpyruvate, tissue extracts were prepared as described above for aromatic amino acids with the exceptions of using 4-chlorobenzoic acid as an internal standard. For prephenate detection, extract was prepared at pH 10 to degrade endogenous phenylpyruvate and subsequently acidified by 0.25 N HCl for 1 h at 37^{o}C to completely convert endogenous prephenate to phenylpyruvate[10]. For phenylpyruvate detection, petal extracts were prepared at pH 6, in which phenylpyruvate peak represented a sum of endogenous phenylpyruvate and the phenylpyruvate produced by acid conversion of prephenate during extraction. The difference between phenylpyruvate levels in the petal extracts prepared at pH 6 and pH 10, the latter treated with HCl, was used to determine endogenous phenylpyruvate content. Ten µl of the sample was analyzed by LC-MS as above using an Agilent ZORBAX SB-C18 column (4.6 x 150 mm x 3.5 µm) with a 10 min linear gradient from 20 - 70% methanol in 0.1% ammonium acetate (v/v) at a 0.5 ml/min flow rate. Peak quantification was performed based on a calibration curve generated from the authentic standard.

4.5.5 Yeast complementation assays

Coding regions of *PhADT1*, *PhADT2*, and *PhADT3* were first amplified using gene-specific primers (Table 4.4) possessing 5′-extensions that provide annealing sites for subsequent amplification with AttB primers (Invitrogen). The resulting amplicons were inserted into pDONR/Zeo vector by recombination using BP Clonase II (Invitrogen) according to manufacturer’s protocol. The generated constructs were then subjected to recombination with the yeast expression vector pYES-DEST52 using LR Clonase II (Invitrogen) following the manufacturer’s protocol. The *S. cerevisiae PHA2* ORF was acquired in a yeast expression vector to be used as a positive complementation control (Dharmacon, Lafayette, CO), while pYES-DEST52-*Gus*, generated by LR recombination as above with pENTR-Gus vector, was used as a negative control. Yeast expression constructs were transformed into haploid *pha2* knockout *S. cerevisiae* derived from BY4742 strain (Matα, *his*3Δ1, *leu*2Δ0, *lys*2Δ0, *ura*3Δ0, YNL316c:kanMX4; Dharmacon, Lafayette, CO) using the Frozen-EZ Yeast Transformation II kit (Zymo Research, Irving, CA). To test for complementation, yeast were grown overnight at 30° C in synthetic defined uracil dropout media containing 2% raffinose. Resulting cultures were diluted to OD_{600} of 0.05 in synthetic defined phenylalanine dropout media containing 2% galactose, and continued to grow at 30° C. Yeast growth was monitored by absorbance at 600 nm every 24 h.

4.5.6 Enzyme assays

For biochemical characterization of mature PhCM1 (minus predicted transit peptide) and PhCM2 as well as mature PhADT3L and PhADT3S, the coding region of the corresponding gene was amplified using forward and reverse primers (Table 4.4) containing *Nde*I and *BamH*I restriction sites, respectively, for directional cloning into pET-28a expression vector (Novagen, Madison, WI) in frame with an N-terminal 6XHis-tag. After sequence verification, recombinant proteins were produced in *E. coli* and purified on Ni-NTA resin (Qiagen, Hilden, Germany)[10]. Since *E. coli* crude extracts contain endogenous CM and PDT activities derived from a bifunctional CM/PDT enzyme, CM activity was monitored in purified PhADT3L and PhADT3S fractions while PDT activity was checked in purified PhCM1 and PhCM2 fractions to ensure the absence of *E. coli* CM/PDT contamination.

CM and PDT activity assays of recombinant proteins were carried out in 50 µl reaction mixture containing 20 mM Tris-HCl (pH 8.0), 1 mM EDTA, 500 µM chorismate or prephenate and 0.3 - 3 ng (for CM) and 2 µg (for PDT) recombinant enzyme, unless otherwise noted. The reaction mixtures were incubated at 37°C for 20 min and 30 min for CM and PDT activities, respectively. For CM activity, reaction was terminated by adding 50 µl 1N HCl followed by incubation at 37°C for 20 min to convert prephenate into phenylpyruvate. 150 µl 2.5 N NaOH was added before measuring phenylpyruvate formation by spectrophotometer at 320 nm. Due to the need for higher sensitivity at low substrate concentrations, assays with recombinant PhCM2 were performed as above, except that reaction volume was increased to 225 µl, and 10 µl of 10 N HCl was added for the conversion of prephenate to phenylpyruvate while15 µl of 25 N NaOH was added prior to the spectrophotometric analysis. For PDT activity, the reaction was stopped with 200 µl of 2.5 N NaOH and phenylpyruvate formation was measured by spectrophotometer at 320 nm and confirmed by LC-MS.

Chorismate was prepared using *Klebsiella pneumonia*, strain 62-1 (American Type Culture Collection, Manassas, Virginia), in which consumption of chorismate is drastically decreased leading to its secretion to the growth media[68,69]. Briefly, 1 l of sterile growth media (per liter: 2 g yeast extract, 2 g casein hydrolysate, 41 mg tryptophan, 2 g citric acid, 0.2 g anhydrous magnesium sulfate, 13.5 g dibasic sodium phosphate, 1 g monobasic potassium phosphate, and 2 g ammonium chloride) was inoculated with 1 ml of overnight LB culture of *K. pneumonia* and grown with shaking for approximately 6 h at 30^{o}C until OD_{625} reached 1.8. Cells were pelleted by centrifugation at 5000 x *g* for 5 min, the supernatant was discarded, and cells were resuspended in 1 l freshly prepared accumulation media (per liter: 10 g glucose, 19.2 g dibasic sodium phosphate, 2.05 g monobasic potassium phosphate, 2.7 g ammonium chloride, 21 mg magnesium chloride septa-hydrate, and 3 mg tryptophan). Cells were grown for 20 h with shaking at 30^{o}C, then pelleted by centrifugation at 5000 x *g* for 5 min and the supernatant was used for chorismate purification.

After increasing pH to 8.5, the supernatant was loaded under vacuum to the prepared DOWEX column with pH adjusted below 9.0 (30 g of DOWEX-Cl 1 x 8, 200 mesh, Sigma-Aldrich). After washing with 80 ml of water, chorismate was eluted with 2 M ammonium chloride (pH 8.5). Chorismate-containing fractions (6-ml each) were identified by absorption at 275 nm, pooled together and pH was adjusted to 1.5 by HCl. Non-polar contaminants were removed via partitioning with 75 ml dichloromethane three times. The final aqueous phase was extracted three times with 50 ml ethyl acetate to recover the chorismate. The ethyl acetate fractions were combined, dried with anhydrous sodium sulfate, and evaporated under vacuum. The resulting residue was dissolved in 5 ml of 10 mM ammonium acetate (pH 6.0), applied to a 1.5 x 20 cm column packed with 25 g octadecyl-functionalized silica gel (Sigma) that was pre-equilibrated with 250 ml 10 mM ammonium acetate (pH 6.0). Column was eluted with 10 mM ammonium acetate (pH 6.0) at a flow rate of 10 ml/min, and 4-ml fractions were collected. Fractions containing chorismate were pooled and lyophilized. The resulting chorismate powder was resuspended in water, the concentration was determined by absorption at 275 nm ($\varepsilon = 2630$), and aliquots stored at -80^{o}C until needed. Chorismate was assessed by NMR and purity was estimated > 90% by LC-MS.

Prephenate was enzymatically synthesized from chorismate using PhCM2 and purified following an established protocol[70]. Following enzymatic conversion of chorismate to prephenate, the reaction mixture was diluted with water to an approximate prephenate concentration of 20 mM. To each 10 ml of prephenate solution, 3.3 ml of ice-cold $BaBr_2$ solution (1.4% barium bromide in 80% ethanol) was added, and the mixture was incubated for 1 h on ice. Following centrifugation at 13,000 x *g* for 30 min at 4^{o}C, the resulting supernatant was mixed with $BaBr_2$ solution at 2:1 ratio and immediately ethanol was added to final concentration of 85%. The resulting solution was incubated on ice for 16 h, then centrifuged at 13,000 x *g* for 30 min at 4^{o}C and the supernatant discarded. The pellet was washed twice with 100% ethanol, then twice with ethyl ether, and centrifuged at 13,000 x *g* for 10 min at 4^{o}C after each solvent wash. The final pellet was dried by overnight lyophilization, and the resulting barium salt of prephenic acid was dissolved in water. The concentration was determined by absorption at 320 nm after the conversion of prephenate to phenylpyruvate by acid hydrolysis as described above.

All enzyme assays were performed at an appropriate enzyme concentration so that reaction velocity was proportional to enzyme concentration and linear during the incubation time period.

Kinetic data were evaluated by nonlinear regression analysis (GraphPad Prism, version 6.05). Triplicate assays were performed for all data points except as otherwise specified.

4.5.7 Preparation of plastidial cytosolic fractions

Plastidial and cytosolic fractions were prepared from 1- to 3-day old petunia petals harvested at 10:00 h, using established protocol[16] with some modifications. 20 g of petal tissue were submerged in 200 ml chilled homogenizing buffer A containing 0.5 M sorbitol, 20 mM HEPES/NaOH (pH 7.4), 10 mM KCl, 1 mM $MgCl_2{\cdot}6H_2O$, 1 mM Na_2-EDTA, 5 mM EDTA, and 5 mM DTT and blended three times for 2 sec. The homogenate was filtered through two layers of Miracloth (Calbiochem, La Jolla, CA, USA). A 1 ml aliquot was removed to analyze enzyme activities in crude extracts, and the remainder was centrifuged at 2,500 x *g* for 10 min. The pellet was washed and resuspended in 2 ml of buffer B containing 0.66 M sorbitol, 20 mM HEPES/NaOH (pH 7.5), and layered over a Percoll^{TM} gradient consisting of 2 ml 80% and 5 ml 30% Percoll^{TM} in buffer B. Intact plastids were collected from the interface of 80% and 30% Percoll^{TM} after centrifugation at 5,000 x *g* for 20 min at 4^{o}C, with both slow acceleration and deceleration settings. Plastids were washed in buffer B and resuspended in 50 mM Na-phosphate (pH 8.0) and 10% glycerol buffer. For a cytosolic fraction, the remaining supernatant was centrifuged at 12,000 x *g* for an additional 30 min at 4^{o}C to eliminate mitochondria and peroxisomes. The resulting supernatant was then desalted through Sephadex G-50 columns (GE Heathcare) and eluted into 50 mM Na-phosphate (pH 8.0) and 10% glycerol buffer and concentrated using Amicon® Ultra -10K centrifugal filters (EMD Millipore, Billerica, MA, USA). Obtained fractions as well as crude protein extracts were used for analysis of PPA-AT, alcohol dehydrogenase ADH (cytosolic marker), and CM activities.

For detection of PPA-AT activity, assays were conducted in 50 µl of reaction mixture containing 50 mM sodium phosphate buffer (pH 8.0), 20 mM L-aspartate, 200 µM PLP, 2 mM prephenate and 1 to 3 µg of total protein. After incubation at 37^{o}C for 15 min, the reaction was terminated by 25 µl of 1N HCl and further incubated at 37˚C for 20 min for quantitative conversion of arogenate to phenylalanine[21] before neutralization with 25 µl of 1N NaOH. Ten µl of the final reaction mixture was derivatized with *o*-phthalaldehyde (OPA) and subjected to HPLC analysis using an Agilent 1200 HPLC system (Palo Alto, CA) equipped with ZORBAX Eclipse XDB-C18 column (5 µm, 80Å, 150 x 3 mm; Agilent) with a 15 min linear gradient of 15 to 65 % methanol in 20 mM sodium phosphate buffer (pH 6.8). Phenylalanine production was monitored at 336 nm and quantified based on a standard calibration curve generated with authentic standard.

ADH activity assays were conducted in 500 µl of reaction mixture containing 100 mM sodium phosphate buffer (pH 8.0), 1 mM NAD^+, 100 µM ethanol and 1 to 3 µg of total protein. NADH production was measured spectrophotometrically at 340 nm over 5 min incubation at 25^o C, and quantified based on a standard calibration curve.

ADT activity in crude extracts was analyzed in 20 µl reaction mixture containing 500 µM arogenate, 250 mM sodium phosphate buffer (pH 8.2), 1 mM EDTA and 1 to 3 µg of total protein. Mixture was incubated at 37°C for 15 min and reaction was terminated by adding 25 µl of methanol. Produced phenylalanine was quantified as described above.

4.5.8 Non-aqueous fractionation and enzyme assays

To independently evaluate subcellular distribution of phenylalanine biosynthetic enzymes, petal tissue of 2-day-old wild type flowers harvested at 21:00 h was subjected to non-aqueous fractionation[32]. Approximately 0.3 g of dried tissue was resuspended in 2.5 ml heptane/tetrachloroethylene (density = 1.32 g ml^{-1}) and homogenized in a ball mill. The resulting suspension was layered atop a freshly prepared heptane/ tetrachloroethylene density gradient, then centrifuged for 90 min at 13,000 x *g*, 4^oC. The resolved gradient was divided into six fractions and all solvent was evaporated under nitrogen flow. The resulting fraction residues were resuspended in 1 ml of protein resuspension buffer (50 mM Tricine-NaOH, 10% glycerol, pH 8.4), centrifuged, and metabolites were removed using Zeba™ Spin Desalting Columns (7K MWCO, Thermo Scientific). The resulting fractions were first assayed for marker activities: NADP-glyceraldehyde-3-phosphate dehydrogenase (GAPDH) for plastids and phospho*enol*pyruvate (PEP) carboxylase for cytosol. Then, activities of phenylalanine ammonia lyase (PAL), a well-known cytosolic enzyme, and PPA-AT, a plastidial enzyme, were used to validate the subcellular resolution. Finally, CM assays were performed across a gradient in the presence of 20 µM and 500 µM of chorismate as well as PDT activities were analyzed as described above. PPY-AT activity was analyzed in 50 µl reaction mixture containing 50 mM HEPES pH 10, 10 mM tyrosine, 20 mM phenylpyruvate, and 200 mM PLP. The reaction was initiated by adding 10 µl of fractionated protein and incubated at 30^oC for 20 min. After termination of reaction with 50 µl of 1N HCl and centrifugation, 10 µl of the final reaction mixture was derivatized with OPA and phenylalanine production was analyzed by HPLC as described above.

For GAPDH activity assays[71], 37.5 µl of fractionated protein was incubated in 50 µl activation mixture containing 10 mM DTT, 5 mM ATP, 20 mM sodium phosphate buffer (pH 8.4), and 50 mM Tricine-NaOH (pH 8.4). After 10-min incubation at room temperature, 200 µl of reaction mixture (50 mM Tricine-NaOH pH 8.4, 25 mM $MgCl_2$, 10 mM DTT, 5 mM ATP, 50 µM NADPH, 10 mM 3-phosphoglycerate, 3 units of phosphoglycerate kinase) was added. NADPH consumption was measured spectrophotometrically at 340 nm (ε = 6200 M^{-1} cm^{-1}) over 5 min incubation at 25°C.

PEP carboxylase assays essentially followed the protocol described in[72] using a 250 µl volume containing 50 mM Tricine-NaOH (pH8.4), 5 mM $MgCl_2$, 5 mM DTT, 10 mM $NaHCO_3$, 2.5 mM PEP, 0.2 mM NADH, 2 units of malate dehydrogenase and 20 µl of fractionated protein. For PAL activity assays[73], reaction mixture contained 5 µl of fractionated protein and 2 mM L-phenylalanine in 50 µl assay buffer (100 mM $Na_2B_4O_7$ pH 8.8 and 2 mM DTT). After incubation for 30 min at 30°C, the reaction was stopped with 25 µl of 1N HCl and conversion of phenylalanine to *trans*-cinnamic acid was measured by HPLC. Distribution of enzymatic activities between compartments was solved by best fit algorithm[38].

4.5.9 Shikimate feeding

2-day-old *PhCM2*-RNAi and control petunia petals were fed with 100 mM shikimate for seven hours (from 15:00 h to 22:00 h). Levels of phenylalanine, tyrosine, tryptophan, arogenate, prephenate and phenylpyruvate were analyzed by LC-MS as described above.

4.5.10 Metabolic flux analysis with ^{15}N-tyrosine labeling

2-day-old *PhCM2*-RNAi and control petunia petals were fed with 10 mM ^{15}N-tyrosine (Cambridge Isotope Laboratories) starting at 18:00 h. After 2 h, 4 h and 6 h of feeding, the isotopic abundances and pool sizes of phenylalanine, tyrosine and arogenate were analyzed by LC-MS and used for metabolic flux analysis[16,32]. No labeling of arogenate was detected at any timepoint.

4.5.11 PhADT3 immunodetection and proteomic analyses

PhADT3 was immunoprecipitated from 0.5 g petals of 2-day-old wild type flowers harvested at 10:00 h using rabbit anti-PhADT3 antibodies and Pierce™ Classic IP Kit (Thermo Scientific) according to the manufacturer's protocol. Rabbit anti-PhADT3 polyclonal antibodies were generated against a synthetic PhADT3 peptide CFKTSIVFAHDKGTS and purified by cross-absorption with PhADT1 specific peptide CFKTSIVFAHEGTGV to increase antibodies specificity and prevent cross-reactivity with PhADT1 (Genscript, Piscataway, NJ). 1 mg of total protein crude extract was incubated with 1.5 µg of anti-PhADT3 polyclonal antibodies at 4°C overnight. The PhADT3 immune complex was recovered in 100 µl of elution buffer and was subjected to Western blot and proteomic analyses.

Western blot analysis of isolated PhADT3 immune complex (4 µl) was carried out as previously[74]. Immunodetection was performed on 0.06 µg of protein using rabbit anti-PhADT3 antibodies (1: 5000 dilution) and Pierce™ goat anti-rabbit IgG (H+L) horseradish peroxidase conjugate (1: 10000 dilution) as secondary antibodies (Catalog # 31460, Thermo Scientific). Antigen bands were visualized using chemiluminescent substrate for detection of horseradish peroxidase (Pierce™ ECL Western Blotting Substrate, Thermo Scientific) according to manufacturer's protocol and exposing the membranes on UltraCruz® Autoradiography Film (Santa Cruz Biotechnology). Purified recombinant mature PhADT3L (~42kD), PhADT3S (~33kD), and PhADT1 proteins as well as preparations from *E. coli* carrying empty pET28 expression vector were used as controls.

Sixty µl of isolated PhADT3 immune complex prepared from crude extract were loaded on a gel and used for proteomics analysis. Approximately 0.3 cm sections were excised from SDS-PAGE gels from positions corresponding to the bands detected in immunoblots from identical gels with anti-PhADT3 antibodies. Gel sections were destained and digested with trypsin (Sequencing grade, Promega) overnight[75] and analyzed at the Proteomics Facilities (Bindley Bioscience Center, Purdue University) as follows. Samples were subjected to reverse-phase HPLC-ESI-MS/MS using the Dionex UltiMate 3000 RSLC nano System (Thermo Fisher Scientific) coupled to the Q-Exactive High Field (HF) Hybrid Quadrupole Orbitrap MS (Thermo Fisher Scientific) and a Nano-electrospray Flex ion source (Thermo Fisher Scientific). Purified peptides were loaded onto a trap column (300 µm ID x 5 mm) packed with 5 µm 100 Å PepMap C18 medium and washed using a flow rate of 5 µl/min with 98% purified water/2% acetonitrile (ACN)/0.01% formic acid (FA). After 5 min the trap column was switched in-line with the analytical column. Peptides were separated using a reverse phase Acclaim PepMap RSLC C18 (75 µm x 15 cm) analytical column using a 120 min method at a flow rate of 300 nl/min. The analytical column was packed with 2 µm 100 Å PepMap C18 medium (Thermo Scientific). Mobile phase A consisted of 0.01% FA in water and a mobile phase B consisted of 0.01 % FA in 80% ACN. The linear gradient started at 5% B and reached 30% B in 80 min, 45% B in 91 min, and 100% B in 93 min. The column was held at 100% B for the next 5 min before being brought back to 5% B and held for 20 min. Sample was injected into the QE HF through the Nanospray Flex™ Ion Source fitted with an emission tip from Thermo Scientific. Column temperature was maintained at 35^{o}C. MS data were acquired with a Top20 data-dependent MS/MS scan method. The full scan MS spectra were collected over 300 - 1,650 m/z range with a maximum injection time of 100 msec, a resolution of 120,000 at 200 m/z, spray voltage of 2 and AGC target of 1 $\times 10^{6}$. Fragmentation of precursor ions was performed by high-energy C-trap dissociation (HCD) with the normalized collision energy of 27 eV. MS/MS scans were acquired at a resolution of 30,000 at m/z. The dynamic exclusion was set at 20 sec to avoid repeated scanning of identical peptides. Instrument optimization and recalibration was carried out at the start of each batch run using Pierce calibration solution. The sensitivity of the instrument was also monitored using *E. coli* digest at the start of the sample run.

LC-MS/MS data were searched using MaxQuant software (v. 1.5.3.28)[76–78] with its built-in Andromeda search engine[76] for protein identification and label free MS1 quantitation. The MS/MS spectra were searched against the *Solanum lycopersicum* protein database downloaded from the NCBI. The minimal length of six amino acids was required in the database search. The database search was performed with the precursor mass tolerance set to 10 ppm and MS/MS fragment ions tolerance was set to 20 ppm. Database search was performed with enzyme specificity for trypsin/LysC, allowing up to two missed cleavages. Oxidation of methionine was defined as a variable modification, and carbamidomethylation of cysteine was defined as a fixed modification. The ‘unique plus razor peptides’ were used for peptide quantitation. Razor peptides are the non-unique peptides assigned to the protein group with the most other peptides. The false discovery rate (FDR) of peptides and proteins identification was set at 1%. At this stringency, only one peptide corresponding to known ADT enzymes was identified. This peptide (LVDDANVGTAK) was common to both PhADT1 and PhADT3 at a position downstream of the second methionine, and was present in both the high and low molecular weight bands. To verify the presence of the target protein, a direct database search was performed as above using PhADT3 as query, which led to the identification of the three peptides AVLPIENSLGGSIHR, NYDLLLR, and

VAYQGVPGAYSEAAAGK, the first of which is exclusive to PhADT3 among petunia ADT proteins.

4.5.12 Subcellular localization of PhADT3S

The coding region of PhADT3S was amplified both with and without the native stop codon using gene-specific primers (Table 4.4) possessing 5′-extensions that provide annealing sites for subsequent amplification with AttB primers (Invitrogen). The resulting amplicons were inserted into pDONR/Zeo vector by recombination using BP Clonase II (Invitrogen) according to manufacturer's protocol. The generated constructs with and without the stop codon were then subjected to recombination with binary GFP-fusion vectors pK7WGF2 (N-terminal GFP) and pK7FWG2 (C-terminal GFP), respectively, both containing the CaMV 35S promoter[79], using LR Clonase II (Invitrogen) according to the manufacturer's protocol. The constructs and a GFP cytosolic control were transformed into *Agrobacterium tumefaciens* (GV3101) and infiltrated into *Nicotiana benthamiana* leaves[80]. Five days after infiltration leaf tissue was imaged by using Zeiss LSM710 laser spectral scanning confocal microscope with a C-Apochromat 40 x/1.20W objective (Zeiss, Thornwood, NY, USA). GFP was excited with an Argon laser at wavelength 488 nm and emissions were collected over a 493–598 nm bandpass[16]. Chlorophyll fluorescence was excited by a HeNe laser at wavelength 633 nm and emissions were collected over a 647–721 nm bandpass[16].

4.5.13 *PhpCAT* overexpression and *PhADT3* downregulation in planta

Transient *PhpCAT* overexpression in wild type and *PhCM2* RNAi petunia flowers was performed using previously generated pART27-derived *PhpCAT* overexpression construct[32]. Transient *PhpCAT* overexpression[16] was achieved using vacuum infiltration of at least 20 total 1-day-old petunia flowers from each genetic background with *Agrobacterium tumefaciens* strain GV3101 containing pART27-LIS-*PhpCAT* and pART27-LIS vector (control) at OD_{600} of 0.4. Forty-eight hours after infiltration, scent was collected for 6 h from 18:00 h to 24:00 h and analyzed by GC-MS. Immediately following scent collection petal tissue was used for RNA analysis and metabolic profiling as described above.

For *PhADT3* RNAi downregulation, DNA containing two spliced *PhADT3* cDNA fragments of the coding region corresponding to nucleotides 2 to 549 and 2 to 340, the latter in antisense orientation to create a hairpin structure, was synthesized with flanking AttL1 and AttL2 recombination sites (Genscript, NJ). The resulting cassette was subcloned into the binary vector pB2GW7 (Invitrogen, Carlsbad, CA, USA) under control of the cauliflower mosaic virus 35S promoter using the Gateway LR Clonase II (Invitrogen) and used for transient downregulation[116] as described above.

4.6 Tables and Figures

Table 4.1 Kinetic parameters of recombinant petunia PhCM2

Enzyme	**K_m (μM)**	**V_{max} (μmol min^{-1} mg^{-1})**	**k_{cat}/K_m (M^{-1} s^{-1})**
PhCM1	174 ± 27	45.7 ± 1.5	144,000
PhCM2	8.6 ± 1.2	114 ± 4	7,136,000

Data are the mean ± SEM (n = 3).

Table 4.2 Changes in flux in flowers from control and *PhCM2*-RNAi petunia lines at t_{0h} and t_{6h}

	Plastidial synthesis rate v_1 (nmol gFW^{-1} h^{-1})			**Cytosolic synthesis rate v_2 (nmol gFW^{-1} h^{-1})**		
	t_{0h}	t_{6h}	Relative change at t_{6h}	t_{0h}	t_{6h}	Relative change at t_{6h}
Control	266±21.2	255±20.5	-3.95%	0.627±0.0560	11.1±1.08	+1660%
PhCM2 RNAi	162±8.28	160±8.22	-1.17%	0.147±0.0168	1.64±0.131	+993%
Relative change in *PhCM2* RNAi	-39.0%	-37.3%		-76.2%	-85.2%	

v_1 – absolute flux through the plastidial arogenate pathway;
v_2 – absolute flux through the cytosolic phenylpyruvate pathway;
(-) - indicates a decrease in flux at t_{6h} versus t_{0h} or in *PhCM2* RNAi versus control
(+) - indicates an increase in flux at t_{6h} versus t_{0h}

Table 4.3 Kinetic parameters of recombinant petunia PhADT3 isoforms with prephenate as substrate

Enzyme	**K_m (μM)**	**V_{max} (μmol min^{-1} mg^{-1})**	**k_{cat}/K_m (M^{-1} s^{-1})**
PhADT3L	358 ± 32	0.125 ± 0.060	252
PhADT3S	433 ± 73	0.113 ± 0.006	186

Data are the mean ± SEM (n = 3)

Table 4.4 Primers used in this project

Primer Name	**Sequence**	**Purpose**
AtCM2 LB GSP	5'-GGATTCGGGTTCTGGTTGTT-3'	Genotyping
AtCM2 RB GSP	5'-TCGCAGGCTCGTAATCTTGT-3'	Genotyping
p745	5'-AACGTCCGCAATGTGTTATTAAGTTGTC-3'	Genotyping
o8409	5'-ATATTGACCATCATACTCATTGC-3'	Genotyping
AtCM2 F	5'-GGGAGCTCCATATGGCAAGAGTCTTCGAATCGGA-3'	RT-PCR
AtCM2 R	5'-CCCTCGAGGCATGCTCAATCGAGACGACGTAGAA-3'	RT-PCR
AtUbc F	5'-ATGCAGGCATCAAGAGCG-3'	RT-PCR
AtUbc R	5'-TCATCCTTTCTTAGGCATAGCG-3'	RT-PCR
AtCM2 qRT F	5'-GAAAGCAGAAACGTTTGGACAA-3'	qRT-PCR
AtCM2 qRT R	5'-AGATGCGAGAGGCAAGCAAT-3'	qRT-PCR
AtUbc qRT F	5'-CTGCGACTCAGGGAATCTTCTAA-3'	qRT-PCR
AtUbc qRT R	5'-TTGTGCCATTGAATTGAACCC-3'	qRT-PCR
AtADT6 qRT F1	5'-ACATGTTTTTCTACATTCTCGACTTTG-3'	qRT-PCR
AtADT6 qRT R1	5'-CCGGCTGGCTAGCACCTAA-3'	qRT-PCR
AtADT6 qRT F2	5'-AGGAACCAGCGTGCTTTTCA-3'	qRT-PCR
AtADT6 qRT R2	5'-CCTGATCGGACGGTTGTGAT-3'	qRT-PCR
PhCM2 RNAi F	5'-CTCGAGTCTAGAATCAAATTCCCAATAAATTCCACC-3'	Cloning
PhCM2 RNAi R	5'-GAATTC GGATCCTGAATATCACAGGCAGCAGT-3'	Cloning
PhCM1 F	5'-CATATGCAAGCTTCTGCAACTTCTC-3'	Cloning
PhCM1 R	5'-GGATCCCTAATCCAGTCTTCTCAG-3'	Cloning
PhCM2 F	5'-CATATGGCCTGTGGTGATTATG-3'	Cloning
PhCM2 R	5'-GGATCCCAAACTAACTTCTATCTAA-3'	Cloning
PhADT3S F	5'-CATATGATGCACGGGGCGCAGCT-3'	Cloning
PhADT3S R	5'-GGATCCTTAAGCATCCCTGGAAGG-3'	Cloning
PhADT1 GTW F	5'-AAAAAGCAGGCTTCATGCAGTCCCTTACTCCT-3'	Gateway Cloning
PhADT1 GTW NS R	5'-AGAAAGCTGGGTCTTCATCCCTAGAAGGACAG-3'	Gateway Cloning
PhADT2 GTW F	5'-AAAAAGCAGGCTTCATGGCAGCCACCACTACAC-3'	Gateway Cloning
PhADT2 GTW NS R	5'-AGAAAGCTGGGTCAGCTATTCCACTATCTGAC-3'	Gateway Cloning
PhADT3 GTW F	5'-AAAAAGCAGGCTTCATGCAGTCCCTTACTCCATC-3'	Gateway Cloning
PhADT3S GTW F	5'-AAAAAGCAGGCTTCATGCACGGGGCGCAGCTG-3'	Gateway Cloning
PhADT3 GTW NS R	5'-AGAAAGCTGGGTCAGCATCCCTGGAAGGAGAC-3'	Gateway Cloning
PhADT3 GTW R	5'-AGAAAGCTGGGTCTTAAGCATCCCTGGAAGGA-5'	Gateway Cloning

Table 4.4 Continued

PhUBQ qRT F	5'-GTTAGATTGTCTGCTGTCGATGGT-3'	qRT-PCR
PhUBQ qRT R	5'-AGGAGCCAATTAAAGCACTTATCAA-3'	qRT-PCR
PhEF1-α F	5'-CCTGGTCAAATTGGAAACGG-3'	qRT-PCR
PhEF1-α R	5'-CAGATCGCCTGTCAATCTTGG-3'	qRT-PCR
PhCM1 qRT F	5'-CCTGCTGTTGAAGAGGCTATCA-3'	qRT-PCR
PhCM1 qRT R	5'-CAGGGTCACCTCCATTTTCTG-3'	qRT-PCR
PhCM2 qRT F	5'-TGCAACTACTGCTGCCTGTGAT-3'	qRT-PCR
PhCM2 qRT R	5'-TCGTCAGAGCAATCCCTGAAT-3'	qRT-PCR
DAHPS qRT F	5'-CAAAGCTCCGTGTGGTCTTAAA-3'	qRT-PCR
DAHPS qRT R	5'-TCCTGGGTGGCTTCCTTCTT-3'	qRT-PCR
EPSPS qRT F	5'-CACCCCACCGGAGAAACTAA-3'	qRT-PCR
EPSPS qRT R	5'-TGACGGGAACATCTGCACAA-3'	qRT-PCR
ODO1 qRT F	5'-ATTCGCCATGGGAATTTCC-3'	qRT-PCR
ODO1 qRT R	5'-GAAAGTGTCTTCCCAGGATGTCA-3'	qRT-PCR
PhADT1 qRT F1	5'-GAGCTCCGGCGAGTTACAAC-3'	qRT-PCR
PhADT1 qRT R1	5'-GTGTCCGGCTGCTGTGAGA-3'	qRT-PCR
PhADT1 qRT F2	5'-TAACTGCGAAGCCATTCCCTGC-3'	qRT-PCR
PhADT1 qRT R2	5'-CTCTACTGGTAGAACTGCGCG-3'	qRT-PCR
PhADT2 qRT F3	5'-ACCATCTCATCTCCCGCTCTT-3'	qRT-PCR
PhADT2 qRT R3	5'-TGTAGTGGTGGCTGCCATTG-3'	qRT-PCR
PhADT2 qRT F4	5'-ACGAAGTTGGGTTTGGTCAG-3'	qRT-PCR
PhADT2 qRT R4	5'-TGCCCCTGCATCTTTTAGTT-3'	qRT-PCR
PhADT3 qRT F5	5'-AGCAGCCGCCGTAAACAC-3'	qRT-PCR
PhADT3 qRT R5	5'-TGCACACGAACTCTGCCAAT-3'	qRT-PCR
PhADT3 qRT F6	5'-CAAAATGTGAAGCTATTCCTTGTG-3'	qRT-PCR
PhADT3 qRT R6	5'-TTCGATCGGTAAAACAGCACG-3'	qRT-PCR
PhADT2 GSP	5'-TGCCCCTGCATCTTTTAGTT-3'	5' RACE
PhADT3 GSP	5'-GCTCTTACGTCCGCCATTGACGCT-3'	5' RACE

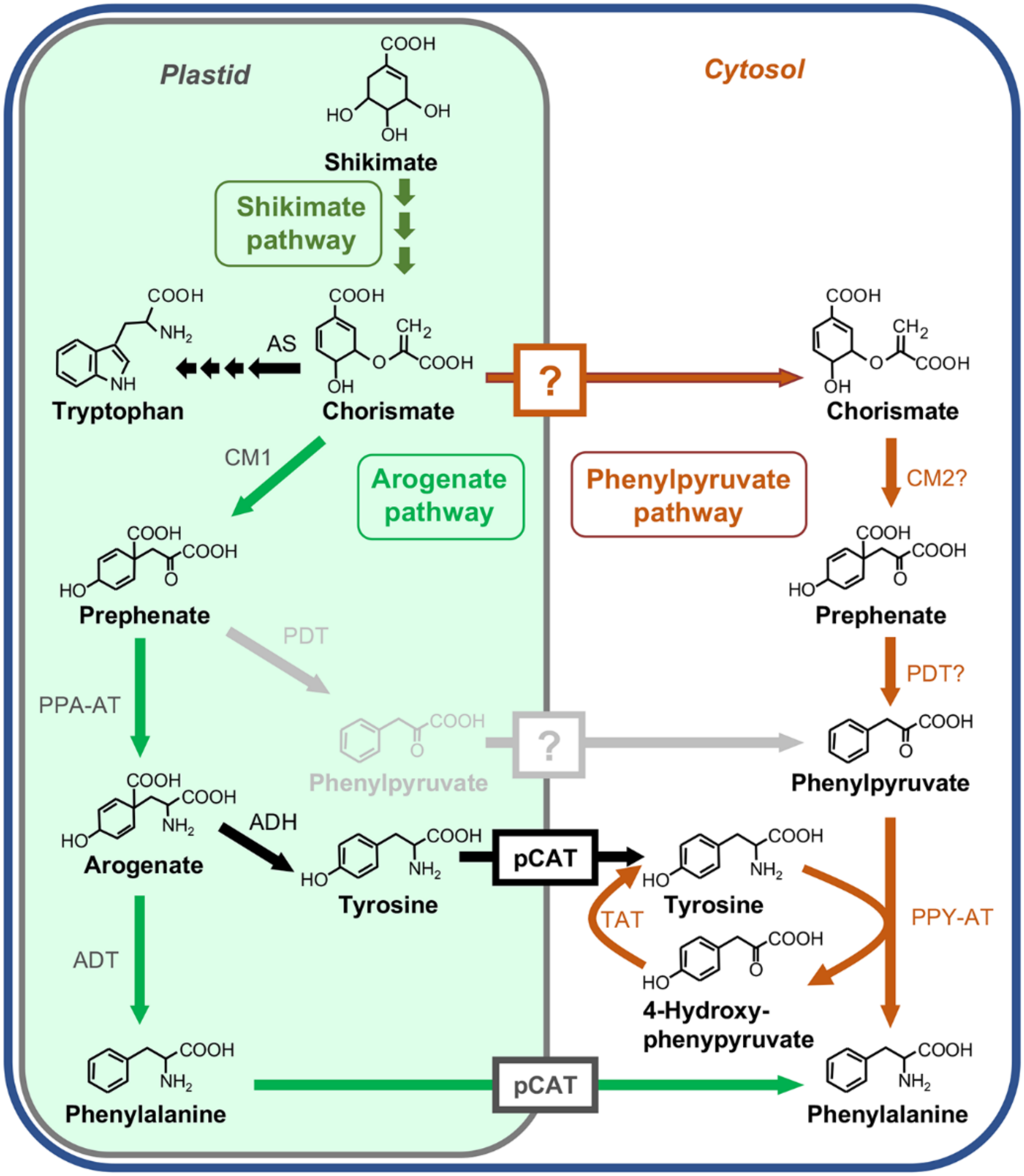
Plastid
Cytosol
COOH
HO
OH
OH
Shikimate
Shikimate pathway
COOH
NH2
NH
Tryptophan
AS
COOH
CH2
O
COOH
OH
Chorismate
?
COOH
CH2
O
COOH
OH
Chorismate
CM1
Arogenate pathway
Phenylpyruvate pathway
CM2?
COOH
COOH
HO
O
Prephenate
COOH
COOH
HO
O
Prephenate
PDT
PPA-AT
PDT?
COOH
O
Phenylpyruvate
?
COOH
O
Phenylpyruvate
COOH
COOH
NH2
HO
Arogenate
ADH
COOH
NH2
HO
Tyrosine
pCAT
COOH
NH2
HO
Tyrosine
TAT
PPY-AT
COOH
O
HO
4-Hydroxy-phenypyruvate
ADT
COOH
NH2
Phenylalanine
pCAT
COOH
NH2
Phenylalanine

Figure 4.1 Proposed plant phenylalanine biosynthetic pathways

Characterized enzymes and transporters are shown in solid colors. Uncharacterized enzymes and transporters are shown in grey. Abbreviations: ADH, arogenate dehydrogenase; ADT, arogenate dehydratase; AS, anthranilate synthase; pCAT, plastidial cationic amino-acid transporter; CM, chorismate mutase; PDT, prephenate dehydratase; PPA-AT, prephenate aminotransferase; PPY-AT, phenylpyruvate aminotransferase; TAT, tyrosine aminotransferase. Boxes with question marks indicate unknown transporters/ transport steps.

Figure 4.2 Metabolic effects of *PhCM2* RNAi downregulation in petunia flowers

(**a**) *PhCM2* mRNA levels in 2-day-old petunia petals at 20:00 h. Expression levels in transgenic lines (white bars) are shown as a percentage of *PhCM2* expression in control (black bar) petals set as 100% (n ≥ 3 biological replicates). (**b**) CM activities with 500 μM chorismate in crude extracts (striped bars), and cytosolic (grey bars) and plastidial (back bars) fractions prepared from corollas of 1 to 3 day-old wild type and *PhCM2* RNAi petunia flowers harvested at 10:00 h (n = 3 biological replicates). (**c**) Internal pools of shikimate, prephenate, arogenate and aromatic amino acids as well as total volatile emission (n ≥ 6 biological replicates). Metabolite levels were measured in 2-day-old petunia petals at 20:00 h and are shown in nmol g FW^{-1}. Pink background indicates metabolites with potential dual subcellular localization, in the cytosol and plastids. Emitted volatiles were collected from 2-day-old wild type and transgenic *PhCM2* RNAi petunia flowers from 18:00 h to 22:00 h. Black and white bars represent wild type and transgenic lines, respectively. Data are means ± SE. * $P < 0.05$, **$P < 0.01$ as determined by paired two-tailed Student's *t* test. Abbreviations: ADT, arogenate dehydratase; ADH, arogenate dehydrogenase; CM, chorismate mutase; E4P, erythrose 4-phosphate; pCAT, plastidial cationic amino-acid transporter; PDT, prephenate dehydratase; PEP, phospho*enol*pyruvate; PPA-AT, prephenate aminotransferase; PPY-AT, phenylpyruvate aminotransferase, FW, fresh weight.

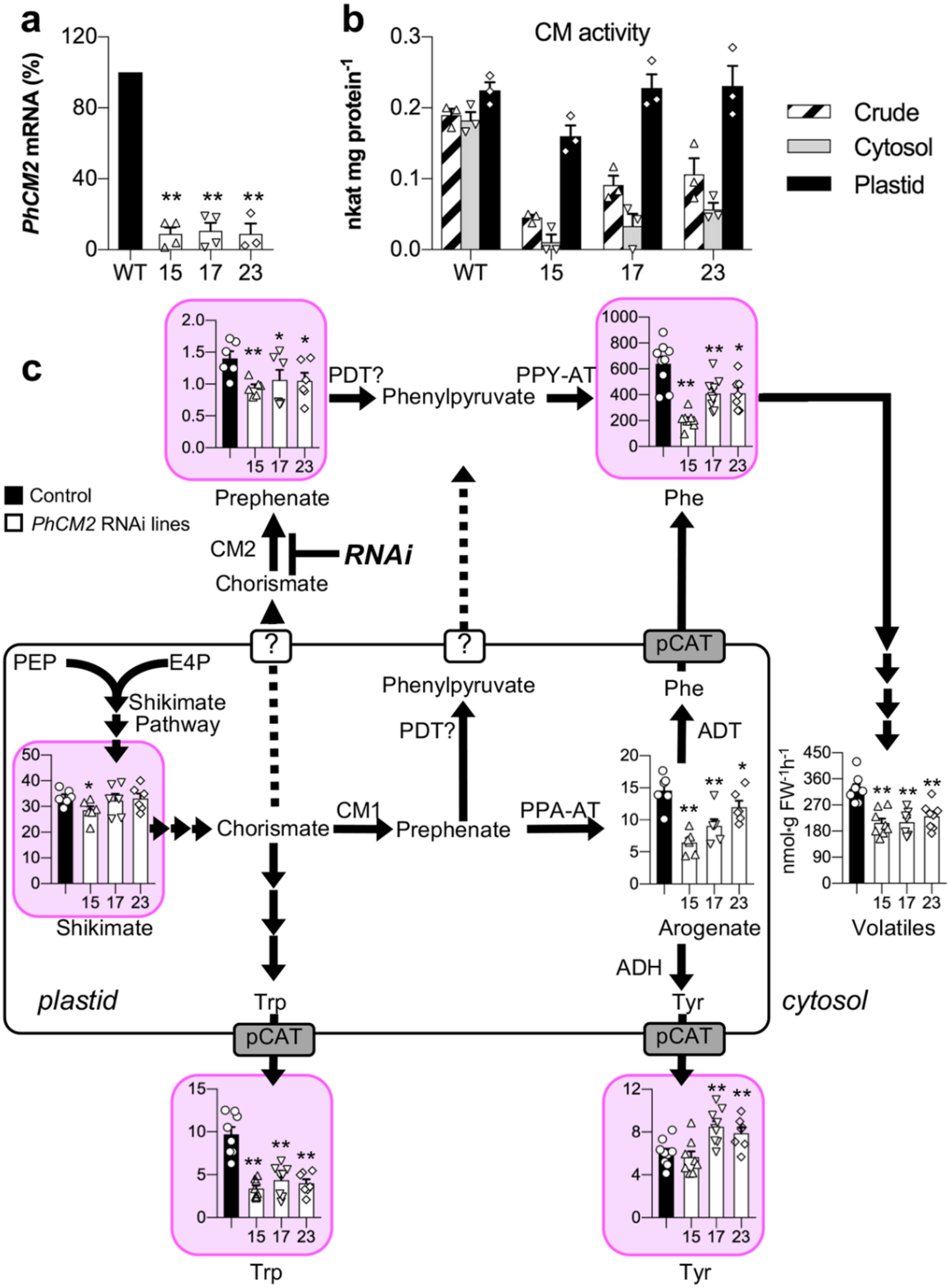
a
PhCM2 mRNA (%)
120
80
40
0
WT
15
17
23
**
b
CM activity
nkat mg protein^{-1}
0.3
0.2
0.1
0.0
Crude
Cytosol
Plastid
c
Control
PhCM2 RNAi lines
Prephenate
PDT?
Phenylpyruvate
PPY-AT
Phe
CM2
RNAi
Chorismate
?
pCAT
PEP
E4P
Shikimate Pathway
Shikimate
Chorismate
CM1
Prephenate
PPA-AT
Arogenate
ADT
ADH
Tyr
Trp
plastid
cytosol
nmol·g FW^{-1}h^{-1}
Volatiles
*
**

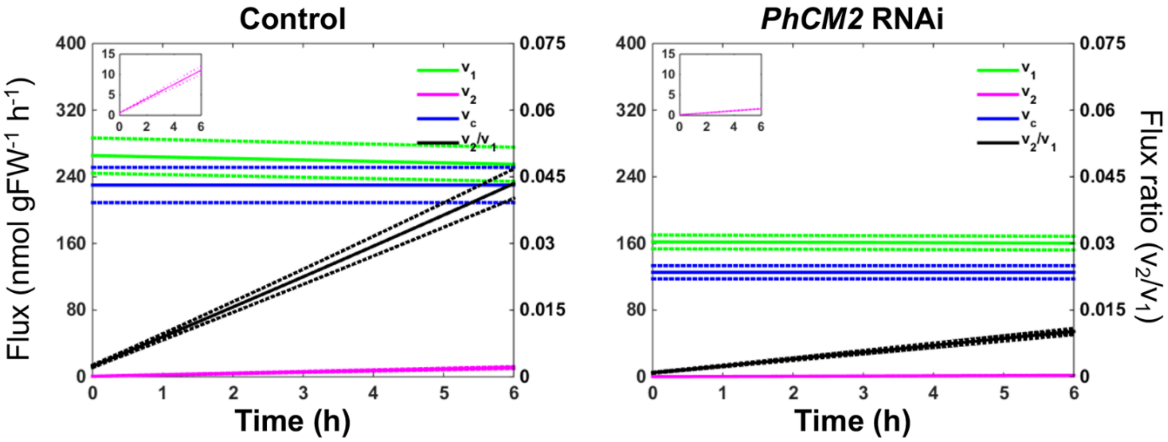

Figure 4.3 Metabolic modeling of phenylalanine biosynthetic pathways in control and *PhCM2* RNAi petunia flowers

Flux models representing the phenylalanine biosynthetic network in 2-day-old control and *PhCM2* RNAi petunia flowers. Metabolic modeling was performed using pool sizes and isotopic abundances of phenylalanine and tyrosine, and measurements of phenylalanine-derived volatile emission (consumption flux, v_c, blue lines) from petunia petals supplied with 10mM ^{15}N-tyrosine for up to 6 h starting at 18:00 h (n = 3 biological replicates). v_1, flux through the plastidial arogenate pathway (green lines); v_2, flux through the cytosolic phenylpyruvate (pink lines, also is enlarged in inserts). v_2/v_1 ratio is shown by black lines. Solid lines are estimated values and dotted lines are standard deviation for each flux value.

Figure 4.4 Characterization of the Arabidopsis *cm2* mutants

(**a**) Structure of the *AtCM2* gene showing the T-DNA insertion sites in *cm2-1* and *cm2-2* mutant lines. Black boxes represent exons. Arrows indicate the positions of primers used for analysis. (**b**) Genotyping of the Arabidopsis *cm2* mutants by PCR analysis using primers specific to genomic regions flanking each T-DNA as well as T-DNA specific primers. (**c**) RT-PCR analysis of *AtCM2* transcripts in wild type (ecotype Col-0) and the *cm2* mutants. Transcript levels of *AtUBC* encoding ubiquitin-conjugating enzyme were used as endogenous control. (**d**) Aromatic amino acid levels in leaves of Arabidopsis wild type (ecotype Col-0; black bars) and *cm2* mutants (white bars). Data are means ± SE (n ≥ 3 biological replicates). (**e**) Phenylacetaldehyde emission from leaves of Arabidopsis wild type and *cm2* mutants upon mechanical wounding. Volatiles were collected from intact (black bars) and wounded (grey bars) leaves for 24 h and analyzed by GC-MS. Data are means ± SE (n ≥ 7 biological replicates). * $P < 0.05$ as determined by paired two-tailed Student's *t*-test. (**f**) *AtAAS* transcript levels in Arabidopsis leaves of wild type and *cm2* mutants upon mechanical wounding, as determined by qRT-PCR. (**g**) *AtCM2* transcript levels in wild type Arabidopsis leaves upon mechanical wounding, as determined by qRT-PCR. In **f** and **g** data are presented as relative to untreated wild type control plants set as 100%, and bar colors are same as in **e**. Data are means ± SE (n =3 biological replicates). * $P < 0.05$ as determined by paired two-tailed Student's *t*-test.

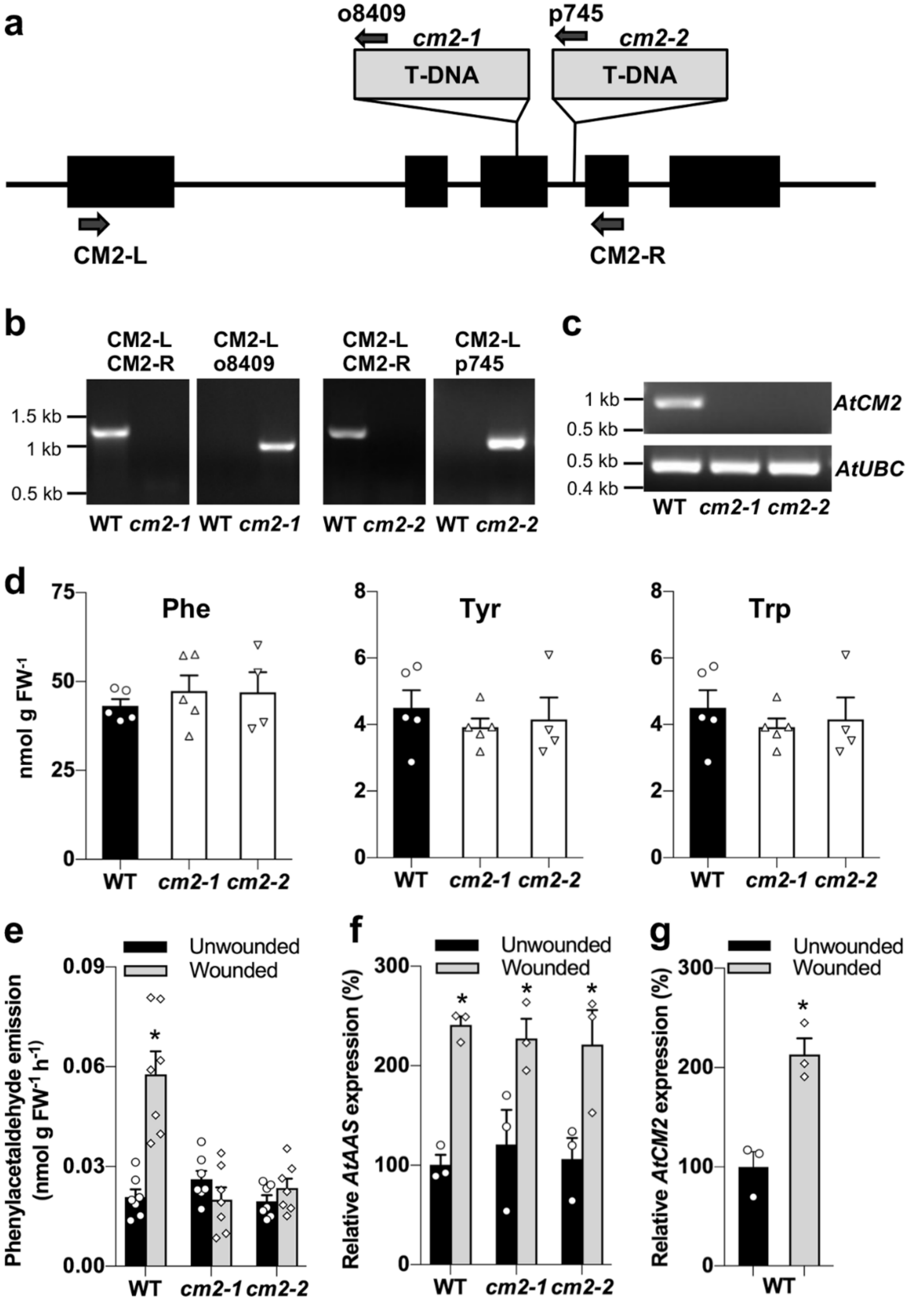
a
o8409
cm2-1
T-DNA
p745
cm2-2
T-DNA
CM2-L
CM2-R
b
CM2-L CM2-R
CM2-L o8409
CM2-L CM2-R
CM2-L p745
1.5 kb
1 kb
0.5 kb
WT cm2-1 WT cm2-1
WT cm2-2 WT cm2-2
c
1 kb
0.5 kb
AtCM2
0.5 kb
0.4 kb
AtUBC
WT cm2-1 cm2-2
d
Phe
Tyr
Trp
nmol g FW⁻¹
75
50
25
0
8
6
4
2
0
WT cm2-1 cm2-2
e
Unwounded
Wounded
Phenylacetaldehyde emission (nmol g FW⁻¹ h⁻¹)
0.09
0.06
0.03
0.00
*
WT cm2-1 cm2-2
f
Unwounded
Wounded
Relative AtAAS expression (%)
300
200
100
0
* * *
WT cm2-1 cm2-2
g
Unwounded
Wounded
Relative AtCM2 expression (%)
300
200
100
0
*
WT

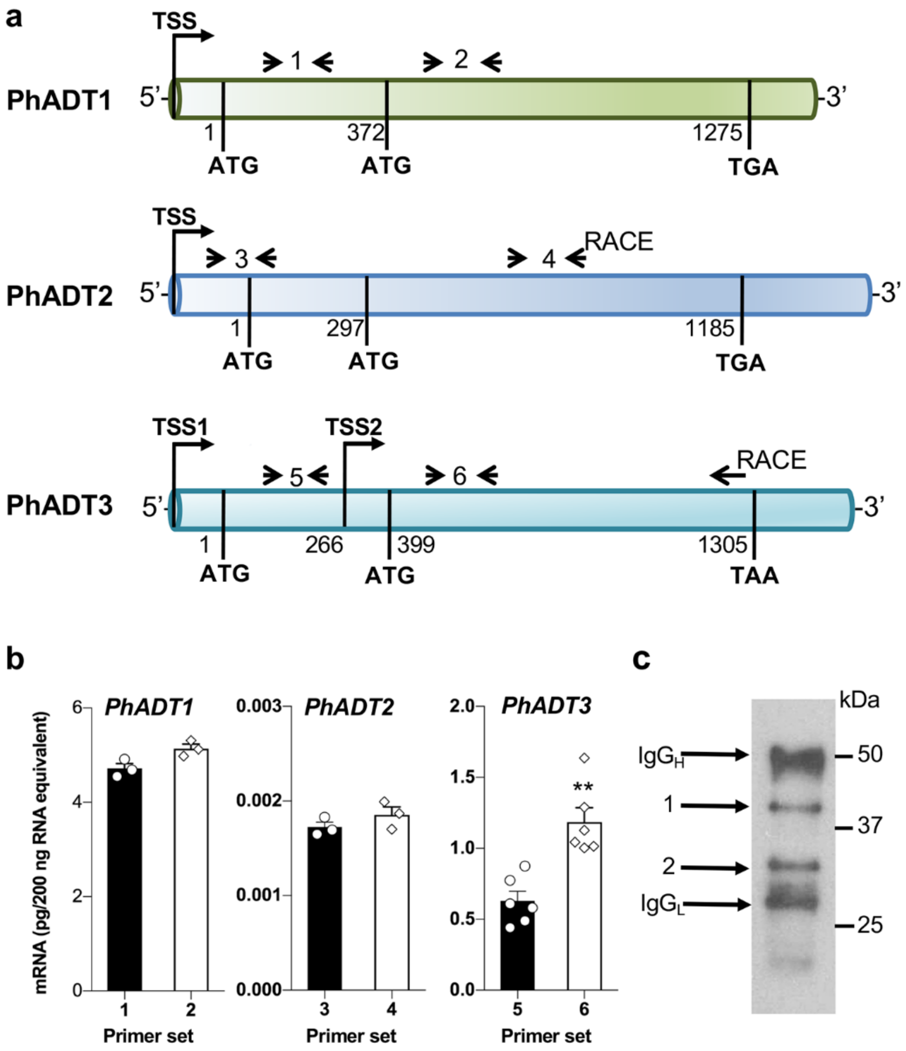

Figure 4.5 Alternative *PhADT3* transcript yields a cytosolic isoform in petunia flowers

(**a**) Schematic presentation of *PhADT1*, *PhADT2* and *PhADT3* mRNA and positions of gene-specific primer sets shown in Supplementary Table 1. The translation initiation codons as well as stop codons are indicated in bold. Nucleotide positions are referred to the first translation initiation codon. TSS, transcription start site, RACE depicts the position of primers used for 5′-RLM-RACE. (**b**) Alternative *PhADT3* transcripts in petunia flowers. The absolute transcript levels of *PhADT1*, *PhADT2* and *PhADT3* were determined at 5′ end (black bars) and 3′ end (white bars) of mRNAs by qRT-PCR and are shown as pg/200 ng total RNA. mRNA was obtained from petunia flowers harvested at 20:00 h on day 2 post-anthesis. Data are means ± SE (n=3 biological replicates for *PhADT1* and *PhADT2*; n=6 biological replicates for *PhADT3*). ** $P<0.01$ as determined by paired two-tailed Student's *t*-test. (**c**) Representative immunoblot (out of seven) using anti-PhADT3 antibodies against PhADT3 immune complex prepared from 1 mg protein from crude extract of 2-day-old petunia petals harvested at 10:00 h. 4 μl of isolated PhADT3 immune complex were loaded on a gel. Regions corresponding to bands 1 and 2 of the SDS-PAGE gel were excised and used for proteomics analysis. IgG$_{H}$ and IgG$_{L}$ correspond to the heavy and light chains of IgG, respectively.

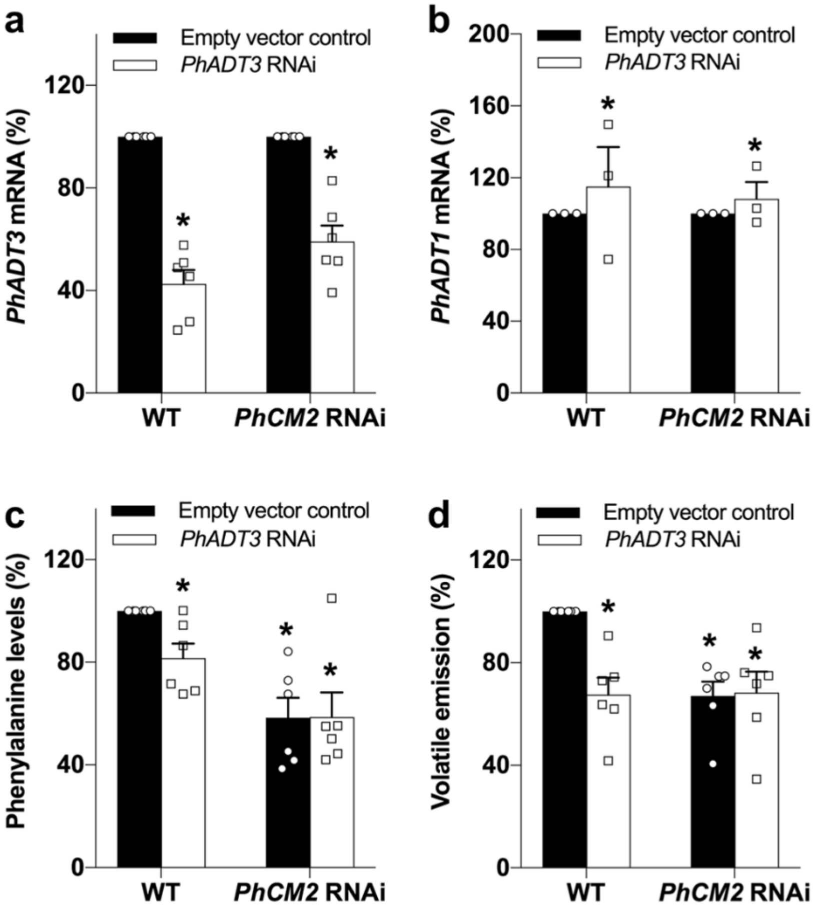

Figure 4.6 Effect of *PhADT3* RNAi down-regulation in wild type and *PhCM2* RNAi petunia flowers

(**a, b**) *PhADT3* mRNA (**a**) and *PhADT1* mRNA (**b**) levels in wild type and *PhCM2* RNAi line15 petunia flowers. For each genetic background, black and white bars represent flowers infiltrated with empty vector or the *PhADT3* RNAi construct, respectively. Data are presented as a percentage relative to the corresponding empty-vector reference. (**c**, **d**) Levels of phenylalanine (**c**) and phenylalanine-derived volatiles (**d**) in petunia flowers of wild type and *PhCM2* RNAi line 15 infiltrated with agrobacterium carrying the empty vector (black bars) or the *PhADT3* RNAi construct (white bars). For **c** and **d**, data are presented as a percentage relative to the WT empty vector reference. Data are means ± SE (n = 6 biological replicates). * $P < 0.01$ as determined by paired two-tailed Student’s *t*-test.

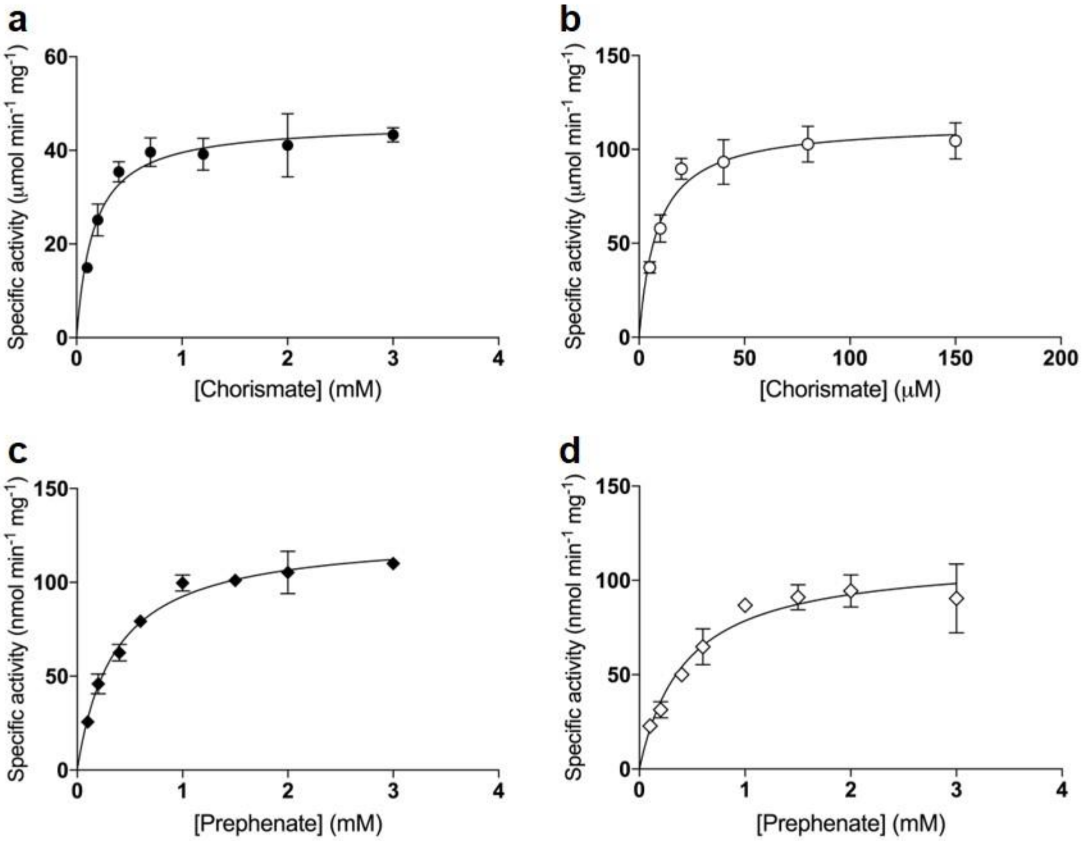

Figure 4.7 Michaelis-Menten kinetics for PhCM1 (a), PhCM2 (b), PhADT3L (c) and PhADT3S (d).

Data are means ± SE (n=3).

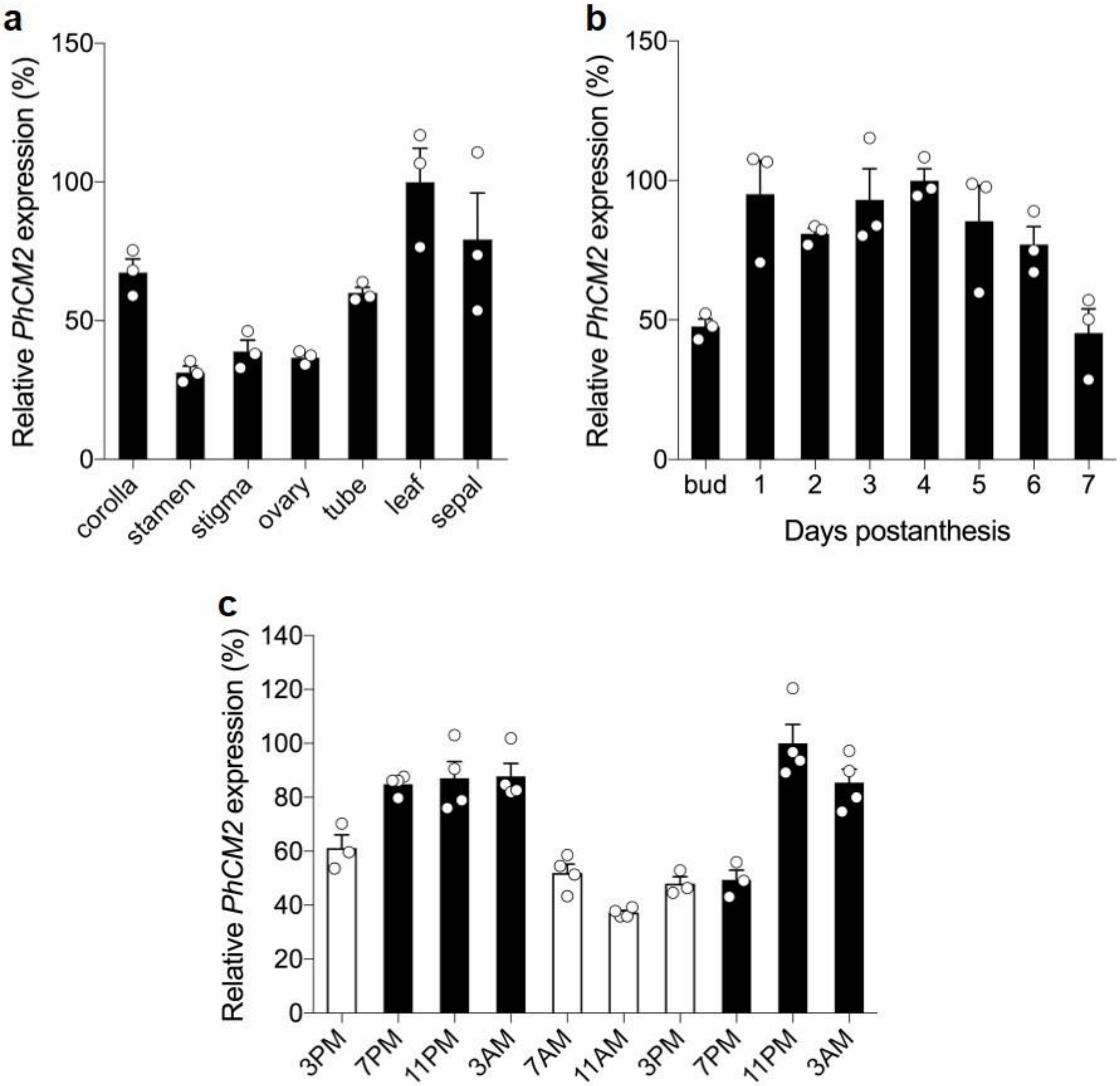

Figure 4.8 Expression profiles of *PhCM2* in petunia flowers.

(a) Tissue-specific expression of *PhCM2* presented relative to the level in leaf tissue set as 100%. (b) Developmental *PhCM2* expression profile in petunia corolla from mature buds to day 7 post-anthesis determined by qRT-PCR. Data are presented relative to the 4-day level. (c) Changes in *PhCM2* transcript levels during a normal light/day cycle in petunia corolla harvested at 15:00 h on day 1 to 03:00 h on day 3 post-anthesis. Black and white bars correspond to night and day sampling points, respectively. Data are presented relative to the transcript level at 23:00 h on day 2 post-anthesis set as 100%. All data are means ± SE (n = 3 biological replicates).

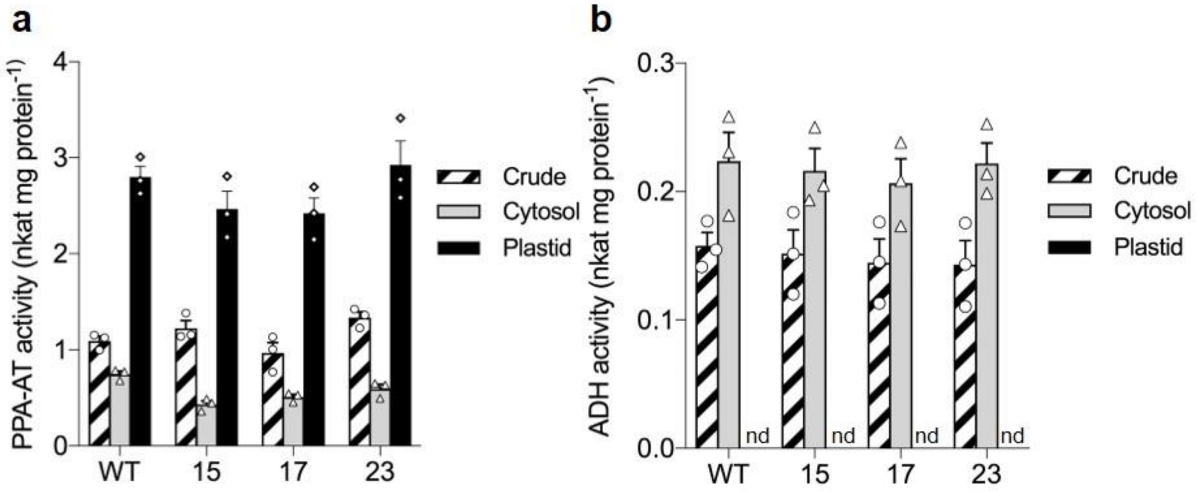

Figure 4.9 Activities of marker enzymes in WT and *PhCM2* RNAi petunia petals.

Prephenate aminotransferase (PPA-AT) (a) and alcohol dehydrogenase (ADH) (b) activities were used as a plastidial and cytosolic marker, respectively. Enzyme activities were measured in crude extracts, cytosolic and plastidic fractions prepared from corollas of 1 to 3 day-old wild type and *PhCM2* RNAi petunia flowers (lines 15, 17, and 23) harvested at 10:00 h. Data are means ± SE. (n=3 biological replicates). nd, not detected.

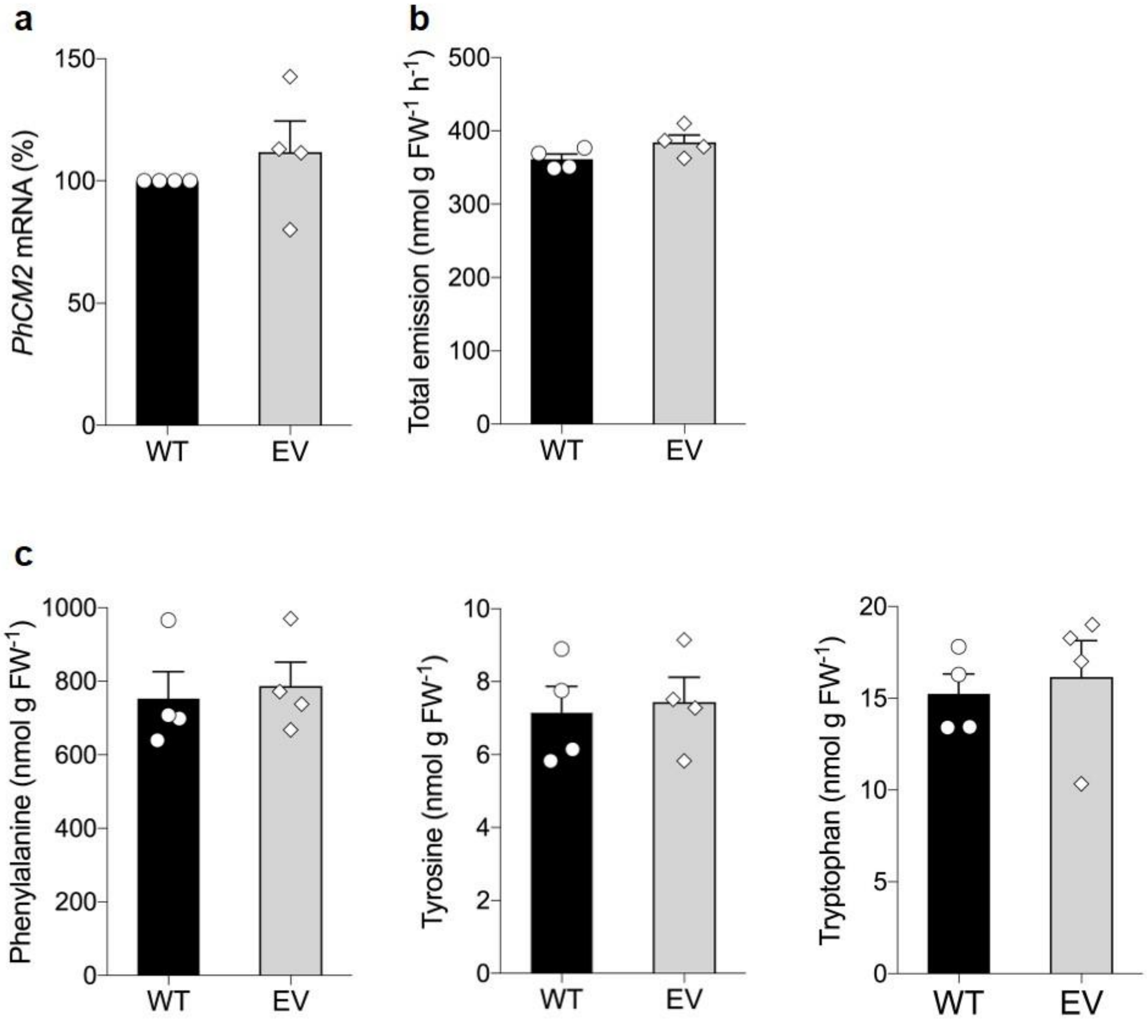

Figure 4.10 Levels of *PhCM2* transcripts (a), emitted phenylalanine-derived volatiles (b) and internal pools of aromatic amino acids (c) in petunia flowers of wild type (WT) and empty vector (EV) control lines.

Petal tissue for RNA isolation and aromatic amino acid extraction was harvested at 20:00 h on 2 day post-anthesis. Volatiles were collected from 2 day-old wild type and transgenic petunia flowers expressing empty vector from 18:00 h to 22:00 h. *PhCM2* mRNA levels are presented as percentage of levels in wild-type set at 100%. Data are means ± SE (n = 4 biological replicates).

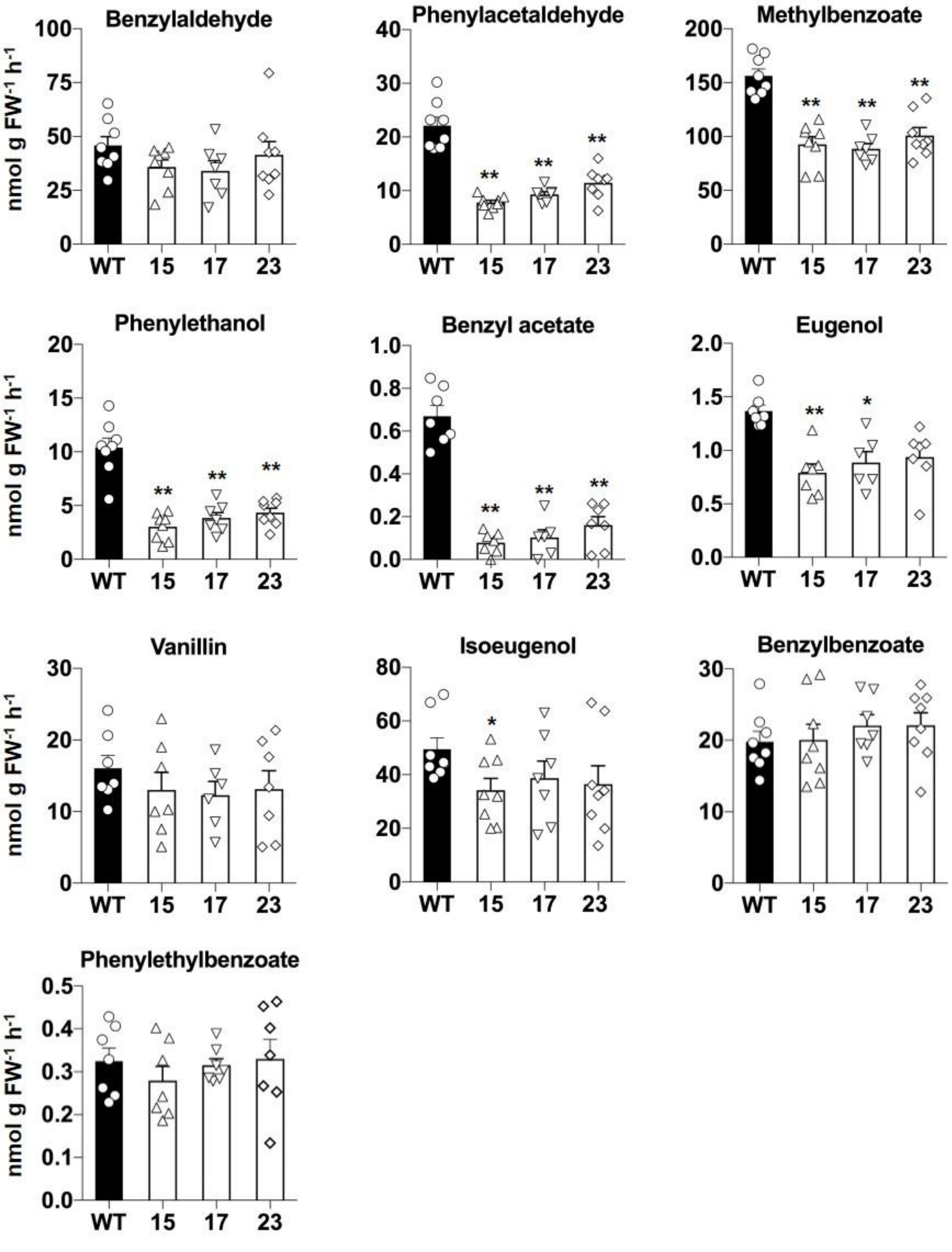

Figure 4.11 Effect of *PhCM2* RNAi downregulation on emission of individual phenylalanine-derived volatiles from petunia flowers.

Volatiles were collected from wild type and transgenic *PhCM2* RNAi petunia flowers from 18:00 h to 22:00 h on day 2 post-anthesis. Data are means ± SE (n ≥ 6 biological replicates). * $P < 0.05$, ** $P < 0.01$ as determined by two-tailed Student's *t*-test.

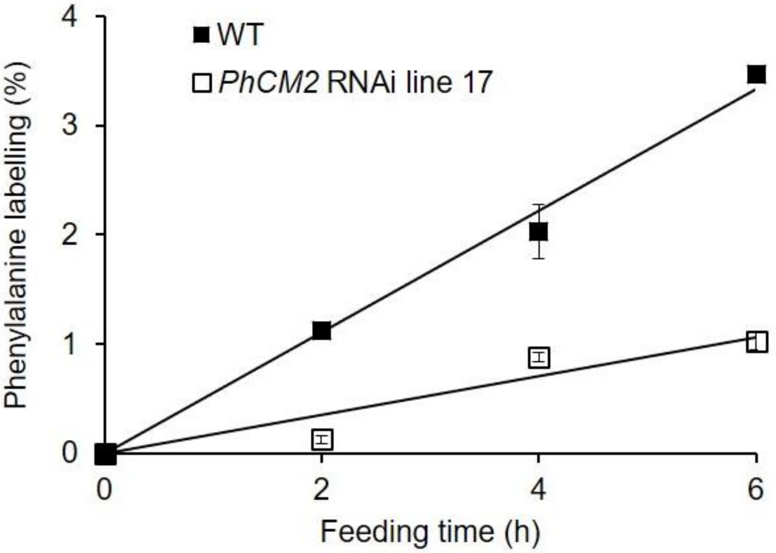

Figure 4.12 Isotopic labeling of phenylalanine from ^{15}N-tyrosine in petunia flowers.

10mM ^{15}N-Tyrosine was fed to 2 day-old control (solid square), and the *PhCM2* RNAi line 17 (open square) petunia flowers for 2, 4, 6 h beginning at 18:00 h. Labeling of phenylalanine pools were analyzed by TOF LC-MS. Data are means ± SE (n = 3 biological replicates). Incorporation of ^{15}N label in phenylalanine was linear over the 6-h time course ($R^2 = 0.991$ and 0.968 for control and the *PhCM2* RNAi line, respectively).

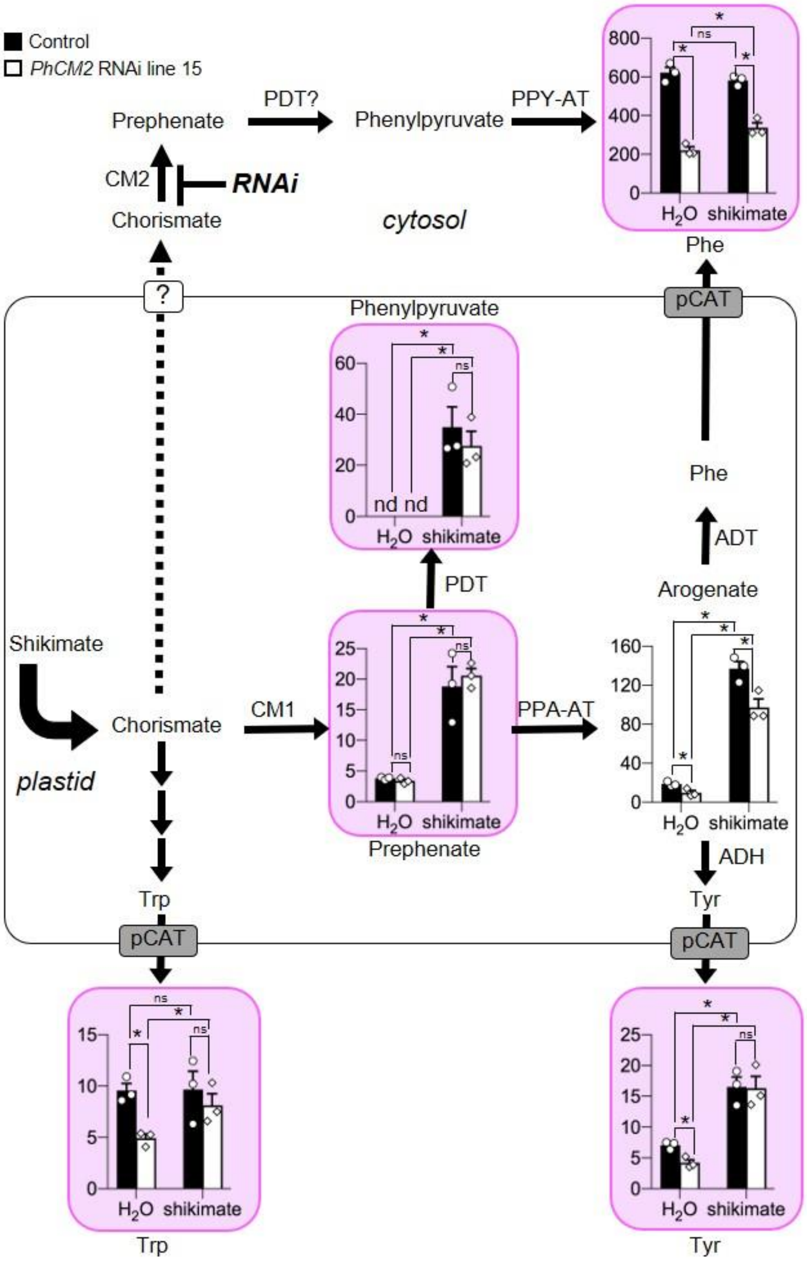

Figure 4.13 Effects of feeding with exogenous shikimate on the levels of aromatic amino acids, arogenate, prephenate and phenylpyruvate in wild type and *PhCM2* RNAi petunia petals.

Excised petals of wild type and *PhCM2* RNAi line 15 (black and white bars, respectively) were fed with water and 100 mM shikimate for 7 h (from 15:00 h till 22:00 h), and the levels of phenylalanine, tyrosine, tryptophan, arogenate, prephenate, and phenylpyruvate were analyzed. Metabolite levels are shown in nmol g FW^{-1}. Pink background indicates metabolites with potential dual subcellular localization, in the cytosol and plastids. Data are means ± SE (n = 3 biological replicates). * $P < 0.05$ as determined by paired two-tailed Student's *t* test. nd, not detected; ns, not significant.

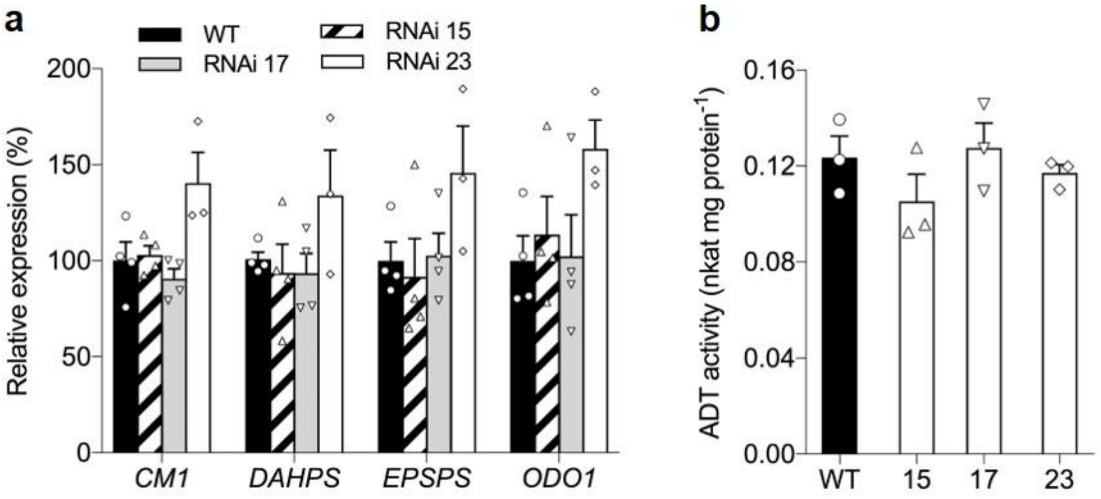

Figure 4.14 Effect of *PhCM2* downregulation on expression levels of shikimate pathway genes and ODO1 transcription factor, and plastidial ADT activity.

(**a**) Expression levels of *CM1,* 3-deoxy-D-arabino-heptulosonate 7-phosphate synthase (DAHPS), and 5-enolpyruvylshikimate 3-phosphate synthase (*EPSPS*), and their transcriptional activator ODORANT1 (*ODO1*) were analyzed in the corollas of wild-type and *PhCM2* RNAi (lines 15, 17, and 23) petunia flowers harvested at 20:00 h 2 day post-anthesis. Expression values in *PhCM2* lines are presented as a percentage of corresponding transcript level in wild-type set as 100%. Data are means ± SE (n = 3 biological replicates). (**b**) ADT activities were measured in plastids isolated from corollas of 1 to 3 day-old wild type and *PhCM2* RNAi petunia flowers (lines 15, 17, and 23) harvested at 10:00 h. Data are means ± SE. (n=3 biological replicates).

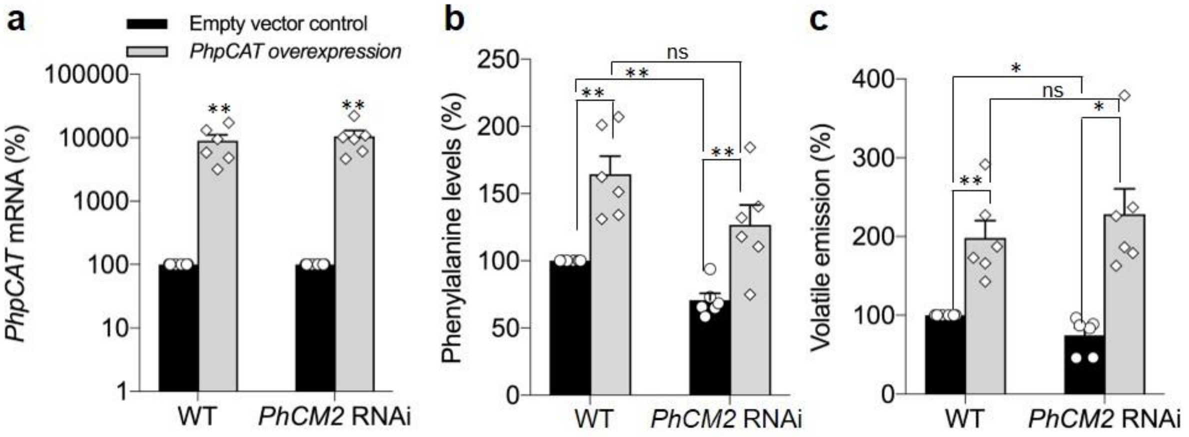

Figure 4.15 Effect of *PhpCAT* overexpression on levels of phenylalanine and phenylalanine-derived volatiles in wild-type and *PhCM2* RNAi petunia flowers.

(**a**) *PhpCAT* mRNA levels in wild type and *PhCM2* RNAi line15 petunia flowers. For each genetic background, black and gray bars represent flowers infiltrated with empty vector or the *PhpCAT* overexpression construct, respectively. Data are presented as a percentage relative to the corresponding empty-vector reference. (**b**, **c**) Levels of phenylalanine (**b**) and phenylalanine-derived volatiles (**c**) in petunia flowers of wild type and *PhCM2* RNAi line 15 infiltrated with agrobacterium carrying the empty vector (black bars) or the *PhpCAT* overexpression construct (gray bars). For **b** and **c**, data are presented as a percentage relative to the WT empty vector reference. Data are means ± SE (n = 6 biological replicates). ns, not significant; * $P < 0.05$ and ** $P < 0.01$ as determined by paired two-tailed Student's *t*-test.

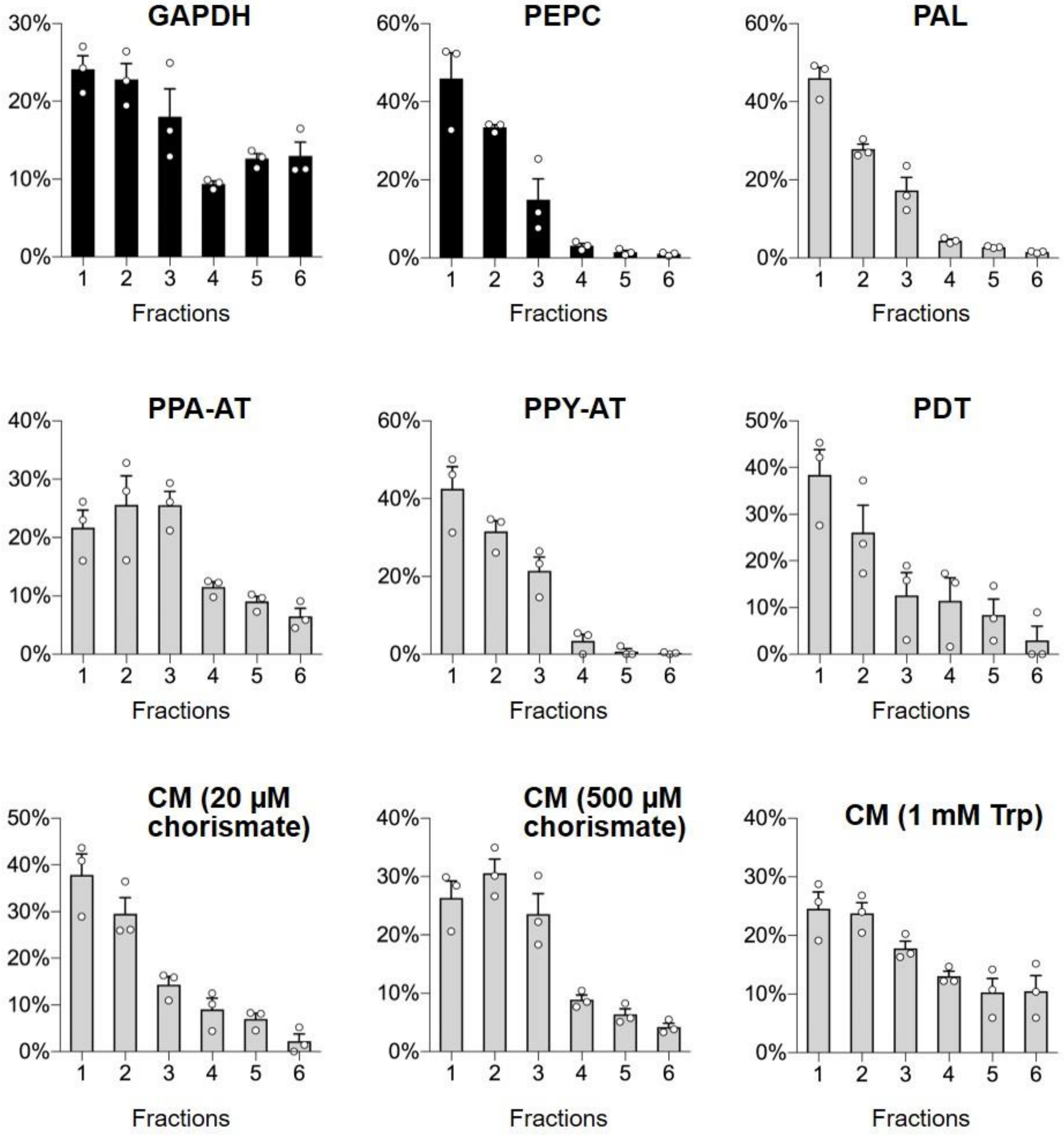

Figure 4.16 Distribution of enzyme activities across the six fractions of decreasing density obtained by non-aqueous fractionation of petunia petals.

Data. are shown as the percentage of total activity recovered across all fractions and are the means ± SE (n=3). GAPDH, NADPH-dependent glyceraldehyde-3-phosphate dehydrogenase; PEPC, phosphor(enol)pyruvate carboxylase; PAL, phenylalanine ammonia lyase; PPA-AT, prephenate aminotransferase; PDT, prephenate dehydratase; PPY-AT, phenylpyruvate aminotransferase; CM (20 µM), chorismate mutase assayed with 20 µM substrate; CM (500 µM), chorismate mutase assayed with 500 µM substrate; CM (1 mM Trp), chorismate mutase assayed with 500 µM substrate in the presence of 1 mM tryptophan.

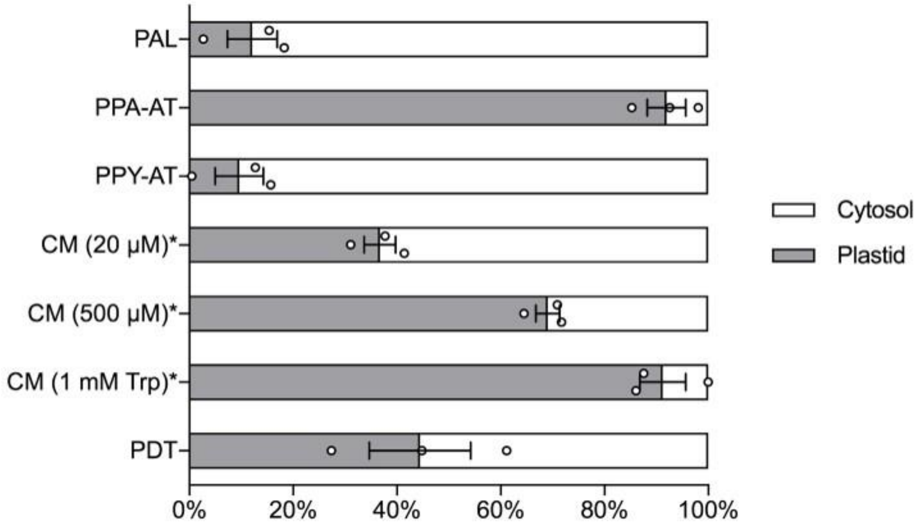

Figure 4.17 Relative distribution of enzyme activities between plastids and cytosol, as determined by non-aqueous fractionation.

Plastidic and cytosolic fractions are shown in grey and white, respectively. Data are means ± SE (n=3). PAL, phenylalanine ammonia lyase; PPA-AT, prephenate aminotransferase; PPY-AT, phenylpyruvate aminotransferase; CM, chorismate mutase; PDT, prephenate dehydratase.

*Distribution of chorismate mutase activities was determined at substrate concentrations of 20 µM and 500 µM, and at 500 µM substrate with 1 mM tryptophan, as indicated. PDT activity was measured at 2 mM of prephenate.

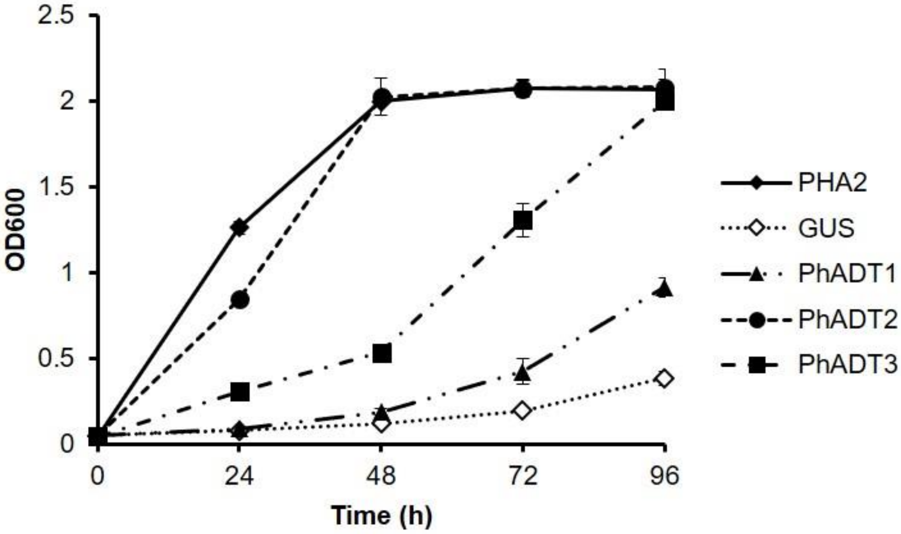

Figure 4.18 Expression of *PhADTs* in a *pha2 S. cerevisiae* mutant.

The *pha2 S. cerevisiae* mutant was transformed with expression vectors carrying *PhADT1*, *PhADT2*, *PhADT3*, *S. cerevisiae PHA2* ORF (a positive control) and GUS (a negative control) under the control of the GAL promoter. The growth of the *pha2* strain is phenylalanine dependent. All strains were first grown to stationary phase in raffinose media containing phenylalanine, then transferred at an initial OD600 of 0.05 to galactose media lacking phenylalanine and grown with shaking at 30°C for 4 days. All data are means ± SE of three independent cultures.

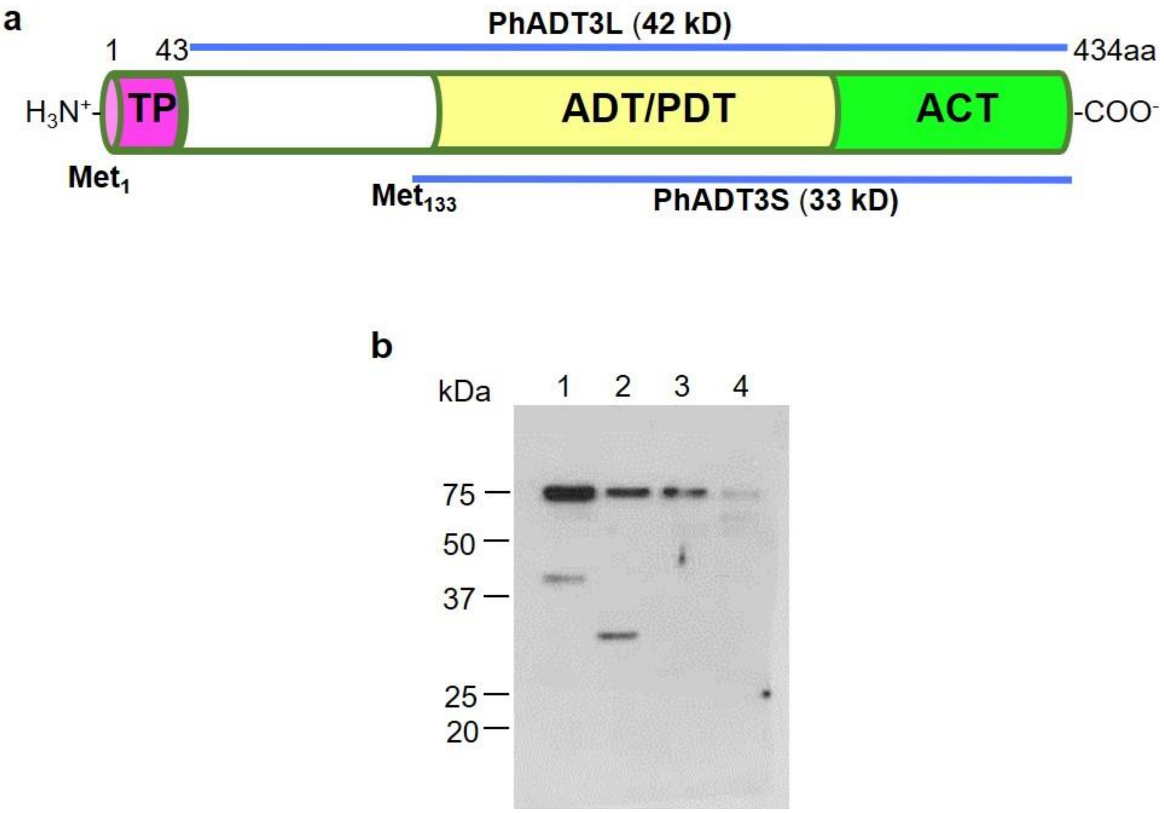

Figure 4.19 Immunodetection of the cytosolic PhADT3 isoform.

Structure of the PhADT3 protein showing positions of plastidial transit peptide (TP), arogenate/prephenate dehydratase (ADT/PDT) catalytic domain, and ACT regulatory amino acid binding domain according to (Zhang et al., 1998). Molecular mass of mature PhADT3L and PhADT3S isoforms are shown. (**b**) Specificity of anti-PhADT3 antibodies. Representative immunoblot using anti-PhADT3 antibodies against purified recombinant mature PhADT3L (lane 1) and PhADT3S (lane 2) isoforms, preparations from *E. coli* carrying empty pET28 expression vector (lane 3) and mature PhADT1 protein (lane 4). 1 µg of total protein was loaded in each lane.

Zhang, S. *et al.* Chorismate mutase-prephenate dehydratase from *Escherichia coli* study of catalytic and regulatory domains using genetically engineered proteins. *J. Biol. Chem.* **273,** 6248-6253 (1998).

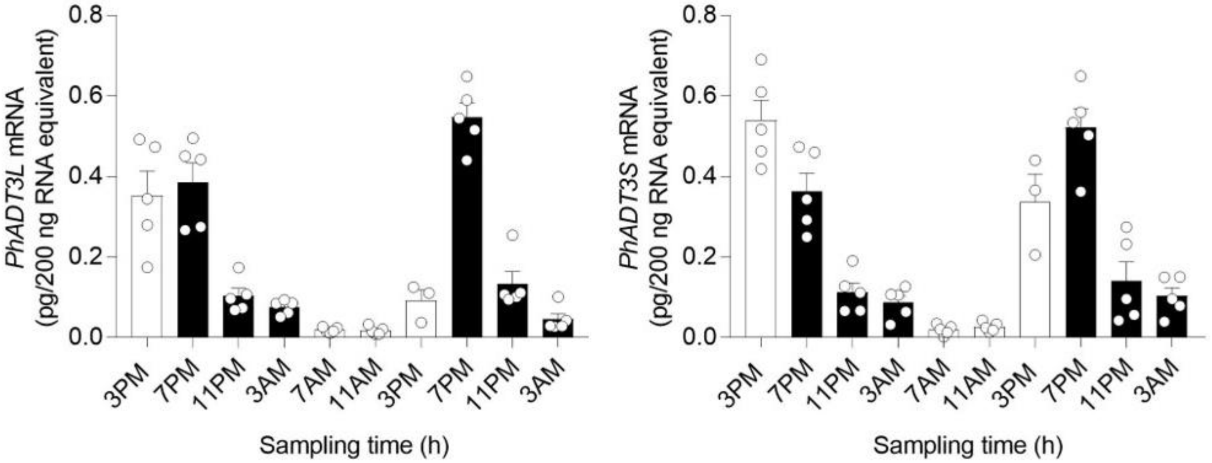

Figure 4.20 Expression profiles of *PhADT3L* and *PhADT3S* transcripts in petunia flowers over a daily light/dark cycle.

Changes in *PhADT3* transcript levels during a normal light/day cycle in petunia corolla harvested at 15:00 h on day 1 to 03:00 h on day 3 post-anthesis. *PhADT3L* mRNA levels were determined using primer set 5 (Fig. 3.5b) while *PhADT3S* mRNA levels were determined by subtracting the quantity of mRNA measured with primer set 5 from that of primer set 6 (Fig. 3.5b), as primer set 5 detects only *PhADT3L* and primer set 6 detects the entire *PhADT3* transcript population (*PhADT3L* plus *PhADT3S*). Black and white bars correspond to night and day sampling points, respectively. All data are means ± SE (n = 5 biological replicates, except for 15:00 h on day 2 post-anthesis n = 3).

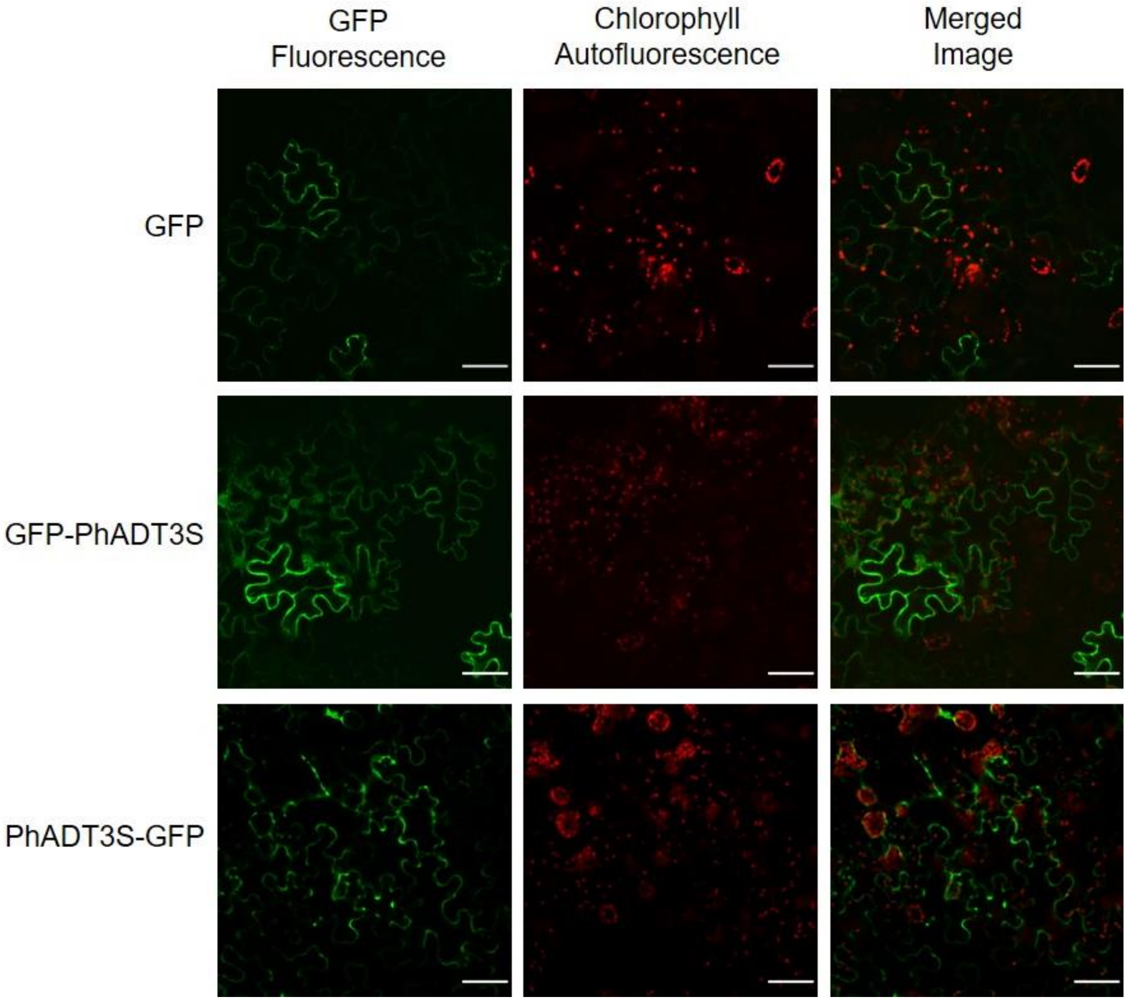
GFP
Fluorescence
Chlorophyll
Autofluorescence
Merged
Image
GFP
GFP-PhADT3S
PhADT3S-GFP

Figure 4.21 Subcellular localization of PhADT3S.

PhADT3S was transiently expressed in *Nicotiana benthamiana* leaves with either an N-terminal (GFP-PhADT3S) or C-terminal (PhADT3S-GFP) fused GFP tag. GFP fluorescence and chlorophyll autofluorescence are shown (*Left* and *Center* panels, respectively), while the merged panels (*Right*) show the overlay of GFP and chlorophyll autofluorescence. GFP alone and chlorophyll autofluorescence were used as cytosolic and plastidic markers, respectively. Scale bars, 50 µm.

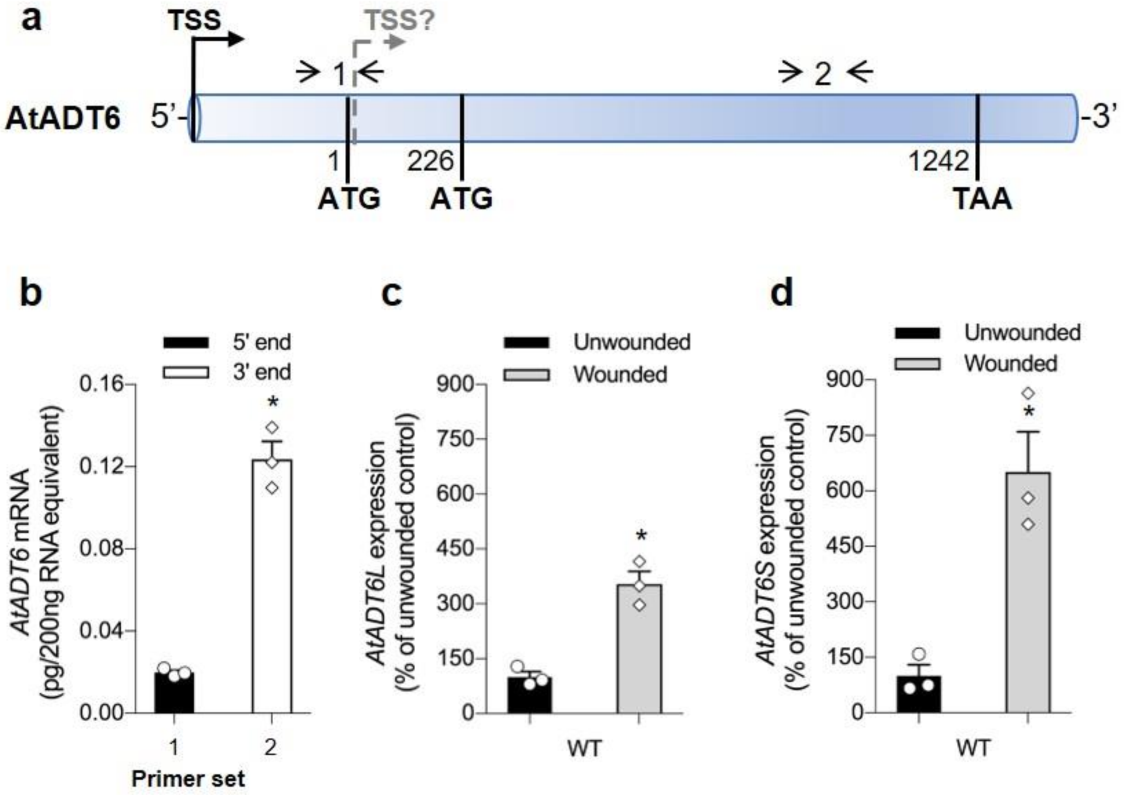

Figure 4.22 Potential alternative *AtADT6* transcripts.

(**a**) Schematic presentation of *AtADT6* mRNA and positions of gene-specific primer sets shown in Table 3.4. The translation initiation codons as well as stop codons are indicated in bold. Nucleotide positions are referred to the first translation initiation codon. TTS, transcription start sites. TTS?, predicted TSS2. (**b**) The absolute levels of *AtADT6* transcripts were determined at 5′ end (black) and 3′ end (white) of mRNAs by qRT-PCR and are shown as pg/200 ng total RNA. Data are means ± SE (n=3 biological replicates). (**c**, **d**) *AtADT6L* (**c**) and *AtADT6S* (**d**) transcript levels in wild type Arabidopsis leaves upon mechanical wounding, as determined by qRT-PCR. Data are presented as percentage to levels of *AtADT6L* and *AtADT6S* transcripts in unwounded leaves, set as 100%. Data are means ± SE (n = 3 biological replicates). * $P < 0.05$ as determined by Student's *t*-test.

4.7 References

1. Maeda, H. & Dudareva, N. The shikimate pathway and aromatic amino acid biosynthesis in plants. *Annual Review of Plant Biology* **63,** 73–105 (2012).
2. Vlot, A. C., Dempsey, D. A. & Klessig, D. F. Salicylic acid, a multifaceted hormone to combat disease. *Annu. Rev. Phytopathol.* **47,** 177–206 (2009).
3. Block, A. *et al.* The origin and biosynthesis of the benzenoid moiety of ubiquinone (Coenzyme Q) in Arabidopsis. *Plant Cell* **26,** 1938–1948 (2014).
4. Dudareva, N., Negre, F., Nagegowda, D. A. & Orlova, I. Plant volatiles: Recent advances and future perspectives. *Crit. Rev. Plant Sci.* **25,** 417–440 (2006).
5. Dudareva, N., Klempien, A., Muhlemann, J. K. & Kaplan, I. Biosynthesis, function and metabolic engineering of plant volatile organic compounds. *New Phytol.* **198,** 16-32 (2013).
6. Vogt, T. Phenylpropanoid biosynthesis. *Mol. Plant* **3,** 2–20 (2010).
7. Bonawitz, N. D. & Chapple, C. The genetics of lignin biosynthesis: Connecting genotype to phenotype. *Annu. Rev. Genet.* **44,** 337–363 (2010).
8. Huang, W. Y., Cai, Y. Z. & Zhang, Y. Natural phenolic compounds from medicinal herbs and dietary plants: Potential use for cancer prevention. *Nutr. Cancer* **62,** 1–20 (2010).
9. Costa, M. A. *et al.* Transgenic hybrid poplar for sustainable and scalable production of the commodity/specialty chemical, 2-phenylethanol. *PLoS One* **8,** e83169 (2013).
10. Maeda, H. *et al.* RNAi suppression of Arogenate dehydratase1 reveals that phenylalanine is synthesized predominantly via the arogenate pathway in petunia petals. *Plant Cell* **22,** 832–849 (2010).
11. Corea, O. R. A. *et al.* Arogenate dehydratase isoenzymes profoundly and differentially modulate carbon flux into lignins. *J. Biol. Chem.* **287,** 11446–11459 (2012).
12. Dal Cin, V. *et al.* Identification of genes in the phenylalanine metabolic pathway by ectopic expression of a MYB transcription factor in tomato fruit. *Plant Cell* **23,** 2738–2753 (2011).
13. Tzin, V. & Galili, G. The biosynthetic pathways for shikimate and aromatic amino acids in *Arabidopsis thaliana*. *Arab. B.* **8,** e0132 (2010).
14. Tzin, V., Malitsky, S., Aharoni, A. & Galili, G. Expression of a bacterial bi-functional chorismate mutase/prephenate dehydratase modulates primary and secondary metabolism associated with aromatic amino acids in Arabidopsis. *Plant J.* **60,** 156–167 (2009).

15. Oliva, M. *et al.* Phenylpyruvate contributes to the synthesis of fragrant benzenoid–phenylpropanoids in *Petunia* × *hybrida* flowers. *Front. Plant Sci.* **8,** 1–13 (2017).
16. Yoo, H. *et al.* An alternative pathway contributes to phenylalanine biosynthesis in plants via a cytosolic tyrosine:phenylpyruvate aminotransferase. *Nat. Commun.* **4,** 2833 (2013).
17. Cho, M.-H. *et al.* Phenylalanine biosynthesis in *Arabidopsis thaliana*: Identification and characterization of arogenate dehydratases. *J. Biol. Chem.* **282,** 30827–30835 (2007).
18. Yamada, T. *et al.* Mutation of a rice gene encoding a phenylalanine biosynthetic enzyme results in accumulation of phenylalanine and tryptophan. *Plant Cell* **20,** 1316–1329 (2008).
19. El-Azaz, J., de la Torre, F., Ávila, C. & Cánovas, F. M. Identification of a small protein domain present in all plant lineages that confers high prephenate dehydratase activity. *Plant J.* **87,** 215–229 (2016).
20. Rippert, P., Puyaubert, J., Grisollet, D., Derrier, L. & Matringe, M. Tyrosine and phenylalanine are synthesized within the plastids in Arabidopsis. *Plant Physiol.* **149,** 1251–1260 (2009).
21. Maeda, H., Yoo, H. & Dudareva, N. Prephenate aminotransferase directs plant phenylalanine biosynthesis via arogenate. *Nat. Chem. Biol.* **7,** 19–21 (2011).
22. Colquhoun, T. a. *et al.* A petunia chorismate mutase specialized for the production of floral volatiles. *Plant J.* **61,** 145–155 (2010).
23. Eberhard, J. *et al.* Cytosolic and plastidic chorismate mutase isozymes from Arabidopsis thaliana: molecular characterization and enzymatic properties. *Plant J.* **10,** 815–821 (1996).
24. Mobley, E. M., Kunkel, B. N. & Keith, B. Identification, characterization and comparative analysis of a novel chorismate mutase gene in *Arabidopsis thaliana*. *Gene* **240,** 115–123 (1999).
25. Goers, S. K. & Jensen, R. A. The differential allosteric regulation of two chorismate-mutase isoenzymes of *Nicotiana silvestris*. *Planta* **162,** 117–124 (1984).
26. Poulsen, C. & Verpoorte, R. Roles of chorismate mutase, isochorismate synthase and anthranilate synthase in plants. *Phytochemistry* **30,** 377–386 (1991).
27. Singh, B. K., Lonergan, S. G. & Conn, E. E. Chorismate mutase isoenzymes from selected plants and their immunological comparison with the isoenzymes from *Sorghum bicolor*. *Plant Physiol.* **81,** 717–722 (1986).

28. Westfall, C. S., Xu, A. & Jez, J. M. Structural evolution of differential amino acid effector regulation in plant chorismate mutases. *J. Biol. Chem.* **289,** 28619–28628 (2014).
29. Boatright, J. *et al.* Understanding *in vivo* benzenoid metabolism in petunia petal tissue. *Plant Physiol.* **135,** 1993–2011 (2004).
30. Verdonk, J. C. *et al.* Regulation of floral scent production in petunia revealed by targeted metabolomics. *Phytochemistry* **62,** 997–1008 (2003).
31. Orlova, I. *et al.* Reduction of benzenoid synthesis in petunia flowers reveals multiple pathways to benzoic acid and enhancement in auxin transport. *Plant Cell* **18,** 3458–3475 (2006).
32. Widhalm, J. R. *et al.* Identification of a plastidial phenylalanine exporter that influences flux distribution through the phenylalanine biosynthetic network. *Nat. Commun.* **6,** 8142 (2015).
33. Bentley, R. & Haslam, E. The shikimate pathway - A metabolic tree with many branche. *Crit. Rev. Biochem. Mol. Biol.* **25,** 307–384 (1990).
34. Herrmann, K. M. & Weaver, L. M. The shikimate pathway. *Annu. Rev. Plant Physiol. Plant Mol. Biol.* **50,** 473–503 (1999).
35. Verdonk, J. C., Haring, M. A., Tunen, A. J. Van & Schuurink, R. C. ODORANT1 regulates fragrance biosynthesis in petunia flowers. *Plant Cell* **17,** 1612–1624 (2005).
36. Gutensohn, M. *et al.* Role of aromatic aldehyde synthase in wounding/herbivory response and flower scent production in different Arabidopsis ecotypes. *Plant J.* **66,** 591–602 (2011).
37. Warpeha, K. M. *et al.* G-protein-coupled receptor 1, G-protein Galpha-subunit 1, and prephenate dehydratase 1 are required for blue light-induced production of phenylalanine in etiolated Arabidopsis. *Plant Physiol.* **140,** 844–855 (2006).
38. Krueger, S. *et al.* A topological map of the compartmentalized Arabidopsis thaliana leaf metabolome. *PLoS One* **6,** e17806 (2011).
39. Achnine, L., Blancaflor, E. B., Rasmussen, S. & Dixon, R. A. Colocalization of L-phenylalanine ammonia-lyase and cinnamate 4-hydroxylase for metabolic channeling in phenylpropanoid biosynthesis. *Plant Cell* **16,** 3098–3109 (2004).
40. Cunillera, N., Boronat, A. & Ferrer, A. The *Arabidopsis thaliana* FPS1 gene generates a novel mRNA that encodes a mitochondrial farnesyl-diphosphate synthase isoform. *J. Biol. Chem.* **272,** 15381–15388 (1997).

41. Thatcher, L. F. *et al.* Differential gene expression and subcellular targeting of Arabidopsis glutathione S-transferase F8 is achieved through alternative transcription start sites. *J. Biol. Chem.* **282,** 28915–28928 (2007).
42. Phillips, M. A., D'Auria, J. C., Gershenzon, J. & Pichersky, E. The *Arabidopsis thaliana* type I isopentenyl diphosphate isomerases are targeted to multiple subcellular compartments and have overlapping functions in isoprenoid biosynthesis. *Plant Cell* **20,** 677–696 (2008).
43. Daras, G. *et al.* Alternative transcription initiation and the AUG context configuration control dual-organellar targeting and functional competence of Arabidopsis Lon1 protease. *Mol. Plant* **7,** 989–1005 (2014).
44. Lescot, M. *et al.* PlantCARE, a database of plant cis-acting regulatory elements and a portal to tools for in silico analysis of promoter sequences. *Nucleic Acids Res.* **30,** 325–327 (2002).
45. Grebenok, R. J. *et al.* Green-fluorescent protein fusions for efficient characterization of nuclear targeting. *Plant J.* **11,** 573–586 (1997).
46. Haslam, E. *Shikimic Acid: Metabolism and Metabolites*. (John Wiley & Sons Inc, 1993).
47. Graindorge, M. *et al.* Identification of a plant gene encoding glutamate/aspartate-prephenate aminotransferase: The last homeless enzyme of aromatic amino acids biosynthesis. *FEBS Lett.* **584,** 4357–4360 (2010).
48. Berry, A., Ahmad, S., Liss, A. & Jensen, R. A. Enzymological features of aromatic amino acid biosynthesis reflect the phylogeny of mycoplasmas. *J. Gen. Microbiol.* **133,** 2147–2154 (1987).
49. Fischer, R. S., Bonner, C. A., Boone, D. R. & Jensen, R. A. Clues from a halophilic methanogen about aromatic amino acid biosynthesis in archaebacteria. *Arch. Microbiol.* **160,** 440–446 (1993).
50. Prakash, P., Pathak, N. & Hasnain, S. E. pheA (Rv3838c) of *Mycobacterium tuberculosis* encodes an allosterically regulated monofunctional prephenate dehydratase that requires both catalytic and regulatory domains for optimum activity. *J. Biol. Chem.* **280,** 20666–20671 (2005).
51. Whitaker, R. J., Byng, G. S., Gherna, R. L. & Jensen, R. A. Diverse enzymological patterns of phenylalanine biosynthesis in pseudomonads are conserved in parallel with deoxyribonucleic acid homology groupings. *J. Bacteriol.* **147,** 526–534 (1981).

52. Tohge, T., Watanabe, M., Hoefgen, R. & Fernie, A. R. Shikimate and phenylalanine biosynthesis in the green lineage. *Front. Plant Sci.* **4,** 62 (2013).
53. Bross, C. D. *et al.* Complementation of the pha2 yeast mutant suggests functional differences for arogenate dehydratases from *Arabidopsis thaliana*. *Plant Physiol. Biochem.* **49,** 882–890 (2011).
54. Kleeb, A. C., Kast, P. & Hilvert, D. A monofunctional and thermostable prephenate dehydratase from the archaeon *Methanocaldococcus jannaschii*. *Biochemistry* **45,** 14101–14110 (2006).
55. Miura, F. *et al.* A large-scale full-length cDNA analysis to explore the budding yeast transcriptome. *Proc. Natl. Acad. Sci.* **103,** 17846–17851 (2006).
56. Kimura, K. *et al.* Diversification of transcriptional modulation: large-scale identification and characterization of putative alternative promoters of human genes. *Genome Res.* **16,** 55–65 (2006).
57. Tanaka, T., Koyanagi, K. O. & Itoh, T. Highly diversified molecular evolution of downstream transcription start sites in rice and Arabidopsis. *Plant Physiol.* **149,** 1316–1324 (2009).
58. Shahmuradov, I. A., Umarov, R. K. & Solovyev, V. V. TSSPlant: a new tool for prediction of plant Pol II promoters. *Nucleic Acids Res.* **45,** e65 (2017).
59. Hieno, A. *et al.* Ppdb: Plant promoter database version 3.0. *Nucleic Acids Res.* **42,** 1188–1192 (2014).
60. Para, A. *et al.* The dehydratase ADT3 affects ROS homeostasis and cotyledon development. *Plant Physiol.* **172,** 1045–1060 (2016).
61. Canales, J. *et al.* De novo assembly of maritime pine transcriptome: Implications for forest breeding and biotechnology. *Plant Biotechnol. J.* **12,** 286–299 (2014).
62. Tzin, V. & Galili, G. New insights into the shikimate and aromatic amino acids biosynthesis pathways in plants. *Mol. Plant* **3,** 956–972 (2010).
63. Ayoubi, T. A. & Van De Ven, W. J. Regulation of gene expression by alternative promoters. *FASEB J.* **10,** 453–460 (1996).
64. Schenck, C. a, Chen, S., Siehl, D. L. & Maeda, H. a. Non-plastidic, tyrosine-insensitive prephenate dehydrogenases from legumes. *Nat. Chem. Biol.* **11,** 52–57 (2015).

65. Gleave, A. P. A versatile binary vector system with a T-DNA organisational structure conducive to efficient integration of cloned DNA into the plant genome. *Plant Mol. Biol.* **20,** 1203–1207 (1992).

66. Klempien, A. *et al.* Contribution of CoA ligases to benzenoid biosynthesis in petunia flowers. *Plant Cell* **24,** 2015–2030 (2012).

67. Qualley, A. V, Widhalm, J. R., Adebesin, F., Kish, C. M. & Dudareva, N. Completion of the core β-oxidative pathway of benzoic acid biosynthesis in plants. *Proc. Natl. Acad. Sci. U. S. A.* **109,** 16383–16388 (2012).

68. Rieger, C. E. & Turnbull, J. L. Small scale biosynthesis and purification of gram quantities of chorismic acid. *Prep. Biochem. Biotechnol.* **26,** 67–76 (1996).

69. Grisostomi, C., Kast, P., Pulido, R., Huynh, J. & Hilvert, D. Efficient in vivo synthesis and rapid purification of chorismic acid using an e ngineered *Escherichia coli* strain. *Bioorg. Chem.* **25,** 297–305 (1997).

70. Duziński, P. K. & Morrison, J. F. The preparation and purification of sodium prephenate. *Prep. Biochem.* **6,** 113–121 (1976).

71. Widhalm, J. R., van Oostende, C., Furt, F. & Basset, G. J. C. A dedicated thioesterase of the Hotdog-fold family is required for the biosynthesis of the naphthoquinone ring of vitamin K1. *Proc. Natl. Acad. Sci. U. S. A.* **106,** 5599–5603 (2009).

72. Walker, G. H., Ku, M. S. & Edwards, G. E. Catalytic activity of maize leaf phosphoenolpyruvate carboxylase in relation to oligomerization. *Plant Physiol.* **80,** 848–855 (1986).

73. Kim, J. I., Dolan, W. L., Anderson, N. A. & Chapple, C. Indole glucosinolate biosynthesis limits phenylpropanoid accumulation in *Arabidopsis thaliana*. *Plant Cell* **27,** 1529–1546 (2015).

74. Dudareva, N. *et al.* Developmental regulation of methyl benzoate biosynthesis and emission in snapdragon flowers. *Plant Cell* **12,** 949–961 (2000).

75. Eissler, C. L. *et al.* A general strategy for studying multisite protein phosphorylation using label-free selected reaction monitoring mass spectrometry. *Anal. Biochem.* **418,** 267–275 (2011).

76. Cox, J. *et al.* Andromeda: A peptide search engine integrated into the MaxQuant environment. *J. Proteome Res.* **10,** 1794–1805 (2011).

77. Cox, J. *et al.* Accurate proteome-wide label-free quantification by delayed normalization and maximal peptide ratio extraction, termed MaxLFQ. *Mol. Cell. Proteomics* **13,** 2513–2526 (2014).
78. Cox, J. & Mann, M. MaxQuant enables high peptide identification rates, individualized p.p.b.-range mass accuracies and proteome-wide protein quantification. *Nat. Biotechnol.* **26,** 1367–1372 (2008).
79. Karimi, M., Inzé, D. & Depicker, A. GATEWAY^{TM} vectors for Agrobacterium-mediated plant transformation. *Trends Plant Sci.* **7,** 193–195 (2002).
80. Sparkes, I. A., Runions, J., Kearns, A. & Hawes, C. Rapid, transient expression of fluorescent fusion proteins in tobacco plants and generation of stably transformed plants. *Nat. Protoc.* **1,** 2019–2025 (2006).

CHAPTER 5. MODULATION OF AUXIN FORMATION BY THE CYTOSOLIC PHENYLALANINE BIOSYNTHETIC PATHWAY[4]

5.1 Abstract

In plants, biosynthesis of phenylalanine occurs via two compartmentally separated pathways with the major carbon flux flowing through the plastidial arogenate route. To evaluate the metabolic potential of the alternative cytosolic phenylpyruvate pathway, we generated transgenic petunia plants overexpressing *petunia chorismite mutase 2* (*PhCM2*), catalyzing the first committed step. Unexpectedly, phenylalanine levels and emission of phenylalanine-derived volatiles in three independent transgenic lines were reduced on average by 33% and 15%, respectively, despite the flux through the cytosolic pathway was increased by 34% relative to control plants. Electron microscopy, metabolic profiling and metabolic flux analysis revealed that the number of leucoplasts, starch levels and flux through the plastidial pathway were all reduced while the amount of auxin and its biosynthetic intermediate, indole-3-pyruvic acid (IPA), was elevated by approximately 1.9- and 4-fold, respectively. Overexpression of Arabidopsis VAS1, an aminotransferase that converts IPA back to tryptophan, in *PhCM2* overexpression background reduced auxin levels and recovered levels of phenylalanine and phenylalanine-derived volatiles, demonstrating the existence of a metabolic crosstalk between the cytosolic phenylalanine pathway and tryptophan-dependent auxin biosynthesis.

[4] This chapter is a manuscript in preparation.

Qian, Y., Lynch, J. H., Guo, L., Louie, G., Bowman, M. E. , Noel, J. P., Morgan, J. A., & Dudareva, N. (2019) Modulation of auxin formation by the cytosolic phenylalanine biosynthetic pathway

5.2 Introduction

In plants, up to 30% of photosynthetically fixed carbon is directed towards formation of aromatic amino acids and their downstream products, making this biosynthetic network one of the most metabolically intensive[1]. Plants have a high demand for aromatic amino acids since they serve as precursors for the formation of proteins and numerous aromatic primary and specialized metabolites with prominent, and even vital, roles in plant growth, development, reproduction, and defense[2-7]. Within the network, the highest carbon flux is directed to phenylalanine, a common precursor of >8000 phenolic compounds, which fulfill broad physiological functions and are ubiquitous throughout the plant kingdom. In contrast to plants, animals are unable to synthesize phenylalanine, which is thus an essential component of their diet. In addition, phenylalanine-derived compounds are widely used by humans as nutritional supplements, flavors, fragrances, pharmaceuticals and biofuels[8,9].

It has long been accepted that aromatic amino acid biosynthesis occurs exclusively in plastids where it is subject to complex feedback regulation both at the entry point into the network and at the committed steps towards individual aromatic amino acids[1] (Figure 5.1). However, we have recently demonstrated that phenylalanine is also synthesized in the cytosol via the microbial-like phenylpyruvate pathway, which branches from the known plastidial arogenate pathway at chorismate[13]. In contrast to arogenate pathway, the phenylpyruvate route is subject to less stringent feedback regulation, because cytosolic chorismite mutase 2 (CM2), catalyzing the entry step in the pathway, is insensitive to allosteric regulation by aromatic amino acids[14].

The cytosolic pathway can serve to conditionally provide rapid increases in phenylalanine levels, as was recently demonstrated by the CM2-dependent production of phenylacetaldehyde, a direct product from phenylalanine, in response to mechanical wounding in Arabidopsis[13]. Moreover, fluxes through the cytosolic phenylalanine biosynthetic pathway have been shown to increase in petunia transgenic plants in which the plastidial pathway is either downregulated[12] or feedback inhibited[19], suggesting the cytosolic pathway is able to redirect the flux to increase phenylalanine production in the cytosol *in planta*. However, when the *E. coli* bifunctional chorismate mutase/prephenate dehydratase gene (*PheA*) was constitutively expressed in the cytosol in Arabidopsis, there were no reported changes in aromatic amino acid levels[15]. These inconsistent impacts of the cytosolic pathway on phenylalanine production raise the question as how the metabolic potential of the cytosolic phenylpyruvate pathway is utilized *in planta*.

5.3 Results

5.3.1 Plastidial phenylalanine biosynthesis flux decreased in *PhCM2* overexpression lines

Petunia hybrida produces high levels of phenylalanine and phenylalanine-derived benzenoid/phenylpropanoid volatiles[16,17]. To evaluate the metabolic potential of the cytosolic phenylpyruvate pathway, we overexpressed *PhCM2* in petunia flowers to direct carbon flux towards the phenylpyruvate pathway in the cytosol. Transient *PhCM2* overexpression in fully developed, 2-day-old, flowers resulted in more than 3-fold increase in emission of phenylalanine-derived volatiles, suggesting that cytosolic pathway can produce high levels of phenylalanine (Figure 5.2a). However, consistent with *PheA* overexpression in Arabidopsis[15], stable transgenic petunia lines overexpressing *PhCM2* under the control of the petal-specific promoter[18] did not exhibit any increase in phenylalanine or phenylalanine-derived volatiles. Instead, three independent transgenic lines with highest expression of *PhCM2*, ranging from a 49-fold to 64-fold increase in transcript abundance and up to 3-fold increase in cytosolic CM activity (Figure 5.2b), displayed an unexpected decrease in phenylalanine levels by 25% - 41%, and a subsequent 15% decrease on average in emission of phenylalanine-derived volatiles (Figure 5.2c). At the same time, the levels of phenylpyruvate, an intermediate in the cytosolic phenylalanine pathway, were increased to detectable levels, while the levels of arogenate, an intermediate in the plastidial phenylalanine biosynthetic pathway, was decreased by 31% - 42% (Figure 5.2c). Analysis of the flux through the phenylalanine biosynthetic network using ^{15}N-tyrosine labeling[12] and recently developed metabolic flux model[19] revealed that indeed flux through the cytosolic pathway, v_2, was increased by 24% and 34% ($p < 0.05$, two tailed Student's *t*-test, n=8, Bonferroni corrected) at t_0 and t_6, respectively, in *PhCM2* transgenic lines relative to control (Figure 5.4 and Table 5.1) further supporting that *PhCM2* overexpression does increase production of phenylalanine via the cytosolic pathway. In contrast, the flux through the plastidial pathway, v_1, in transgenics was decreased by 24% ($p < 0.01$, two tailed Student's *t*-test, n=8, Bonferroni corrected) at both t_0 and t_6 time points, relative to control, which was consistent with the redirection of carbon flux towards the cytosolic phenylalanine pathway as well as the observed decrease in internal pools of arogenate (Figure 5.2c). Therefore, the overall decrease in phenylalanine biosynthesis was due to the net difference between increased flux via the cytosolic pathway and decreased flux via the plastidial pathway, the latter of which is the dominant pathway for phenylalanine production in plants[10,20,21].

5.3.2 Plastid development is impaired in *PhCM2* overexpression lines

While testing CM activity, we came across that although the specific CM activity in plastidial extracts was similar in transgenic and wild-type flowers, the yield of plastidial proteins was on average 34% lower in preparations from the transgenic flowers relative to control (Table 5.2). Transmission electron microscopy of the epidermal conical cells, the predominant location for phenylalanine-derived volatiles biosynthesis, did not identify any alterations in plastidial structure (Figure 5.5b); however, fewer leucoplasts, the predominant form of flower petal plastids, were visible in cross-sections of transgenic petals (on average 1.2 ± 0.3 per cell, n = 7 cells) versus control (on average 2.4 ± 0.4 per cell, n = 7 cells) (Figure 5.5a), suggesting perturbations of plastid development. Consistent with the decrease in the number of leucoplasts, the levels of starch were also reduced by 20 - 39% in transgenic lines relative to control (Figure 5.6a), as starch is mainly stored in leucoplasts. Taken together, these data suggest that the different metabolic phenotypes observed upon transient versus stable overexpression of *PhCM2* are due to alterations occurring during flower development that result in decreased production of leucoplasts.

In plants colorless leucoplasts are mainly formed via redifferentiation of chloroplasts, in addition to their formation directly from proplastid[22,23]. It has been shown that plastid organogenesis relies on the cytokinin/auxin signaling pathway[24]. Indeed, increased auxin signaling represses plastid development in Arabidopsis roots[24] and the effective development of amyloplasts, a sub-class of leucoplasts, which accumulate starch, depends on auxin in cultured Bright Yellow-2 (BY-2) tobacco cells[25]. As auxins and phenylalanine share common biosynthetic precursors[1], we hypothesized that the decrease in number of plastids and a subsequent reduction in the flux via the arogenate phenylalanine biosynthetic pathway in *PhCM2* overexpressors are due to changes in auxin homeostasis. To test this hypothesis, we analyzed the levels of indole-3-acetic acid (IAA, an endogenous auxin) and indole-3-pyruvic acid (IPA), an intermediate in the major tryptophan dependent auxin biosynthetic pathway[26-29]. Both IAA and IPA were elevated in all three transgenic petunia lines (by ~1.9- and ~4-fold, respectively) relative to control (Figure 5.6b), correlating with the observed decrease in leucoplast content (Figure 5.5a) and suggesting the existence of cytosol-specific interactions between the phenylalanine and auxin biosynthetic pathways.

5.3.3 Overexpressing *AtVAS1* in *PhCM2* overexpression line rescued phenylalanine levels

To independently test whether the decrease in flux through the plastidial biosynthetic pathway in *PhCM2*-overexpressing flowers is due to elevation of IPA and IAA levels, we reduced endogenous auxin levels through overexpression of Arabidopsis VAS1, an aminotransferase that converts IPA back to tryptophan[30]. Several independent *AtVAS1* overexpression lines were generated in the background of *PhCM2*-overexpression line 28, and three with the highest *AtVAS1* mRNA levels were used for further analysis (Figure 5.3a). In all three lines, starch levels were recovered to wild-type levels (Figure 5.3c), indicating overexpression of *AtVAS1* is capable of complementing the leucoplast-development deficiency of the *PhCM2* overexpression line, leading to recovery of arogenate levels (Figure 5.3e), phenylalanine and phenylalanine-derived volatiles emission (Figure 5.3d).

5.4 Discussion

In the *PhCM2* overexpression lines, an increase in IAA and IPA levels was not expected, since increased expression of *PhCM2* would be anticipated to increase consumption of chorismate, leaving less chorismate available to be directed towards production of the auxins by anthranilate synthase[32]. Additionally, when the consumption of chorismate was increased by the overexpression of bacterial PheA, a bifunctional chorismate mutase/prephenate dehydratase, in the plastids, no phenotypic changes associated with altered auxin signaling were reported[15]. These results suggest there exists a cytosol-specific interaction between the phenylalanine and auxin biosynthetic pathways. Moreover, recent characterization of an Arabidopsis Shade AVoidance deficient mutant (*sav3*) identified a novel cytosolic pathway for the production of IAA via deamination of tryptophan to form IPA, an auxin biosynthesis intermediate[28]. *In vitro* biochemical characterization of the responsible aminotransferase SAV3, also known as tryptophan aminotransferase of Arabidopsis (TAA1), demonstrated that tryptophan is the preferred amino donor with pyruvate serving as the amino acceptor[28]. Further investigation is required to clarify if TAA1 may also use phenylpyruvate, the intermediate of the cytosolic phenylalanine biosynthetic pathway, as amino acceptor, thus the increased auxin production in *PhCM2* overexpression lines could be a result of the increased phenylpyruvate levels (Figure 5.7), connecting the cytosolic phenylalanine production and auxin biosynthesis.

A combination of reverse genetics, biochemistry, targeted metabolic profiling and metabolic flux modelling used in this study supports the existence of a metabolic crosstalk between the cytosolic phenylalanine pathway and tryptophan-dependent auxin biosynthesis. Despite the relatively low direct contribution of the cytosolic phenylpyruvate pathway to phenylalanine biosynthesis, plants likely use it for rapid production of phenylalanine in response to biotic and abiotic stresses[13]. Thus, the existence of a crosstalk between phenylalanine and auxin biosynthesis might provide an efficient metabolic mechanism for tissue-specific coordination of defense responses with plant growth and development. Since the auxin pathway intersects with other plant hormones' pathways[30], modulation of auxin levels via the cytosolic phenylalanine biosynthetic pathway can have a broader impact on plant growth and development, especially under stress conditions.

5.5 Materials and Methods

5.5.1 Generation of *PhCM2* overexpression and *AtVAS1xPhCM2* overexpression plants

Petunia hybrida cv Mitchell plants were grown under standard greenhouse conditions with a light period from 6:00 h to 21:00 h. For the *PhCM2* overexpression construct, *PhCM2* coding region (792 bp) was amplified by PCR using gene-specific primers (Table 5.3). The PCR fragment was subcloned into the polylinker site (*Eco*RI/*BamH*I) of a modified pRNA69 vector, containing the *Clarkia breweri linalool synthase* (*LIS*) petal specific promoter[18]. The entire cassette containing the *LIS* promoter and the *PhCM2* coding region was released by *Sac*I/*Not*I digestion and ligated into the corresponding sites of the pART27 binary vector[31]. The final *PhCM2* overexpression construct in the binary vector was used for *Agrobacterium tumefaciens* (GV3101) mediated transformation of *Petunia hybrida* cv. Mitchell using the standard leaf disk transformation method. For the *AtVAS1* overexpression construct, the coding region of *AtVAS1* was amplified using gene-specific primers (Table 5.3) possessing 5′-extensions that provide annealing sites for subsequent amplification with AttB primers (Invitrogen). The resulting amplicons were inserted into pDONR/Zeo vector by recombination using BP Clonase II (Invitrogen) according to the manufacturer's protocol. The generated construct was confirmed by sequencing, then subjected to recombination with binary vector pB2GW7 (containing the CaMV 35S promoter, using LR Clonase II (Invitrogen) according to the manufacturer's protocol. The final *AtVAS1* overexpression construct in the binary vector was used for *Agrobacterium tumefaciens* (GV3101) mediated transformation on *PhCM2* overexpression line 28 background using the standard leaf disk transformation method.

5.5.2 RNA isolation and qRT-PCR analysis

Sample collection, RNA isolation and qRT-PCR were performed as described in 4.5.3. Relative quantification of *PhCM2* transcript levels were performed by qRT-PCR analysis with gene specific primers (Table 5.3) relative to the reference genes *UBQ10* for petunia[10]. For absolute quantification of *AtVAS1* transcript levels, pB2GW7 vector carrying *AtVAS1* coding region was used. Concentration of was determined with the NanoDrop 1000 spectrophotometer (Thermo Scientific, West Palm Beach, FL, USA). Several dilutions were prepared from 1 ng/ml to 6.4 pg/ml and used to obtain standard curves in qRT-PCR with *AtVAS1*-specific primers[30] (Table 5.3). On the basis of the standard curves, absolute quantity of *AtVAS1* transcript was calculated and expressed as pg per 200 ng total RNA.

5.5.3 Metabolic profiling

Volatiles collection and analysis, internal pools of aromatic amino acids and organic acids (shikimate, prephenate, arogenate and phenylpyruvate) analysis for wild type control and transgenic petals were performed as described in 4.5.4.

5.5.4 Enzyme assays

CM activity assays were performed as described in 4.5.6.

5.5.5 Preparation of plastidial and cytosolic fractions

Plastidial and cytosolic fractions were prepared from 1- to 3-day old *PhCM2* overexpression , *AtVAS1xPhCM2* overexpression and wild type control petunia petals harvested at 10:00 h, using established protocol[12] described in 4.5.7.

5.5.6 Metabolic flux analysis with ^{15}N-tyrosine labelling

Two-day-old *PhCM2* overexpression and wild type control petunia petals were fed with 10 mM ^{15}N-tyrosine (Cambridge Isotope Laboratories) starting at 18:00 h. After 2 h, 4 h and 6 h of feeding, the isotopic abundances and pool sizes of phenylalanine and tyrosine were analyzed by LC-MS and used for metabolic flux analysis[12,19].

5.5.7 Starch extraction and analysis

The extraction and quantification of starch was performed as previously reported[33]. Starch was extracted from 0.5 g petunia flowers harvested at 20:00 h on day 2 postanthesis. Weighted Flower tissue was ground in liquid nitrogen, mixed with 5 ml of 80% ethanol in a 15ml tube and then incubate at 100°C for 3 minutes. After centrifugation at 4000 g for 15 minutes at room temperature, discard the supernatant and repeat the process 5 more times. For glucose assay, pellet was transferred to a mortar and homogenized in 4.5 ml 80% ethanol. Distribute the homogenate into 8 tightly sealed screw-cap microcentrifuge tubes, each containing an aliquot of 0.5 ml of the homogenate. The tubes were incubated at 100°C for 10 minutes to gelatinize starch granules. After adding 0.5 ml of 200 mM sodium acetate (pH 5.5) to each tube, 4 tubes were treated with 6 units of a-amyloglucosidase and 0.5 units of a-amylase dissolved in 100 mM sodium acetate (pH 5.5), while the other 4 tubes without enzyme treatment were treated as control groups. Then samples were incubated at 37°C for 4 hours to convert starch into glucose. The quantification of starch was performed as previously reported[33] with some modification. After incubation, the samples were centrifuged at 10000g for 5 minutes at room temperature. The supernatant containing glucose was collected for further analysis. 150 μl of butter containing 50 mM triethanolamine (pH 7.6), 100 mM ATP, 0.5 M MgCl2 and 14 mM NADP was added into a quartz cuvette, then 100 μl of glucose sample, 12.5 units of G-6-P-DH and 0.2 units of Hexokinase was subsequently added. Production of NADPH was measured by spectrophotometer at 340 nm before the addition of 0.2 units of hexokinase and 5 minutes afterward.

5.5.8 IPA and IAA extraction and analysis

A typical extraction was done as previously reported[34] through a dispersive liquid-liquid microextraction (DLLME). Add 3 ml extraction buffer containing 80% methanol/1mM butylated hydroxytoluene to 0.5 g of day 2 petunia petal tissue harvested at 20:00 h. Each sample was spiked with 10 μl of 10 μM d-IAA standard. The extraction was then wrapped in aluminum foil and incubate overnight at 4°C. After centrifugation at 10000 g for 15 minutes at 4°C, the supernatant was collected in a 15 mL tube and stored at 4°C. The pellet was resuspended in 1 ml of 80%

methanol/1mM butylated hydroxytoluene and incubated at 4°C for 1 hour. Centrifuge and combine the supernatant with previously collected supernatant. An aliquot of 1 ml combined supernatant was mixed with 1ml 9% NaCl solution in a 15ml tube. Adjust the pH to 4.0 with HCl. After vortexing, add 50 μl of chloroform and 1 ml of acetone. Vortex the tubes for six seconds. After centrifugation at 4500 rpm for 3 minutes, the layer of chloroform was collected by a 25 μl syringe, and then placed into a fresh test tube. Four chloroform fractions from the same plant tissue were combined into total volume100 μl, which was then desiccated in nitrogen. Desiccated samples were resuspended into 40 μl 80% methanol/1mM butylated hydroxytoluene. Samples were analyzed by LC/MS using a Zorbax SB-C18 column (Agilent) with a 10 minutes linear gradient of 15-90% 0.1% formic acid ACN in 0.1% formic acid (v/v) at 0.3 ml/min flow rate. The amount of IAA and IPA were calculated in ratio against the spiked d-IAA standard.

5.6 Tables and Figures

Table 5.1 Changes in flux in flowers from control and *PhCM2* overexpressing petunia lines at t_{0h} and t_{6h}.

	Plastidial synthesis rate v_1 (nmol gFW^{-1} h^{-1})			Cytosolic synthesis rate v_2 (nmol gFW^{-1} h^{-1})		
	t_{0h}	t_{6h}	Relative change at t_{6h}	t_{0h}	t_{6h}	Relative change at t_{6h}
Control	806.3±80.6	774.6±77.8	-3.9%	0.45±0.16	32.07±5.56	+7027%***
PhCM2 OX	628.4±62.7	586.1±59.2	-6.7%	0.56±0.19	42.91±7.06	+7563%***
Relative change in *PhCM2 OX*	-22.1%**	-24.3%***		+24.4%	+33.8%*	

v_1 – absolute flux through the plastidial arogenate pathway;
v_2 – absolute flux through the cytosolic phenylpyruvate pathway;
(-) - indicates a decrease in flux at t_{6h} versus t_{0h} or in *PhCM2 OX* versus control
(+) - indicates an increase in flux at t_{6h} versus t_{0h} or in *PhCM2 OX* versus control
* $p < 0.05$; ** $p < 0.01$; *** $p < 0.001$. *P*-values are calculated from unpaired, two-tailed t-tests, Bonferroni corrected for multiple tests (n = 8).

Table 5.2 Protein yield from control and *PhCM2* overexpression petunia petals

	WT	**11**	**28**	**35**
Crude	2.82±0.19	2.79±0.23	2.85±0.25	2.94±0.24
Cytosolic	1.82±0.18	2.05±0.08	1.86±0.14	2.24±0.35
Plastidial	0.00451±0.00014	0.00342±0.00025*	0.00306±0.00021*	0.00244±0.00050*

Protein concentration in mg protein/g FW.
FW, fresh weight
Data are means ± s.e.m. (n = 3 independent experiments).
* $p < 0.05$ by paired Student's t test of transgenic relative to wild type control.

Table 5.3 Primers used in this project

Primer Name	**Sequence**	**Purpose**
PhCM2 F	5'-GGAATTCATGGCCTGTGGTGATTATGATGATA-3'	Cloning
PhCM2 R	5'-CGGATCCTTAGATAGAAGTTAGTTTGTTCTGATCAAGA-3'	Cloning
AtVAS1 GTW F	5'-AAAAAGCAGGCTTCATGGGTTCGTTTGGGA-3'	Gateway Cloning
AtVAS1 GTW R	5'-AGAAAGCTGGGTCTCACTCCACCATTCCATG-3'	Gateway Cloning
PhUBQ qRT F	5'-GTTAGATTGTCTGCTGTCGATGGT-3'	qRT-PCR
PhUBQ qRT R	5'-AGGAGCCAATTAAAGCACTTATCAA-3'	qRT-PCR
PhCM2 qRT F	5'-TGCAACTACTGCTGCCTGTGAT-3'	qRT-PCR
PhCM2 qRT R	5'-TCGTCAGAGCAATCCCTGAAT-3'	qRT-PCR
AtVAS1 qRT F	5′-TGGTAACCCAAGTGGCACCT-3′	qRT-PCR
AtVAS1 qRT R	5′-GCAATCCTCTTAAGCAGCGGT-3′	qRT-PCR

Figure 5.1 Proposed plant phenylalanine biosynthetic pathways and feedback regulation by aromatic amino acids.

Characterized enzymes and transporters are shown in solid colors. Phe, Tyr and Trp allosterically inhibit the committed enzymatic steps (ADT, ADH and AS respectively) in each pathway. Phe and Tyr inhibit CM, while Trp enhance CM activity. Abbreviations: ADH, arogenate dehydrogenase; ADT, arogenate dehydratase; AS, anthranilate synthase; pCAT, plastidial cationic amino-acid transporter; CM, chorismate mutase; DAHPS, 3-deoxy-D-arabino-heptulosonate 7-phosphate synthase; E4P, erythrose 4-phosphate; PEP, phosphenolpyruvate; PDT, prephenate dehydratase; PPA-AT, prephenate aminotransferase; PPY-AT, phenylpyruvate aminotransferase; TAT, tyrosine aminotransferase. Uncharacterized enzymatic steps are shown in grey. Boxes with question marks indicate unknown transporters/transport steps.

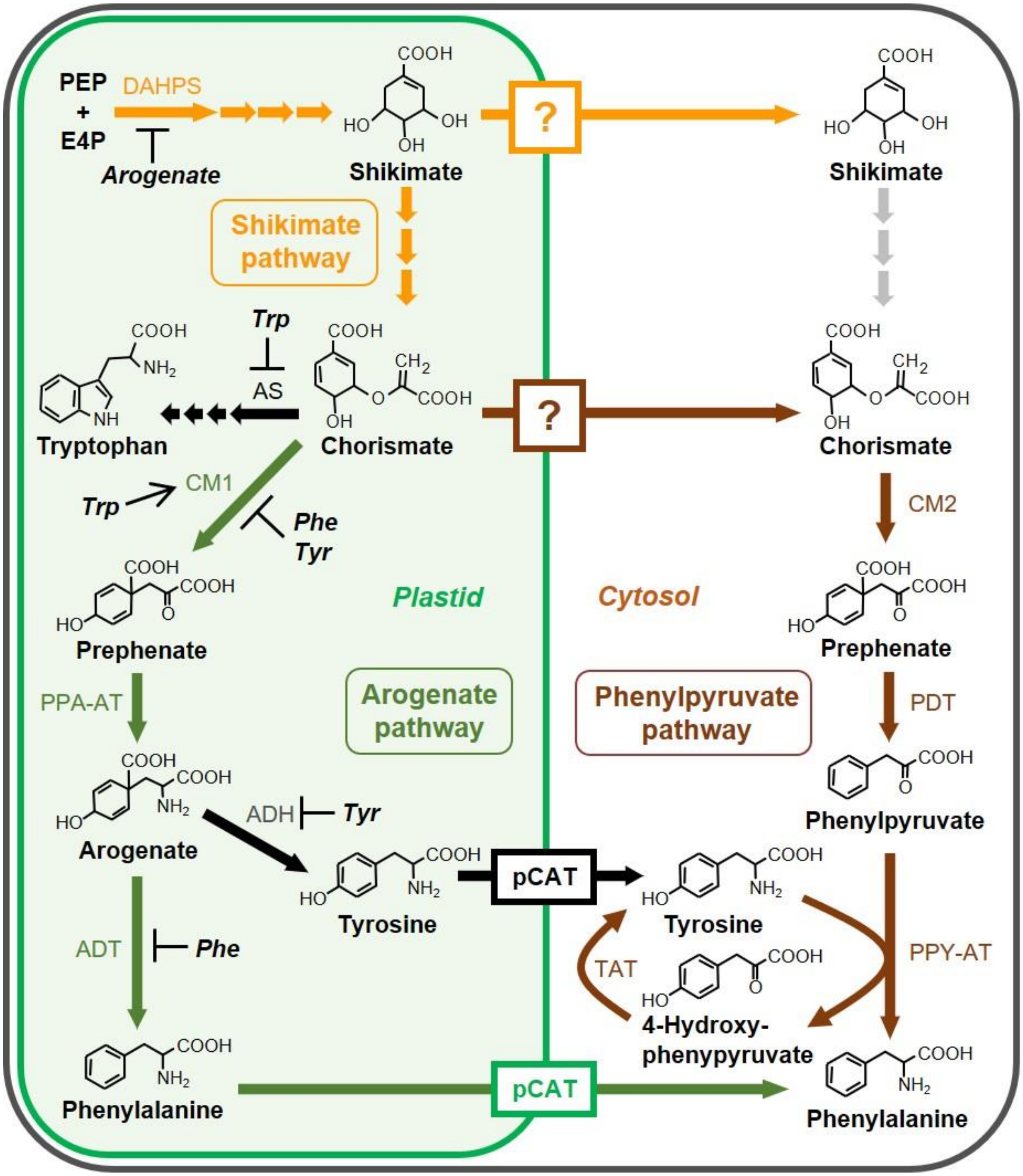
PEP
+
E4P
DAHPS
Arogenate
COOH
HO
OH
OH
Shikimate
?
COOH
HO
OH
OH
Shikimate
Shikimate pathway
Trp
AS
COOH
NH2
NH
Tryptophan
COOH
CH2
O
COOH
OH
Chorismate
?
COOH
CH2
O
COOH
OH
Chorismate
CM1
Trp
Phe
Tyr
CM2
COOH
COOH
O
HO
Prephenate
Plastid
Cytosol
COOH
COOH
O
HO
Prephenate
PPA-AT
Arogenate pathway
Phenylpyruvate pathway
PDT
COOH
COOH
NH2
HO
Arogenate
ADH
Tyr
COOH
O
Phenylpyruvate
COOH
NH2
HO
Tyrosine
pCAT
COOH
NH2
HO
Tyrosine
ADT
Phe
TAT
COOH
O
HO
4-Hydroxy-phenypyruvate
PPY-AT
COOH
NH2
Phenylalanine
pCAT
COOH
NH2
Phenylalanine

Figure 5.2 Metabolic effects of *PhCM2* overexpression in petunia flowers.

(**a**) *PhCM2* mRNA levels in wild type petunia flowers infiltrated with empty vector (black bar) and *PhCM2* overexpression construct (white bar). Data are presented as a percentage relative to the empty-vector reference. Levels of phenylalanine-derived volatiles in wild type petunia flowers infiltrated with empty vector (black bar) and *PhCM2* overexpression construct (white bar). Data are presented as a percentage relative to the empty vector reference. Data are means ± SE. (n=4 biological replicates). (**b**) *PhCM2* mRNA levels in 2-day-old petunia petals at 20:00 h. Expression levels in transgenic lines (white bars) are shown as a percentage of *PhCM2* expression in control (black bar) petals set as 100% (n = 3 biological replicates). CM activities with 500 μM chorismate in cytosolic fractions prepared from corollas of 1 to 3 day-old wild type and *PhCM2* OX petunia flowers harvested at 10:00 h (n = 3 biological replicates). (**c**) Internal pools of shikimate, prephenate, arogenate and aromatic amino acids as well as total volatile emission ($n \geq 6$ biological replicates). Metabolite levels were measured in 2-day-old petunia petals at 20:00 h and are shown in nmol g FW^{-1}. Pink background indicates metabolites with potential dual subcellular localization, in the cytosol and plastids. Emitted volatiles were collected from 2-day-old wild type and transgenic *PhCM2* OX petunia flowers from 18:00 h to 22:00 h. Black and white bars represent wild type and transgenic lines, respectively. Data are means ± SE. * $P < 0.05$, **$P < 0.01$ as determined by paired two-tailed Student's *t*-test. Abbreviations: ADT, arogenate dehydratase; ADH, arogenate dehydrogenase; CM, chorismate mutase; E4P, erythrose 4-phosphate; pCAT, plastidial cationic amino-acid transporter; PDT, prephenate dehydratase; PEP, phosphoenolpyruvate; PPA-AT, prephenate aminotransferase; PPY-AT, phenylpyruvate aminotransferase, FW, fresh weight.

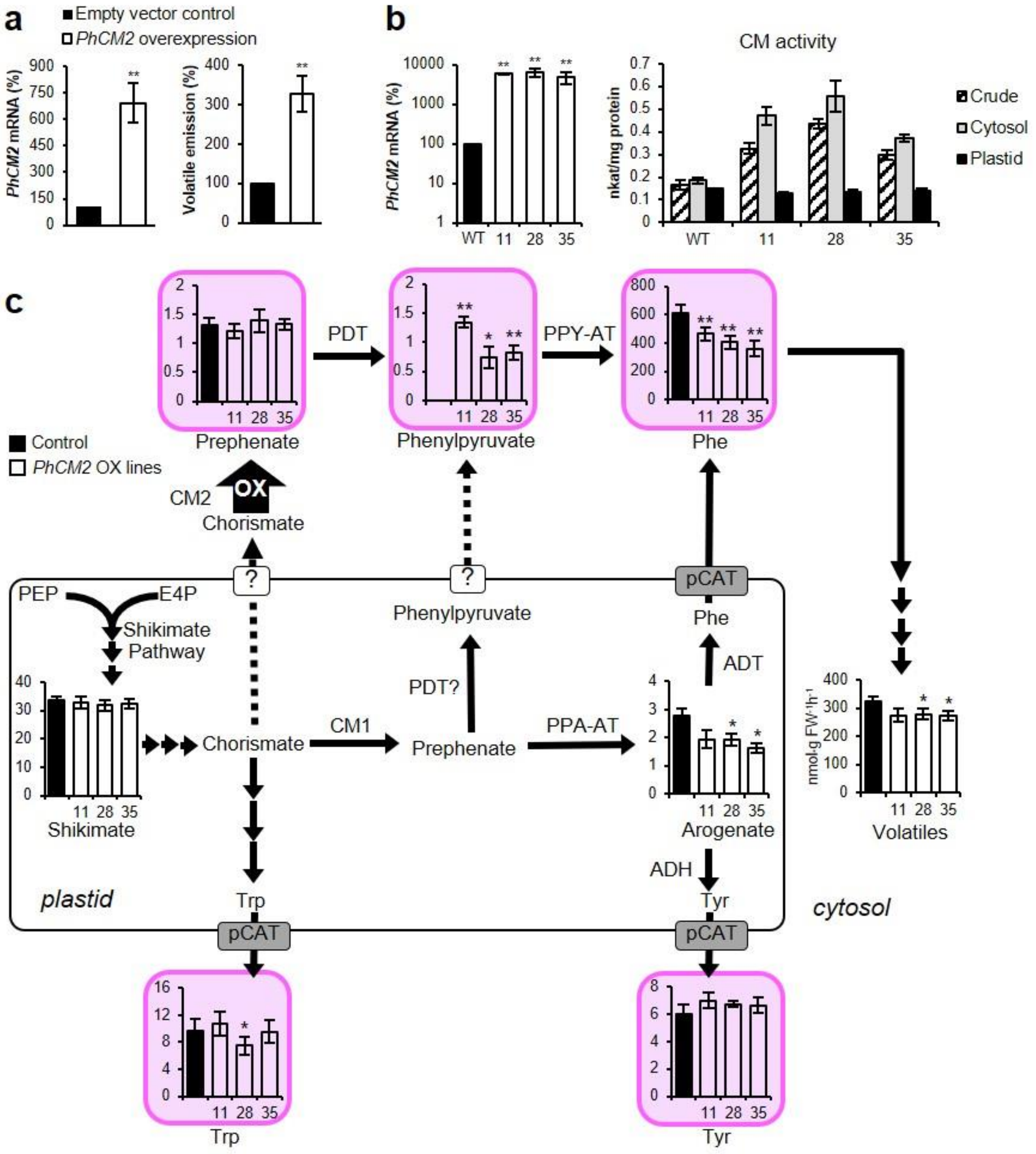
a
■ Empty vector control
☐ PhCM2 overexpression
PhCM2 mRNA (%)
0
150
300
450
600
750
900
**
Volatile emission (%)
0
100
200
300
400
**
b
PhCM2 mRNA (%)
1
10
100
1000
10000
** ** **
WT 11 28 35
CM activity
nkat/mg protein
0
0.1
0.2
0.3
0.4
0.5
0.6
0.7
WT 11 28 35
▨ Crude
☐ Cytosol
■ Plastid
c
■ Control
☐ PhCM2 OX lines
Prephenate
PDT
Phenylpyruvate
PPY-AT
Phe
** * **
** ** **
11 28 35
CM2
OX
Chorismate
?
?
pCAT
PEP
E4P
Shikimate Pathway
Phenylpyruvate
Phe
ADT
PDT?
Shikimate
Chorismate
CM1
Prephenate
PPA-AT
Arogenate
* *
ADH
Tyr
Trp
plastid
cytosol
pCAT
pCAT
Volatiles
nmol·g FW⁻¹h⁻¹
* *
Trp
*
Tyr

Figure 5.3 Metabolic effects of *AtVAS1* overexpression upon *PhCM2* overexpression petunia flowers.

(**a**) The absolute transcript levels of *AtVAS1* in wild type, *PhCM2* overexpression line, *AtVAS1 x PhCM2* overexpression lines (white bars) were determined by qRT-PCR and are shown as pg/200ng total RNA. mRNA was obtained from petunia flowers harvested at 20:00 h on day 2 post anthesis (n = 4 biological replicates). (**b**) *PhCM2* mRNA levels in 2-day-old petunia petals at 20:00 h. Expression levels in *PhCM2* overexpression line (grey bar), *AtVAS1 x PhCM2* overexpression lines (white bars) are shown as a percentage of *PhCM2* expression in wild type (black bar) petals set as 100% (n = 4 biological replicates). CM activities with 500 μM chorismate in cytosolic fractions prepared from corollas of 1 to 3 day-old wild type (black bar), *PhCM2* overexpression (grey bar) and *AtVAS1 x PhCM2* overexpression (white bars) petunia flowers harvested at 10:00 h (n = 3 biological replicates). Data are means ± SE. * $P < 0.05$, **$P < 0.01$ compared to wild type, as determined by paired two-tailed Student's *t* test. (**c**) Starch levels (n = 4 biological replicates), (**d**) total volatile emission and (**e**) internal pools of arogenate and aromatic amino acids (n = 6 biological replicates). Emitted volatiles were collected from 2-day-old wild type (black bar), *PhCM2* overexpression (grey bar) and *AtVAS1 x PhCM2* overexpression (white bars) petunia flowers from 18:00 h to 22:00 h. Metabolite levels were measured in 2-day-old petunia petals at 20:00 h and are shown in nmol g FW^{-1}. Data are means ± SE (n=6 biological replicates). Columns with the same letters above are not significantly different, as determined by Tukey's test ($p < 0.05$; one-way ANOVA). Abbreviations: CM, chorismate mutase; FW, fresh weight; N.D., not detectable.

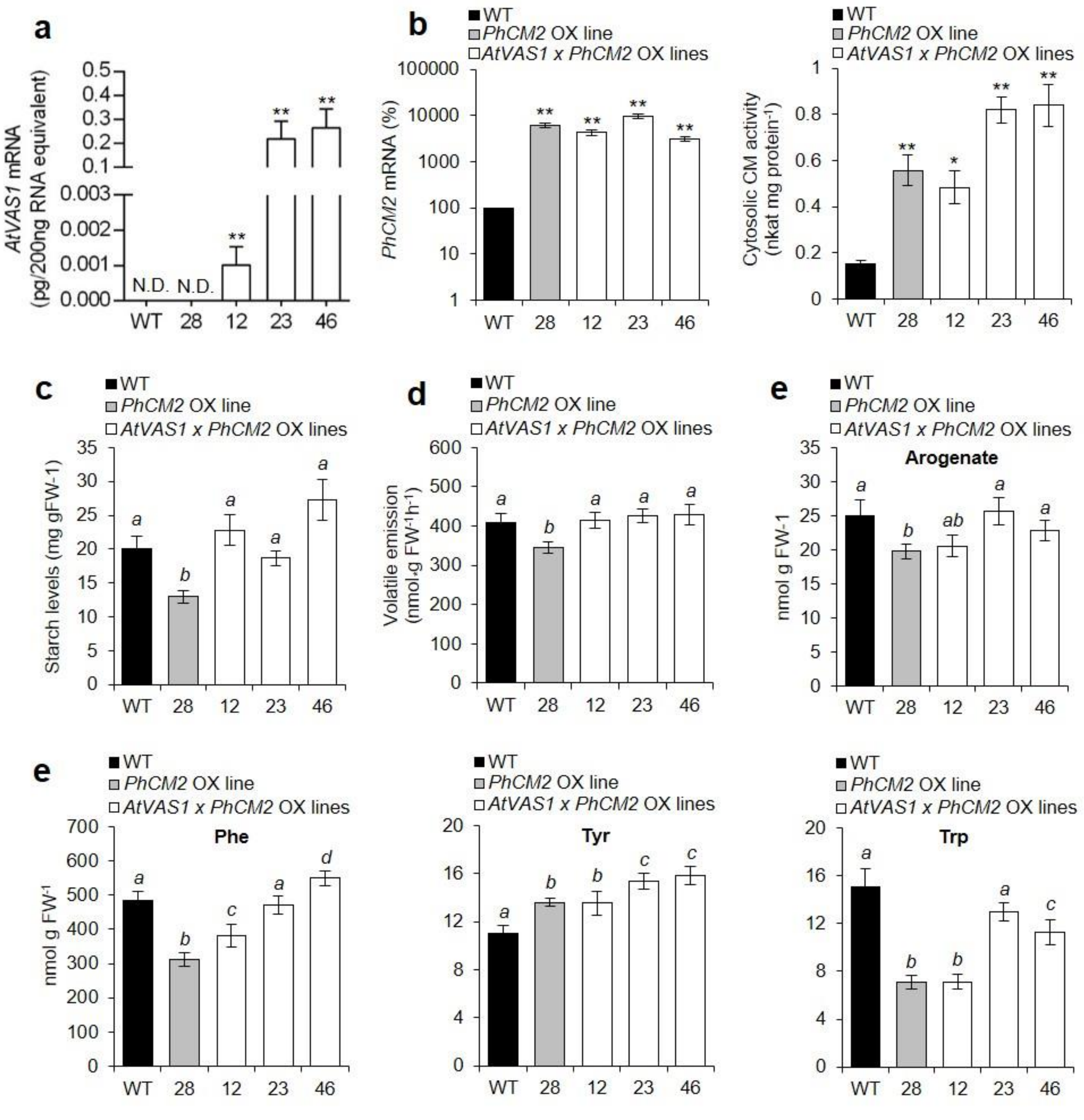
a
AtVAS1 mRNA (pg/200ng RNA equivalent)
0.5
0.4
0.3
0.2
0.1
0.003
0.002
0.001
0.000
N.D.
N.D.
**
**
**
WT
28
12
23
46
b
■ WT
▨ PhCM2 OX line
☐ AtVAS1 x PhCM2 OX lines
PhCM2 mRNA (%)
100000
10000
1000
100
10
1
**
**
**
**
WT
28
12
23
46
■ WT
▨ PhCM2 OX line
☐ AtVAS1 x PhCM2 OX lines
Cytosolic CM activity (nkat mg protein-1)
1
0.8
0.6
0.4
0.2
0
**
*
**
**
WT
28
12
23
46
c
■ WT
▨ PhCM2 OX line
☐ AtVAS1 x PhCM2 OX lines
Starch levels (mg gFW-1)
35
30
25
20
15
10
5
0
a
b
a
a
a
WT
28
12
23
46
d
■ WT
▨ PhCM2 OX line
☐ AtVAS1 x PhCM2 OX lines
Volatile emission (nmol.g FW-1h-1)
600
500
400
300
200
100
0
a
b
a
a
a
WT
28
12
23
46
e
■ WT
▨ PhCM2 OX line
☐ AtVAS1 x PhCM2 OX lines
Arogenate
nmol g FW-1
35
30
25
20
15
10
5
0
a
b
ab
a
a
WT
28
12
23
46
e
■ WT
▨ PhCM2 OX line
☐ AtVAS1 x PhCM2 OX lines
Phe
nmol g FW-1
700
600
500
400
300
200
100
0
a
b
c
a
d
WT
28
12
23
46
■ WT
▨ PhCM2 OX line
☐ AtVAS1 x PhCM2 OX lines
Tyr
20
16
12
8
4
0
a
b
b
c
c
WT
28
12
23
46
■ WT
▨ PhCM2 OX line
☐ AtVAS1 x PhCM2 OX lines
Trp
20
16
12
8
4
0
a
b
b
a
c
WT
28
12
23
46

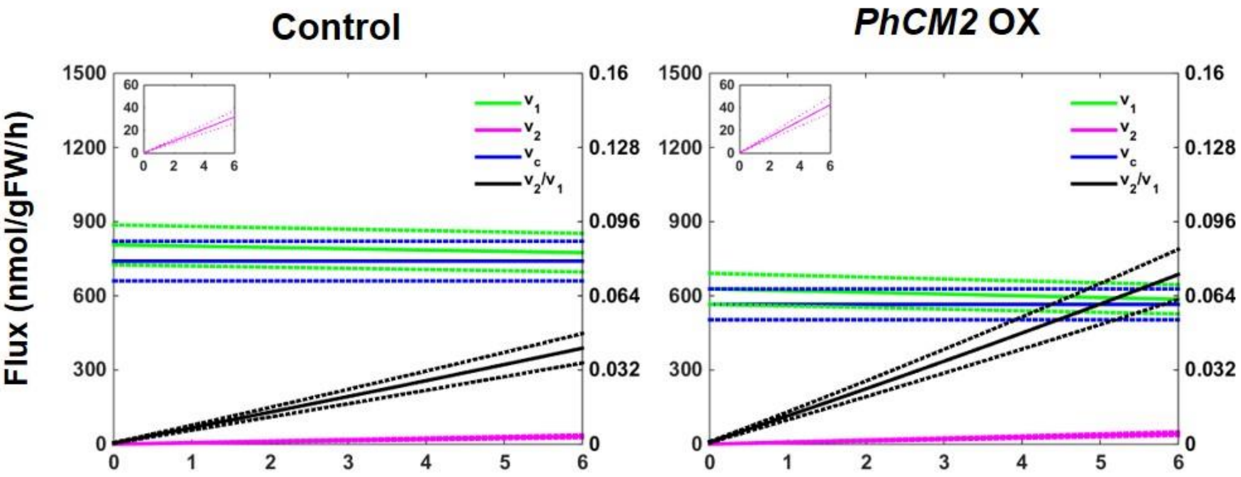

Figure 5.4 Metabolic modeling of phenylalanine biosynthetic pathways in control and *PhCM2* overexpression petunia flowers.

Flux models representing the phenylalanine biosynthetic network in 2-day-old control and *PhCM2* overexpression petunia flowers. Metabolic modeling was performed using pool sizes and isotopic abundances of phenylalanine and tyrosine, and measurements of phenylalanine-derived volatile emission (consumption flux, v_c, blue lines) from petunia petals supplied with 10mM ^{15}N-tyrosine for up to 6 h starting at 18:00 h (n = 8 biological replicates). v_1, flux through the plastidial arogenate pathway (green lines); v_2, flux through the cytosolic phenylpyruvate (pink lines, also is enlarged in inserts). v_2/v_1 ratio is shown by black lines. Solid lines are estimated values and dotted lines are standard deviation for each flux value.

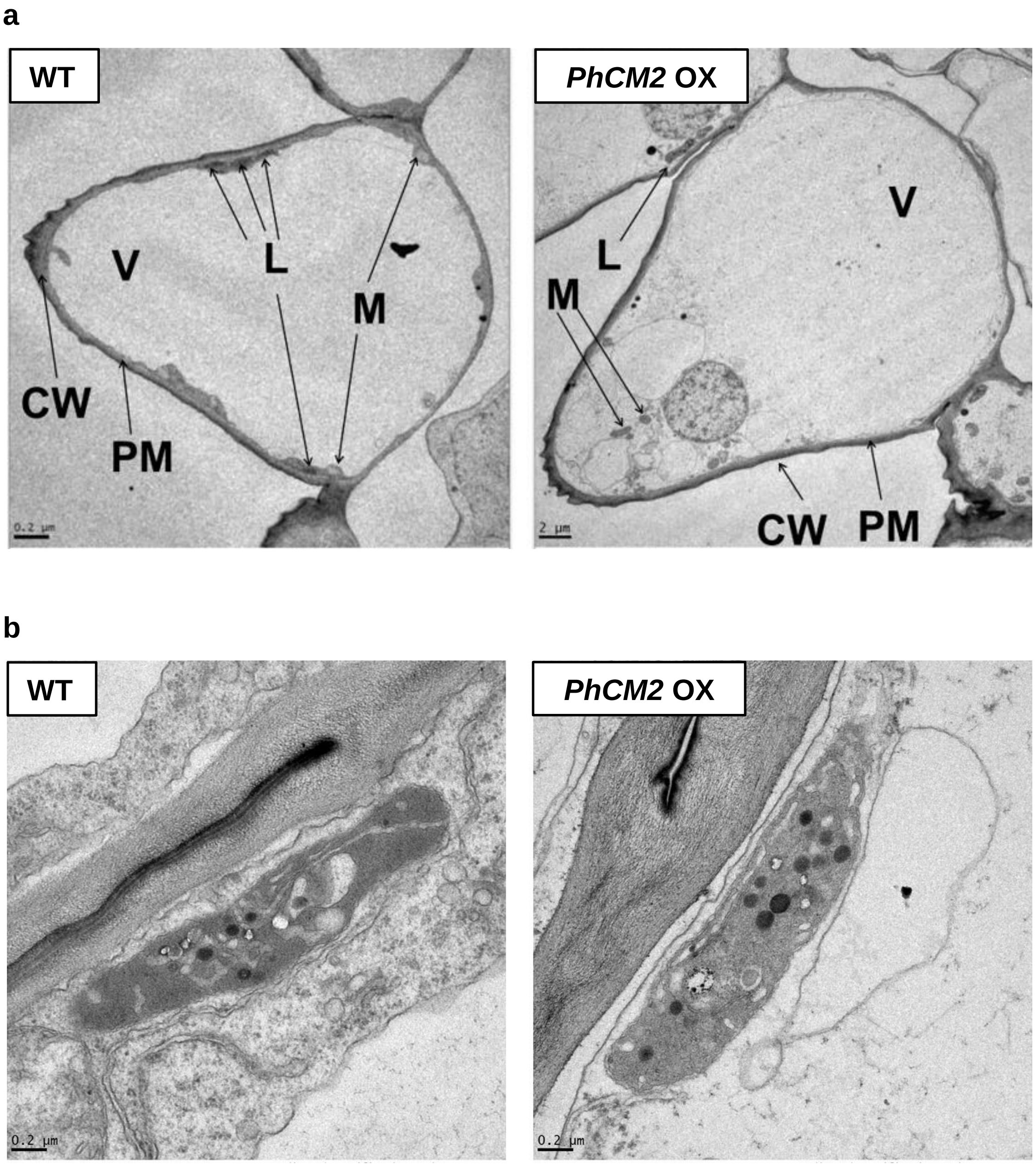
a
WT
V
L
M
CW
PM
0.2 µm
PhCM2 OX
V
L
M
CW
PM
2 µm
b
WT
0.2 µm
PhCM2 OX
0.2 µm

Figure 5.5 Transmission electron microscopy of wild type and *PhCM2* overexpression petunia petal cells.

(a) The number of leucoplast in *PhCM2* overexpressor (right) is less than wild type (left). **(b)**There is no difference in leucoplast morphology between *PhCM2* overexpressor (right) and wild type control (left). Abbreviations: CW, cell wall; L, leucoplast; M, mitochondria; PM, plasma membrane; V, vacuole.

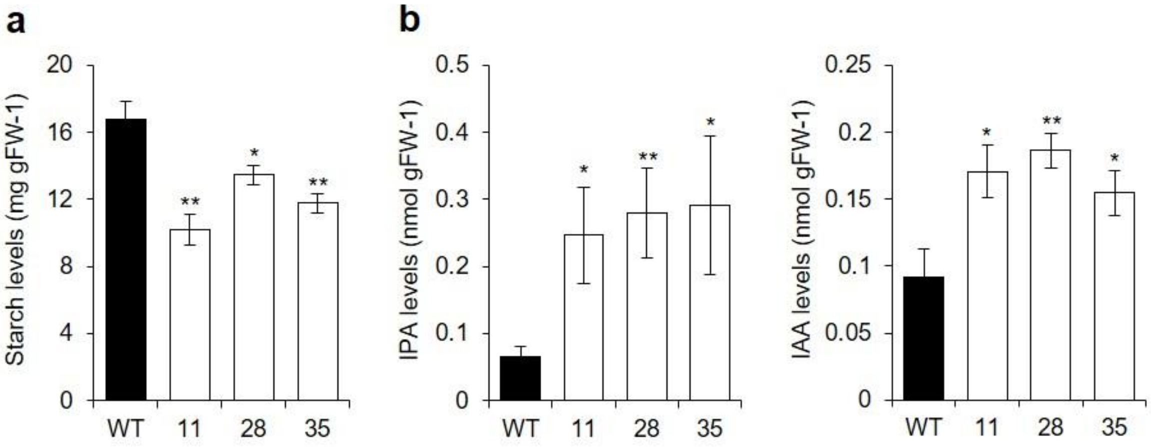

Figure 5.6 Effect of *PhCM2* overexpression on starch, IPA and IAA levels in petunia petals

(**a**) Starch levels from 2-day-old wild type (black bar) and *PhCM2* overexpression (white bars) petunia petals collected at 20:00 h (n = 4 biological replicates). (**b**) IPA and IAA levels of wild type (black bar) and *PhCM2* overexpression (white bars) petunia flowers collected at 20:00 h. (n ≥ 7 biological replicates). Data are means ± SE. *P < 0.05 and **P < 0.01 as determined by Student's *t* test. Abbreviations: IPA, indole-3-pyruvic acid (IPA); IAA, indole-3-acetic acid; FW, fresh weight.

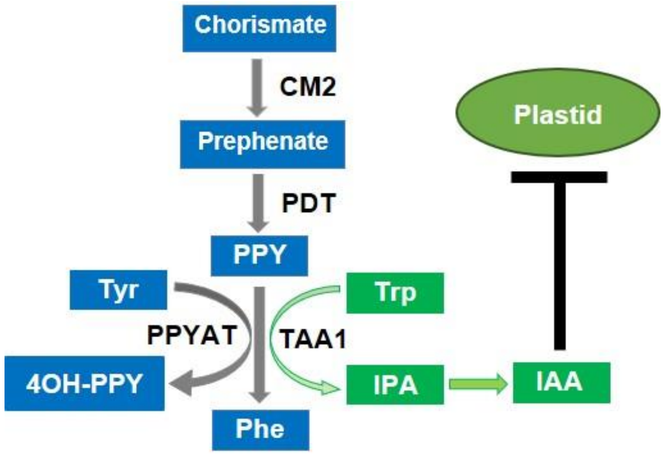
Chorismate
CM2
Prephenate
PDT
PPY
Tyr
PPYAT
4OH-PPY
Phe
Trp
TAA1
IPA
IAA
Plastid

Figure 5.7 Scheme of proposed metabolic crosstalk between phenylpyruvate pathway and tryptophan-dependent auxin biosynthesis

Abbreviations: CM2, chorismate mutase 2; IAA, indole-3-acetic acid; IPA, indole-3-pyruvic acid; 4OH-PPY, 4-hydroxyphenylpyruvate; PPY, phenylpyruvate; PPYAT, phenylpyruvate aminotransferase; TAA1, tryptophan aminotransferease.

5.7 References

1. Maeda, H. & Dudareva, N. The shikimate pathway and aromatic amino acid biosynthesis in plants. *Annual Review of Plant Biology* **63,** 73–105 (2012).
2. Vlot, A. C., Dempsey, D. A. & Klessig, D. F. Salicylic acid, a multifaceted hormone to combat disease. *Annu. Rev. Phytopathol.* **47,** 177–206 (2009).
3. Block, A. *et al.* The origin and biosynthesis of the benzenoid moiety of ubiquinone (Coenzyme Q) in Arabidopsis. *Plant Cell* **26,** 1938–1948 (2014).
4. Dudareva, N., Negre, F., Nagegowda, D. A. & Orlova, I. Plant volatiles: Recent advances and future perspectives. *Crit. Rev. Plant Sci.* **25,** 417–440 (2006).
5. Dudareva, N., Klempien, A., Muhlemann, J. K. & Kaplan, I. Biosynthesis, function and metabolic engineering of plant volatile organic compounds. *New Phytol.* **198,** 16-32 (2013).
6. Vogt, T. Phenylpropanoid biosynthesis. *Mol. Plant* **3,** 2–20 (2010).
7. Bonawitz, N. D. & Chapple, C. The genetics of lignin biosynthesis: Connecting genotype to phenotype. *Annu. Rev. Genet.* **44,** 337–363 (2010).
8. Huang, W. Y., Cai, Y. Z. & Zhang, Y. Natural phenolic compounds from medicinal herbs and dietary plants: Potential use for cancer prevention. *Nutr. Cancer* **62,** 1–20 (2010).
9. Costa, M. A. *et al.* Transgenic hybrid poplar for sustainable and scalable production of the commodity/specialty chemical, 2-phenylethanol. *PLoS One* **8,** e83169 (2013).
10. Maeda, H. *et al.* RNAi suppression of Arogenate dehydratase1 reveals that phenylalanine is synthesized predominantly via the arogenate pathway in petunia petals. *Plant Cell* **22,** 832–849 (2010).
11. Maeda, H., Yoo, H. & Dudareva, N. Prephenate aminotransferase directs plant phenylalanine biosynthesis via arogenate. *Nat. Chem. Biol.* **7,** 19–21 (2011).
12. Yoo, H. *et al.* An alternative pathway contributes to phenylalanine biosynthesis in plants via a cytosolic tyrosine:phenylpyruvate aminotransferase. *Nat. Commun.* **4,** 2833 (2013).
13. Qian, Y., *et al.* Completion of the cytosolic post-chorismate phenylalanine biosynthetic pathway in plants. *Nat. Commun.* **10,** 15 (2019)
14. Westfall, C. S., Xu, A. & Jez, J. M. Structural evolution of differential amino acid effector regulation in plant chorismate mutases. *J. Biol. Chem.* **289,** 28619–28628 (2014).

15. Tzin, V. *et al.* Expression of a bacterial bi-functional chorismate mutase/prephenate dehydratase modulates primary and secondary metabolism associated with aromatic amino acids in Arabidopsis. *Plant J.* **60,** 156–167 (2009).
16. Boatright, J. *et al.* Understanding *in vivo* benzenoid metabolism in petunia petal tissue. *Plant Physiol.* **135,** 1993–2011 (2004).
17. Verdonk, J. C. *et al.* Regulation of floral scent production in petunia revealed by targeted metabolomics. *Phytochemistry* **62,** 997–1008 (2003).
18. Orlova, I. *et al.* Reduction of benzenoid synthesis in petunia flowers reveals multiple pathways to benzoic acid and enhancement in auxin transport. *Plant Cell* **18,** 3458–3475 (2006).
19. Widhalm, J. R. *et al.* Identification of a plastidial phenylalanine exporter that influences flux distribution through the phenylalanine biosynthetic network. *Nat. Commun.* **6,** 8142 (2015).
20. Corea, O. R. A. *et al.* Arogenate dehydratase isoenzymes profoundly and differentially modulate carbon flux into lignins. *J. Biol. Chem.* **287,** 11446–11459 (2012).
21. Dal Cin, V. *et al.* Identification of genes in the phenylalanine metabolic pathway by ectopic expression of a MYB transcription factor in tomato fruit. *Plant Cell* **23,** 2738–2753 (2011).
22. Marano, M. R., Serra, E. C., Orellano, E. G., & Carrillo, N. The path of chromoplast development in fruits and flowers. *Plant Science* **94,** 1-17 (1993).
23. Pyke, K. A., & Page, A. M. Plastid ontogeny during petal development in Arabidopsis. *Plant Physiology* **116,** 797-803 (1998).
24. Kobayashi, K. *et al*. Regulation of root greening by light and auxin/cytokinin signaling in Arabidopsis. *Plant Cell* **24,** 1081-1095 (2012).
25. Miyazawa, Y. *et al.* Auxin and cytokinin have opposite effects on amyloplast development and the expression of starch synthesis genes in cultured bright yellow-2 tobacco cells. *Plant Physiology* **121,** 461-470 (1999).
26. Mashiguchi, K. *et al.* The main auxin biosynthesis pathway in Arabidopsis. *Proc. Natl. Acad. Sci.* **108,** 18512-18517 (2011).
27. Stepanova, A. N. *et al.* TAA1-mediated auxin biosynthesis is essential for hormone crosstalk and plant development. *Cell* **133,** 177-191 (2008).
28. Tao, Y. *et al.* Rapid synthesis of auxin via a new tryptophan-dependent pathway is required for shade avoidance in plants. *Cell* **133,** 164-176 (2008).

29. Zhao, Y. Auxin biosynthesis: a simple two-step pathway converts tryptophan to indole-3-acetic acid in plants. *Molecular plant* **5,** 334-338 (2012).
30. Zheng, Z. *et al.* Coordination of auxin and ethylene biosynthesis by the aminotransferase VAS1. *Nat. Chem. Biol.* **9,** 244 (2013).
31. Gleave, A. P. A versatile binary vector system with a T-DNA organisational structure conducive to efficient integration of cloned DNA into the plant genome. *Plant Mol. Biol.* **20,** 1203–1207 (1992).
32. Mano, Y., & Nemoto, K. The pathway of auxin biosynthesis in plants. *Journal of experimental Botany* **63,** 2853-2872 (2012).
33. Smith, A. M., & Zeeman, S. C. Quantification of starch in plant tissues. *Nat. Protoc.* **1,** 1342 (2006).
34. Lu, Q. *et al.* Extraction and analysis of auxins in plants using dispersive liquid-liquid microextraction followed by high-performance liquid chromatography with fluorescence detection. *Journal of agricultural and food chemistry* **58,** 2763-2770 (2010).

CHAPTER 6. FUTURE DIRECTIONS

6.1 Introduction

Previous researches have revealed that phenylalanine (Phe) is predominantly synthesized in the plastids in plants[1]. Researches covered in this work discovered and completed a cytosolic phenylpyruvate pathway for Phe biosynthesis in plants (Chapter 2 and Chapter 4), identified and characterized a plastidial Phe transporter (Chapter 3), and elucidated carbon flux regulation throughout the Phe biosynthetic network (as discussed in all chapters). Discoveries from this work provide us with new genetic tools to identify molecular players in Phe biosynthesis and metabolism, as well as new analytical methods *in planta* to answer prolonged questions such as the carbon flux regulation through the shikimate pathway. These new observations also raised questions about potential crosstalk between cytosolic Phe biosynthesis and auxin homeostasis (Chapter 5), expanding the impact of Phe biosynthetic pathway beyond aromatic amino acid metabolism.

6.2 Objectives of future research

6.2.1 Understand regulation mechanism of plant DAHPS

DAHPS catalyzes the first step in the shikimate pathway in plastids and is subject to feedback regulation (Figure 5.1). While bacterial DAHPS(s) have been demonstrated to be inhibited by all 3 aromatic amino acids, the regulation mechanism of plant DAHPS is still unclear[1]. Though Phe-sensitive DAHPS has not been reported in plants yet[2,3], *in vitro* assays have shown that DAHPS(s) from plants can be inhibited by Phe biosynthesis intermediate arogenate and prephenate[4,5], as well as Tyr[6]. Trp can either inhibit[7] or enhance DAHPS activity to a smaller extent[8,9] However, none of these feedback regulations have been demonstrated *in vivo* yet. The newly elucidated regulation mechanism of plant DAHPS, combined with knowledge of regulations in Phe biosynthesis, will provide us with a clearer picture how flux is directed through the aromatic amino acids biosynthesis network. On the other hand, though the shikimate pathway is localized in the plastids, cytosolic DAHPS activity has also been reported in plants[10,11]. However, no genes encoding plant cytosolic DAHPS(s) have been identified. This provides us with another opportunity to understand the regulation of shikimate pathway by discovering molecular players in the cytosol that exihibit similar biological functions as those in the plastidial shikimate pathway.

6.2.2 Identify shikimate and chorismate transporters

Shikimate is synthesized in the plastids through the shikimate pathway. Other than being a precursor for Phe, it has been reported that shikimate also serves as a co-substrate in phenylpropanoid and lignin biosynthesis in the cytosol[12,13], thus requiring a plastidial transporter to export shikimate from plastids into cytosol (Figure 5.1).

The existence of a functional CM2 in cytosol raises questions about the origin of the cytosolic pool of chorismate. Although there is a cytosolic shikimate pool, the enzymatic activities converting shikimate to chorismate in the cytosol still have not been reported, making it unlikely to synthesize chorismate from shikimate in the cytosol. Increased flux through cytosolic phenylpyruvate pathway when PhCM1 is feedback inhibited indicates chorismate needs to be exported from the plastids to the cytosol[14] (Figure 5.1). Identifying shikimate and chorismate transporter candidates could also show us if shikimate and chorismate is exported through transportation capacity from known transporters, or through shikimate- and/or chorismate-specific transporters.

6.2.3 Characterize petunia TAA1

In Arabidopsis, the first step in the IPA pathway of auxin biosynthesis is catalyzed by tryptophan aminotransferase TAA1, also known as Shade AVoidance 3 (SAV3)[15], which converts tryptophan to IPA. TAA1 biochemical characterization showed that tryptophan is the preferred substrate with pyruvate serving as the amino acceptor[15]. Since aminotransferase contains broad substrate specificity and phenylpyruvate contains pyruvate as a structural component, we hypothesized that TAA1 may also be able to use phenylpyruvate, the intermediate in the cytosolic phenylalanine biosynthetic pathway, as amino acceptors, and therefore the increased auxin production in *PhCM2* overexpression lines could be driven by the increased phenylpyruvate levels (Figure 5.7). To test this hypothesis, a petunia tryptophan aminotransferase (PhTAA1) candidate was identified from searching our petunia RNA-seq dataset for genes encoding proteins homologous to Arabidopsis TAA1 (At1g70560). Biochemical characterization of PhTAA1 will be performed to determine if phenylpyruvate is the a preferred substrate for PhTAA1, and hereby reveal the interconnection between cytosolic phenylpyruvate pathway and auxin biosynthesis in plants.

6.3 References

1. Maeda, H., & Dudareva, N. The shikimate pathway and aromatic amino acid biosynthesis in plants. *Annual review of plant biology* **63,** 73-105 (2012).
2. Huisman, O. C., & Kosuge, T. Regulation of aromatic amino acid biosynthesis in higher plants II. 3-Deoxy-arabino-heptulosonic acid 7-phosphate synthetase from cauliflower. *Journal of Biological Chemistry* **249,** 6842-6848 (1974).
3. Herrmann, K. M. The shikimate pathway: early steps in the biosynthesis of aromatic compounds. *Plant Cell* **7,** 907-919 (1995).
4. Rubin, J. L., & Jensen, R. A. Differentially regulated isozymes of 3-deoxy-D-arabino-heptulosonate-7-phosphate synthase from seedlings of Vigna radiata [L.] Wilczek. *Plant physiology* **79,** 711-718 (1985).
5. Doong, R. L., Ganson, R. J., & Jensen, R. A. Plastid-localized 3-deoxy-D-arabino-heptulosonate 7-phosphate synthase (DS-Mn): the early-pathway target of sequential feedback inhibition in higher plants. *Plant, Cell & Environment* **16,** 393-402 (1993).
6. Reinink, M., & Borstlap, A. C. 3-Deoxy-D-arabino-heptulosonate 7-phosphate synthase from pea leaves: inhibition by L-tyrosine. *Plant Science Letters* **26,** 167-171 (1982).
7. Graziana, A., & Boudet, A. M. 3-Deoxy-D-arabino heptulosonate 7-phosphate synthase from Zea mays: General properties and regulation by tryptophan. *Plant and cell physiology* **21,** 793-802 (1980).
8. Suzich, J. A., Dean, J. F., & Herrmann, K. M. 3-Deoxy-D-arabino-heptulosonate 7-phosphate synthase from carrot root (Daucus carota) is a hysteretic enzyme. *Plant physiology* **79,** 765-770 (1985).
9. Pinto, J. E., Suzich, J. A., & Herrmann, K. M. 3-Deoxy-D-arabino-heptulosonate 7-phosphate synthase from potato tuber (Solanum tuberosum L.). *Plant Physiol*. **82,** 1040-1044 (1986).
10. Schmid, J., & Amrhein, N. Molecular organization of the shikimate pathway in higher plants. *Phytochemistry* **39,** 737-749 (1995).
11. Ganson, R. J., d'Amato, T. A., & Jensen, R. A. The two-isozyme system of 3-deoxy-D-arabino-heptulosonate 7-phosphate synthase in Nicotiana silvestris and other higher plants. *Plant physiology* **82,** 203-210 (1986).

12. Hoffmann, L. *et al.* Purification, cloning, and properties of an acyltransferase controlling shikimate and quinate ester intermediates in phenylpropanoid metabolism. *Journal of biological chemistry* **278,** 95-103 (2003).
13. Vanholme, R. *et al.* Caffeoyl shikimate esterase (CSE) is an enzyme in the lignin biosynthetic pathway in Arabidopsis. *Science* **341**, 1103-1106 (2013).
14. Widhalm, J. R. *et al.* Identification of a plastidial phenylalanine exporter that influences flux distribution through the phenylalanine biosynthetic network. *Nat. Commun.* **6,** 8142 (2015).
15. Tao, Y. *et al.* Rapid synthesis of auxin via a new tryptophan-dependent pathway is required for shade avoidance in plants. *Cell* **133,** 164-176 (2008).

PUBLICATIONS

1. **Qian, Y.,** Lynch, J. H., Guo, L., Louie, G., Bowman, M. E. , Noel, J. P., Morgan, J. A., & Dudareva, N. (2019) Modulation of auxin formation by the cytosolic phenylalanine biosynthetic pathway (manuscript in preparation)

2. **Qian, Y.,** Lynch, J. H., Guo, L., Rhodes, D., Morgan, J. A., & Dudareva, N. (2019). Completion of the cytosolic post-chorismate phenylalanine biosynthetic pathway in plants. *Nature communications*, *10*(1), 15.

3. Widhalm, J. R., Gutensohn, M., Yoo, H., Adebesin, F., **Qian, Y.,** Guo, L., ... & Dudareva, N. (2015). Identification of a plastidial phenylalanine exporter that influences flux distribution through the phenylalanine biosynthetic network. *Nature communications*, *6*, 8142.

4. Yoo, H., Widhalm, J. R., **Qian, Y.,** Maeda, H., Cooper, B. R., Jannasch, A. S., ... & Dudareva, N. (2013). An alternative pathway contributes to phenylalanine biosynthesis in plants via a cytosolic tyrosine: phenylpyruvate aminotransferase. *Nature communications*, *4*, 2833.

5. Lin, B. F., Megley, K. A., Viswanathan, N., Krogstad, D. V., Drews, L. B., Kade, M. J., **Qian, Y.,** & Tirrell, M. V. (2012). pH-responsive branched peptide amphiphile hydrogel designed for applications in regenerative medicine with potential as injectable tissue scaffolds. *Journal of Materials Chemistry*, *22*(37), 19447-19454.